

The Influence of Processing Conditions on the
Thermo-physical Properties and Morphology of
Polycarbonate / Poly (butylene terephthalate) Blends

by

Allan Rogalsky

A thesis
presented to the University of Waterloo
in fulfilment of the
thesis requirement for the degree of
Master of Applied Science
in
Mechanical Engineering

Waterloo, Ontario, Canada, 2009

© Allan David Rogalsky 2009

Author's Declaration

I hereby declare that I am the sole author of this thesis. This is a true copy of the thesis, including any required final revisions, as accepted by my examiners.

I understand that my thesis may be made electronically available to the public.

Abstract

The objective of this work is to determine the effect of four process variables on the properties of blends composed of bisphenol-A polycarbonate (PC) and poly (butylene terephthalate) (PBT) polymers which are compounded using a large scale commercial extruder. The four variables studied are blend composition, specific energy consumption, residence time and shear rate. The last three factors were varied using the extruder screw speed and feed rate. The PC/PBT blends, commercially known as XENOY, were compounded using a WP ZSK 58 mm co-rotating twin screw extruder at the facility of SABIC Innovative Plastics in Cobourg Ontario. The extruder was instrumented to measure online the die pressure, specific energy consumption and blend temperature.

The blends were characterized using differential scanning calorimetry, (DSC), scanning electron microscopy, (SEM), gel permeation chromatography, (GPC), and melt volume flow rate, (MVR). After processing, the blend properties determined were melting temperature, glass transition temperature, crystallinity, amorphous phase weight fraction, amorphous phase composition, phase morphology, PBT-rich-phase size, blend molecular weight distribution, and MVR. Using principles available in the literature, a linear regression model was developed to relate the process variables with the online measured properties and output blend properties. Fitting this model allowed the relative importance of each process variable to be estimated for each property. An attempt was also made to identify the general type of PC/PBT blend studied and how it compares with published PC/PBT blend data.

It was found that the blends studied were well stabilized since there was no evidence of significant co-polymer formation during processing. Small decreases in molecular weight were attributed to mechanical degradation. Blending increased the crystallization and melting temperatures, as well as blend crystallinity. No practically significant difference in melting temperatures was observed between the different processing conditions. Analysis of glass transitions indicated that the blend components were partially miscible. The amorphous phase compositions were unaffected by blend composition or processing; however, the weight fraction PC-rich-phase present in the blend was strongly influenced by the screw speed. The phase structure of as-extruded blends could not be resolved using the SEM. Therefore, the

blends were annealed to coarsen the phases. After annealing, a continuous PC-rich-phase and a discrete PBT-rich-phase were observed. The PBT phase size increased with increasing PBT content. No other statistically significant effects on phase size were observed but this is not conclusive due to the large scatter in the measurements. MVR was primarily influenced by blend composition and specific energy consumption, with the effects of composition being dominant.

Further study using higher imaging resolution is required if the phase structures of as-received blend pellets are to be characterized. Contrary to current practice, it is recommended that the Utracki-Jukes equation be used rather than the Fox equation for determining amorphous phase composition from glass transition data in PC/PBT blends.

Acknowledgements

I would like to acknowledge Dr Shuihan Zhu, Dr Anthony Shin and Dr Ding for their help with staining, sample preparation and SEM operation. My collaborator Vahid Noeei is acknowledged for his experimental work which provided the starting point and support for this one. Finally I would like to thank my family, friends and my God for putting up with me and bearing me up through all my stress.

Table of Contents

LIST OF FIGURES	IX
LIST OF TABLES	XI
NOMENCLATURE.....	XII
1.0 INTRODUCTION	1
1.1 MOTIVATION FOR WORK	1
1.2 OBJECTIVE AND SCOPE OF RESEARCH.....	3
1.3 CHEMICAL CHARACTERISTICS	5
1.3.1 Syntheses and Structure	5
1.3.2 Molecular Weight / Molecular Weight Distribution	5
1.3.3 Hydrolysis.....	8
1.3.4 Direct Ester-Carbonate Exchange (Transesterification).....	9
1.3.5 End group Attack (Alcoholysis, Acidolysis).....	10
1.3.6 Thermal Degradation	11
1.3.7 Mechanical Degradation.....	12
1.3.8 Additives	12
1.3.9 Solvent Resistance	12
1.3.10 Tests of Blend Stability	12
1.4 THERMAL PROPERTIES.....	14
1.4.1 Idealized Thermal Model for Polymer Blends.....	14
1.4.2 Polymer Crystallization / Melting Theory	14
1.4.3 Glass Transition Theory	18
1.5 PHASE MORPHOLOGY	20
1.5.1 Equilibrium Phase Diagrams for Polymers.....	20
1.5.2 Characterization Techniques.....	21
1.6 RHEOLOGY	23
1.6.1 Introduction	23
1.6.2 Property Measurement	23
1.6.3 Homo-polymer Rheology and Theory.....	26
1.6.4 Blend Rheology.....	28
1.7 MECHANICAL PROPERTIES.....	31
1.7.1 Effect of Co-Polymer	31
1.7.2 Tensile Strength, Elastic Modulus, and Elongation.....	31
1.7.3 Critical Ligament Thickness and Impact Resistance	32
1.7.4 Vicat Temperature	33
2.0 LITERATURE REVIEW ON THE INTERACTION BETWEEN PROCESSING AND PC/PBT BLEND PROPERTIES	34
2.1 THERMAL PROPERTIES.....	34
2.1.1 Effects of Transesterification on Thermal Properties.....	34
2.1.2 PBT Crystallization and Melting, Pure PBT and Low-Reaction Blends	34
2.1.3 Glass Transitions in PC, PBT and blends	37
2.2 BLEND MORPHOLOGY	39
2.2.1 Low-Reaction Blend.....	39
2.2.2 Influence of Co-polymer	40
2.3 RHEOLOGY OF PC/PBT BLENDS.....	43
2.4 PROCESSING AND COMPOUNDING.....	44
2.4.1 Blending Equipment and Process Variables.....	44
2.4.2 Typical Co-rotating Twin Screw Extruder Operation	44

3.0	EXPERIMENTS	48
3.1	EXTRUDER FACTORIAL EXPERIMENT	48
3.2	MOLECULAR WEIGHT BY GEL PERMEATION CHROMATOGRAPHY (GPC)	50
3.2.1	<i>Purpose and Experimental Setup</i>	50
3.2.2	<i>Blend to Individual Polymer Comparison</i>	50
3.3	THERMAL ANALYSIS	52
3.3.1	<i>Purpose</i>	52
3.3.2	<i>Differential Scanning Calorimetry Analysis</i>	52
3.3.3	<i>Sample Preparation</i>	55
3.3.4	<i>Heating Rate Optimization</i>	55
3.3.5	<i>Test Procedures for Full Test Runs</i>	56
3.3.6	<i>Instrument Setup and Calibration</i>	56
3.3.7	<i>Calibration with Sapphire Standard</i>	57
3.3.8	<i>DSC Data Analysis</i>	58
3.4	PHASE STRUCTURE	60
3.4.1	<i>Characterization of Blend Morphology by Electron Microscopy</i>	60
3.4.2	<i>SEM Instrument Considerations</i>	61
3.4.3	<i>Sample Preparation</i>	63
3.4.4	<i>Heat Treatment</i>	65
3.4.5	<i>Instrument and Settings</i>	66
3.4.6	<i>Image Analysis</i>	67
4.0	RESULTS AND DISCUSSION	69
4.1	LINEAR REGRESSION ANALYSIS	70
4.1.1	<i>Model Development</i>	70
4.1.2	<i>Regression Implementation</i>	72
4.2	BLEND PROPERTIES	74
4.2.1	<i>Crystalline Phases</i>	74
4.2.2	<i>Amorphous Phases</i>	75
4.2.3	<i>Phase Structure</i>	77
4.3	PROCESSING ENVIRONMENT	80
4.3.1	<i>Specific Energy Consumption (SEC)</i>	80
4.3.2	<i>Die Pressure and Blend Temperature at Extruder Exit</i>	80
4.4	EFFECTS OF PROCESSING	83
4.4.1	<i>Molecular Weight</i>	83
4.4.2	<i>Volumetric Melt Flow Rate</i>	84
4.4.3	<i>Phase Size</i>	84
4.4.4	<i>PBT Melting Temperatures</i>	84
4.4.5	<i>Fraction PC-Rich-Phase</i>	86
5.0	CONCLUSIONS AND RECOMMENDATIONS	87
5.1	BLEND PROPERTIES	87
5.2	PROCESSING CONDITIONS	88
5.3	RECOMMENDATIONS	89
	REFERENCES	90

Appendices

APPENDIX A: FTIR ANALYSIS OF PC/ PBT BLENDS	96
APPENDIX B: UNIVERSAL ANALYSIS MACROS FOR DATA ANALYSIS	105
APPENDIX C: DSC CURVE ANALYSIS RESULTS	108

APPENDIX D: BLEND AND PHASE COMPOSITION FROM DSC	115
APPENDIX E: RULE OF MIXTURES DSC CURVE SUPERPOSITION.....	117
APPENDIX F: MATERIAL SAFETY DATA SHEETS FOR STAINING COMPOUNDS	130
APPENDIX G: SEM IMAGES OF ANNEALED BLEND	140
APPENDIX H: LINEAR REGRESSION MATLAB CODE	147
APPENDIX I: JOINT CONFIDENCE INTERVALS FOR REGRESSION RESULTS.....	150

List of Figures

Figure 1: Schematic of PC/PBT Blend Formulation	1
Figure 2: Thesis Organization Flow Chart.....	3
Figure 3: Fields of study and their relationship to blend properties	4
Figure 4: Polycarbonate Repeat Unit.....	5
Figure 5: Poly(butylene terephthalate).....	5
Figure 6: Molecular Weight Distribution (Theoretical Condensation Polymers)	6
Figure 7: Transesterification Reaction – Initial AB Block Polymers	9
Figure 8: Decomposition Rate vs. Temperature by TGA, 10°C/min heating	11
Figure 9: Ideal Thermodynamic Transitions.....	15
Figure 10: Spinodal Decomposition: Phase Diagram and Schematic Morphology	20
Figure 11: Typical Polymer Phase Diagrams	21
Figure 12: Rheometer Geometry	25
Figure 13: G' and G'' master curves for a typical polymer melt	25
Figure 14: Stress vs. Shear Rate for Pseudoplastic Materials.....	27
Figure 15: Polymer Viscosity vs. Molecular Weight.....	27
Figure 16: Yield Stress and Elastic Modulus vs. Co-Polymer content.....	31
Figure 17: Percent Elongation and Tensile Strength vs. Co-Polymer content	31
Figure 18: Impact Strength vs. Co-Polymer	32
Figure 19: Percent Elongation vs. wt% PC]	32
Figure 20: Yield Stress vs. wt% PC.....	32
Figure 21: Elastic Modulus vs. wt% PC	32
Figure 22: Vicat Temperature vs. Molecular Weight	33
Figure 23: PBT crystallinity versus crystallization temperature.....	35
Figure 24: PBT melting behavior by DSC.....	35
Figure 25: PC/PBT Phase Diagram	39
Figure 26: Low Reaction Blend by TEM	39
Figure 27: Phase Preferences vs. Molecular Weight	40
Figure 28: PC Tg vs Co-polymer content	41
Figure 29: Low-Reaction Blend by SEM	41
Figure 30: Highly Reacted blend by SEM.....	41
Figure 31: Typical Co-Rotating twin screw extruder operation.	45
Figure 32: Statistical Model, Coded Variables	49
Figure 33: Molecular Weight Curves – Experimental and Rule of Mixtures.....	51
Figure 34: Schematic Disk Type Heat Flux DSC.....	52
Figure 35: Transition Analysis.....	54
Figure 36: Heating Rate Optimization Results	56
Figure 37: DSC Calibration Using Sapphire	57
Figure 38: Typical DSC Analysis Results	58
Figure 39: Raw and Averaged Experimental DSC Curves.....	59
Figure 40: The effect of work distance in a typical SEM.....	61
Figure 41: Secondary Electron Contrast.....	62
Figure 42: Back Scatter Coefficient vs. Atomic Number	62
Figure 43: SEM Sample Preparation	63
Figure 44: Samples arranged for staining.	64

Figure 45: Sample positioned in holder for staining.....	65
Figure 46: Annealing Time Comparison	66
Figure 47: Image Analysis Stages.....	68
Figure 48: Linear Independence Check for Factor Pairs	71
Figure 49: Linear Independence Check for Three factor Groups	72
Figure 50: Crystalline fraction and crystallinity versus blend PBT content.....	74
Figure 51: Typical melting results	74
Figure 52: Typical glass transition results	75
Figure 53: Blend composition calculated using DSC results.....	76
Figure 54: Typical Phase Structure of an Annealed Blend.....	78
Figure 55: Phase Size Regression Results	79
Figure 56: SEC Regression Results	80
Figure 57: Die Pressure Regression Results	82
Figure 58: Melt Exit Temperature Results.....	82
Figure 59: Molecular Weight Change due to Blending	83
Figure 60: MVR Regression Results	84
Figure 61: Blends with identical composition but different processing.	85
Figure 62: PC-Rich-Phase Regression Results	86

List of Tables

Table 1: Molecular Weight Averages	6
Table 2: Chain End Groups.....	8
Table 3: Drying Conditions Reported in the Literature	8
Table 4: New Linkages formed by Transesterification.....	10
Table 5: Abusive DSC Procedure	13
Table 6: Thermal Properties of Pure PC and PBT	14
Table 7: Avrami exponent summary.....	16
Table 8: Avrami Parameters for PBT in blends with PC.....	36
Table 9: T _g by DMA	38
Table 10: Factorial Experiment Statistical Model	48
Table 11: Un-Coded Screw Speed and Feed Rate	49
Table 12: Un-Coded Blend Composition	49
Table 13: DSC Thermal Treatments	56
Table 14: Staining Supply List	64
Table 15: Staining Batch and SEM Session for Annealed Blends.	67
Table 16: Regressor Variables for Property Modeling	70
Table 17: Significance Levels for Fit Quality Categories	73
Table 18: Crystalline Phase Result Summary.....	74
Table 19: Amorphous Phase Composition Results.....	76
Table 20: PC Rich Phase Glass Transitions.....	77
Table 21: Phase Area Statistics in μm^2	79
Table 22: Phase Size Regression Results.....	79
Table 23: SEC Regression Results	80
Table 24: Die Pressure Regression Results	82
Table 25: Melt Exit Temperature Results.....	82
Table 26: MVR Regression Results.....	84
Table 27: Main Melting Regression Results.....	85
Table 28: Small Melting Regression Results.....	85
Table 29: PC-Rich-Phase Regression Results	86

Nomenclature

Symbol	Description
a	Mark-Houwink exponent
A	Area
A_f	Extruder Screw Free Cross-sectional Area
c_2	Polymer Concentration in Solution
c_p	Specific Heat Capacity
C_p	Heat Capacity
D	Extruder Diameter
d_p	SEM Probe Diameter
f	Extruder Degree of Fill
G'	Dynamic Storage Modulus
G''	Dynamic Loss Modulus
G_N°	Plateau Modulus
H	Extruder Channel Depth
i	Number of Flights in Extruder Screw
i_{BSE}	SEM Backscatter Signal Current
i_p	SEM Probe Current
J_s°	Recoverable Compliance
K	Mark-Houwink constant; Fox-Flory constant
k	Utracki-Jukes Miscibility Parameter; Crystallization Rate; Thermal Conductivity
K(T)	DSC Calibration Constant
L	Crystal Lamella Thickness
l_c	Reverse Element Length in Extruder Screw
L_c	Extruder Screw Conveying Section Length
LCST	Lower Critical Solution Temperature
L_m	Mixing Area Length in Extruder Screw
M	Molecular Weight; Torque
m	Mass
M_c	Critical Molecular Weight for Entanglement
MI	Melt Flow Index
M_n	Number Average Molecular Weight
M_v	Viscosity Average Molecular Weight
MVR	Volumetric Melt Flow Rate
M_w	Weight Average Molecular Weight
M_z	'Z' Average Molecular Weight
M_{z+1}	'Z + 1' Average Molecular Weight
n	Avrami exponent
N	Extruder Screw Speed
N_1	First Normal Stress Difference
P	Polymerization Reaction Extent; Mol-Fraction Crystallisable Units
PDI	Poly-dispersity Index

Symbol	Description
Q	Flow rate Through Extruder
R	Ideal Gas Constant; Rheometer Cone Radius
SEC	Specific Energy Consumption
T_m^*	Melting Temperature of Extended Chain Crystal
T_m°	Equilibrium Melting Temperature
T_g	Glass Transition Temperature
T_m	Apparent Melting Temperature
UCST	Upper Critical Solution Temperature
V_h	Polymer Empty Volume
V_p	Extra Extruder Conveying Section Volume Filled due to Back Pressure
V_s	Polymer Filled Volume
w_i	Weight Fraction
X_c	Crystallinity / Crystalline Fraction
α_p	SEM Beam Divergence
$\dot{\gamma}$	Shear Rate
γ_o	Shear Magnitude
ΔC_p	Heat Capacity Change at Glass Transition
ΔG_m	Free Energy of Mixing
ΔH_f	Latent Heat of Fusion
ΔL	DSC sample to reference distance
ΔQ_f	Apparent Heat of Fusion
$\Delta \Phi_{rs}$	DSC Heat Flow Difference
η	Viscosity
η^*	Complex Viscosity
η_{BSE}	SEM Electron Backscatter Coefficient
η_o	Zero Shear Viscosity; Pure Solvent Viscosity in Polymer Solutions
Θ	Rheometer Cone Angle
λ	Viscosity Ratio in Emulsions
ν_e	Crystal Surface Energy
ρ	Density
σ	Shear Stress
τ_o	Characteristic Relaxation Time
ϕ	Extruder Screw Pitch
χ_{12}	Binary Interaction Parameter
ω	Frequency
Ω	Rheometer Rotational Velocity
$[\eta]$	Intrinsic Viscosity

1.0 INTRODUCTION

1.1 Motivation for Work

Bisphenol-A-Polycarbonate (PC) is a widely used engineering thermoplastic known for its high temperature stiffness and impact resistance. However, its high melt viscosity, poor hydrocarbon resistance and lack of low temperature toughness prevent its use in some applications [1,2]. PC is increasingly being blended with other thermoplastics to modify its properties. A schematic of one of the more common blends is shown in Figure 1. Poly(butylene terephthalate), (PBT), is a semi crystalline polyester with low melt viscosity and good hydrocarbon resistance but poor high temperature stiffness [2,3]. Blends of the two polymers inherit the properties of both. Their main application is the manufacturing of automotive parts as the blend offers high impact and solvent resistance as well as stiffness at elevated temperatures [1]. Although they can be tailored to most hot forming techniques, PC/PBT blends are primarily formed by injection moulding where the viscosity lowering effect of PBT is useful [3]. Careful control over processing conditions is necessary in producing good PC/PBT blends [4].

The blend compounding operation requires accurate mixtures of both polymer components and thorough blending to ensure consistency in the final blend resin pellets. Compounding requires a significant effort in set-up and process control. It is not uncommon to generate large amounts of scrap in the initial stages of the compounding process until optimum conditions are achieved. When large volumes are processed, high scrap rates are more

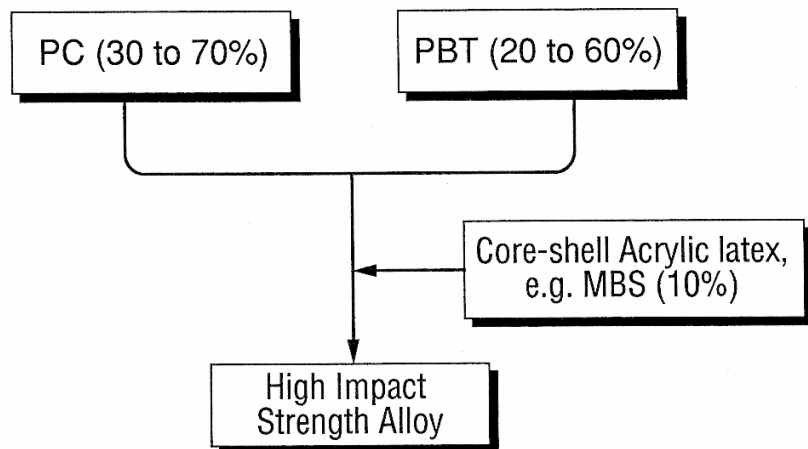


Figure 1: Schematic of PC/PBT Blend Formulation [4]

acceptable. On small production runs, however, as many blend pellets may be wasted as are sold. Attempts to predict the optimum equipment settings so far have not been well established due to a poor understanding of process dynamics. To the best of the author's knowledge, commercial scale compounding of this blend and its effect on blend properties have not been studied anywhere in the open literature. This work is part of a wider study aimed at characterizing the compounding process of a large scale extruding operation to improve the consistency in blend resin properties. The study is conducted in parallel with the investigation by Noeei [5].

1.2 Objective and Scope of research

A wider experimental study of a PC/PBT compounding process in a large scale extrusion facility is currently being undertaken [5]. The main investigation involves online property measurement prediction and control to allow better fault detection and faster optimization of processing conditions. The objective of this specific work is to determine the relationship between online measurements and the final blend properties. Results on this work will provide a better understanding of the relative importance of four extrusion process conditions studied.

A flow chart outlining the organization of this work is provided in Figure 2. Figure 3 provides a schematic of the interrelated factors influencing properties in polymer blends. A general background on these factors is provided as background in sections 1.3 to 1.7 below. For the PC/PBT blend, characteristics such as morphology, co-polymer content, molecular weight, and crystallinity have been widely studied, as have their relationships with the desired properties of solvent resistance, impact toughness and high temperature stiffness. These relationships are also described in this chapter. In Chapter 2, the current knowledge on the relationship between processing conditions and blend characteristics is reviewed. It will be shown that there is a void in the current literature with regard to understanding how extrusion conditions in a large scale commercial process affect PC/PBT blend properties. The present

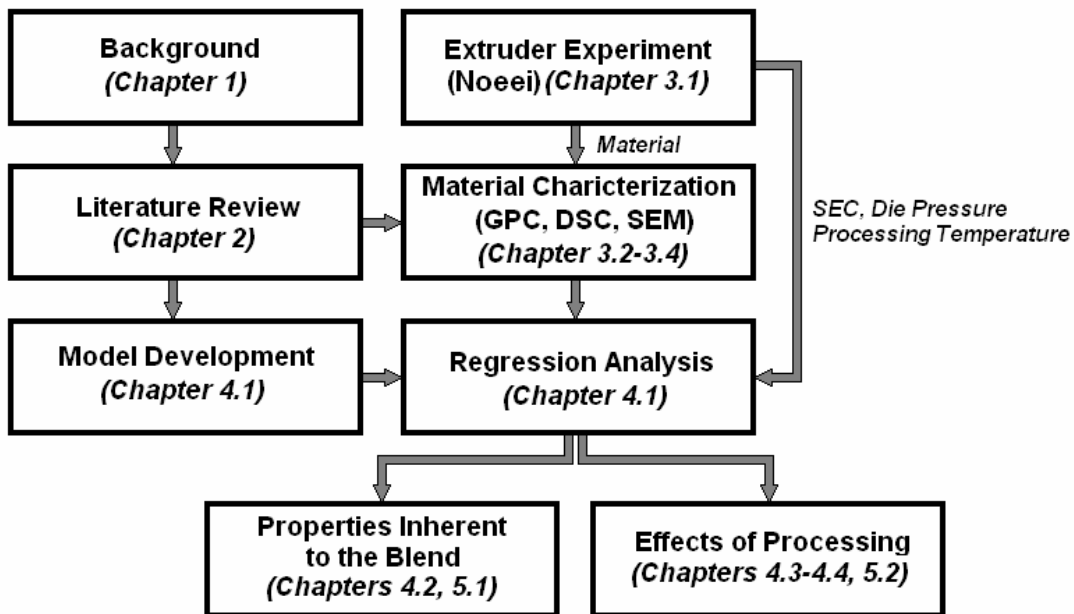


Figure 2: Thesis Organization Flow Chart

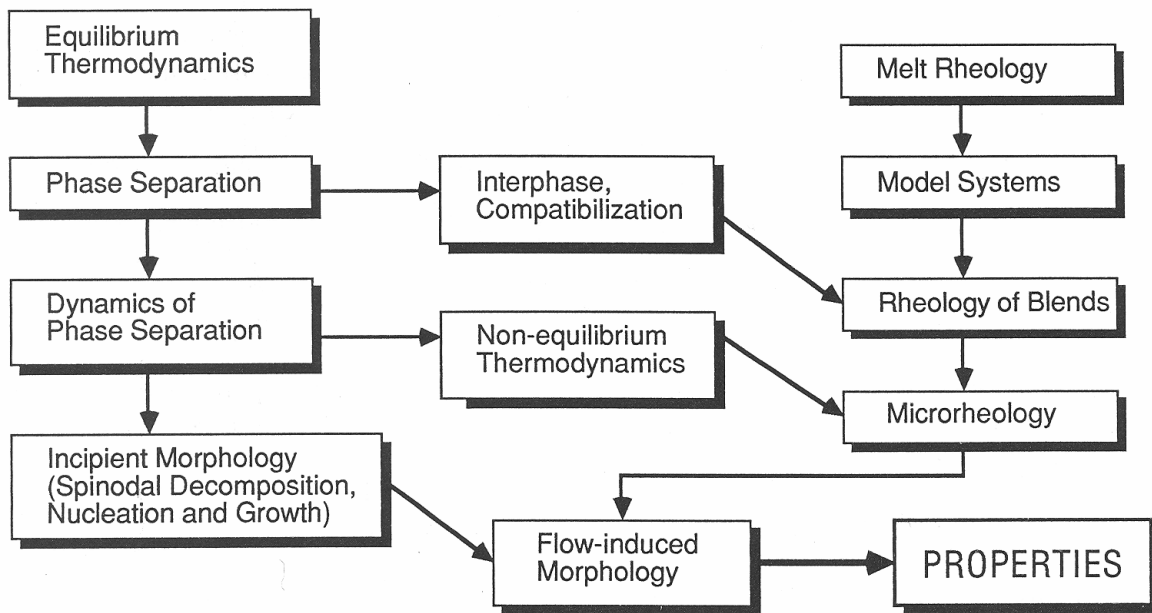


Figure 3: Fields of study and their relationship to blend properties [6]

investigation intends to fill the gap by characterizing the thermophysical properties and morphology of PC/PBT blends for a set of processing conditions.

The morphology of the PC/PBT blend is analyzed using differential scanning calorimetry (DSC) and by direct observation using scanning electron microscopy (SEM). This allows estimation of crystallinity and phase composition. Inferences about co-polymer content can be drawn through its effects on interphase compatibilization and crystallinity. To allow comparison with results from the literature the molecular weights of the blend components studied have been determined.

Due to differences between thermal and geometric scaling, the process conditions between research laboratory and commercial scale equipment are not similar. For this reason, representative resin samples have to be taken from commercial size compounding equipment. The current research investigation has received material samples from a commercial scale co-rotating twin screw extruder at SABIC plastics facility in Coburg Ontario. Section 2.5.1 compares the advantages and disadvantages of various equipment types and will demonstrate that co-rotating twin screw extruders represent one of the best options for commercial scale compounding. The scope of this work is focused on studying four main parameters in the extrusion process, namely, shear rate, specific energy consumption (SEC), blend composition and residence time.

1.3 Chemical Characteristics

1.3.1 Syntheses and Structure

PC and PBT which are both synthesized through step growth condensation reactions [3] to form the chemical structures seen in Figures 4 and 5. Several different reactions can take place between PC and PBT to form co-polymers. These reactions and their implications will be discussed later in this section. PC does not crystallize under commercial processing conditions while PBT is semi-crystalline. Crystallization from the melt produces the ‘ α ’ crystal form characterized by a gauche-trans-gauche, g-t-g, conformation of the aliphatic chain. Deformation produces the ‘ β ’ crystal form. This form is more difficult to differentiate chemically from the amorphous fraction as both are characterized by a t-t-t conformation [7,8]. The importance of these conformational differences is discussed in Appendix A: FTIR characterization of PC/PBT blends.

1.3.2 Molecular Weight / Molecular Weight Distribution

Blend miscibility [9], glass transitions, crystallization [10], and mechanical properties [11], are affected by molecular weight. Unlike low molecular weight substances polymers can not be characterized by a single molecular weight. This is a result of the random nature of a polymerization reaction which produces a range of chain lengths. In step growth polymers a “most probable” molecular weight distribution can be theoretically determined using the kinetics of the reaction. Table 1 lists different molecular weight averages used to summarize polymer molecular weight. Figure 6 plots the “most probable” distribution and provides an illustration of the relationship between the different averages. It is noted that the dependence on the high molecular weight tail increases with the order of the average. For this reason, the weight average molecular weight is always greater than the number average molecular weight. This fact can be used to provide an estimate of the distribution width called the polydispersity index, Equation 1. Using the “most probable” distribution, it can be shown that in condensation polymers the molecular weight averages and polydispersity index are all

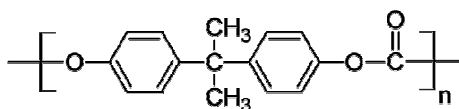


Figure 4: Polycarbonate Repeat Unit [3]

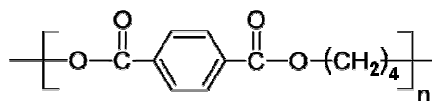


Figure 5: Poly(butylene terephthalate) [3]

functions of the reaction conversion fraction, ‘p’.[12] Useful polymers are only produced by conversions approaching one, resulting in a polydispersity index slightly less than two for step growth polymers such as PC and PBT.

$$PDI = \frac{M_w}{M_n} = 1 + p \leq 2 \quad [12] \quad \text{Equation 1}$$

There are several methods for determining molecular weight. Number average molecular weight can be determined by end group analysis, and osmotic pressure, while light scattering provides weight average molecular weight [13]. Intrinsic viscosity by itself is only a relative

Table 1: Molecular Weight Averages 13 [14]

Symbol	Name and Significance	Formula
M_n	Number Average Molecular Weight – <i>estimates the mean of the chain frequency distribution</i>	$\bar{M}_n = \frac{\sum N_i M_i}{\sum N_i} = M_0 \frac{1}{1-p}$
M_v	Viscosity Average Molecular Weight – <i>estimate based on the random coil size distribution for a specific solvent/ temperature pair</i>	$\bar{M}_v = \left(\frac{\sum N_i M_i^{1+a}}{\sum N_i M_i} \right)^{1/a} = M_0 \left((p-1)^2 \sum_{n=1}^{\infty} n^{1+a} p^{n-1} \right)^{1/a}$
M_w	Weight Average Molecular Weight – <i>estimates the mean of the chain mass distribution</i>	$\bar{M}_w = \frac{\sum N_i M_i^2}{\sum N_i M_i} = M_0 \frac{1+p}{1-p}$
M_z	“Z” Average Molecular Weight – <i>estimates extent of high molecular weight tail</i>	$\bar{M}_z = \frac{\sum N_i M_i^3}{\sum N_i M_i^2} = M_0 \frac{p^2 + 4p + 1}{(1-p)(1+p)}$
M_{z+1}	“Z + 1” Average Molecular Weight – <i>provides more significance to high molecular weight tail</i> [15]	$\bar{M}_w = \frac{\sum N_i M_i^4}{\sum N_i M_i^3} = M_0 \frac{p^3 + 11p^2 + 11p + 1}{(p^2 + 4p + 1)(1-p)}$

M_i ≡ molecular weight of the ith fraction

N_i ≡ number molecules of the ith molecular weight

a ≡ Mark-Houwink exponent for solvent/temperature pair

p ≡ reaction extent, condensation polymers

M_0 ≡ molecular weight of repeat unit

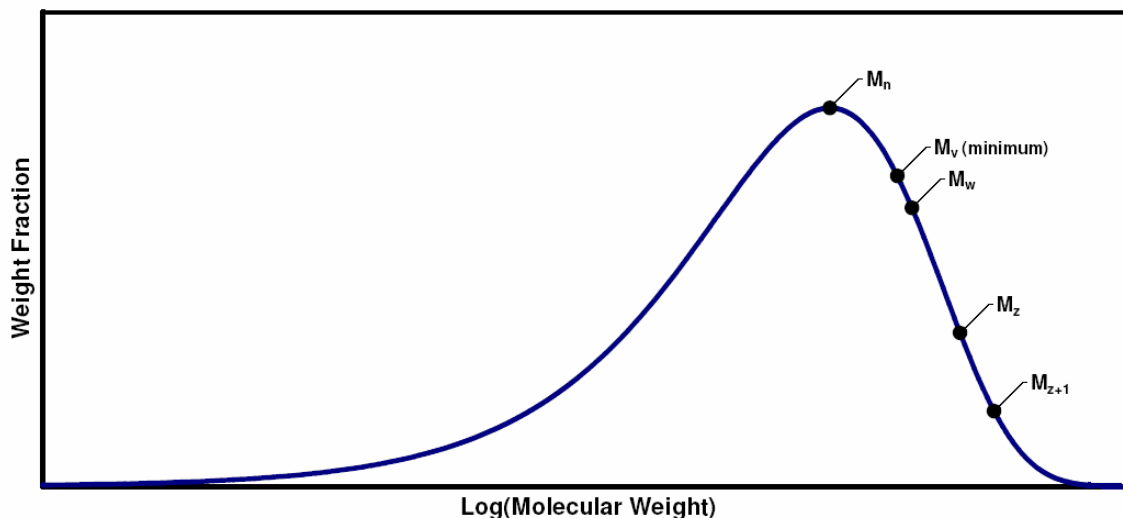


Figure 6: Molecular Weight Distribution (Theoretical Condensation Polymers)

estimate of molecular weight because it is dependent on the conditions under which it was determined. It is found by measuring the viscosity of a dilute polymer solution at a variety of concentrations, c_2 . The viscosity is then extrapolated to zero concentration according to Equation 2, where η is the viscosity of the solution, η_0 is the viscosity of the pure solvent [15,16, 17]. Both the temperature and choice of solvent affect the final value and therefore should be sighted if intrinsic viscosity is to have any meaning [15]. If these conditions are known the viscosity average molecular weight can be calculated using the Mark-Houwink equation, Equation 3 [15,16,18]. Reference [16] tabulates the Mark-Houwink constants for PC in several solvents.

$$[\eta] = \lim_{c_2 \rightarrow 0} \left(\frac{\eta - \eta_0}{c_2 \eta_0} \right) \quad [15,16,17] \quad \text{Equation 2}$$

$$[\eta] = KM_v^a \quad [15,16,18] \quad \text{Equation 3}$$

If the entire molecular weight distribution is desired the simplest method is gel permeation chromatography, (GPC) [15]. GPC separates molecules by their hydrodynamic volume. It does this by using a column packed with pellets containing pores similar to the size of the polymer molecules. When the solution is forced through the column small molecules fit into many pores resulting in a circuitous path through the column. Large molecules pass through more directly. Calibration using standards of known molecular weight allows the resulting concentration vs. exit time curve to be converted into a molecular weight distribution. Often standards are not available for the polymer being tested. Two options are available in this situation. The best option is the use of a universal calibration based on a known relationship between retention time, hydrodynamic volume and intrinsic viscosity. (For a complete description of this technique see reference [19]). As universal calibration requires a more sophisticated instrument, calibration is commonly performed with the available standards and the resulting molecular weights quoted as relative that of the standard polymer. Similar to intrinsic viscosity, relative molecular weight is only directly comparable if measured using the same standard, solvent and operating conditions [19].

1.3.3 Hydrolysis

Both PBT and PC can be degraded by the presence of water [28,29,30]. The water splits the chain generating carboxylic acid and alcohol end groups in PBT [29]. In PC the reaction splits the chain at the carbonate linkage resulting in phenol end groups and the generation of CO₂, see Table 2. PC initial degradation of 2.54×10^{-2} % chain scissions followed by a steady rate of 6.92×10^{-4} % scissions/h was reported in samples exposed to 100% relative humidity at 90°C. The reaction rate was observed to increase with temperature requiring that PC be dried before melt processing [30]. Some hydrolytic degradation is expected during the drying process as evidenced by the measured degradation of PBT sheet of varying thicknesses aged and dried identically. PBT pellets of approximately 3 mm diameter and PBT sheet of similar thickness evidenced 1.20×10^{-3} % scissions/h while only 0.92×10^{-3} % scissions/h was calculated for 0.77 mm sheet. As the reverse trend would be expected if the increase in degradation were due to poor water penetration of the polymer during ageing, it can be concluded that 23% of the total degradation is due to drying. Ageing conditions were 95% R.H. 85°C. Drying conditions were 3 hours at 150°C in vacuum [30]. As can be seen from Table 3 this drying temperature is higher than any of those recorded in the literature for PC /

Table 2: Chain End Groups

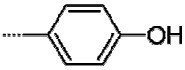
Alcoholic	Carboxylic	Phenol
$\text{---}(\text{CH}_2)_4\text{OH}$	$\text{---}\overset{\text{O}}{\parallel}{\text{C}}\text{---OH}$	

Table 3: Drying Conditions Reported in the Literature

Temperature	Environment	Sample Type	Time	Source
60°C	Air	Pellets	1 week	[20]
60°C	Vacuum	Pellets	1 week	[21]
80°C	Air	Pellets	4h	[1,22]
115°C	Air	Plaques	>2h	[9]
115±5°C	Air	Pellets	4-5h	[23]
120°C	Air	Pellets	2h	[24]
120°C	Vacuum	Particulate	4h	[2,22]
120°C	Air	Pellets	5h	[25]
120°C	Air	Pellets	18h	[1]
120°C	Vacuum	Pellets	24h	[26]
120°C	Air	Pellets	48h	[27]
125°C	Air	Pellets	>3h	[9]

PBT blends. GE Plastics recommended drying conditions are 3 to 6 hours in air at no more than 120°C [31,32].

1.3.4 Direct Ester-Carbonate Exchange (Transesterification)

PC/PBT blends are known to react under certain conditions. Devaux et al. have determined that direct ester-carbonate exchange or transesterification is the dominant reaction taking place in these blends [25]. Residual quantities of organometallic Ti compounds from the manufacture of PBT have been detected in both raw PBT [33] and in PC/PBT blends [2]. These compounds have been found to also catalyze the transesterification between PC and PBT [7,9,34] with a reaction rate proportional to the catalyst content [7]. Transesterification stabilizers for this blend typically operate by inactivating the catalyst; however complete suppression can not be proven. The reaction has been observed to occur at temperatures as low as 200°C [3] and has been predicted to proceed un-catalyzed at 250°C with an initial rate of 3.11×10^{-7} mol/(g min). The catalyzed reaction rate is as much as two orders of magnitude higher [25] in one experiment producing 100% co-polymer in 5min at 240°C [21]. Several authors agree that in melt blending operations small but significant copolymer concentrations are achieved prior to catalyst inactivation [3,25,35]. To produce blends unaffected by the presence of a catalyst, it should be neutralized by ether solvent [35] or melt [9] blending the PBT with a stabilizer prior to compounding with PC.

As seen in the reaction scheme outlined in Figure 7 transesterification initially produces A-B type block co-polymers. As the reaction continues the number of blocks in each chain

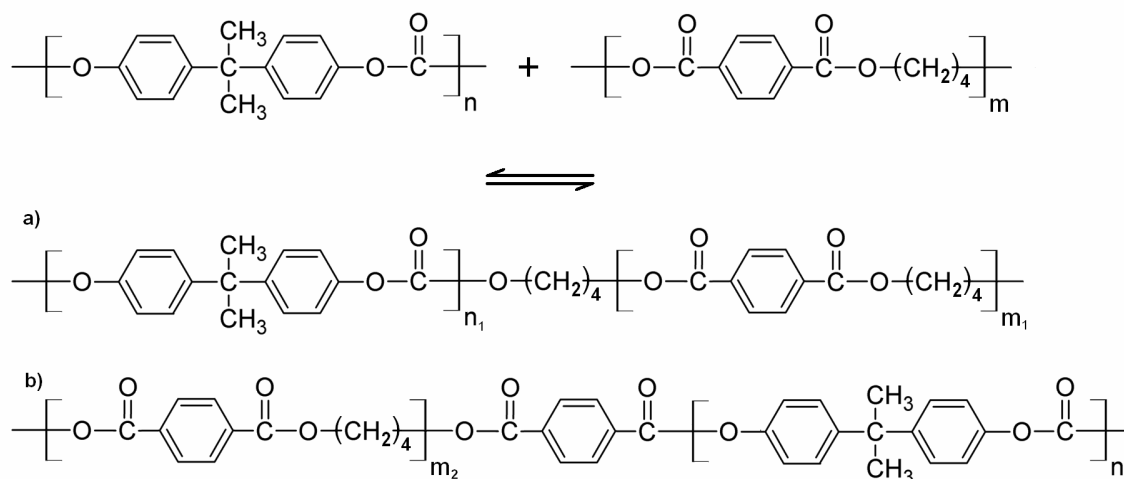


Figure 7: Transesterification Reaction – Initial AB Block Polymers [21, 25]

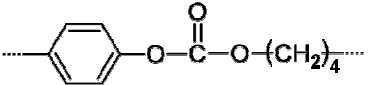
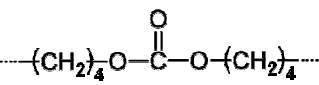
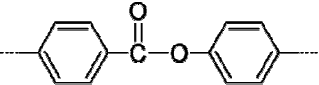
increase while the block length decreases. The final result is a random statistical co-polymer [25,36]. Transesterification is believed to be a fully reversible reaction and do not result in the evolution of carbon dioxide [25]. Carbon dioxide evolution observed during reactive processing is attributed to ether acidolysis of PC by PBT terminated with carboxylic groups [25], see section 1.3.5, or the thermal decomposition of less stable aliphatic carbonates formed by the reaction [9], Figure 7a. In addition to the aliphatic aromatic carbonate [25], and aromatic ester [25,37], formed by the initial transesterification, the reaction products can react further to produce fully aliphatic carbonates [7]. See Table 4 for new structures formed by the reactions.

The presence of co-polymers in the blend affects blend miscibility [35], phase structure [38,39], thermal properties [35], mechanical properties [39] and solvent resistance [25,36]. Low reaction extent blends exhibit the phase separated structure and thermal properties of a low miscibility blend [36] combined with increased mechanical properties. The one exception to this is impact resistance which is immediately decreased [39]. This is one reason commercial blends typically try to keep co-polymer content as low as possible [3,9]. Increased solvent resistance occurs in blends containing large components of A-B block co-polymers [25,36], while nearly all properties are severely reduced if the reaction is allowed to progress to the formation of statistical co-polymers [3,9]. The specific effects of co-polymers summarized here are discussed in more detail in the sections on mechanical properties, thermal properties and phase structure. Other co-polymer forming reactions exist besides transesterification. These are discussed in the following sections.

1.3.5 End group Attack (Alcoholysis, Acidolysis)

Alcoholic and carboxylic end groups on PBT react readily with PC. In an un-catalyzed melt mixing experiment the reaction went to completion in approximately 5min at 240°C. The co-polymer content was significant at approximately 50wt% for 50/50mol% blend [21]. The PC phenol end groups formed were found to be un-reactive to 270°C which was the maximum

Table 4: New Linkages formed by Transesterification

Aromatic Aliphatic Carbonate [25]	Fully Aliphatic Carbonate [7]	Aromatic Ester [25,37]
		

temperature studied [25]. For this reason at lower temperatures the reaction stops when all reactive PBT end groups are consumed and a block co-polymer and low molecular weight PC are formed rather than a statistical copolymer [25,21]. To prevent this reaction PBT ends can be capped [21]. No carbon dioxide is formed by the alcoholysis reaction however it is formed by acidolysis [25, 21]. This can result in destructive foaming during extrusion [9].

1.3.6 Thermal Degradation

Though its degradation onset has been measured at as low as 266°C [37], pure PC exhibits negligible degradation to 300°C. The PBT degradation onset temperature is known to be below 240°C with an initial rate of thermal degradation of 9.1×10^{-8} mol/(g min) at 250°C [25]. PBT samples with capped ends did not generate alcoholic or carboxylic end groups by thermal decomposition when heated to 290°C for 1h. This degradation was detected at 310°C and has been reported in the literature in significant quantities at 300°C [21]. Blends of PBT and PC have lower degradation onset temperatures than their parent polymers suggesting transesterification produces less stable structures [20, 37]. Aliphatic carbonates have been implicated [9, 20], while completely aromatic esters were found to be more stable than the parent polymers [20]. See Figure 8 for TGA data for the two parent polymers and their blends.

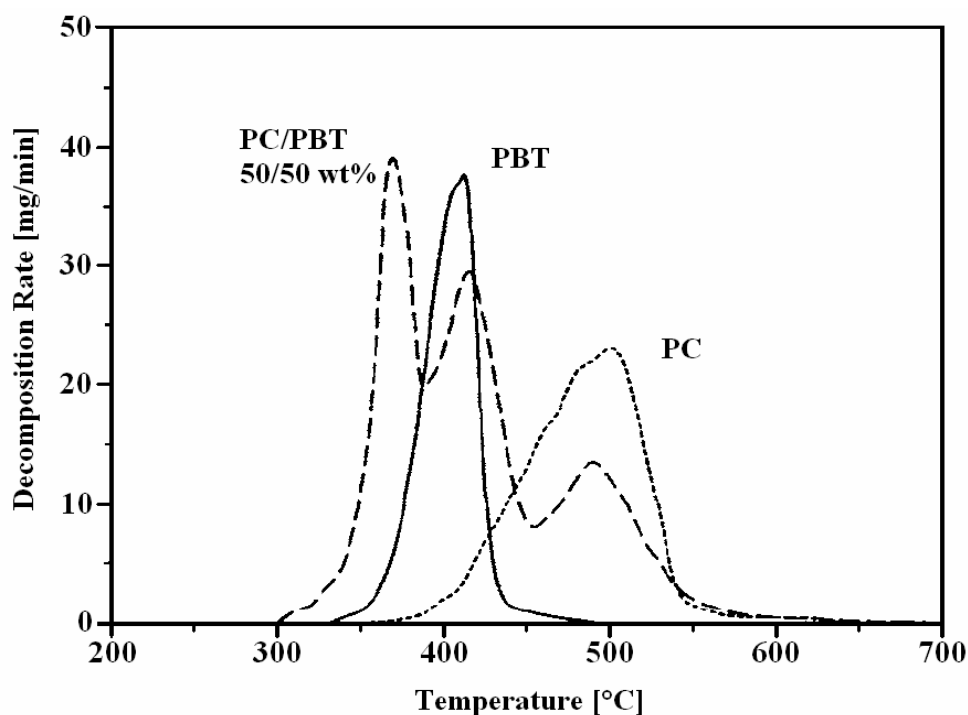


Figure 8: Decomposition Rate vs. Temperature by TGA, 10°C/min heating [20]

1.3.7 Mechanical Degradation

Polymers can be degraded by excessive shear stress during processing. This has the effect of breaking polymer chains and reducing molecular weight. Data from polymer solutions suggests that entanglements between chains attenuate the stress and reduce the chance of chain failure as initial molecular weight increases [40]. At a given shear stress polymer molecular weight is found to eventually stabilize after long processing intervals [41].

1.3.8 Additives

Santos and Guthrie, [3], provided a good summary of additives typically used in PC/PBT blends. According to them, blends typically contain 15-20 wt% MBS rubber as an impact modifier. Inorganic pigments typically make between 0.1 and 2.0 wt% of the blend. Though pigments are only intended to affect appearance they have been shown to affect transesterification [3], UV stabilization [42], and other properties. Heat stabilizers added to the blend are free radical quenchants and as such also protect against free radicals produced by UV-light, exposure to oxygen and mechanical degradation of the polymer. Phosphates and phosphorous containing acids are often used as transesterification inhibitors. As mentioned previously these “inhibitors” primary role is to inactivate the residual catalyst found in the PBT, slowing, but not stopping the transesterification reaction [3].

1.3.9 Solvent Resistance

Chemical resistance of blends is directly proportional to PBT content. PBT chemical resistances is attributed to its crystallinity which is as high as 40% when blended with PC [3], but which is reduced by high reaction extent transesterification [3,9]. The A-B type block copolymers formed by initial transesterification have high solvent resistance, as evidenced by the minimum in solubility data published by Devaux et al., however the random co-polymer is fully soluble in most solvents for either polymer [25]. The total loss of crystallinity observed in fully reacted blends [3,9] is likely a contributing factor, as is the fact that in a random co-polymer there will be many sites which exhibit favourable interaction with solvents for either of its constituents.

1.3.10 Tests of Blend Stability

Given the importance of characterizing or estimating the co-polymer content and its rate of change in PC / PBT blends, many tests of stability have been developed. To quantify

the exact co-polymer concentration the best methods are Fourier transfer infrared (FTIR) [7,25,26, 37] and nuclear magnetic resonance (NMR) [7,25,26]. Both of these detect the new chemical groups formed. NMR can detect co-polymer at concentrations of less than 0.5mol%. FTIR is limited to aromatic ester concentrations greater than 3.5mol% with aliphatic carbonates not being detectable at concentrations below 23mol% due to overlap with existing PC and PBT bands [7]. Appendix A provides more information.

If only verification of blend stabilization and the absence of significant co-polymer concentrations are necessary several other techniques have been attempted. Hamilton and Gallucci, [9], have outlined a procedure they call “Abusive DSC” which exploits the negative effect on PBT crystallinity of high transesterification reaction extent, see Table 5. Poor stabilization is indicated by drops in melting temperature and crystallinity during the final scan. As will be seen in the thermal properties section, the AB type co-polymers produced by end group attack or at the early stages of transesterification do not greatly affect melting and crystallization behaviour. Because of this abusive DSC mainly verifies that little or no random copolymer is present [9]. Other authors have used changes in solvent resistance [1,27,26]. Solubility of the blend is measured in methylene chloride, a good PC but poor PBT solvent. If the dissolved fraction matches the original PC fraction it is assumed no reaction occurred. However blends declared un-reacted by this method showed decreased PBT crystallinity [27], a sign of reaction according to Hamilton and Gallucci [9]. For this reason solvent extraction is probably best used to improve the resolution of FTIR in the manner of Birley and Chen [1], rather than a stand alone method. Evaluation of blend reaction extent may also be possible by observing morphological changes. Blend phase size is known to decrease with increasing co-polymer concentration [36]. More details are provided in the section on blend morphology.

Table 5: Abusive DSC Procedure [9]

Description	Cycle Parameters
First Scan	Heat 40-290°C at 20°C/min
	Hold at 290°C for 15 min
	Cool 290-40°C at 80°C/min
Second Scan	Heat 40-290°C at 20°C/min

1.4 Thermal Properties

1.4.1 Idealized Thermal Model for Polymer Blends

In thermal analysis, semi-crystalline polymers are typically modeled as two phase mixtures consisting of completely amorphous and completely crystalline phases [43]. Similarly un-reacted PC/PBT blend behaviour, ignoring impact modifier, can be modeled as a three-phase mixture. Leaving the morphological arguments on this model for later, and assuming in the most general case partial miscibility, the phases consist of a crystalline PBT phase and two amorphous phases, one rich in PC and the other in PBT [3]. Under such a model full thermal characterization of the polymer blend consists of characterizing each of the phases in terms of its characteristic temperatures and behaviour as well as the relative proportions of these phases. The behaviour of the whole is described by the superposition of all phase behaviours using the rule of mixtures, Equation 4 [44]. A summary of typical thermal properties for both PC and PBT is listed in Table 6. Discussion regarding key properties follows.

$$c_p = \sum_i (w_i \cdot c_{p,i}) \quad [44] \quad \text{Equation 4}$$

1.4.2 Polymer Crystallization / Melting Theory

The polymer melting temperature is not as sharply defined as that of metals or low molecular weight compounds. Even so polymer melting can be classified as a first order phase

Table 6: Thermal Properties of Pure PC and PBT

Description	Symbol	Material	Value
Latent Heat of Fusion	ΔH_f	Crystalline PBT	140±1.5 J/g, 144 J/g [45] 142 J/g [46]
Crystal Surface Energy	ν_e	PBT	$57-75 \times 10^{-7} \text{ J/cm}^2$ [47]
Equilibrium Melting Temperature	T_m°	PBT	236-260°C [47] 244°C [48]
Apparent Melting Temperature (Dependent on Processing)	T_m	PBT	Multiple Peaks [48,49] 215°C [1] - 230°C [48]
Maximum Crystallinity	X_c	PBT	38-40% [7,50]
Heat Capacity Change at Glass Transition	ΔC_p	PC	0.24 J/(gK) [51]
		Semi-crystalline PBT	0.35 J/(gK) [48]
		Amorphous PBT	0.49 J/(gK) [48]
Glass Transition Temperature	T_g	PC	< 155°C [52]
		Semi-crystalline PBT	22-80°C [48]
		Amorphous PBT	-25°C [48]

transformation thermodynamically [53]. An ideal first order phase transition is characterized by a change in the slope of the Gibbs free energy versus temperature curve resulting from a discontinuity in one of its derivatives, Figure 9a. The crystal represents a much more ordered state than the melt resulting in a step change in entropy. Theory predicts a sharp “infinity point” in the second derivative of free energy, and therefore the heat capacity curve, but in practice “a broad melting peak” is observed [54]. This deviation from theory is due to kinetic factors. The area under this peak, taking the theoretical heat capacity curve as a base line, represents the enthalpy difference between the crystal and the liquid [55], which when normalized with respect to mass is customarily called the latent heat of fusion, ΔH_f .

The kinetics of polymer crystallization at constant temperature are well described by the Avrami equation, Equation 5, where $X_{c,t}$ is the crystal fraction at time t , k is the crystallization rate constant and n is the Avrami exponent [56,57,58]. The Avrami exponent is related to the “primary nucleation and growth geometry” of the crystals [56,58]. Table 7 summarizes the Avrami exponents expected. Polymer crystals often grow in large spherical super structures called “spherulites”, with all crystals radiating from a common center. For this growth geometry an Avrami exponent of 3 is expected. As can be seen, the Avrami exponent by itself is not a definitive indicator of crystal growth mode but merely an indicator, eliminating some options [59]. Small angle light scattering and other morphological characterization methods can be used to narrow the field further [58].

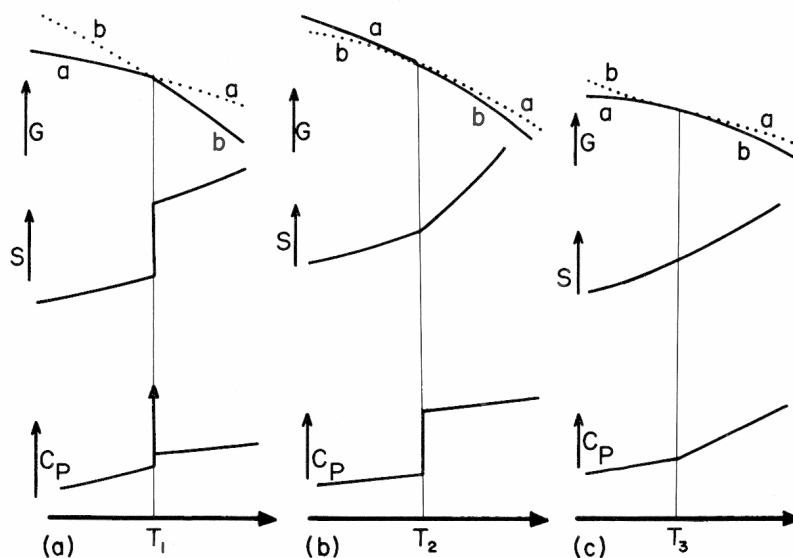


Figure 9: Ideal Thermodynamic Transitions; First order (a), Second order (b), Third order (c). [54]

Table 7: Avrami exponent summary [59]

Growth Habit	← Homogenous Nucleation →				Linear Growth
	← Heterogeneous Nucleation →				
	Linear Growth		Diffusion Controlled Growth		
	Steady State	t = 0*	Steady State	t = 0*	
Sheaf-like	6	5	3.5	2.5	5 ≤ n ≤ 6
Three-dimensional	4	3	2.5	1.5	3 ≤ n ≤ 4
Two-dimensional	3	2	2	1	2 ≤ n ≤ 3
One-dimensional	2	1	1.5	0.5	1 ≤ n ≤ 2

*All nuclei are activated at t = 0

$$\frac{X_{c,t}}{X_{c,t=\infty}} = 1 - \exp(-kt^n) \quad [58]$$

Equation 5

In polymers, crystallization kinetics favour the formation of relatively small metastable crystals rather than the large crystals favoured by equilibrium [60]. The ideal equilibrium crystal must have the lowest free energy possible. This is obtained by creating a crystal with the largest volume to surface area ratio. Relatively slow growth along the chain direction, compared perpendicular to it results in polymer crystals that are plate-like regardless of their size [61]. Due to this constraint the ideal equilibrium crystal is one in which all polymer chains are extended linearly, maximizing thickness. The maximum crystal thickness obtainable is therefore dependent on molecular weight [62]. Such a crystal can only form at the equilibrium melting temperature, as the kinetic factor mentioned above favours the growth of thinner crystal lamella in which the chain snakes back and forth. This growth pattern maximizes growth perpendicular to the chain axis and minimizes it along the axis. The lamella thickness therefore decreases with crystallization temperature, a fact that has been experimentally verified [63].

Similar to crystallization, the melting temperature is influenced by molecular weight and crystallite thickness. For polymers, such as PBT, following the “most probable” molecular weight distribution, the dependence of the melting temperature of an extended chain crystal, T_m^* , on molecular weight is provided by Equation 6. In this case T_m° represents the equilibrium melting temperature of an infinite molecular weight extended chain crystal, ΔH_u is the latent heat of fusion of a single chain repeat unit, R is the ideal gas constant, and \bar{x}_n is the number-average degree of polymerization [64]. The effect of lamella thickness, L, on apparent melting temperature is described by Equation 7. T_m° is now the melting temperature of an

equilibrium extended chain crystal of finite molecular weight [56] similar to T_m^* above. As at useful values for polymers the effect of molecular weight is small [44], this second definition is what is typically quoted in the literature as the equilibrium melting temperature [45,46]. ΔH_f is the latent heat of fusion of the bulk polymer and v_e is the interfacial energy for the lamella ends [56].

$$\frac{1}{T_m^*} - \frac{1}{T_m^0} = \frac{R}{\Delta H_u} \frac{2}{\bar{x}_n} \quad [64] \quad \text{Equation 6}$$

$$T_m = T_m^0 \left(1 - \frac{2v_e}{\Delta H_f L} \right) \quad [56] \quad \text{Equation 7}$$

As PC and PBT can react to form block and random co-polymers, the melting and crystallization of co-polymers is relevant to this blend. Equation 8, provides the dependence of melting temperature on, p , the “probability that a crystallisable unit in the co-polymer is succeeded by another such unit”. T_m^0 is again the melting temperature of an equilibrium extended chain crystal of finite molecular weight. The other terms in the equation are similar to those in Equations 6 and 7 above. For an A-B type block co-polymer p approaches unity, and very little decrease in melting temperature is expected. As the block length decreases p also decreases to the limiting case of a random co-polymer, for which p is equal to the mol fraction of crystallisable units [65]. In the case of a PC / PBT blend this will be equal to the mol fraction PBT units remaining, which due to the new linkages formed by reaction will be less than the mol fraction PBT originally present in the blend.

$$\frac{1}{T_m^*} - \frac{1}{T_m^0} = \frac{R}{\Delta H_u} \ln p \quad [65] \quad \text{Equation 8}$$

The above discussion is based on comparison to equilibrium and so is most accurate in the regions around the equilibrium melting temperature T_m^0 [62,63,66]. The rates of crystal nucleation and growth are both dependent on the degree of under cooling below T_m^0 and three crystallization regimes have been identified based on the balance between these forces. Type I crystallization occurs at temperatures just below T_m^0 . In this regime nucleation is slow and each successive layer of a crystal finishes its growth prior to the nucleation of the next layer. Crystals from this regime are expected to be the largest and contain the least imperfections. Type II crystallization occurs at greater undercoolings where nucleation is comparable to

growth. In this regime several nucleation events will occur on each layer of the crystal, increasing the rate of crystallization but introducing defects. As the temperature is lowered further the crystallization rate decreases as the rate of nucleation exceeds that of growth. This condition is entitled regime III. Nuclei have almost no room to grow and crystals are very small, consisting of little more than stable nuclei. The transitions between these regimes are generally diffuse. It is a matter of some debate if hard boundaries can be assigned or if the regimes merely summarize the extremes of a continuum. Theory does predict that if a hard boundary between regimes II and III does exist it will fall near the temperature of maximum crystallization rate; which for many polymers is given by Equation 9. T_{\max} and T_m° are both in °C. [67]

$$T_{\max} = (0.82 \pm 0.005)T_m^\circ \quad [67] \qquad \text{Equation 9}$$

1.4.3 Glass Transition Theory

The exact nature of the glass transition is not entirely understood. It is often defined as the point where “the characteristic time of molecular motions...becomes longer than the timescale of the experiment.”[68] Due to this dependence on experimental time scale, the exact temperature of transition measured will be lower at slower cooling and heating rates. However, the dependence is small and therefore the experimental conditions are often not specified [69]. Phenomena associated with glass transition include: lowered molecular mobility, a step in the heat capacity curve, and a large increase in rigidity [70]. The existence of a heat capacity change suggests that a second order thermodynamic transition may be taking place, Figure 9b, but a large kinetic component prevents equilibrium from being reached as would be the case for an ideal thermodynamic transition [71]. Similar to ΔH_f during melting, the height of the heat capacity change, ΔC_p , can be related to the amount of material undergoing a transition [72].

As molecular motions are influenced by molecular weight, molecular structure and molecular environment, it is not surprising that all three have an impact on the glass transition [73]. Though it was originally derived semi-empirically, both the free volume theory and the Gibbs-DiMarzio thermodynamic theory predict glass transition molecular weight dependence to follow the form of the Flory-Fox equation, Equation 10. Similar to other molecular weight dependences, a maximum value for the glass transition temperature, $T_g(\infty)$, is approached as the molecular weight approaches infinity. Under the free volume theory this can be interpreted

as a decreasing effect of the more mobile chain ends as chain length increases [74]. Other aspects of molecular structure, such as main chain rigidity also have a pronounced effect on the glass transition temperature. For this reason, PBT with its four carbon aliphatic sections has a much lower glass transition than PC. The impact of molecular environment can be seen in the increase of PBT glass transition temperature observed in semi-crystalline PBT as opposed to wholly amorphous PBT. Rigid constraint is imposed on the amorphous phase by the hard crystalline phase reducing its mobility and therefore increasing its glass transition temperature [73].

$$T_g(M) = T_g(\infty) - \frac{K}{M} \quad [74] \quad \text{Equation 10}$$

The effects of molecular environment are particularly important when discussing polymer blends and co-polymers. If phase size is of less than 2 to 15 nm diameter, or co-polymer sequence length is smaller than this value, a single glass transition between those of the parent polymers will be observed. This result is typically taken as proof of miscibility, but according to Utracki, this is not precisely the case in thermodynamic terms. Solvent cast blends of immiscible polymers have been produced which exhibit a single glass transition initially but after annealing exhibit two distinct transition temperatures, demonstrating the effect of phase size [75]. The Fox equation, Equation 11, is often used to provide an estimate of the glass transition temperature of the mixture based on the weight fractions, w_i , and glass transition temperatures $T_{g,i}$ of its components. Utracki recommends Equation 12 for fully miscible blends and Equation 13 if blends are partially miscible. The parameter k is empirically determined and accounts for the entropy of mixing, which is usually assumed to be negligible but may not be in partly miscible blends [76].

$$\sum_i \left[w_i \left(1 - \frac{T_g}{T_{g,i}} \right) \right] = 0 \quad [76] \quad \text{Equation 11}$$

$$\frac{\ln T_g}{T_g} = \sum_i \frac{w_i \ln T_{g,i}}{T_{g,i}} \quad [76] \quad \text{Equation 12}$$

$$w_1 \ln \left(\frac{T_g}{T_{g,1}} \right) + k \cdot w_2 \ln \left(\frac{T_g}{T_{g,2}} \right) = 0 \quad [76] \quad \text{Equation 13}$$

1.5 Phase Morphology

1.5.1 Equilibrium Phase Diagrams for Polymers

Polymers approach equilibrium slowly due to their low rate of self diffusion [77,78]. In the melt, equilibrium may be easily reached. However, as a polymer is cooled, slow diffusion may allow non-equilibrium structures to persist until they are locked in by the glass transition. Even so, equilibrium phase diagrams are important as over their life time polymer parts will tend towards equilibrium with accompanied improvement or deterioration of properties [78]. Figure 10 provides a schematic phase diagram and its relation to the free energy of mixing, ΔG_m . A detailed description of the thermodynamics of phase separation is given by Utracki [79], along with a comprehensive summary of many of the theories that attempt to describe phase separation for polymers [78]. The key to understanding morphology in PC/PBT blends is the existence of two mechanisms for phase separation. The binodal line represents the point at which a two phase region becomes thermodynamically favoured. Separation occurs by the mechanism of nucleation and growth. An induction time is required for nucleation, preventing instantaneous separation. Under the spinodal line, the driving force for phase separation is great enough that any compositional difference closer than the average to the two equilibrium phases is favoured. No nucleation is required and phases start as ripples of concentration that maintain a continuous composition gradient between extremes. As shown schematically in Figure 10, during spinodal decomposition the ripples present at time, t_1 , expand until by time,

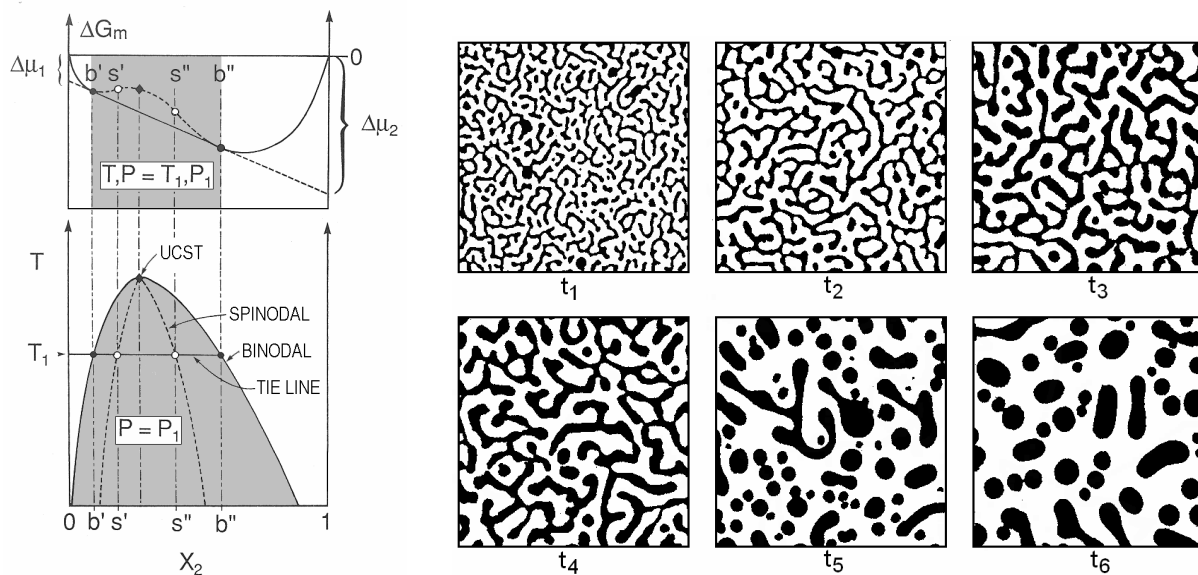


Figure 10: Spinodal Decomposition: Phase Diagram and Schematic Morphology [79]

t_6 , surface tension breaks them into individual globules [79].

Polymers often have phase diagrams where maximum miscibility is obtained at an intermediate temperature, Figure 11a. The long chains reduce the significance of the entropy of mixing when compared to low molecular weight compounds. This increases the relative importance of chemical attractions and repulsions. These are measured by the binary interaction parameter, χ_{12} [78]. A negative interaction parameter is required for miscibility [77]. The maximum in miscibility has been explained by the effects on χ_{12} of free volume and dispersion forces, Figure 11b. The upper critical solution temperature, UCST, and lower critical solution temperature, LCST, define the extremes of miscibility [77]. Multiple critical temperatures have been measured in some blends, suggesting that the relationship between χ_{12} and composition is at least second order. Molecular weight has been shown to have a large effect on miscibility. Phase diagrams between the extremes of Figure 11a and c can be generated for a given polymer pair by varying molecular weight. Pressure is also important, though less studied. The effect of pressure on LCST has been found to be ten times greater than the effect on UCST. For polymers that have been studied, pressure effects on critical temperatures are on the order of 10°C/MPa. [78]

1.5.2 Characterization Techniques

Utracki provides a summary of techniques that can be used for morphological characterization along with discussion of their advantages and disadvantages [80]. Discussion here will be limited to the techniques commonly used for PC/PBT blends. For direct

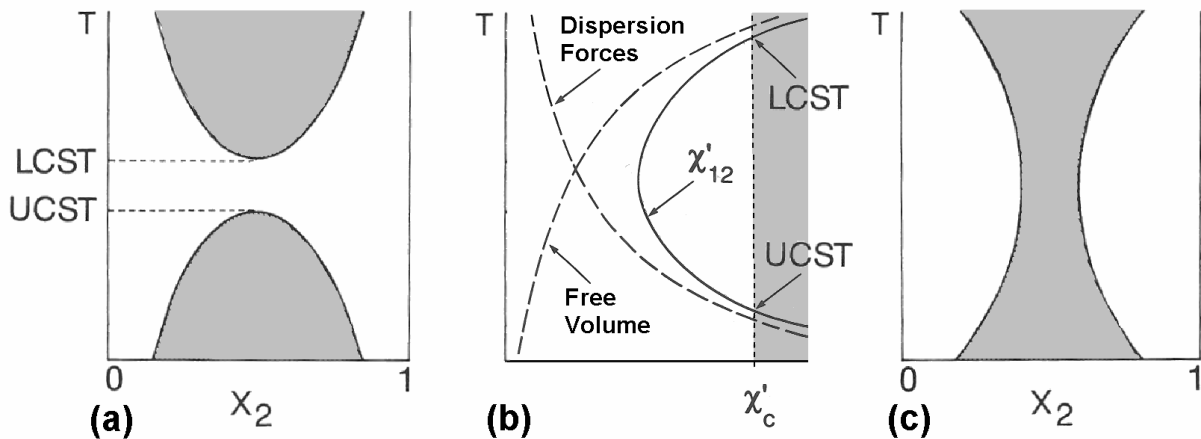


Figure 11: Typical Polymer Phase Diagrams. Shaded regions are two phase. [78,77]

observation of morphology electron microscopy techniques are best. The microscopic methods used in this work will be described in Chapter 3. Other techniques that have been used in the literature include light scattering, FTIR microscopy, DSC and inverse gas chromatography.

Light scattering has been used to characterize both phase separation in PC/PBT blends [81], while an attempt at measuring phase composition was made by FTIR-Microscopy [7]. For a successful measurement in a PC/PBT blend the phase size must be greater than approximately 12 μm , (See Appendix A), which is larger than what was reported by Tatum, Cole and Wilkinson [38]. Typically estimates of phase composition are made from changes in glass transition temperature by DSC [75,82]. (See sections 1.4.3 and 3.3.2) Inverse Gas Chromatography has been used to investigate phase interactions, and can be used to calculate the binary interaction parameter [83]. Even with this information the complexity of PC/PBT phase behaviour has prevented the use of thermodynamic theory to generate a phase diagram [3].

1.6 Rheology

1.6.1 Introduction

Rheology is often defined as the study of fluid flow. The viscosity (η) of non-Newtonian fluids, such as many molten polymers, is dependent on strain rate ($\dot{\gamma}$) resulting in a more complex relationship between strain rate and shear stress (σ) than that described by Newton's equation, (Equation 14). The increased complexity results from visco-elastic behaviour, that is, behaviour somewhere between the viscous response of a liquid, and the elastic response of a solid. Rheological characterization techniques attempt to determine the dependence of flow on the applied loads [84], often though the dependence of viscosity on strain rate. Theoretical treatment of polymer rheology attempts to describe this dependence, and also the known dependences of viscosity on temperature and molecular weight [85]. The rheology of polymer blends is further complicated by the presence of multiple phases. The effect of phase structure on flow behaviour is important and must be understood before useful measurements and predictions can be made [86]. With this background, the flow characteristics of PC, PBT and their blends presented at the end of this section can be understood in the proper context.

$$\sigma = \eta\dot{\gamma}$$

Equation 14

1.6.2 Property Measurement

Rheological characterization techniques can be classified as dynamic or steady state. Large strains are induced in steady state tests elongating and orienting droplets. The resultant data therefore is on the oriented material rather than the original [87]. This can reduce reproducibility and the generality of results because the exact geometry of the test equipment may have a large influence on the resultant morphology. Dynamic testing of blends provides excellent reproducibility [88]. Only small deformations are used for dynamic tests, allowing the information gathered to be specific to the original material [87]. Small deformations are necessary to maintain measurements in the linear visco-elastic region, where stress is proportional to strain. This necessity, though good for direct property determination limits the use of dynamic tests as process models. Processing strain rates and deformations are more similar to those of steady state tests making the results directly applicable to design problems provided proper attention is given to matching flow geometries [88]. The empirical Cox-Merz rule, Equation 15, often used to relate steady state and dynamic results in homopolymers

should only be used with extreme caution in blends due to the morphological differences induced by different test techniques [87].

$$\eta(\dot{\gamma}) = [\eta^*(\omega)]_{\omega=\dot{\gamma}} \quad \text{[89]} \quad \text{Equation 15}$$

Both drag flow and pressure drop can be used to induce shear stresses on polymers. Pressure drop instruments are limited to determining steady shear viscosity, $\eta(\dot{\gamma})$, [90] however they have the advantage simple construction and a wide range of shear rates, (5 to 1000s⁻¹). At their simplest, pressure drop instruments consist of a piston that applies a known pressure, forcing molten polymer through a channel or capillary of known dimensions. In such an instrument the viscosity of the polymer at the applied shear rate can be calculated from the measured pressure drop and flow rate provided the correction factors for entrance pressure drop and wall shear rate are known. In non-Newtonian fluids such as polymers the correction factors must be determined experimentally, requiring that many tests be conducted with varying pressure drops and channel dimensions. This is not a great hardship if the full viscosity curve is to be determined; however it does prevent the melt flow or melt volume indices, (MI, MVR respectively) from being directly relatable to viscosity. Both MI and MVR are used in industry as classifications for polymer melts. The MI is equal to the mass of polymer which flows through a standard capillary under a standard pressure in a given time. It is often quoted in units of g/10min. The MVR is simply the MI adjusted for density and therefore is quoted in units of cm³/10min. Both are typically determined under a single set of conditions preventing correction. As the standard capillaries are short, a significant portion of the pressure drop is due to entrance effects reducing the dependence on viscosity. Despite these limitations, melt indices are significant due to their role as the sole rheological classification parameter quoted for commercial polymers [91]. The use of melt indices in polymer blends is even more questionable than in homo-polymers due to morphological changes induced by the flow. In the worst case the low viscosity phase will concentrate at the capillary walls lubricating the flow and obscuring the condition of the other constituent [92]. More information on capillary rheometers can be found in [91].

Drag flow rheometers produce more uniform shear rates than pressure flow and also are more flexible, usable for both steady and dynamic shear studies [90]. Parallel plate, concentric cylinder and plate and cone geometries are all used. Though concentric cylinders have certain theoretical advantages [93], they have practical limitations regarding sample loading and

therefore are not often used. Most common is the cone and plate geometry pictured in Figure 12. Given several simplifying assumptions this geometry provides uniform shear stress, and allows shear rate, shear stress, and first normal stress difference (N_1 , another rheological important parameter) to be calculated using Equations 16 through 18. In these equations F represents the normal force separating the plates, M is the torque transmitted by the polymer, R is the fixture radius, Θ is the cone angle and Ω is the rotational speed in radians per second [94]. In dynamic mode an oscillatory shear of the form given in Equation 19 is applied where γ_o is the magnitude and ω is the oscillation frequency. The output, Equation 20, provides the definition for the dynamic storage, G' , and loss, G'' , moduli, where G' describes the elastic or solid like response of the polymer melt and G'' describes the viscous or liquid like behaviour [95]. The vector sum of these is the complex viscosity given by Equation 21 [89].

$$\dot{\gamma} = \frac{\Omega}{\Theta} \quad [94] \quad \text{Equation 16}$$

$$\sigma = \frac{3M}{2\pi R^3} \quad [94] \quad \text{Equation 17}$$

$$N_1 = \frac{2F}{\pi R^2} \quad [94] \quad \text{Equation 18}$$

$$\gamma(t) = \gamma_o \sin(\omega t) \quad [95] \quad \text{Equation 19}$$

$$\frac{\sigma(t)}{\gamma_o} = G'(\omega) \sin(\omega t) + G''(\omega) \cos(\omega t) \quad [95] \quad \text{Equation 20}$$

$$\eta^*(\omega) = \frac{1}{\omega} \sqrt{G'(\omega) + G''(\omega)} \quad [89] \quad \text{Equation 21}$$

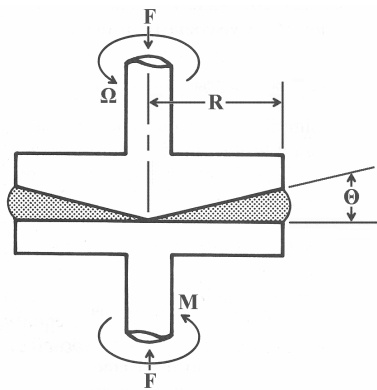


Figure 12: Rheometer Geometry [94]

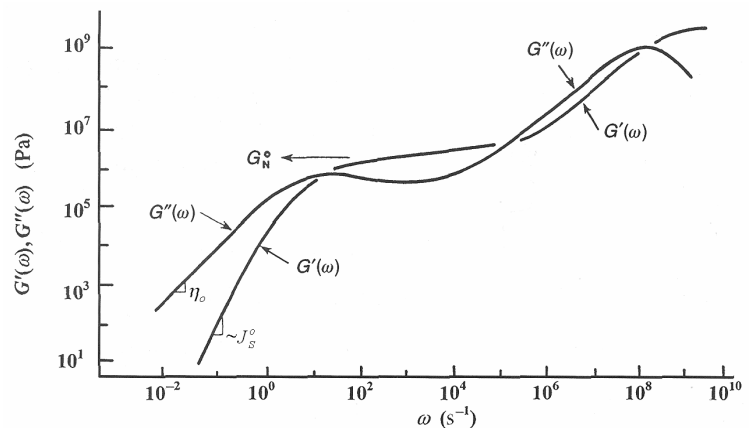


Figure 13: G' and G'' master curves for a typical polymer melt [95]

To determine the viscosity vs. frequency/shear rate dependence a wide range of test frequencies are required, however even the best test equipment is limited to five orders of magnitude. To produce master curves for homo-polymers, such as the one seen in Figure 13, time-temperature-superposition is used [95]. This is based on the assumption of thermo-rheological-simplicity that states decreasing temperature or increasing time have the same effect on polymer flow behaviour. This requires that major changes in material viscosity are linear functions of temperature meaning that no transition temperatures are crossed while shifting data [96]. In homo-polymers, above the glass transition temperature, the Williams, Landel, Ferry equation (WLF), provides a good fit for shift factors, allowing the shear rate dependence of a material to be extrapolated to many temperatures [95]. In polymer blends the situation is more complicated. Temperature induced changes may result in many transitions in blend morphology making regions of consistency too narrow to justify time-temperature superposition, and requiring that experiments be conducted at each temperature to determine the precise material behaviour [96]. If a master curve can be produced, linear-visco-elastic properties such as the zero shear viscosity (η_o), recoverable compliance (J_s^o), and plateau modulus (G_N^o), can be determined (Figure 13, Equations 22 and 23). These are important in modeling polymer rheology. In particular η_o and J_s^o , allow calculation of the characteristic relaxation time, τ_o (Equation 24), which among other things, defines the onset of non-linear visco-elastic behaviour in steady shear flows [95].

$$\eta_o = \lim_{\omega \rightarrow 0} \frac{G''(\omega)}{\omega} \quad [95] \quad \text{Equation 22}$$

$$J_s^o = \frac{1}{\eta_o^2} \lim_{\omega \rightarrow 0} \frac{G'(\omega)}{\omega^2} \quad [95] \quad \text{Equation 23}$$

$$\tau_o = \eta_o J_s^o \quad [95] \quad \text{Equation 24}$$

1.6.3 Homo-polymer Rheology and Theory

Homo-polymers are typically pseudoplastic, meaning that their viscosity decreases with increasing strain rate, (See Figure 14). Though often used due to their simplicity, power law equations relating viscosity to shear rate, (see Equation 25), are purely empirical and typically only provide a good fit over a few orders of magnitude [97]. A much better fit is obtained using the Eyring equation particularly when a relaxation spectrum rather than a single

relaxation time is used, (Equation 26). In its derivation all terms have physical significance, however due to its many parameters care must be taken during the fitting procedure to ensure that the result maintains the original meaning of the terms rather than just a good empirical fit. The rational behind the Eyring equation is that visco-elasticity originates from chain segments being deformed faster than they can relax into their equilibrium configuration. For n equals 1 it is assumed that only one characteristic relaxation time τ is necessary. Greater values of n indicate a spectrum of times. Existence of a spectrum of times is theoretically justified by noting that chain segments will be under a varying amount of constraint. The proportion of segments having a given relaxation time is given by f_i . Free volume influences on where segments can move to are accounted for in the ratio V_s/V_h which represents the ratio of filled volume over empty volume [98]. Empty volume increases with temperature through thermal expansion, preventing the apparent increase in viscosity with temperature that might otherwise be inferred from Equation 26.

$$\eta = \eta_r \left(\frac{\dot{\gamma}}{\dot{\gamma}_r} \right)^{m-1} \quad [97] \quad \text{Equation 25}$$

$$\eta = \frac{2RT}{V_h} \sum_{i=1}^n \left[f_i \beta_i \frac{\sinh^{-1}(\beta_i \dot{\gamma})}{\beta_i \dot{\gamma}} \right], \quad \beta_i = \frac{1}{2} \frac{V_s}{V_h} \tau_i \quad [98] \quad \text{Equation 26}$$

The effect of molecular weight on viscosity is seen in Figure 15. Equation 27 accurately describes this behaviour, where M_c is the critical molecular weight before entanglement. M_c is not temperature dependent indicating that its effects are wholly due to chain geometry [99]. As

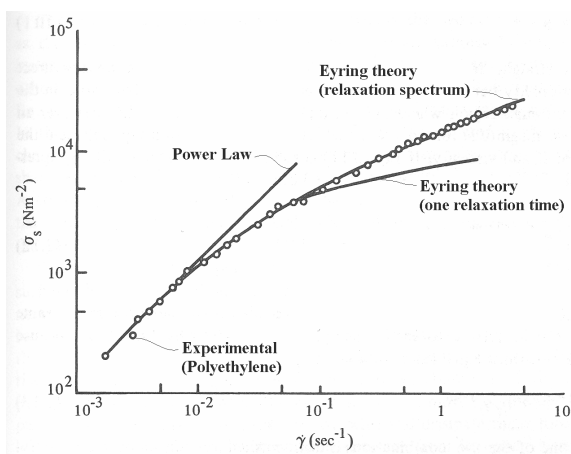


Figure 14: Stress vs. Shear Rate for Pseudoplastic Materials [97]

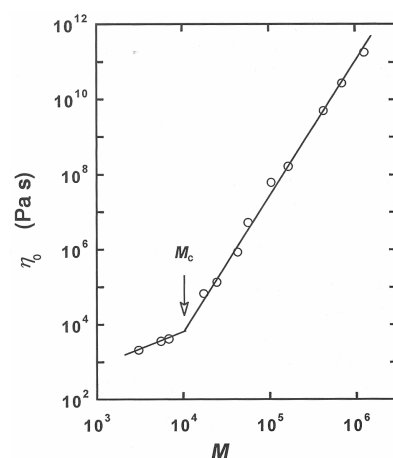


Figure 15: Polymer Viscosity vs. Molecular Weight [99]

the plateau in the dynamic storage modulus curve also appears at M_c it is also attributed to entanglements [100]. Theories attempting to explain the molecular weight dependence of viscosity are divided in applicability between those that work well below M_c and those that work above it. Below M_c the Debye viscosity equation [101], and the Rouse model are used. The Rouse model deals with polydispersity and gives predictions for τ_o and J_s^o in addition to viscosity. The prediction for J_s^o in particular provides a good fit to experiment with no flexible parameters [85]. Above M_c , Bueche Theory [102] and the Reptation model of Gennes, Doi, and Edwards are options [103]. Though Bueche predicts a similar relationship to Equation 25, the model does not do as well at predicting other aspects of polymer rheology [102]. The Reptation model builds on Rouse, assuming rouse like molecules trapped in tubes defined by entangling chains. It has been extended to polydisperse liquids through double reptation and though it does not deal well with long chain branching it is otherwise very good [104]. More information about the models can be found in their respective references.

$$\begin{aligned}
 M < M_c, \quad \eta \propto M \\
 M > M_c, \quad \eta \propto M^{3.4}
 \end{aligned}
 \quad [105,106]
 \qquad \text{Equation 27}$$

1.6.4 Blend Rheology

Utracki provides a good review of blend rheology [107]. As it is long and involved the main points for PC/PBT blends are summarized here. Miscible blends are modeled using solutions and homologous blends, (blends of one polymer with itself). Immiscible blends are modeled using suspensions, emulsions or block co-polymers. Partially miscible blends processed near their spinodal temperature are modeled as mixtures of two liquids near their critical solution temperature [86]. The viscosity of polymer blends with respect to composition is often modeled using the “log-additively rule”, Equation 28, where η_o is the viscosity of the blend, x_i can be mole fraction, volume fraction or weight fraction, and $\eta_{o,i}$ are the viscosities of blend components. The effects of blend structure on blend viscosity are often discussed in terms of negative or positive deviations to this rule. For thermodynamic miscibility a small positive deviation will exist [108].

$$\log \eta_o = \sum_i (x_i \log \eta_{o,i}) \quad [108]
 \qquad \text{Equation 28}$$

Block-Co-polymers model highly mixed blends and compatibilized blends. In these blends immiscible polymers form sub micron scale ordered structures. Viscosity is highly dependent on structure and is typically higher than what would be expected based on composition due to the necessity of disrupting the structure to induce flow. Coarser blends are modeled on emulsions or suspensions depending on the viscosity ratio, Equation 29. The viscosity ratio governs the deformation behavior of dispersed droplets in a liquid matrix. Unless it is much greater than 1, blends are best modeled as emulsions [109]. Emulsions have been found to be nearly Newtonian provided that the volume fraction dispersed phase is less than 0.3. Between this and some critical value emulsions are pseudoplastic, while above the critical value solid like properties are exhibited [95]. Carefully constructed commercial emulsions can have as much as 90% dispersed phase. Polymer blends typically undergo a phase inversion long before this occurs. Phase inversion occurs at lower volume fraction when the dispersed phase has the lower viscosity [110]. Emulsion viscosity is increased slowly by volume fraction below values of 0.3 and much more rapidly above this. A maximum is expected at phase inversion where the volume fraction dispersed phase is at a maximum [109].

$$\lambda = \frac{\eta_{dispersed}}{\eta_{continuous}} \quad [111]$$

Equation 29

In concentrated emulsions two types of morphology exist, those that are formed by a shear field, and those that are formed by liquid / liquid interactions. At equilibrium the later case dominates and the interface area is equal to that that can be protected by a surfactant. In most emulsions, many droplet sizes are present and droplets form strings or clusters [112]. At moderate shear rates droplets are expected to stratify into layers with decreasing droplet size and layer spacing with increasing shear rate. Coagulation of droplets is expected to become more difficult between layers as shear rate increases; however within a given layer at high shear rates coagulation may destroy the emulsion producing a layered liquid morphology. In this morphology the low viscosity component is expected to lubricate the flow of the higher viscosity component. The emulsion may re-form upon return to a lower shear rate [95].

In partially miscible blends small positive deviations to log additivity are observed in regions outside of the binodal. (See Figure 25 for reference phase diagram) Viscosity drops sharply upon entering the two phase region resulting in negative deviations. A local maximum within this region is observed, possibly representing the point of phase inversion. In blends

where shear induces crystallization, deformation tends to reduce miscibility. In other blends an increase in miscibility with increasing shear rate is observed [113].

1.7 Mechanical Properties

1.7.1 Effect of Co-Polymer

The effect of co-polymer content on PC/PBT blend properties is seen in Figures 16-18. The blend composition of 60/40wt% PC/PBT is similar to that of commercial blends. All properties besides impact resistance initially increase. As the blends were produced by blending highly reacted PC/PBT with virgin polymer, the exact co-polymer content is unknown, however it is reasonable to assume the co-polymer content is similar to the proportion of reacted blend. (Reacted blend is assumed to be 100% co-polymer, additional co-polymer production during blending assumed to be negligible.) This places the maximum for mechanical properties at or below 2wt% co-polymer [39].

1.7.2 Tensile Strength, Elastic Modulus, and Elongation

In Figures 19-21 the effect of blend composition on mechanical properties is observed. Improvements in yield strength over rule-of-mixtures behaviour were attributed to crack bridging and massive plastic deformation of the PC phase made possible by cavitation at the PC/PBT interface. Blends with 20 to 50% PBT had a strong interface, attributed to *in-situ*-formed co-polymer [33]. Similar synergistic behaviour but at a lesser degree was observed by Sanchez et al. for yield strength [27]. Unlike Wu and co-workers [33], a significant deviation was observed for modulus following the same trend as yield strength. This was attributed to free volume effects. The opposing trends for strength and elongation are viewed as typical of most materials [27]. Lower values for elongation were observed by other authors in the 50/50wt% range [1,22]. Blend processing and structure may be responsible.

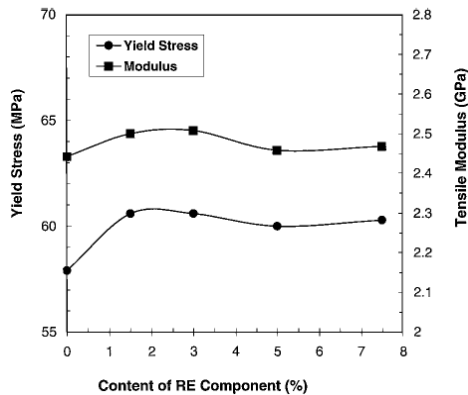


Figure 16: Yield Stress and Elastic Modulus vs. Co-Polymer content [39]

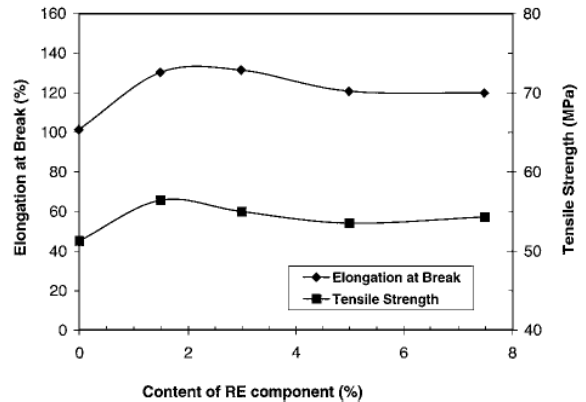


Figure 17: Percent Elongation and Tensile Strength vs. Co-Polymer content [39]

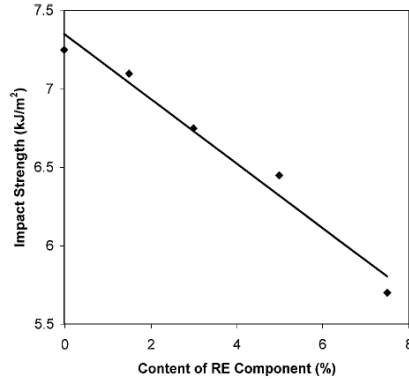


Figure 18: Impact Strength vs. Co-Polymer [39]

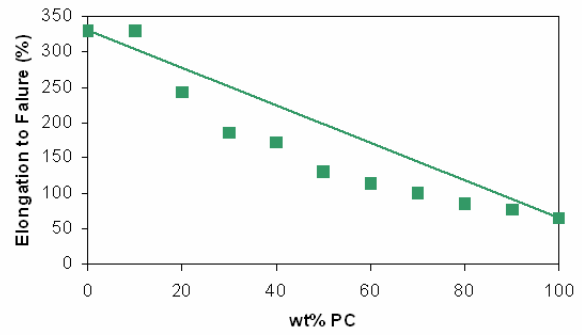


Figure 19: Percent Elongation vs. wt% PC [27]

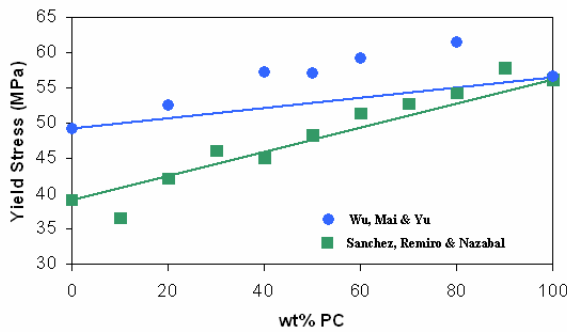


Figure 20: Yield Stress vs. wt% PC [27,33]

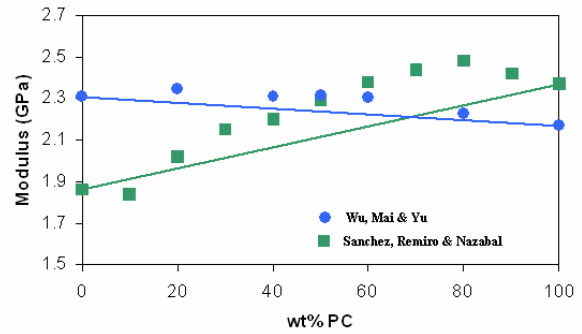


Figure 21: Elastic Modulus vs. wt% PC [27,33]

1.7.3 Critical Ligament Thickness and Impact Resistance

In addition to interfacial modifiers such as co-polymers, ligament thickness has a significant effect on blend impact strength. Impact strength is improved by adding a rubber impact modifier to the blend in the form of small particles. This rubber deforms easily even at high strain rates. Provided the polymer ligament separating rubber particles is below a critical thickness, rubber deformation reduces the constraint on the surrounding polymer allowing a shear deformation mode. This results in large plastic deformations of the ligament absorbing large amounts of energy. The critical ligament thickness is expected to depend on temperature, strain rate, and blend component elastic moduli. As it affects both elastic modulus and blend morphology, crystallinity is expected to have an effect [2,22]. In 50/50wt% PC/PBT blends, a critical ligament thickness of 0.52 μ m was achieved with the addition of at least 4.5wt% 50/50wt% blend of ethylene-butylacrylate-glycidyl methacrylate co-polymer (PTW) and ethylene-1-octylene co-polymer (POE) [22]. 5 and 7wt% of POE and PTW alone were required for 0.55 and 0.40 μ m critical ligament thicknesses respectively [2]. This compares to 20wt% methyl methacrylate-butadiene-styrene co-polymer, (MBS), required for good impact

resistance in PC/PBT blends [22]. MBS is the material used for impact modification in the Xenoy family of PC/PBT blends [1].

1.7.4 Vicat Temperature

The vicat temperature is often used as a measure of high temperature stiffness. It is measured by applying a standard load to a standard specimen and measuring the temperature at which a specific deflection is reached. ASTM 1525 covers one such set of standard conditions. Figure 22 shows the effects of molecular weight on the vicat temperature. Comparing to the polycarbonate glass transitions measured by Hamilton and Galuchi in Figure 27 it can be seen that there is a strong correlation between glass transition and vicat temperatures [9]. The low vicat-temperatures observed by other authors, [22,2], might be attributed to partial miscibility of low molecular weight polymer or transesterification due to lack of stabilization.

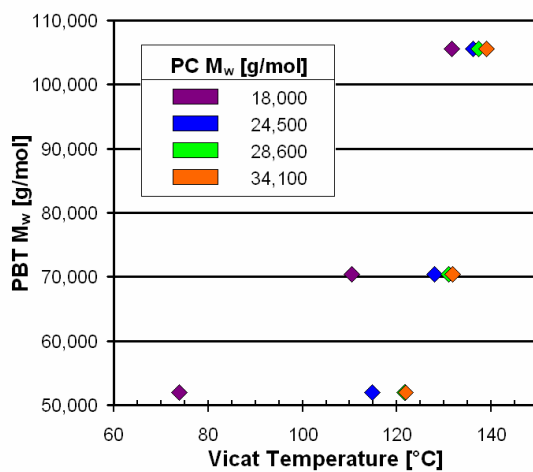


Figure 22: Vicat Temperature vs. Molecular Weight [27]

2.0 LITERATURE REVIEW ON THE INTERACTION BETWEEN PROCESSING AND PC/PBT BLEND PROPERTIES

As stated in Chapter 1, the objective of this work is to investigate the interaction between four process variables in commercial scale twin screw co-rotating extrusion and PC/PBT blend properties. The blend thermophysical properties will be characterized using Differential Scanning Calorimetry (DSC) while Scanning Electron Microscopy (SEM) will be used to study blend morphology. This chapter describes the current state of knowledge in these areas based on a comprehensive review of the open literature. Also described is the current knowledge of PC/PBT blend rheology and processing in co-rotating twin screw extruders.

2.1 Thermal Properties

2.1.1 Effects of Transesterification on Thermal Properties

In un-stabilized blends rapid transesterification is expected to produce random copolymers. Depending on the extent of the transesterification reaction a range of blend property changes will result. Changes listed in order of increasing co-polymer content are, decreased crystallinity [2,7,22], decreased PC-rich-phase glass transition temperature [1,2], or wholly amorphous polymer. In the last case a single glass transition with temperature predicted by the Fox equation, Equation 11, is expected [36]. Should any of these indications of reaction are found, it is clear that the blend stability should be verified prior to further study [9].

2.1.2 PBT Crystallization and Melting, Pure PBT and Low-Reaction Blends

For PBT, no experimentally determined maximum crystallization rate has been reported [114]. However theoretical modeling has predicted a maximum growth rate at 211°C [49]. This is in good agreement with the regime change from type II to III crystallization at 210-212°C inferred from crystal growth data by Runt and coworkers [47]. Following the general rule for polymers PBT crystallization kinetics are not highly dependent on molecular weight. Pure PBT with M_w equal to 83,000g/mol and PDI equal to 1.9 was used by Runt [47], while the theoretical work was based on polymer with M_w equal to 39,000g/mol [49]. (Calculated from $M_v = 37,800$ g/mol, $a = 0.871$ using Table 1.) Stein and Misra [50] provide further evidence of a transition with their polarized optical microscopy results. Pure PBT was used, with M_n approximately equal to 20,000g/mol and $[\eta]$ equal to 1.04 at 25°C in HFIP. Two

distinct populations of spherulites with identical crystal unit cell parameters were formed depending on the crystallization temperature. At temperatures below 200°C “unusual” two dimensional spherulites formed, while in the 200°C sample “normal” three dimensional spherulites were detected. In this case “unusual” and “normal” are the terminologies used to describe the different populations, nether being that uncommon in the polymer literature. In samples with a dynamically changing crystallization temperature a mixture of “normal” and “unusual” spherulites was obtained. [50] Figure 23 shows a plot of PBT crystallinity vs. crystallization temperature.

The most notable feature about PBT melting is that when investigated by DSC as many

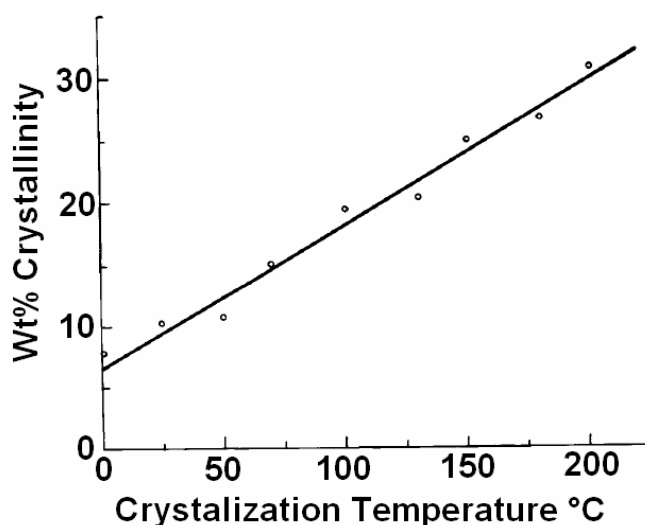


Figure 23: PBT crystallinity versus crystallization temperature [50] ($M_n \approx 20,000$, $[\eta] = 1.04$ @ 25°C in HFIP)

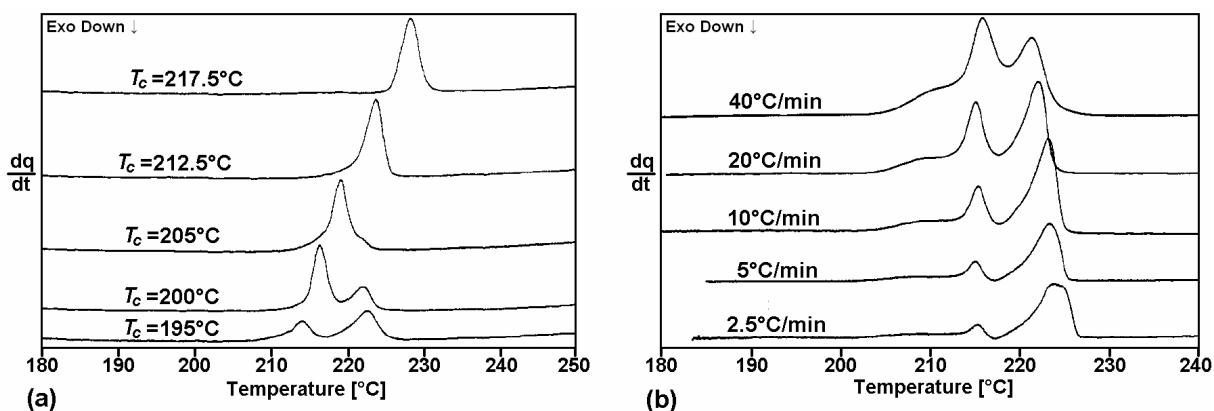


Figure 24: PBT melting behavior by DSC; versus crystallization temperature, 20°C/min heating (a), versus heating rate, $T_c = 200^\circ\text{C}$ (b) ($M_w = 83,000\text{g/mol}$, $\text{PDI} = 1.9$) [47]

as three peaks have been observed even though two are more frequent [47,49], Figure 24. Several theories have been put forward in an attempt to explain this. As the phenomena has been observed in blends with polycarbonate at least one report has attributed the second peak to polymer crystallizing from the PC rich phase [58]. This can not be the complete explanation as pure PBT also exhibits this behaviour. Multiple melting has been attributed to crossing the type II, III transition temperature while cooling [47]. It has also been attributed to the partial melting and reorganization of crystals during a DSC scan. Both events can occur simultaneously. A theoretical treatment of PBT melting by DSC predicted two peaks if a single continuous crystal size distribution was reorganized and three or more for multi-modal distributions [49]. References to “secondary infilling crystallization” [22,2] and “the melting of imperfect crystals” [1] in PC/PBT blends as explanations for double melting could support either mechanism. The existence of different melting points for distinct populations of crystals was demonstrated by Stein and Misra when they observed the complete disappearance of “unusual” spherulites at 223°C and that of “normal” spherulites at 227°C. Both populations had been formed during cooling. However if the “unusual” spherulites were melting or re-crystallizing into the “normal” type during the relatively slow optical observation heating scan was not discussed [50]. Complementary non-thermal techniques such as wide angle x-ray scattering, or FTIR should be used for PBT if the initial crystallinity of the blend is of interest. (See Appendix A)

Table 8 provides Avrami parameters for pure PBT and blends with PC as reported by Halder *et al.* [58]. The exclusion of PC from the PBT crystal structure was inferred from light scattering results. Although no mention of stabilization was made by the authors, the processing temperature was kept below 260°C and the percent crystallinity did not significantly decrease when normalized to 100% PBT [58]. Comparing this result to Hamilton and Gallucci’s “abusive DSC” procedure [9], it is very likely that the blend is largely un-

Table 8: Avrami Parameters for PBT in blends with PC at 50°C [58]

Composition PC/PBT*	$X_{c,t=\infty}$		n	K
	Blend	PBT		
50/50wt%	8.9%	17.8%	1.43	5.27×10^{-3}
30/70wt%	12.4%	17.7%	1.51	7.11×10^{-3}
10/90wt%	16.9%	18.8%	1.66	10.13×10^{-3}
0/100wt%	19.7%	19.7%	2.10	8.06×10^{-3}

* M_w PBT = 55,000g/mol, $[\eta]_{PC}$ = 0.5 DL/g

reacted. Regime III crystallization kinetics are expected, as the blends were quenched from 250°C and crystallized at 50°C. The main conclusion drawn from this data was that neither PBT crystallinity or rate of crystallization is greatly reduced when blended with PC. The initial rate increase at low PC content is what one would expect from an increase in heterogeneous nucleation due to the presence of glassy PC. When the Avrami exponent and light scattering results were compared, Halder *et al.* concluded that in the PC rich blends the crystal growth pattern was two dimensional [58]. This is similar to Stein and Misra's results for regime III crystallized pure PBT [50].

The effect of molecular weight on PBT crystallization in well stabilized PC/PBT blends was studied by Cheng and coworkers [82]. Similar to Halder *et al.* [58], PBT crystallinity in blends with PC was found to be independent of PBT content and in the range of 33-37% total PBT. As Cheng and coworkers crystallized their blends at 200-205°C, near the type II/III transition and above the PC T_g , their higher total crystallinity figures are not surprising. One important observation was that PBT crystallinity was greater in low molecular weight blends, with lower PBT molecular weight having the greatest effect. The study covered all four permutations possible when one PC with M_w of either 36,500 or 19,100g/mol is blended with one PBT of either 108,00 or 65,000g/mol [82].

2.1.3 Glass Transitions in PC, PBT and blends

The Fox-Flory constants for PC are given in Equation 30. No similar relationship was found in the literature for PBT. This is likely due to the difficulty obtaining wholly amorphous polymer because of the fast crystallization kinetics of PBT [48]. In a single sample, the effect of crystallization is greater than that of molecular weight, with glass transition temperatures between 22 and 80°C reported for the rigid amorphous fraction of semi-crystalline PBT, while a glass transition temperature of -25°C reported for wholly amorphous polymer. A study investigating the change in PBT glass transition with molecular weight would therefore not be particularly useful if it pertained to only amorphous polymer. It would also be difficult to define precisely what was studied if a semi-crystalline polymer was studied. A large difference in heat capacity change at glass transition, ΔC_p , was also reported for semi-crystalline vs. wholly amorphous PBT [48], see Table 6. In a 50/50wt% blend with PC, Birley and Chen detected two glass transitions that might be attributable to PBT, one at -80°C and one at 55°C. The presence of an ABS rubber with T_g at -45°C complicates interpretation [1]. However this

evidence combined with the crystallization data in Figure 23 showing that PBT crystallizes at 0°C [50] indicates that even in semi-crystalline PBT a mobile amorphous phase exists well below room temperature.

$$T_{g,PC} = 155 [^{\circ}C] - \frac{2.1 \times 10^5 [g^{\circ}C/mol]}{M_w} \quad [52] \quad \text{Equation 30}$$

Both Cheng and coworkers [82] and Hamilton and Gallucci [9], investigated the interaction between molecular weight and blend miscibility on the PC rich phase T_g in stabilized PC/PBT blends. Both concluded that miscibility increased with decreasing molecular weight [9,82], see Equation 11. Despite concerns about possible transesterification Hamilton and Gallucci's more extensive results are summarized in Table 9 [9]. Although they were well aware of the potential adverse effects of transesterification due to residual catalyst, they did not appear to be aware of the end group reaction mechanism. The use aqueous phosphorus acid solution as a stabilizer will have resulted in some hydrolysis, providing the PBT end groups necessary for co-polymer production by end-group attack. "Abusive DSC" results only verified that no random co-polymer was produced. However, considering that only 0.1 phr of highly concentrated solution was added and that during blending no bubbling or other signs of reaction were observed, the co-polymer content in their stabilized blends is expected to be low. [9]

Table 9: T_g by DMA, 50/50vol% PC/PBT Blends [9]

		PBT			100% PC*	
M _n		25,000	30,600	45,900		
PDI		2.08	2.30	2.30		
PC	8,000	2.25	90.6°C	116.3°C	127.1°C	143.3°C
	10,500	2.33	122.7°C	127.8°C	136.0°C	146.4°C
	12,000	2.38	124.3°C	129.1°C	134.3°C	147.6°C
	13,000	2.62	127.1°C	132.0°C	138.6°C	148.8°C

*Calculated Using Equation 30

2.2 Blend Morphology

2.2.1 Low-Reaction Blend

Delimoy *et al.* [26] investigated the phase preferences in a relatively high molecular weight PC/PBT blend and constructed the phase diagram shown in Figure 25. The blend was well stabilized and FTIR/NMR results confirmed that less than 10^{-3} mol% co-polymer was present. Their predictions were verified by TEM studies of blends corresponding to points D and G [26]. Figure 26 provides a TEM image of a multi phase PC/PBT blend [38]. Though this phase diagram appears to be of the UCST form, Delimoy *et al.* cautioned against any conclusions regarding its form above 260°C emphasizing that the forms of Figure 11a and c are both possible [26]. Santos and Guthrie neither expressed the same concern, nor attempted to explain the different shapes reported for phase diagrams in the literature [3]. The LCST type spinodal of 198°C reported by Okamoto and Inoue [81], is presented in contrast with Delimoy *et al.*'s result by Santos and Guthrie [3], disregarding the fact that Okamoto and Inoue used much lower molecular weight polymers, (PC $M_n = 24,000\text{g/mol}$, PBT $M_n = 27,000\text{g/mol}$), in a 50/50wt% un-stabilized blend [81]. This is in spite of the fact that Delimoy *et al.* highlighted the effects of molecular weight as a major question that needs to be addressed [26].

As previously mentioned, both Cheng and coworkers [82] and Hamilton and Gallucci [9] investigated the effects of molecular weight on PC/PBT blends. Clear trends of increasing miscibility with decreasing molecular weight are visible in Figure 27. Both observed that PBT

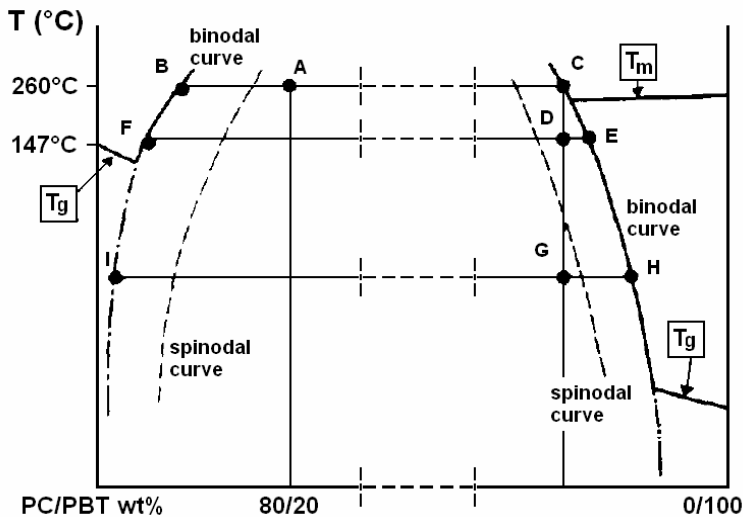


Figure 25: PC/PBT Phase Diagram, PBT $M_w = 110,000\text{g/mol}$, PC $M_w = 35,000\text{ g/mol}$, co-polymer content less than 10^{-3} mol% [26]

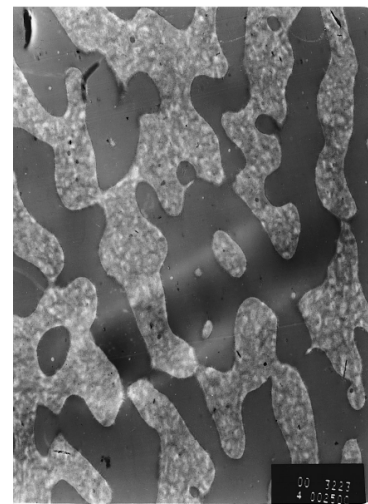


Figure 26: Low Reaction Blend by TEM, 50/50wt%, PC $M_w \approx 19,000\text{g/mol}$ by Equation 30 [38]

molecular weight had a greater effect than PC [9,82]. The blend investigated by Delimoy *et al.* [26], is very similar to the highest molecular weight pair. As can be seen in Figure 27b, the phase composition calculated by Cheng and coworkers using the Fox equation, Equation 11, for the high molecular weight pair agrees well with Figure 25 [82]. If we disregard the un-stabilized nature of Okamoto and Inoue's blend [81], it can be seen that the PBT molecular weight corresponds to the lowest one in Figure 27a. It is not surprising then, that their blend exhibited greater miscibility and a differing phase diagram. In light of the dominance of PBT molecular weight [9,82] an argument can be made that this is the complete explanation, but Okamoto and Inoue used a much higher molecular weight PC than any in Figure 27. The possible impact of un-stabilized nature of their blend [81] should now be recognized.. and the possible impact of co-polymer should now be made. An explanation for the differences observed between Cheng and coworkers well stabilized blend [82], and Hamilton and Gallucci's stabilized, but partially hydrolyzed blend [9], might also be made.

2.2.2 Influence of Co-polymer

Pompe and Haussler [35] have claimed that miscibility in PC/PBT only exists in the presence of co-polymer as presented in Figure 28. Their argument is not that the glass transition behaviour is exclusively due to co-polymer, but that even undetectable co-polymer concentrations can enhance homo-polymer miscibility. They attempt to explain all miscibility variation as an effect of varying co-polymer concentration, however this is likely an oversimplification. They did not address molecular weight, or even cite it for their material

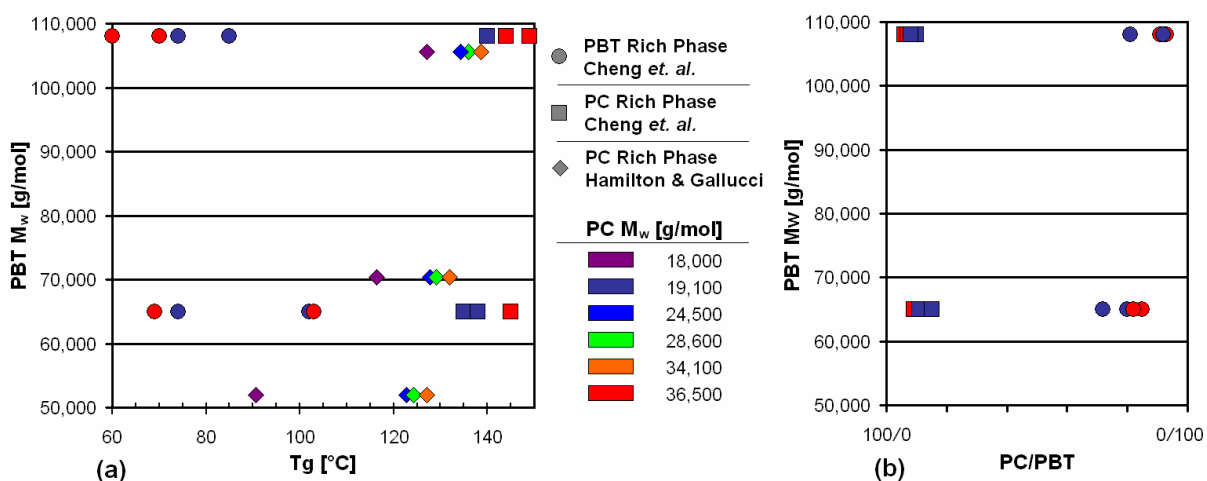


Figure 27: Phase Preferences vs. Molecular Weight, Effect of Molecular Weight on Phase T_g by DMA (a) [9,82], Phase Composition as estimated by the Fox equation from T_g by MDSC (b) [82]

[35]. A superposition of effects is more likely, and would nicely explain why Cheng and coworkers results [82] agree with Delimoy *et al.* [26] but disagree with Hamilton and Gallucci [9]. (See Figure 25 and Figure 27) Okamoto and Inoue's result can similarly be explained [81].

Tatum *et al.* [38] investigated the effects of higher reaction extents on blend morphology. As they do not provide molecular weight data and used relatively low resolution FTIR to characterize co-polymer content, their results are mainly useful for quantitative comparison. They observed similar morphology in the two lowest reaction blends, but with a phase size decrease to 2 μm from 5-10 μm with increased reaction. Figure 29 is an image of the second lowest reaction blend. The next blend, pictured in Figure 30, showed a much finer phase structure, while all subsequent blends provided no image under the SEM. Contrast was produced by selectively dissolving the polycarbonate with dichloromethane. The next two blends were unaffected by the solvent, while the final blend was completely soluble [38]. The

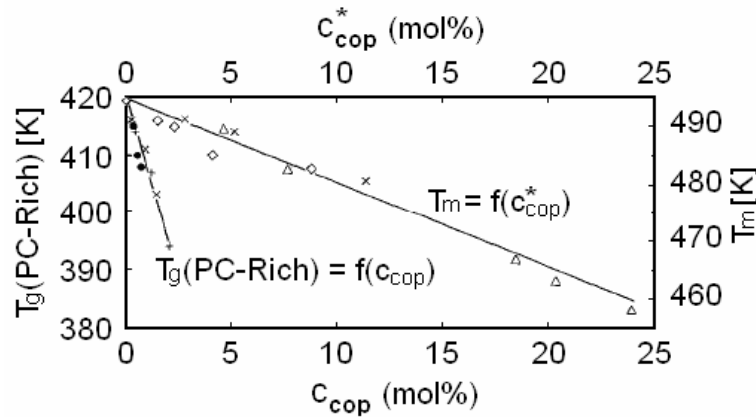


Figure 28: PC Tg vs Co-polymer content, PC $M_w \approx 26,000\text{g/mol}$ by Equation 30 [35]

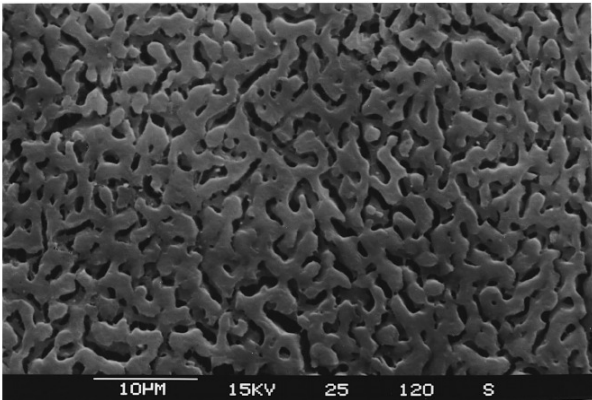


Figure 29: Low-Reaction Blend by SEM, 50/50 wt%, PC $M_w \approx 19,000\text{g/mol}$ by Equation 30 [38]

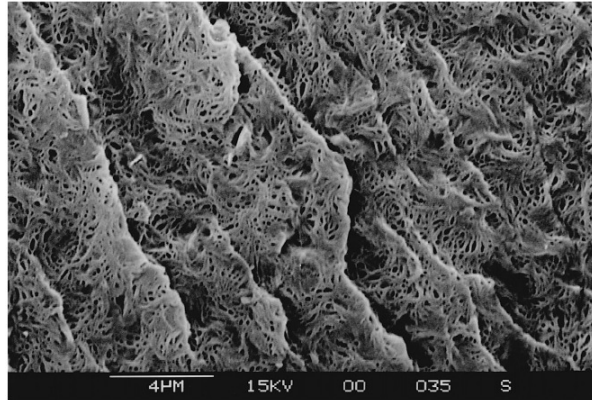


Figure 30: Highly Reacted blend by SEM, 50/50 wt%, PC $M_w \approx 19,000\text{g/mol}$ by Equation 30 [38]

progression of phase size can be easily explained by modeling the co-polymer as a surfactant which modifies the properties of the phase interface. The interfacial area, which is inversely proportional to phase size, is expected to be equal to the area that can be protected by the surfactant [112]. Tatum *et al.* [38] noted the agreement between the results of their etching, and the solvent results of Devaux *et al.* [25].

2.3 Rheology of PC/PBT Blends

Both PC and PBT show typical pseudo-plastic behaviour in their pure state. The rheology of pure PC is well summarized by Robertson [52]. No such summary for pure PBT is available. Several authors have characterized PBT rheology [115-116117118119], but only one lists molecular weight, ($M_n = 22,800$ g/mol), making the data comparable to other studies [117]. A useful finding was that pure PBT, (but not its filled composites), follows the Cox-Merz rule [118]. In contrast, PBT composites, (but not the pure polymer), exhibit shear induced crystallization [119]. The rheology of PC/PBT blends is not well characterized. Though several studies have addressed steady state properties [1,9,27], the only dynamic study is marred by poor transesterification stabilization [23]. In a steady state study PC/PBT blends were found to exhibit negative deviation from log-additivity across the entire composition range at 280°C, a finding consistent with an immiscible blend [27].

2.4 Processing and Compounding

2.4.1 Blending Equipment and Process Variables

A wide variety of processing conditions and equipment types has been used by researchers to produce PC/PBT blends. Co-rotating twin-screw extruders were used by, Wu and co-workers [33,39,120,121], Bai *et al.* [2,22,122] and Okamoto and Inoue [81]. Only one report used a counter-rotating twin-screw extruder [23], while several used single-screw extruders [1,123,124]. Internal mixers are by far the most popular being used by Wilkinson and co-workers [36,38,125] as well as six other research groups [21,24-27,126]. Solvent casting has been used [20,37], but there are concerns that this technique can produce very different morphology than melt blending [35,75]. Co-rotating twin-screw extruders offer excellent distributive mixing [127], uniform high shear stress flow, short residence time, self-wiping, and allow volatiles to dissipate through side ports when run in the typical configuration, (see section 2.5.2 below) [128,129]. Counter-rotating extruders are not self-wiping, requiring higher operating torques [128], but offer better dispersive mixing than their co-rotating cousins due to the high shear rates experienced in the calendar gap. Single screw extruders are not as good at mixing [127], do not have fine control over shear rate and typically exhibit long residence times and dead spaces resulting in possible degradation and inhomogeneity in blends. Their main advantages are that they are inexpensive and widely available [129]. For laboratory purposes internal mixers are excellent, explaining their popularity. They provide good control and uniform stress history but are limited to small batches [129]. Due to their operating scale and control twin screw extruders provide the best option for commercial compounding. As a uniform distribution of PC and PBT is one of the primary objectives of compounding co-rotating extruders with their superior distributive mixing are likely the best.

2.4.2 Typical Co-rotating Twin Screw Extruder Operation

Noeei conducted a review of models for co-rotating twin screw extruders operation [5]. Though in his work he mainly focused on models suitable for online extruder control, specifically physics-based lumped flow model, he identified the work of Meijer and Elemans [128], as particularly good for understanding the role of extruder geometry and processing conditions, such as screw speed, degree of fill, specific energy consumption, and feed rate. The work of Gao *et al.* [130], was identified as providing useful estimates of mean residence

time. Average shear rate was not addressed by Noeei [5], but Mohamed *et al.*'s study, [131], provided useful incite into this parameter. In all these accounts screw speed, N , and feed rate, Q , are the two most important variables governing mechanical operation of co-rotating twin screw extruders [128,130,131]. The effect they play in controlling other variables of interest is summarized in what follows. Figure 31 provides a schematic of an operating extruder.

Shear rate, is significant both for its role in mixing [127], and in mechanical degradation (section 1.3.7). As a variety of shear rates are present within an extruder it may be useful to define an average shear rate that is characteristic of a given operation. Equation 31 providing the relationship between average shear rate and screw speed is largely empirical, though some theoretical basis was presented for its development. β_0 and β_1 are parameters characteristic of a given material, temperature and extruder geometry, but do not assume Newtonian fluid flow in their derivation. They are determined by linear regression analysis [131], making them difficult to use as predictors. It is interesting to note the similarity between Equation 31 and Equation 25, the viscosity relationship for power law materials. From this analysis it can be seen that average shear rate is only dependent on screw speed.

$$\log \dot{\gamma} = \beta_0 + \beta_1 \log N \quad [131] \qquad \text{Equation 31}$$

Specific energy consumption (SEC) is the amount of energy consumed by the extruder per unit mass of material. According to Meijer and Elemans [128], it is closely related to degree of fill (f) of partially filled channel elements. Using a simplified geometry where H is its average height of a rectangular channel, D is the barrel diameter, and ϕ is the screw angle, f can be calculated from Equation 32. Lumping all constants into β_2 it can be seen that f is

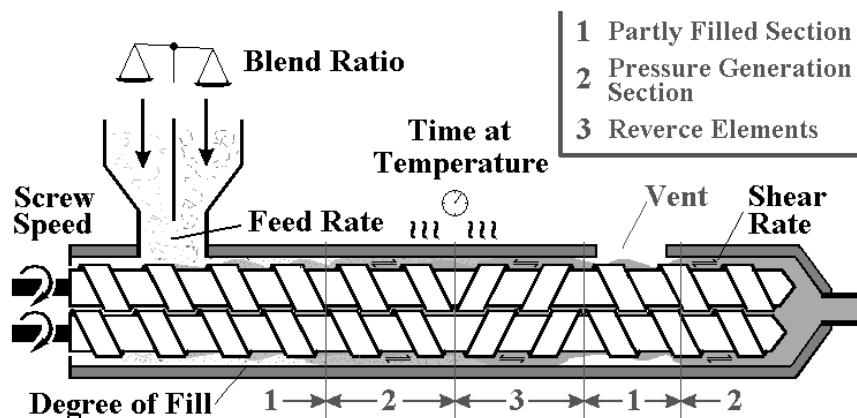


Figure 31: Typical Co-Rotating twin screw extruder operation.

independent of material with its only dependencies being feed rate and screw speed. If f is known Equation 33 can be used to calculate SEC. The first term in the brackets gives the dependence of SEC without reverse elements present. The effect of reverse elements is included in the second term. L is the total length of the screw; l_c is the length of the reverse elements, ρ is the material density and η is its viscosity. In the derivation of Equation 32, screw flight angles and depths were assumed to be constant and the fluid was assumed to be Newtonian. Neither is typically the case in practical applications, however if f is substituted into Equation 33 and the constants lumped into β_3 , and β_4 , the approximate functional form for SEC vs. Q and N is revealed in Equation 34 [128]. Note the parameters dependence on the polymer viscosity and density.

$$f = \frac{2}{H(\pi D)^2 \sin(\varphi)} \frac{Q}{N} = \beta_2 \frac{Q}{N} \quad [128] \quad \text{Equation 32}$$

$$SEC = \frac{\pi \eta D L}{1.8 \rho H^2 \sin \varphi} N \left(1 + l_c \frac{3f + 4}{f} \right) \quad [128] \quad \text{Equation 33}$$

$$SEC = \beta_3 N + \beta_4 \frac{N^2}{Q} \quad [128] \quad \text{Equation 34}$$

Mean residence time t_m , is the average time polymer takes to pass through the extruder. It is significant as it is the time spent at processing temperatures and therefore the reaction time for thermal degradation and transesterification (sections 2.2.4-5). Equation 35 was developed empirically. However, theoretical justification has been provided based on the most basic definition of mean residence time which is the ratio of extruder volume filled over the throughput. The parameter, β_5 , represents the sum of the mixing/melting zone volume and the conveying zone volume filled due to back pressure flow, V_p . Mixing/melting zone volume is calculated by multiplying screw free correctional area A_f , by the length of the mixing area, L_m . β_6 is the conveying zone volume filled due to pure drag flow. Although throughput or feed rate Q appears in the derivation it cancels out leaving this term only dependent on screw speed. L_c is the length of the conveying section and i represents the number of flights on the screw. In the derivation given the parameters have no explicit dependence on material characteristics; however the material can influence the back flow pressure and therefore β_5 . Error less than 10% was reported with use of Equation 35 provided that the percent drag flow did not dominate [130]. The terms for β_6 have been slightly modified to agree with Meijer and

Elemans simplified geometry. It is interesting to note that when this is done the second term reduces to the channel volume multiplied by degree of fill and divided by feed rate. This makes L_c equal to the length of sections 1 and 2 in Figure 31, L_m equal to Meijer and Elemans l_c and V_p equal to the extra volume in section 2 in excess of section 1.

$$t_m = \beta_5 \frac{1}{Q} + \beta_6 \frac{1}{N} \quad [130] \quad \text{Equation 35}$$

$$\beta_5 = A_f L_m + V_p, \beta_6 = \frac{2A_f L_c}{(2i-1)H(\pi D)^2 \sin(\varphi)}$$

3.0 EXPERIMENTS

This chapter describes the three main experimental and analytical techniques used in this study namely, differential scanning calorimetry, scanning electron microscopy and image analysis. As background to the experimental work, the chapter begins with some overview description of the statistical design used for material sampling in this work.

3.1 Extruder Factorial Experiment

As stated earlier, the current work is an extension of a wider study on commercial scale compounding performed by Noeei [5]. Since the sampled materials used in this work are from the same batch, it is useful to provide a summary of the factorial experiment used in that work. The three factors are as shown in Table 10, Figure 32. In the view of the author, Noeei’s use of two separate feed rates for the two hoppers and the screw rate as the three factors in his analysis does not represent the physics of the problem as accurately as the total feed rate and blend composition approach used here. Equations 36 and 37 convert Noeei’s two feeder rates into the feed rate and PBT content used here. To better represent the statistical design the factors have been coded using Equation 38 such that center points are represented as 0, and ± 1 indicates a ten percent increase/decrease relative to the center point. The corresponding uncoded values for each factor are seen in Tables 11 and 12. It should be noted that when run 11 jammed the extruder, screw speed was increased, (Table 10, original design intent shown in brackets).

$$Feed\ Rate\ [kg/h] = Feeder\ 1\ [kg/h] + Feeder\ 2\ [kg/h] \quad \text{Equation 36}$$

$$PBT\ Content\ [wt\%] = \frac{Feeder\ 2\ [kg/h]}{Feed\ Rate\ [kg/h]} \times 100\% \quad \text{Equation 37}$$

Table 10: Factorial Experiment Statistical Model, Coded Variables

Blend Number	Screw Speed	Feed Rate	PBT Content
1	0	0	0
2	+1	+0.2	-1.28
3	+1	-1	0
4	0	0	0
5	-1	-1	0
6	0	0	0
7	-1	+0.2	-1.28

Blend Number	Screw Speed	Feed Rate	PBT Content
8	+1	+1	0
9	0	0	0
10	+1	-0.2	+1.28
11	0 (-1)	+1	0
12	-1	-0.2	+1.28
13	0	0	0

$$\text{Coded Factor} = \frac{\text{Factor} - \text{Center}}{\text{Center}} \times \frac{100\%}{10\%}$$

Equation 38

All materials were processed on a WP ZSK 58 mm co-rotating extruder at the compounding facility of SABIC Innovative Plastics in Cobourg Ontario. The exact screw geometry is confidential but it was assumed that a typical screw for the equipment was used. Therefore, the simplified geometry of Meijer and Elemans [128] as seen in Figure 31 provides a good estimate. The polymer was not dried prior to compounding. Low residence time and the extruder’s devolatizing vents were relied upon to limit hydrolysis. Raw materials consisting of two polycarbonates and one PBT were dispensed from two separate feeders. The polycarbonates and other additives in a fixed ratio seen in Table 12 were in feeder 1. Feeder 2 only contained PBT. The extruder was instrumented for online measurement of, feed rate, screw speed, die pressure, blend exit temperature, and SEC. After achieving a given operating condition, material samples were taken at regular intervals. As this work concerns itself with steady state operation, the sample taken after 19 minutes was used if available. Runs 11 and 12 were the only exceptions with samples taken after 14 and 9 minutes respectively. Although the experimental model was run on two consecutive days with different extruder die plates only material from the first day, (4mm die plate), was analyzed in the following experiments.

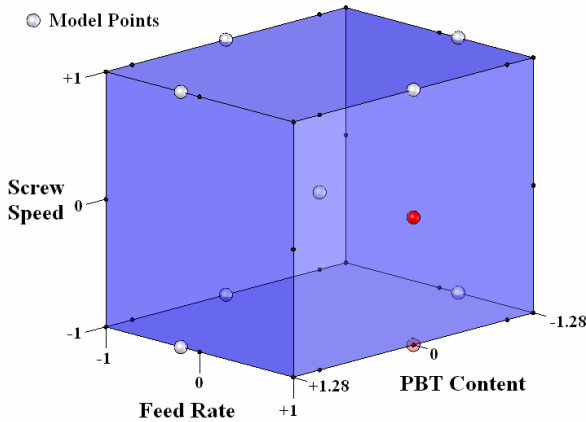


Table 11: Un-Coded Screw Speed and Feed Rate

Code	Screw Speed	Feed Rate
+1	451 rpm	468 kg/h
0	410 rpm	425 kg/h
-1	369 rpm	383 kg/h

Figure 32: Statistical Model, Coded Variables

Table 12: Un-Coded Blend Composition

Code	Feeder 2	Feeder 1		Total
	PBT	PC	Other Additives	
+1.28	44 wt%	46 wt%	10 wt%	100 wt%
0	39 wt%	50 wt%	11 wt%	100 wt%
-1.28	34 wt%	54 wt%	12 wt%	100 wt%

3.2 Molecular Weight by Gel Permeation Chromatography (GPC)

3.2.1 Purpose and Experimental Setup

The purpose of GPC analysis is to determine molecular weight averages of the raw materials used to produce blends, and to estimate the effect of blending on molecular weight. Samples of the two polycarbonates, blend number 9, and the PBT (see section 3.1) were sent to Jordi FLP of Bellingham, Massachusetts to determine molecular weight.

The method used by Jordi is described as follows: “The samples were dissolved in Hexafluoroisopropanol (HFIP) / 0.01M Sodiumtrifluoroacetate (NaTFA) to a concentration of 2.5 mg/ml and placed on an orbital shaker for 24 hours. The samples were filtered using 0.45µm disposable Teflon filters and were then run in duplicate in the same solvent. The system was run at a flow rate of 1.0 ml/min on a JORDI X-stream 10⁵Å column, 250 mm X 10 mm (ID). The column temperature was maintained at 40° C. Injection size was 200µl of the 2.5 mg/ml sample solution. Polymethyl methacrylate standards with a concentration of 0.5 mg/ml were used (Molecular weight as follows: 903K, 701K, 366K, 110K, 89.3K, 31.6K, 14.7K, 5.09K, 2.58K & 402) with injection size of 100 µl. The samples were monitored at a sensitivity of 8 with a WATERS 401 Differential Refractometer. Data acquisition and handling were made with JORDIGPC software.”[132]

3.2.2 Blend to Individual Polymer Comparison

GPC experiments are conducted at very low polymer concentrations so as to prevent interaction between individual chains in solution. This means that PC and PBT in the blend sample will behave identically to the equivalent pure components during the GPC experiments. Furthermore the molecular weight curves for the different polymers are directly comparable as they were tested under identical conditions and all molecular weights are quoted relative to the same reference material. This means that any differences between rule of mixtures behaviour and the experimental curve for the blend are directly attributable to processing effects. Figure 33 shows the GPC results for each blend component and the sample blend. Jordi FLP provided curves normalized with respect to area so that each curve represents the same weight of material. The rule of mixtures result is produced by adding the three component curves according to the blend ratio given in Table 12. To produce comparable points on each curve they were interpolated using cubic splines according to the method described in [133].

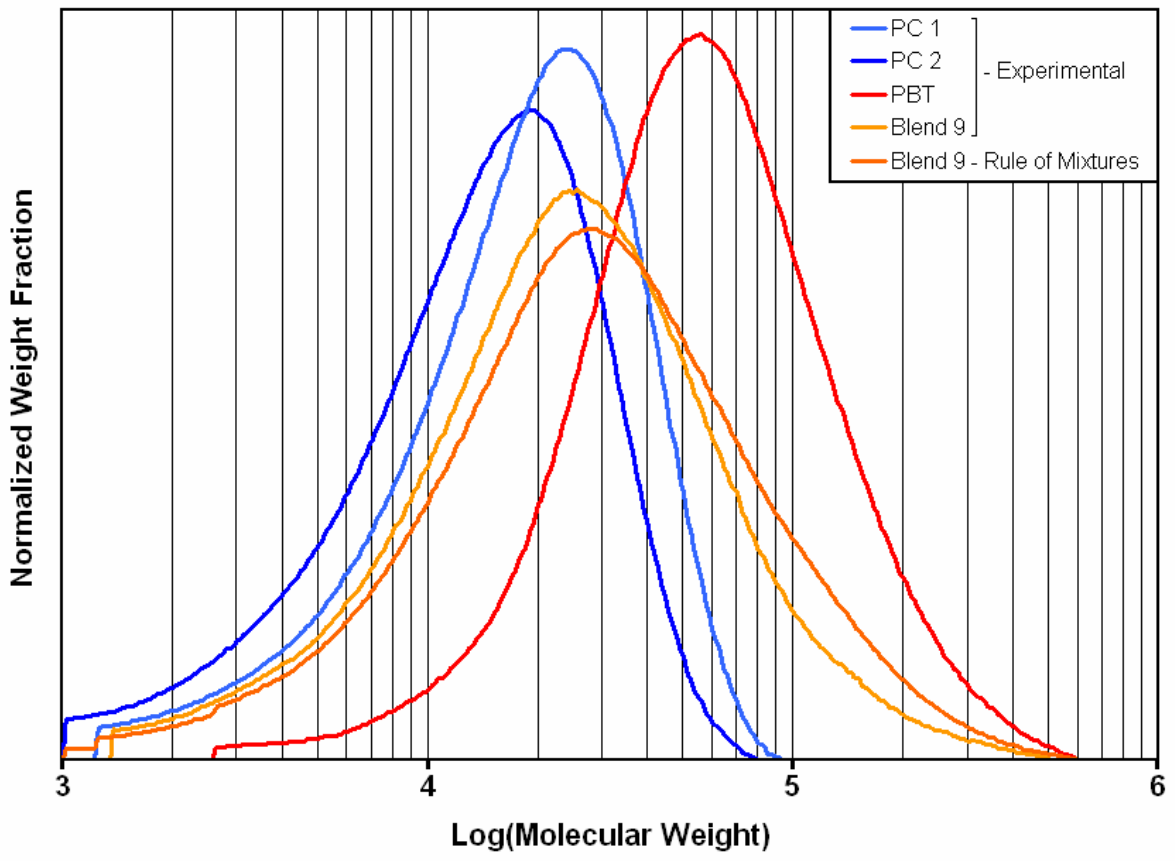


Figure 33: Molecular Weight Curves – Experimental and Rule of Mixtures

3.3 Thermal Analysis

3.3.1 Purpose

A major part of this research study is to characterize the thermophysical properties of PC/PBT blends produced in section 3.1 using a common thermal analysis method, Differential Scanning Calorimetry (DSC). The properties of interest are amorphous phase glass transition temperatures, weight fractions and estimated compositions, as well as PBT crystalline fraction, and melting temperature. These measurements are very useful for determining the effects of compounding on blend structure as they can be directly compared with the raw polymers. If samples are melted and re-solidified at a controlled heating rate prior to property determination, the measured properties closely represent those of the compounded blend after reprocessing into a final product.

3.3.2 Differential Scanning Calorimetry Analysis

There are several different instrument configurations which are referred to as differential scanning calorimeters, DSC. The TA Instruments 2920 DSC machine is a heat flux type which uses a disk type measuring system. As shown in Figure 34 the disk provides a symmetrical heat conduction path from the furnace to both the sample and reference pans. In standard operation, the controller applies a constant heating rate, dT/dt , and measures the sample temperature, $T(t)$, at the disk surface directly beneath the sample. Any difference between the reference and sample will result in a temperature difference, $\Delta T(t)$. In the ideal case, the heat

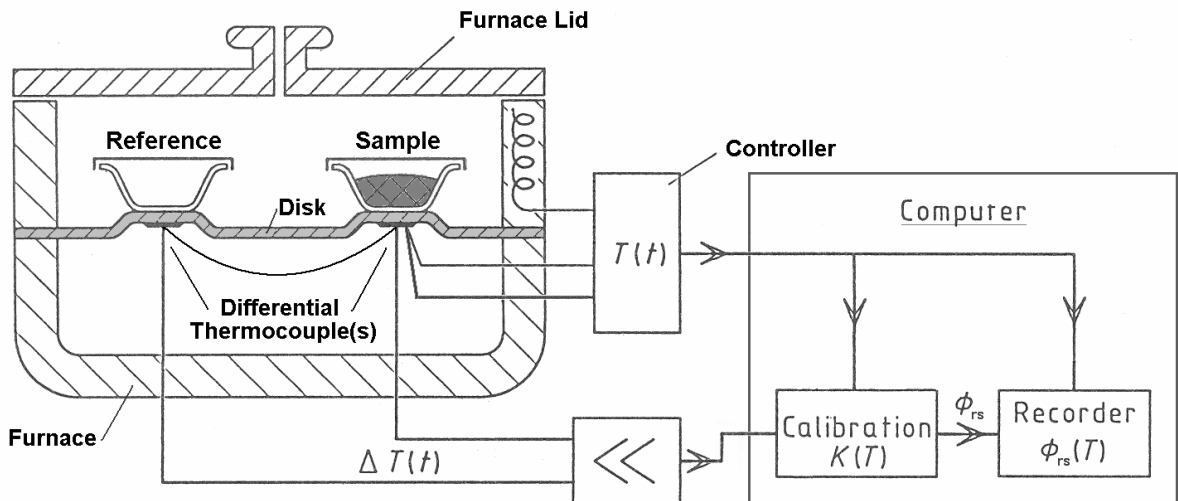


Figure 34: Schematic Disk Type Heat Flux DSC [134]

conduction path is perfectly symmetrical allowing Equation 39 to be used to calculate the heat flow rate difference between the reference and sample, $\Delta\Phi_{rs}$. Noting that the reference heat capacity, C_r , is zero if an empty reference pan is used, $\Delta\Phi_{rs}$ is related to the sample specific heat capacity, c_p , by Equation 40. ΔL is the distance between the sample/reference and the furnace wall, A and k are the disk cross sectional area and thermal conductivity respectively, and m is the sample mass. In actual instruments perfect symmetry is unattainable, requiring that a heating rate and temperature dependent baseline be established by a calibration run under the same conditions as the desired experiment but without the sample present. Typically the calibration constant, $K(T)$, is also evaluated experimentally, either over the entire temperature range by use of a pure substance with known heat capacity, or at a key temperature by measurement of a known first order thermodynamic transition. [135]

$$\Delta\Phi_{rs}(T) = -\left(\frac{A \cdot k}{\Delta L}\right)\Delta T(t) = -K(T) \cdot \Delta T(t) \quad [135] \quad \text{Equation 39}$$

$$m \cdot c_p(T) = C_r - \left(\frac{dT}{dt}\right)^{-1} \Delta\Phi_{rs}(T) \quad [135] \quad \text{Equation 40}$$

During a chemical reaction or thermodynamic transition the relationship between $\Phi_r(t)$, the heat flow into or out of the sample due to the change, and the measured signal, $\Delta T(t)$, is given by Equation 41. Comparing to Equations 39 and 40 it can be seen that the first term of Equation 41 is simply $\Delta\Phi_{rs}$, the second term is the contribution of the sample heat capacity to $\Delta\Phi_{rs}$, while the third term is the energy stored by the sample in response to the rapid change in $\Delta T(t)$ induced by the transition. The existence of a signal delay due to energy storage must be accounted for when interpreting DSC transition results. [135]

$$\Phi_r(t) = -K(T) \cdot \Delta T(t) - \frac{dT}{dt} [m \cdot c_p - C_r] - m \cdot c_p \frac{d\Delta T}{dt} \quad [135] \quad \text{Equation 41}$$

A schematic polymer melting peak is shown in Figure 35a. As can be seen from the diagram, there are several possible definitions of melting temperature. The peak temperature, T_p , has limited physical significance, but is near the inflection point which marks the transition end [136]. The best agreement with other methods comes from using the extrapolated onset temperature, T_{oe} [137]. This represents the best estimate for the start temperature of a first order transition in a heat-flux DSC [136]. It is determined by tracing the tangent to the inflection point back to the base line. As was previously mentioned the baseline for melting

analysis is the heat capacity curve underlying the peak [55,135]. If the liquid and crystalline heat capacities are the same then this is easy to estimate the baseline. When they differ, both experimental evidence and theory based on the Avrami equation suggest a sigmoidal curve provides the best baseline estimate [138]. Integrating the area between this baseline and the peak provides the apparent heat of fusion, ΔQ_f , of a polymer or blend. This differs from the latent heat of fusion, ΔH_f , in that for latent heat a wholly crystalline sample is required. In polymer blends where the crystallizing polymer exhibits both glass transition and melting temperatures Equation 42 can be used to calculate the blend percent crystallinity [72].

$$x_{crystalline} = \frac{\Delta Q_f}{\Delta H_f^0} \approx 1 - \frac{\Delta C_p^{observed}}{\Delta C_p^{amorphous}} \quad [72] \quad \text{Equation 42}$$

The second half of the above equation deals with heat capacity change at glass transition. Figure 35b provides a schematic glass transition curve. In a purely amorphous polymer the heat capacity change measured, $\Delta C_p^{observed}$, will be equal to $\Delta C_p^{amorphous}$. In an immiscible blend or semi-crystalline polymer, the fraction undergoing transition will be reduced proportionately allowing the amorphous fraction to be calculated. Equation 43 provides a direct calculation of the amorphous fraction, while Equation 42 above uses the thermodynamic model for the blend to predict the crystalline fraction from the amorphous fraction [72]. In partially miscible blends with an intermediate glass transition “additivity” of ΔC_p ’s is often assumed, Equation 43, however the accuracy of this assumption as a universal rule is doubtful [139]. In calculating the glass transition temperature, onset temperature, T_o , is sometimes used

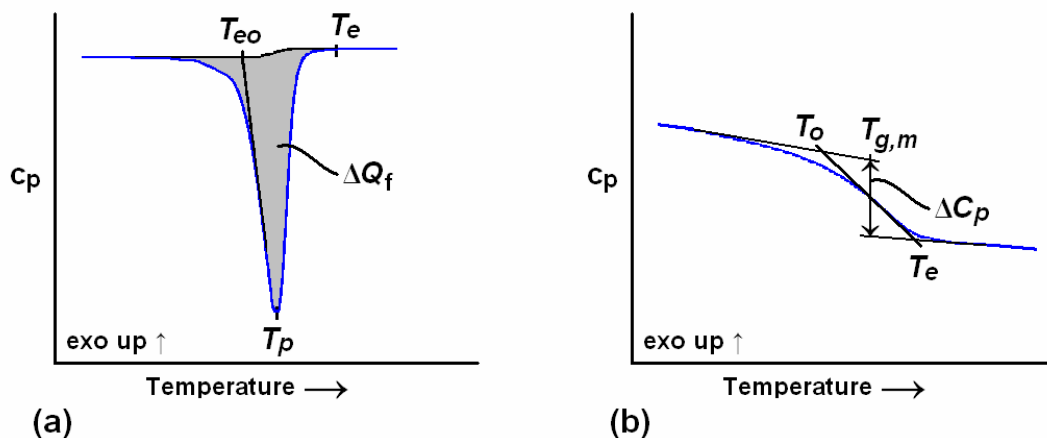


Figure 35: Transition Analysis: Melting (a), Glass Transition (b).

[72], however the “most precise” determination of glass transition temperature is the half transition temperature, $T_{g,m}$, during cooling [140]. If cooling and heating rates are matched, the glass transition temperature and ΔC_p can be precisely determined during heating as well [72,140].

$$x_{amorphous} = \frac{\Delta C_p^{observed}}{\Delta C_p^{amorphous}} \quad [72] \quad \text{Equation 43}$$

$$\Delta C_p^{amorphous} = \sum_i w_i \Delta C_{p,i}^{amorphous} \quad [72] \quad \text{Equation 44}$$

3.3.3 Sample Preparation

Aluminium sample pans are filled with 10 to 14mg of polymer and then placed in a vacuum oven at 120°C for at least three hours to dry samples prior to processing. Within 5 minutes of removal from the oven, lids are used to close the pans. Lids are crimped sealing the dry samples. Blend and pure PBT samples were cut from ‘as received’ pellets. PC was received in a particulate form which did not pack densely enough to provide an adequate sample. For this reason samples were cut from compression moulded plaques. Prior to moulding at 250°C, the particulate was dried using the same oven, temperature, and time as the final samples. A reference pan consisting of an empty aluminium pan with crimped lid was also prepared.

3.3.4 Heating Rate Optimization

Blend samples were tested at heating rates of 2, 5, 10, and 20°C/min to see what rate provided the best signal. The advantage of a low heating rate is reduced thermal lag, resulting in better estimates of transition temperatures. A high heating rate, however, produces larger temperature differences between the sample and reference improving signal strength and therefore the signal-to-noise ratio. At 2°C/min the glass transition signals were too weak to be resolved. As can be seen in Figure 36, two separate melting peaks were observed in the 5°C/min sample, while overlapping of peaks and loss of temperature resolution was observed at greater heating rates. To insure that measured effects of processing were not an artefact of heating rate it was desirable to run at two rates. The initial data set was produced using a 10°C/min rate while 5°C/min was selected as the optimum rate for the final tests. For all rates the same heat cool heat cycle was followed with data taken from the final cycle. This erases prior thermal history thereby reducing the potential for error.

3.3.5 Test Procedures for Full Test Runs

Table 13 lists the thermal treatments for DSC tests. Two sets of tests with different heating rates were conducted. Six samples of each blend produced in section 3.1 were tested at 10°C/min. In the 5°C/min tests three samples of each polymeric material were tested, (13 blends and three raw polymers), as well as three runs with the sapphire standard. Each heating rate was run as a block to eliminate effects of re-calibration between results at each rate. Within each block tests were conducted in a random order to minimize possible error. Samples are held isothermally between heating and cooling steps to eliminate temperature gradients that might exist in the sample prior to subsequent steps.

3.3.6 Instrument Setup and Calibration

A TA DSC 2920 with refrigerated cooling unit, running Thermal Advantage 1.1A control software was used for these experiments. Nitrogen at a flow rate of 20 L/min was the purge gas. Calibration was conducted for each set of experiments at the appropriate heating rate. 10 mg samples of indium and distilled water were used for temperature calibration. The results of the indium run were also used to determine the calibration constant at the indium melting point. For improved accuracy in the final 5°C/min tests the calibration constant as determined experimentally across the entire temperature range using the average results of three calibration runs with a sapphire. Baseline calibration was done using an empty cell. The control software uses a linear approximation of the baseline based on the experimental curve. Some curvature was detected over the 300°C temperature range of the experiment. As error resulting from this curvature is accounted for in the calibration constant calculated using sapphire, it will have been reduced if not completely eliminated in the final results.

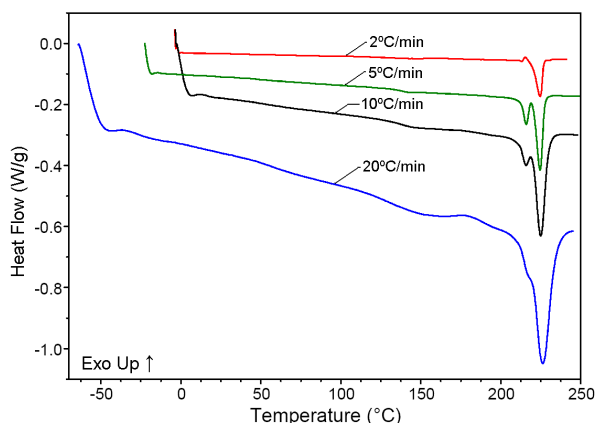


Table 13: DSC Thermal Treatments

Step	5°C/min	10°C/min
1	-20°C → 250°C	~25°C → 250°C
2	hold 2 min	hold 2 min
3	250°C → -20°C	250°C → -20°C
4	hold 4min	hold 4min
5	-20°C → 250°C	-20°C → 250°C

Figure 36: Heating Rate Optimization Results

3.3.7 Calibration with Sapphire Standard

The heat capacity curves from the three sapphire tests are compared to the published values from [141] in Figure 37. It can be seen there is random variation in the absolute values, but minimal difference in the shape of the curves. This error is attributed to sample positioning variation in the cell and instrument drift over time. To obtain the average curve, the three experimental curves are interpolated using cubic splines. The calibration constant $K'(T)$ in Figure 37 is calculated using Equation 45. Note that it is not identical to the constant in Equation 39 because the results have already been corrected by the instrument data acquisition software using the indium based constant. Prior to analysis the heat capacity curves for all 5°C/min test runs were adjusted using Equation 46. Assuming empty reference pans, this equation can be derived from Equation 45 by multiplying both sides by heating rate and mass before substituting Equation 40. Cubic splines were used to interpolate between known $K'(T)$ values to match the temperatures at which experimental data was recorded.

$$K'(T) = \frac{c_{p, Known}}{c_{p, Experimental}} \quad \text{Equation 45}$$

$$\Phi(T)_{Corrected} = K'(T) \cdot \Phi(T)_{Experimental} \quad \text{Equation 46}$$

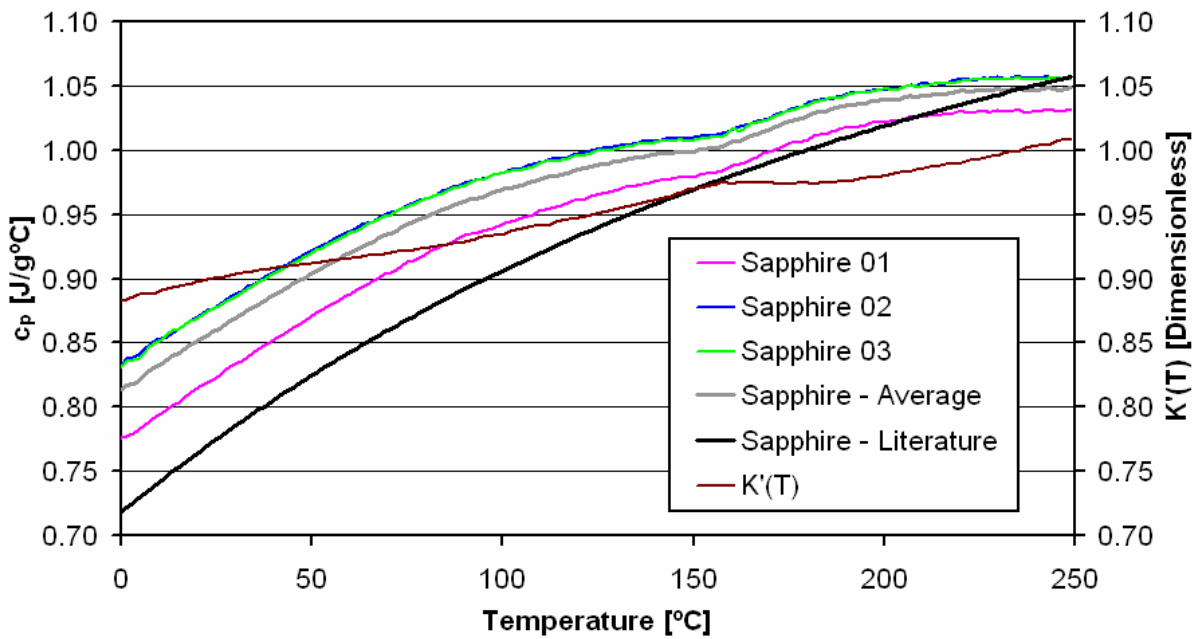


Figure 37: DSC Calibration Using Sapphire

3.3.8 DSC Data Analysis

The software package Universal Analysis 2000 version 1.4D was used to determine peak areas, melting temperatures, glass transition temperatures, and heat capacity changes at glass transition from the DSC curves. To standardize analysis, macros as shown in Appendix B were written. The accompanying documentation states that the software options selected correspond to the procedures outlined above in section 3.3.2. Figure 38 shows typical results as well as analysis limits. Each blend and pure material DSC curve was analyzed individually. For each heating rate the results for each material are averaged to produce a final value. The full results table and averages can be found in Appendix C.

For the 5°C/min tests blend amorphous phase composition and weight fraction were calculated. The composition was calculated using Equations 11-13 and the experimentally determined pure material glass transition temperatures. Following the additivity assumption for ΔC_p , the heat capacity change for a purely amorphous sample was calculated using Equation 44. For PC the experimental heat capacity changes were used; however, as the PBT

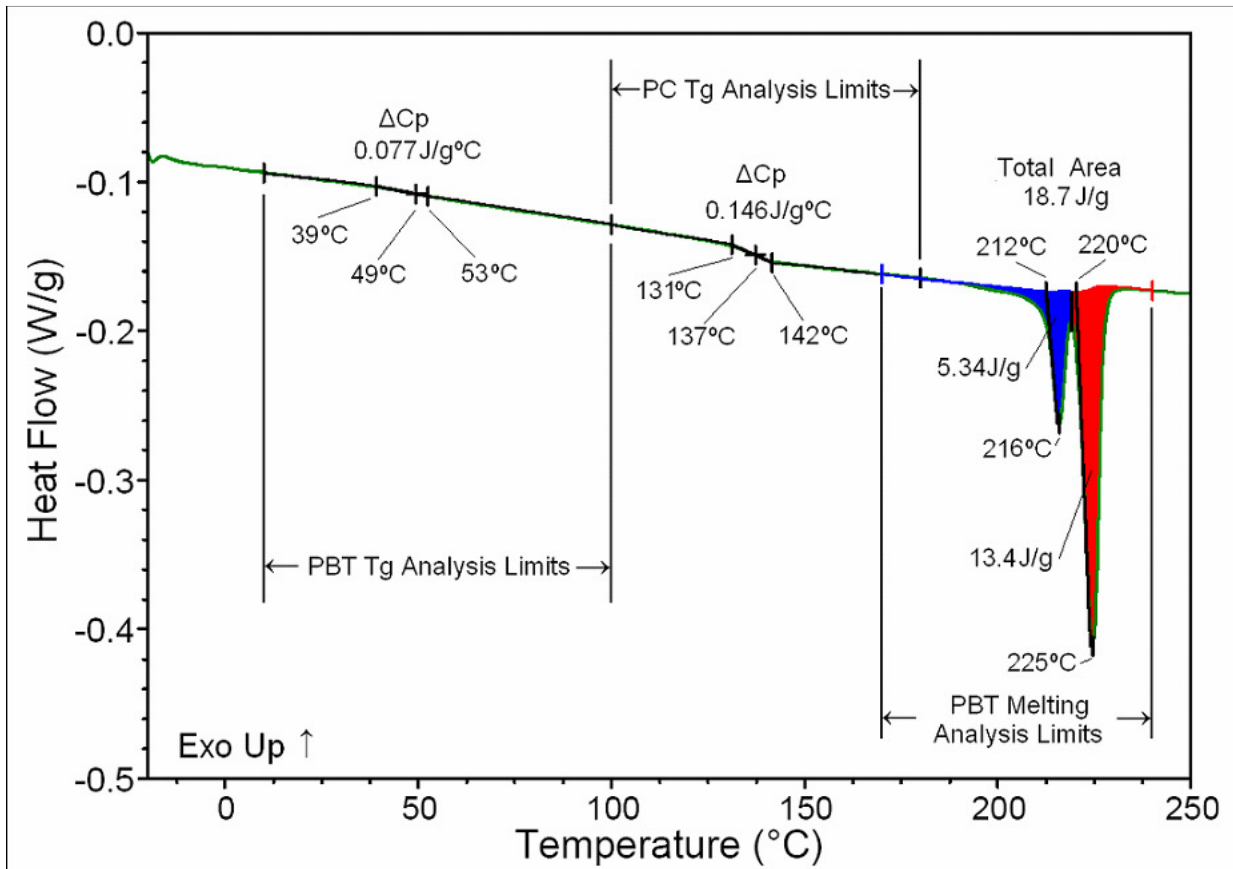


Figure 38: Typical DSC Analysis Results

represents a crystalline-amorphous mixture, the Table 6 value for purely amorphous PBT in a semi-crystalline sample was used. Equation 43 then allows the weight fraction of the amorphous phases to be calculated. The crystalline weight fraction was calculated using Equation 42. From the phase compositions and weight fractions, the weight fraction PC and PBT in the blends can be calculated for comparison with the known values. By minimizing the mean square error between the estimated and known compositions, k in Equation 13 can be estimated. Complete phase composition results are tabulated in Appendix D.

To compare the shape of blend curves to those of the pure constituents, theoretical curves were prepared using the rule-of-mixtures. Thermal Advantage software uses a variable sampling rate based on the signal rate of change necessitating the use of cubic splines to directly compare data. The details of this technique can be found in Rao [133]. Figure 39 shows the three experimental curves for blend number 6 and the resulting average. A similar procedure was conducted on the curves for pure PC and PBT. The pure material curves were combined according to the rule-of-mixtures and the known blend compositions. To better evaluate the effect on glass transitions, the numerical derivatives of these results for the glass transition region were taken. The rule-of-mixtures comparisons for all blends appear in Appendix E.

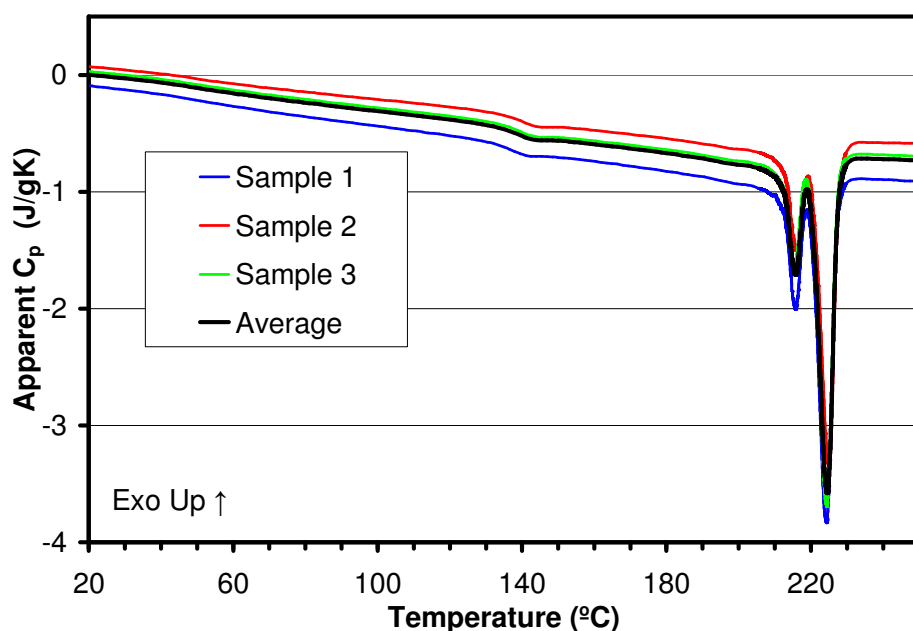


Figure 39: Raw and Averaged Experimental DSC Curves

3.4 Phase Structure

3.4.1 Characterization of Blend Morphology by Electron Microscopy

The DSC scan can only provide information on the presence and composition of multiple phases but not on their size and distribution. In order to directly observe the phase structure of both the as-received blend and that of blends more closely approaching equilibrium, electron microscopy has to be used.

Of the two electron microscopy techniques, transmission electron microscopy, (TEM), provides the highest magnification and finest resolution, but at the cost of the most labour intensive sample preparation [142]. Slices between 30-50 nm thick [26,38] are cut using an ultra-microtome, supported on a copper grid, and stained with combinations ruthenium [26,33,38,120,143] and osmium [143] tetroxide to bring out phase contrast. TEM has been used to investigate crack tip propagation [39,120], the fine microstructures present in reacted [38], or highly mixed [33] blends, and the interior structure of phases [26].

Scanning electron microscopy, SEM, allows for easier sample preparation than TEM, but typically at the cost of decreased resolution [142]. Unlike metals or thermoset-polymers, thermoplastics, particularly PBT which is near its glass transition, should not be sectioned by grinding and polishing as this can smear morphology. Samples are typically prepared by cryofracture or microtoming the specimen [144]. In the latter case the thin shavings used for TEM are discarded and the block they are cut from represents the sample. Some phase contrast can be produced by differing fracture behaviour however often enhancement is still required. Staining, etching, or phase swelling/degradation can all be used to enhance contrast. Staining is the preferred method as it is the least likely to disturb morphology. Etching uses a solvent that selectively removes a single phase; however this will also remove any microstructure internal to the phase. Swelling/degradation uses a compound that will be selectively absorbed or will selectively attack a phase, changing its volume. This can also distort or obscure aspects of microstructure [142].

PC/PBT blends are non-conductive requiring etched or degraded samples to be gold or carbon coated to prevent charging. Coating is not required when using new LVSEM instruments designed to operate at lower accelerating voltages [56]. Staining with ruthenium or osmium tetroxide confers sufficient conductivity for conventional SEM, avoiding contrast

reduction associated with coating [145]. Given the experimental timeline and the most readily available instrument, conventional SEM was selected as the technique of choice for this study.

3.4.2 SEM Instrument Considerations

Figure 40 shows a typical instrument setup. An electron gun produces the illuminating beam which is focused by magnetic lenses to a fine point. An image is formed by scanning the beam across the surface in a grid pattern and detecting the intensity of signal at each point in the grid. Two different signals can be measured mainly secondary and back scattered electrons. Secondary electrons are knocked off the sample surface by the incident beam. A detector, positively charged with respect to the specimen, draws emitted electrons away from the sample. As seen in Figure 41, electrons from the top of peaks have a shorter path and are more easily attracted producing a stronger signal. In this way, contrast is produced by surface roughness allowing topography to be observed. Back scattered electrons are incident beam

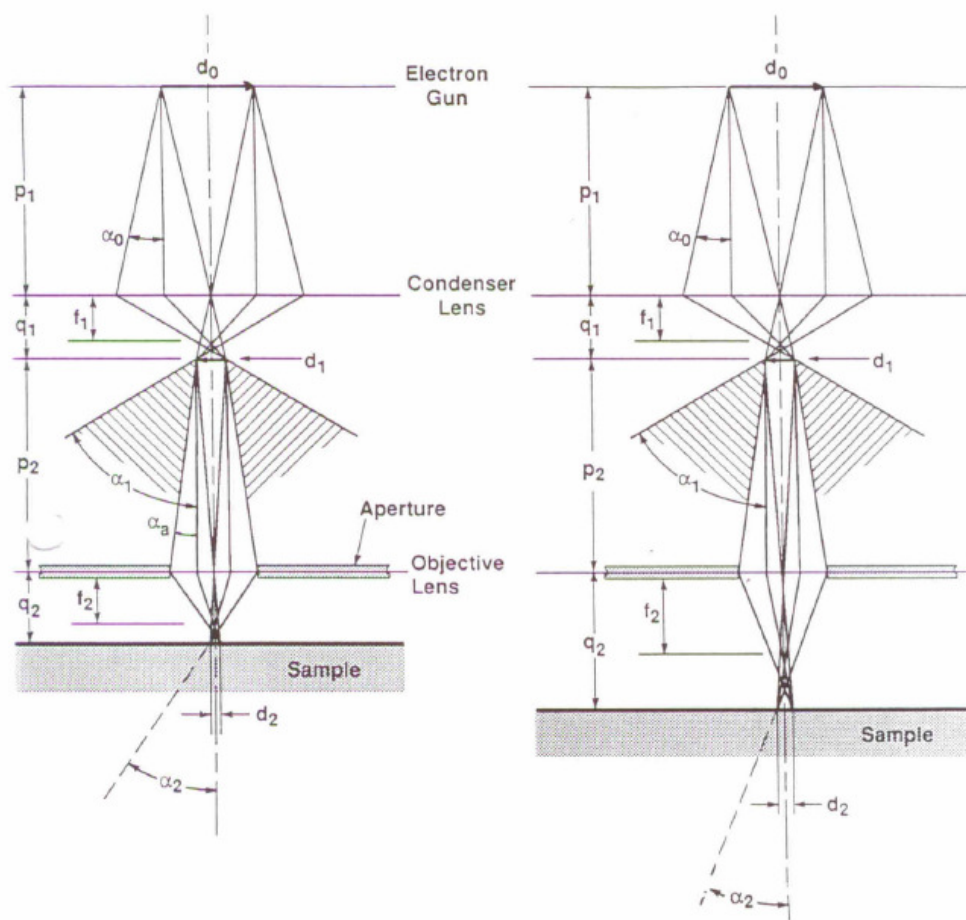


Figure 40: The effect of work distance in a typical SEM [146]

electrons that bounce off of atoms in the sample. As they are higher energy their signal comes from a greater depth and therefore is less affected by the surface. Contrast comes from density and atomic weight fluctuations. The degree of contrast is measured using the back scatter coefficient as defined in Equation 47 where i_{BSE} is the measured current, and i_p is the probe current. Figure 42 shows how high atomic weight materials reflect back more electrons producing stronger signals. PC and PBT have similar average atomic weights necessitating staining to produce back scatter contrast.

$$\eta_{BSE} = \frac{i_{BSE}}{i_p} \tag{Equation 47}$$

The key factors defining good SEM images are resolution, depth of field and brightness. Resolution is the smallest separation of two points that can be distinguished, and is limited by the minimum probe diameter. Depth of field is distance from the focal point at which acceptable resolution is maintained. This is controlled by beam divergence. Figure 40 shows the effect of work distance on beam divergence, α_p and probe diameter d_p . It can be seen that a compromise must be made between resolution and depth of field when choosing a work distance. Brightness is also influenced by these factors; however as can be seen in Equation 48 their effects tend to cancel each other. The primary influence on brightness is probe current. Though probe current is proportional to acceleration voltage, in practice it is mainly controlled by adjusting electron gun heating and aperture size.

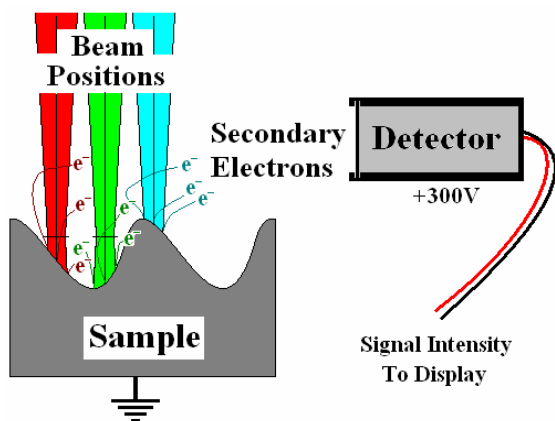


Figure 41: Secondary Electron Contrast

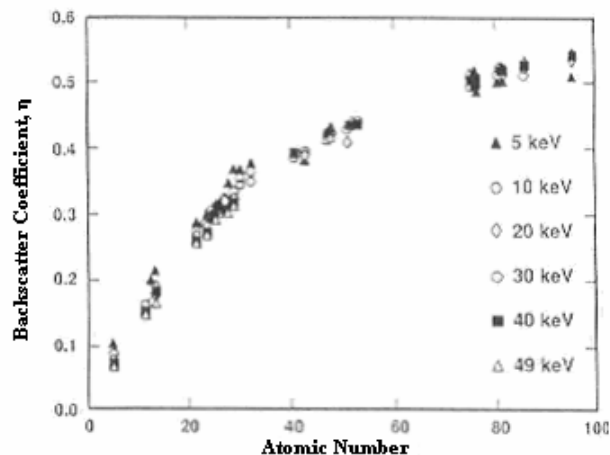


Figure 42: Back Scatter Coefficient vs. Atomic Number [146]

$$\text{Brightness} = \frac{4i_p}{(\pi \cdot d_p \cdot \alpha_p)^2}$$

Equation 48

3.4.3 Sample Preparation

Individual polymer pellets were used as samples. Several stages of sample preparation are shown in Figure 43. In preparation for cutting, samples were encapsulated in commercial epoxy supplied as LECO 812-522-HAZ Lot 110809. Samples were mounted so that the prepared surface was perpendicular to the flow direction in the die. To maintain orientation during encapsulation a pin was driven through the center of a small square of cardboard and into the back of the sample. The sample was lowered on the end of this pin into epoxy filled moulds. Orientation was maintained by the cardboard resting on the lip of the mould and holding the pin vertical. The pin's weight ensured samples stayed at the bottom of the mould.

After curing for 24 hours the samples were removed from the mould, rough ground using a hand grinder under constant water flow, and cut using a Leica EM UC6 ultra microtome. To remove deformation effects the grinding damage was cut away first. Then the sides of the sample were cut to a 45° bevel leaving a truncated rectangular pyramid. Finally to prepare the surface for observation a cut perpendicular to the sample was made. Cutting was done at temperatures below 25°C with freshly broken glass knives to ensure the best surface finish and minimize the risk of smearing.

To produce contrast between phases and insure the necessary sample conductivity cut

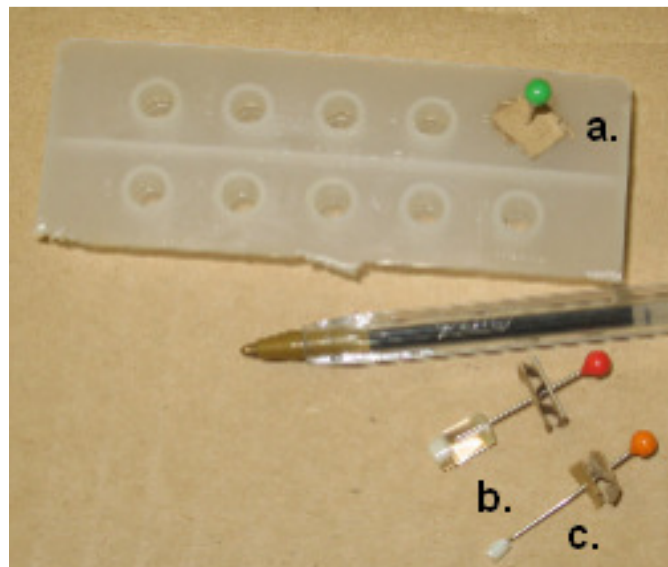


Figure 43: SEM Sample Preparation. sample in mould (a), sample removed from mould and ground (b), sample ready for encapsulation (c)

samples were stained with RuO_4 vapour which is known to stain PC more heavily than PBT [38]. Heavily stained regions bounce electrons back appearing dark in TEM images and light in SEM images. As RuO_4 is toxic and corrosive all staining was conducted in a fume hood. Gloves should be worn while handling chemicals. Material safety data sheets for the chemicals used are provided in Appendix F. Figure 44 shows the layout for staining; Table 14 provides an equipment list. A step by step breakdown of the staining methodology and procedure follows.

1. Four to six mounted samples were placed in custom sample holders as shown in Figure 45. It is important for proper grounding in the SEM that sufficient length of the sample mount be exposed to staining.
2. The lid from a 100mm disposable Petri dish was placed in the fume hood.
3. 0.1g of RuCl_3 powder in an uncovered 10mm disposable Petri dish was placed in the center of the lid.
4. Sample holders were arranged symmetrically in the lid about the central dish.



Table 14: Staining Supply List

Item	Quantity
Sample Holders	6ea
100mm Ø x 15mm Petri Dish & Lid	1ea
35mm Ø x 10mm Petri Dish	1ea
Pipet, 7ml, plastic, disposable	1ea
Vial, poly stopper, 4 dram	1ea
Chemical Spatula	1ea
RuCl_3	0.1g
NaIO_4	0.3g
H_2O	5.0g

Figure 44: Samples arranged for staining.

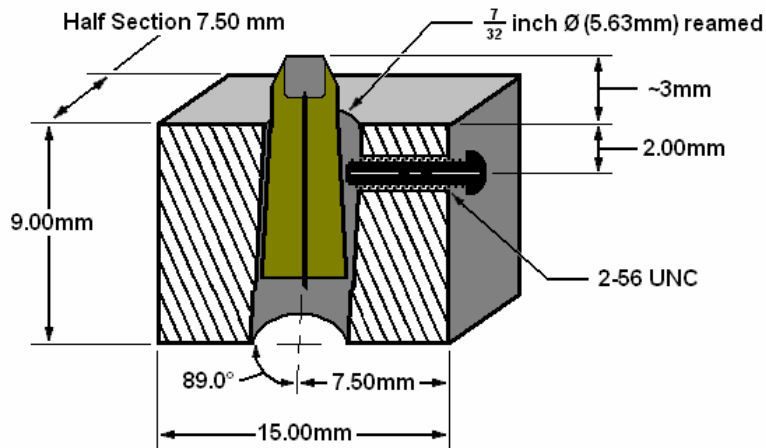


Figure 45: Sample positioned in holder for staining

5. Using a pipette, the lid was flooded with distilled water. Later this water will serve as a seal to prevent RuO_4 from escaping.
6. 0.3g of NaIO_4 was added to 5g of distilled water in a vial. The vial was stoppered and agitated until all crystals dissolved.
7. With the large Petri dish handy the solution from step 6 was poured into the small Petri dish. The large Petri dish was immediately placed on top to contain the RuO_4 vapour produced by the reaction.

To optimize staining time, a set of as-received samples from a single blend were stained for 30, 60, 120 and 180 minutes. The trials showed that at least 3 hours of staining was needed to obtain reasonable contrast. When annealed samples were eventually tested, it was found that 4 hours and longer was sometimes necessary to produce adequate contrast.

3.4.4 Heat Treatment

The purpose of annealing is to erase thermal history of the extruded resin, to equilibrate the blend phases and to improve contrast. The DSC instrument described in section 1.3.6 above was used for sample annealing. Whole pellets were placed in hermetic sealing pans and dried in a vacuum oven at 120°C for at least three hours. Immediately after removal from the oven the pans were placed unsealed and without lids in the DSC where they were heated at $5^\circ\text{C}/\text{minute}$ to 250°C . To determine the best annealing time, they were held at this temperature for 2, 4, and 16 minutes before being cooled at $5^\circ\text{C}/\text{minute}$ to room temperature. In Figure 46, the results of annealing are compared. Minimal changes in phase size are observed between samples after the first 2 minutes. A hold time of 4 minutes was selected for the final test series

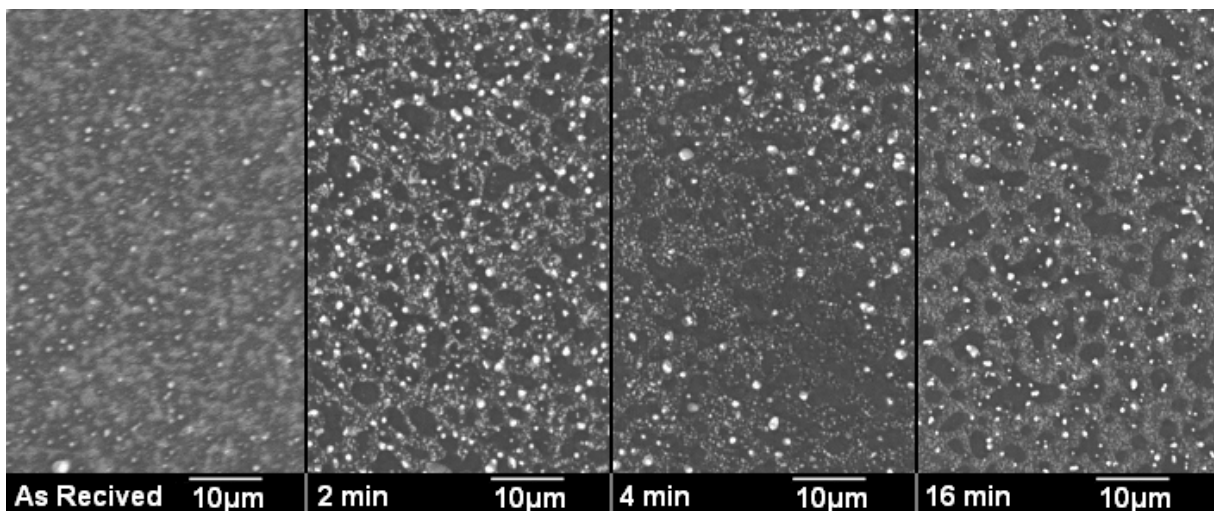


Figure 46: Annealing Time Comparison

with all 13 blends because it provided the best comparison with DSC results. This heat treatment is identical to that received by DSC samples prior to property measurement.

3.4.5 Instrument and Settings

Samples were imaged with a JEOL JSM-6460 SEM. To prevent sample burning or charging acceleration voltages of 10 and 15kv were used. Sample surfaces were almost flat minimizing depth of field as an image quality concern. For this reason, the work distance was kept at a minimum. Under these conditions resolution of approximately 0.5 microns was obtained. This was insufficient to obtain useful detail in as received samples which prevented testing of all 13 blends with these samples. . However, it was possible for the annealed samples which had a phase size was in the order of 10 microns. A maximum of six samples could be stained in a single batch or imaged in a single session necessitating three groups for the full series. Sampling order was randomized to limit session effects on results. Table 15 lists staining batch and SEM session for each of the blends from section 3.1. Appendix G contains a full set of SEM images.

Image contrast was not consistent between SEM sessions. In particular contrast was much better for the first session than subsequent ones. This was initially attributed to staining differences and random variation in electron gun performance. Samples were re-stained for the third session in an attempt to improve contrast. In the re-stained samples improvement was observed but the initial image quality was not obtained. The signal-to-noise ratio in later images was low, and images from the first session were much brighter. Also charging was

Table 15: Staining Batch and SEM Session for Annealed Blends.

Stain Batch	1					2				3,4			
SEM Session	1					2				3,4			
Blend Number	4	3	1	10	2	12	8	6	11	5	9	7	13

markedly higher in the first session. All of these challenges point to a higher probe current which could be caused by larger aperture being used during the first session. It was intended that the standard aperture size of 30µm be used for all sessions because re-alignment of the beam is sometimes necessary for non-standard apertures.

In the first session, the heavily stained PC rich continuous phase showed good conductivity, but apart from a dark ring around their perimeter a flat glow associated with charging obscured PBT rich droplets in secondary electron mode. Good signal-to-noise ratio in back-scatter mode resulted in clear images with adequate contrast to separate PC rich phase sub-structure. Back scatter images from subsequent sessions are noisy but less charging resulted in good secondary electron images. Contrast in back scatter mode was expected and is easily explained due to the atomic weight effect of the Ru on the back-scattering coefficient of stained polymer. The secondary electron contrast can be attributed to the staining agent chemically degrading the blend and possible causing it to swell due to the presence of Ru.

3.4.6 Image Analysis

To obtain a quantitative measurement of phase size, the areas of each particle in each image were measured using ImageJ 1.41g, an image analysis software package developed by the US department of health. The particle measurement module requires a dark/light threshold to be set in order to define phase boundaries. On high contrast images this could be done easily using ImageJ. In noisy or low contrast images, phase boundaries were manually defined over portions of the image using the select similar function in GIMP 2.4.7. This function selects areas of an image that are within a set range of the chosen colour. Figure 47 shows the original image, the threshold mask for image analysis, and the particle boundaries identified by ImageJ. To summarize size data for statistical analysis, phase size statistics were calculated. Because each image contained a distribution of sizes, no one statistic was felt to accurately describe the entire range. For this reason in addition to the average, the median and

upper/lower quartile phase areas are also reported. The reported statistics are calculated on an area basis as this is a better representation of significance within the blend than number average statistics.

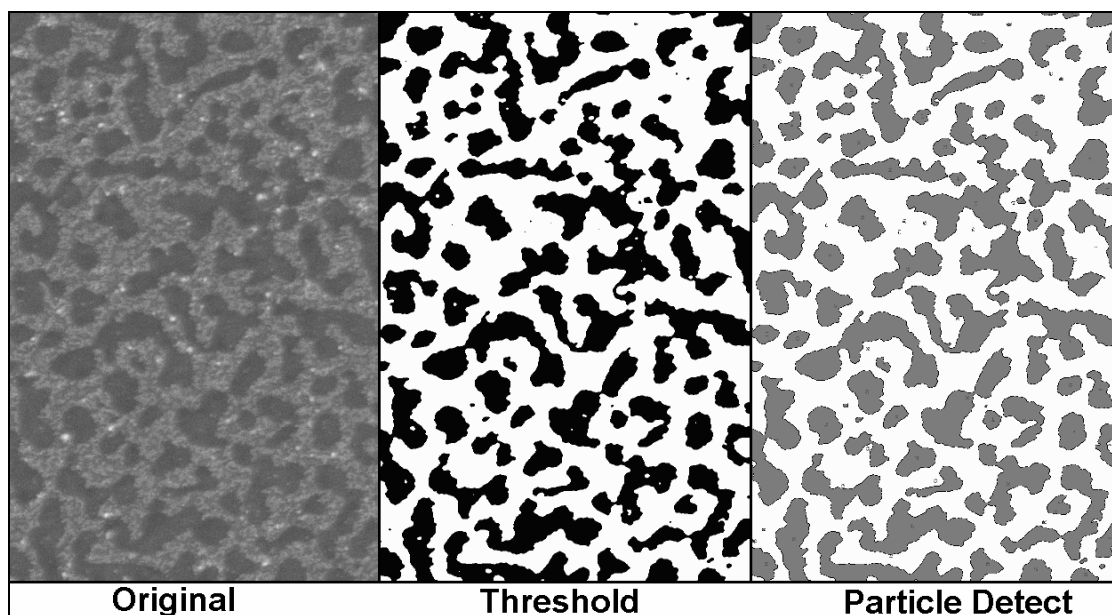


Figure 47: Image Analysis Stages

4.0 RESULTS AND DISCUSSION

In this work, the influence of processing on blend properties has been determined by characterising the blend properties for the set of processing conditions investigated. Blend properties which were analyzed include phase sizes, transition temperatures, estimated phase compositions, estimated phase weight fractions, and MVR measurements. The latter were performed by Noeei [5]. The measured die pressure, specific energy consumption and blend temperature during extrusion were also analyzed to verify the analysis procedures and provide a better understanding of the sensitivity of processing conditions.

The first section of this chapter describes the analysis methodology used followed by results in the subsequent sections. Results are divided into three main categories. First, the effects of blend composition inherent to the blend but not specifically related to processing are discussed under the section “Blend Properties”. An attempt has been made to determine the general type of PC/PBT blend studied and how it compares with respect to published PC/PBT blend data. In the section “Processing environment”, the effects of measured die pressure, specific energy consumption and blend temperature during extrusion are discussed. Finally, the remaining properties and how they are influenced by the process variables are discussed in the “Effects of Processing” section.

4.1 Linear Regression Analysis

4.1.1 Model Development

The statistical design used for the extruder experiment in section 3.1 is similar to those often used for linear regression in that five replicates at one point provide the estimate of variability. Linear regression is used to determine the significance of controlling factors on blend properties.

Of the three factors, only PBT content (composition) has direct physical significance. The significance of the other two factors, screw speed and feed rate, is found in their control of other mechanical processing variables, mainly SEC, residence time, shear rate and extruder degree of fill. Linearized relationships between these factors have been determined by others as described in section 2.4.2. These relationships provide model terms of known physical significance for determining the effects of processing. Accordingly, a new expression given in Equation 49 has been developed to provide the functional form for the most general model. In the equation, the ‘y’ term can represent temperature, phase size or any of the other measured properties. When using coded variables the constant β_0 represents the value of the ‘y’ term at the experimental center point. The source equation and physical significance of the additional terms is summarised in Table 16. Also provided are the coded values for each term calculated using Equation 38 from the conditions measured during the factorial experiment. These

Table 16: Coded Regressor Variables for Property Modeling

Blend Number	Shear	Degree of Fill	Specific Energy Consumption		Residence Time		PBT Content
	Eq. 31	Eq. 32	Eq. 33		Eq. 34		---
	$\log(N)$	Q/N	N	N^2/Q	$1/Q$	$1/N$	w_i
1	0	0	0	0	0	0	0
2	0.16	-0.21	1	1.85	-0.72	-0.91	-1.28
3	0.16	1.1	1	3.43	-1.81	-0.91	0
4	0	0	0	0	0	0	0
5	-0.18	1.1	-1	-1.01	0.01	1.11	0
6	0	0	0	0	0	0	0
7	-0.18	-0.21	-1	-2.07	1.35	1.11	-1.28
8	0.16	-0.92	1	0.99	0.01	-0.91	0.00
9	0	0	0	0	0	0	0
10	0.16	0.22	1	2.36	-1.1	-0.91	1.28
11	0	-0.92	0	-0.92	1.01	0	0
12	-0.18	0.22	-1	-1.72	0.88	1.11	1.28
13	0	0	0	0	0	0	0

provide the ‘x’ values or regressor variables for the linear regression analysis. Values are coded so that the coefficients β_1 to β_7 determined by linear regression analyses represent the effect on the ‘y’ term of a 10% increase in the associated regressor variable.

$$y = \beta_0 + \beta_1 \log N + \beta_2 \frac{Q}{N} + \beta_3 N + \beta_4 \frac{N^2}{Q} + \beta_5 \frac{1}{Q} + \beta_6 \frac{1}{N} + \beta_7 w_i \quad \text{Equation 49}$$

Regressor variables must be linearly independent for analysis to be effective. The functional forms of each term are different making this possible in large data sets. However, due to the limited number of samples in this work, there is the potential problem of co-dependence. This can both mask significant effects, and produce erroneous determinations of significance. Figure 48 plots each of the other mechanical terms against screw speed. It can be seen that the other terms solely dependent on screw speed are closely correlated with it. For this reason they have been removed from the simplified model, Equation 50.

$$y = \beta_0 + \beta_2 \frac{Q}{N} + \beta_3 N + \beta_4 \frac{N^2}{Q} + \beta_5 \frac{1}{Q} + \beta_7 w_i \quad \text{Equation 50}$$

Four mechanical terms remain. The simplest two, N and 1/Q are also the most independent pair. Therefore these two are used to form the basis of three factor clusters. In Figure 49, it can be seen that these are almost linearly dependent. Due to this dependence erroneous results are likely if more than three mechanical factors are fit simultaneously. This

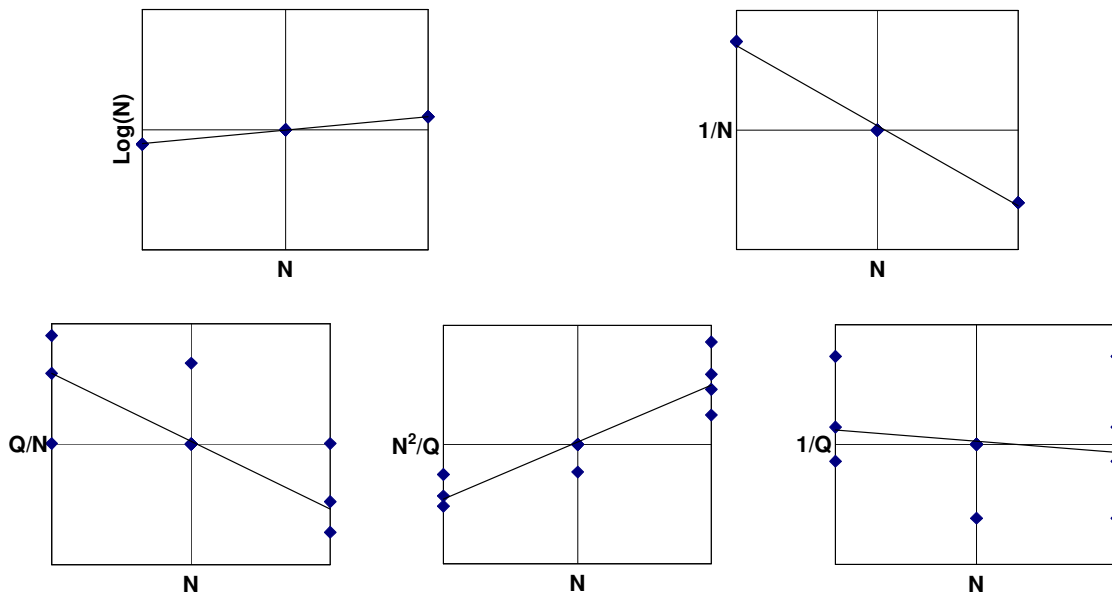


Figure 48: Linear Independence Check for Factor Pairs

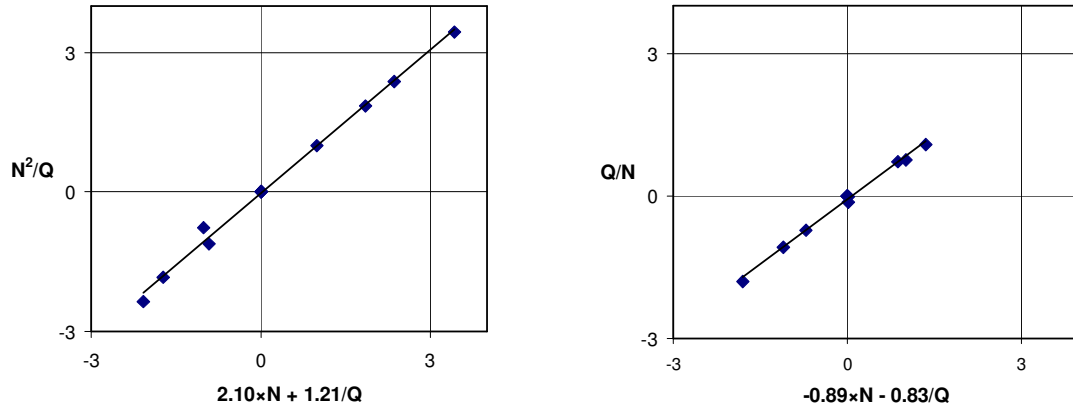


Figure 49: Linear Independence Check for Three factor Groups

gives rise to the final models Equations 51 and 52. Equation 51 assumes that the significance of extruder fill is primarily due to its influence on specific energy consumption. This model was found to be good for analysing the properties of the processed polymer where this assumption holds. In modeling within the processing itself, it was found that the inclusion of degree of fill is required as it affects other non-SEC variables such as die pressure and temperature. For this reason Equation 52 is proposed as a possible alternative when modeling die pressure and temperature.

$$y = \beta_0 + \beta_3 N + \beta_4 \frac{N^2}{Q} + \beta_5 \frac{1}{Q} + \beta_7 w_i \quad \text{Equation 51}$$

$$y = \beta_0 + \beta_2 \frac{Q}{N} + \beta_3 N + \beta_5 \frac{1}{Q} + \beta_7 w_i \quad \text{Equation 52}$$

4.1.2 Regression Implementation

To fit Equations 51 and 52 to the measured and calculated properties and test each term for significance the linear regression procedure outlined by Montgomery [147] was implemented in MATLAB. The MATLAB code provided in Appendix H was validated by comparing results to those obtained in SPSS for a single data set. Moreover, to ensure that only significant terms were included in the fitted model, an iterative procedure was used for each data set. The following 3 steps were followed.

1. The model was fit to using MATLAB code.

2. Student's t tests were conducted on each term using the total error sum of squares.
3. If all terms were significant at a 90% confidence level the model was accepted. Otherwise the least significant term was removed and analysis returned to step 1.

The above procedure prevents the omission of an important mechanical term but might result in an erroneous model with all three mechanical variables present. This is due to induced correlation. A further check on such models was conducted. If all three mechanical terms are important, removing a term should increase the significance of the others. Otherwise removing a term will make the others less significant. In future work a better check of results can be obtained by plotting joint confidence intervals for all model parameters. These have been included for the current work in Appendix I but are not referred to in the discussion.

To evaluate quality of the models significance and lack of fit statistics were calculated. Models were considered significant if 95% confidence level was obtained from the F test between the regression mean square and the total error mean square. Lack of fit was computed by partitioning the error sum of squares into a random error component and a component associated with poor model/data agreement. Mean squares are computed from these components and an F test is again conducted. Table 17 provides the significance levels for each statement regarding the fit statistic. The model results are provided in the following sections.

Table 17: Significance Levels for Fit Quality Categories

Fit Quality	Lack of Fit Significance
Excellent	below 50%
Good	50-80%
Ok	80-90%
Poor	above 90%

4.2 Blend Properties

4.2.1 Crystalline Phases

Figure 50 shows that the weight fraction crystalline material in the blend is proportional to blend composition, but not the PBT crystallinity which is defined as the fraction of PBT that crystallizes. This is consistent with the work of Halder *et al.* [58]. What is, however, surprising is that the crystallinity in blends in Table 18, is greater than that of the pure PBT. This could be attributed to improved nucleation due to the presence of polycarbonate or other additives. The increased crystallization temperature observed for blends further supports this hypothesis. Higher melting temperatures in blends may also be related to this, or be the result of thicker crystal lamella formed at the higher crystallization temperatures. When the rule-of-mixtures calculations are compared in Figure 51 to a typical blend result, it is apparent that

Table 18: Crystalline Phase Result Summary (5°C/min DSC)

		Blends**	Pure PBT**	Probability of Difference
Crystallinity	wt%	32.7±0.5	27.7±3.6	>99%
Crystallization Temperature	°C	198.4±0.2	194.7±7.7	>99%
Small Melting Temperature	°C	212.2±0.2	210.2±1.1	>99%
Small Peak Area*	J/g	12.5±0.5	6.6±2.8	>99%
Main Melting Temperature	°C	220.1±0.1	219.3±0.7	>99%
Main Peak Area*	J/g	33.4±0.7	32.2±4.0	68%

* Normalized To 100% PBT

** ±x Represents 95% Confidence Interval

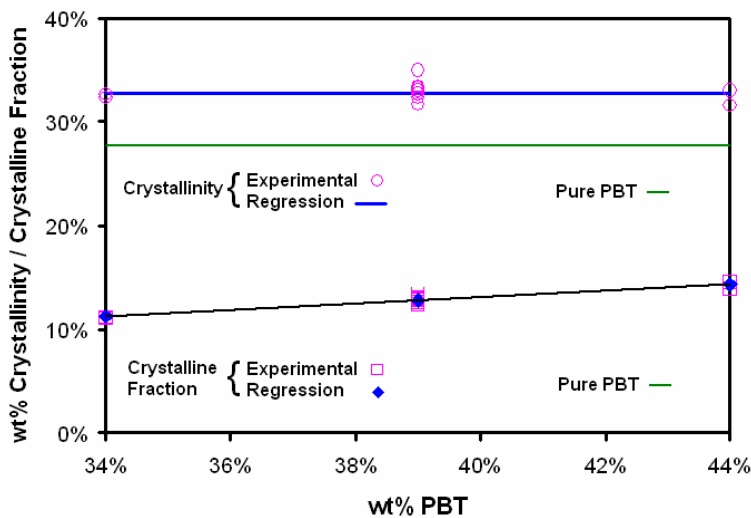


Figure 50: Crystalline fraction and crystallinity versus blend PBT content.

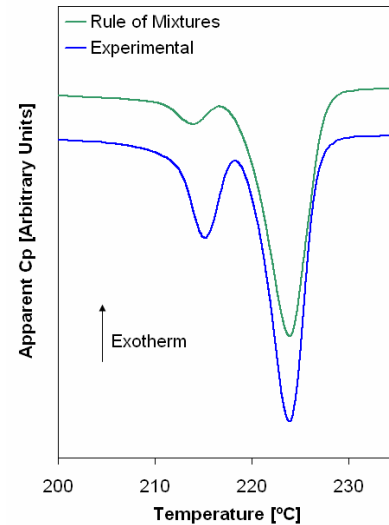


Figure 51: Typical melting results (5°C/min DSC)

much of the increase in blend crystallinity is due to the smaller initial peak. It is difficult to conclude if this is due to secondary crystallization of PBT out of the PC rich phase, or due to changes in the crystal-size distribution resulting from the presence of PC and other additives. All that can be said with certainty is that the effect of blending is concentrated in the lower melting crystals. One other important observation is that the observed crystallization behaviour is similar to that of well stabilized blends containing little co-polymer.

4.2.2 Amorphous Phases

Two glass transitions are identified for the blend in Figure 52, indicating the presence of two amorphous phases. Regression analysis indicates that these temperatures are unaffected by processing and composition. This means that phase compositions are constant in all blends and is in agreement with current knowledge regarding phase diagrams. Comparing the rule of mixtures result in Figure 52 to experimental results, it can be seen that in blends the glass transitions have become more diffuse and have shifted closer together. This is interpreted as partial miscibility between the phases. Phase compositions were calculated using the three different equations available. As seen in Figure 53, the best agreement between known blend composition and calculated composition was found using the Utracki-Jukes equation, Equation 13, with $k = 0.41$. This value is in the same range as that determined by Wilkinson *et al.* [36] for PC/PBT assuming that they used PBT as polymer 1. The amorphous phase compositions determined in this manner are tabulated in Table 19.

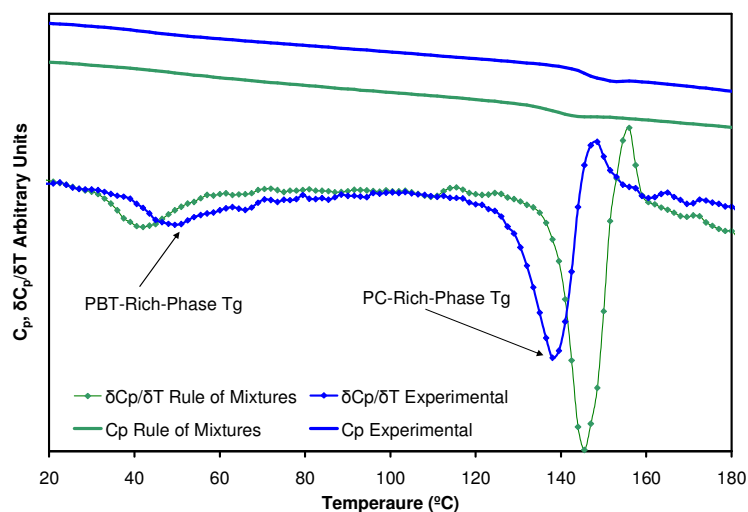


Figure 52: Typical glass transition results (5°C/min DSC)

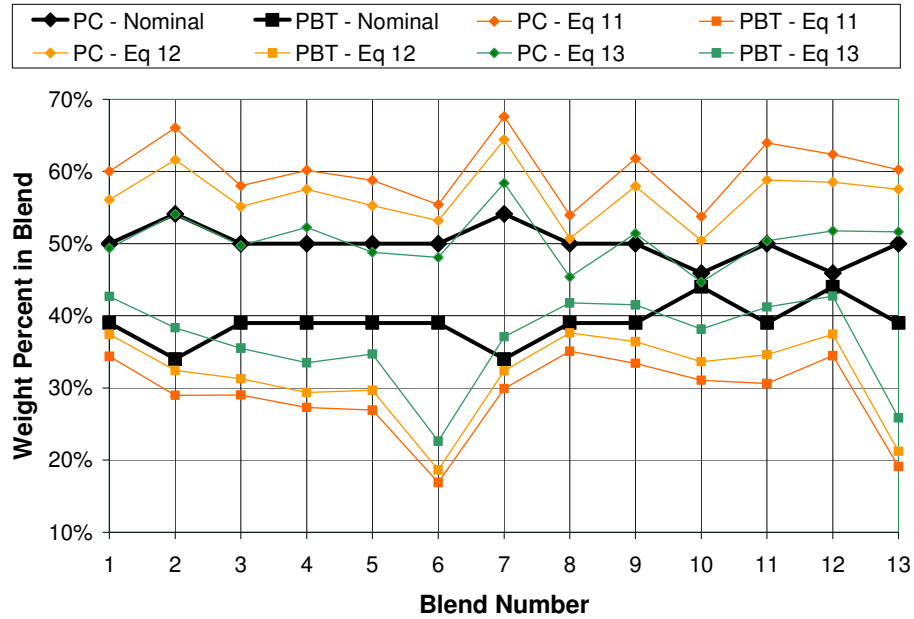


Figure 53: Blend composition calculated using DSC results

One concern with the phase composition results is that contrary to published reports, [26,82], PBT is estimated to be more soluble in PC than PC in PBT. This discrepancy may result from differences between the widely used Fox equation and that of the Utracki Jukes expression. The possibility of an actual composition closer to the Fox equation predictions can be largely ruled out. Crystallinity values in excess of the maximum in Table 6 (Section 1.1.1) are produced if such a low overall PBT content is assumed, which is highly unlikely. One other possible source of error is the assumption of only two phases. Some experimental results in Appendix E show multiple small peaks in the PBT-rich-phase glass transition. These might represent noise in the data, or different amorphous phases formed at different temperatures with different glass transitions. A possible explanation for the low PBT content registered in blends 6 and 13 is the existence of an amorphous phase outside of the studied temperature

Table 19: Amorphous Phase Composition Results (5°C/min DSC)

	PC Rich Phase			PBT Rich Phase			Crystalline PBT*	Blend Totals	
	PC	PBT	wt% in Blend*	PC	PBT	wt% in Blend*		PC*	PBT*
Fox equation (Eq 11)	97%	2.9%	58%	21%	79%	18%	13%	60%	29%
Utracki Jukes (Eq 13)**	87%	13%	57%	5.7%	94%	18%		50%	37%

*Average across all 13 blends

**k = 0.41, PBT = polymer 2

Table 20: PC Rich Phase Glass Transitions

	T _g °C	PBT Mw	PC Mw
Hamilton and Gallucci [9]	116.3	70,380 g/mol	18,000 g/mol
Cheng and coworkers [82]	135-138	65,000 g/mol	19,100 g/mol
Experimental Results*	138.0±0.5	**	**

* ±x Represents a 95% Confidence Interval, 5°C/min DSC

** Exact Molecular Weights are Confidential

range. In addition to the rigid amorphous fraction studied, a wholly amorphous fraction has sometimes been observed in pure PBT. Table 6 (Section 1.1.1) gives a transition temperature of -25°C for this phase.

When comparing the blends studied here to the phase diagram prepared by Delimoy *et al.* [26] both the effects of co-polymer and molecular weight must be taken into account. The PC molecular weights used here are in a similar range to the lowest used in Figure 27 (Section 2.2.2), while the PBT molecular weight is close to the mid range one used by Hamilton and Gallucci [9]. These are significantly lower than those of Delimoy *et al.* [26] but should not be an issue as Figure 27b suggests that provided the blend is well stabilized only minor changes in phase diagram are expected between these molecular weights. Crystallization data has already indicated good stabilization; however, verification is always useful. Table 20 shows that when glass transition temperatures for blends of similar molecular weights are compared those from this study the values are much closer to those of Cheng and coworkers [82] than Hamilton and Galucci's [9]. This is a further sign of good stabilization. Due to their stability and molecular weights the phase diagram for the blends studied here should be similar to Figure 25 (Section 2.2.1). One conclusion that can be drawn from the phase diagram is that all blend / processing condition combinations in this study are within the two phase region. Further more, rapid phase separation by spinodal decomposition is expected.

4.2.3 Phase Structure

In SEM images of annealed blends such as Figure 54, a complex multi phase structure is visible. Darker regions are identified as being rich in PBT, while light regions are rich in PC. Two primary phases are observed to have formed during annealing, a continuous PC-rich-phase and a discrete PBT-rich-phase. As would be expected from Figure 25 (Section 2.2.1), the blend phase diagram, the PC rich phase has separated into two sub phases during cooling. That a similar separation is not observed in the PBT rich phase is also explained by the phase diagram. The time/temperature window for separation to occur during a DSC scan is limited

by glass transitions and crystallization. Before crystallisation, there is half as much time available for separation in the PBT-rich-phase than is available to the PC-rich- phase, Also, the driving force for separation is lower at higher temperatures and PBT can crystallize as it separates out of the PC-rich-phase making separation less reversible and therefore more rapid. The PBT rich phase is expected to have a two-phase structure formed at crystallization; however, the phase size will be in the order of the crystal lamella preventing direct observation by SEM.

Phase size statistics calculated for each blend are given in Table 21. Regression analysis of these results indicates both upper and lower quartile phase sizes are increased by increasing PBT content. Figure 55 graphically compares the regression fit and experimental results, while Table 22 gives the model coefficients and statistical indicators. As can be seen, though excellent fit is found in both cases, the probability of significance is reduced by the large scatter in the data. No trend was found for median and average phase sizes.

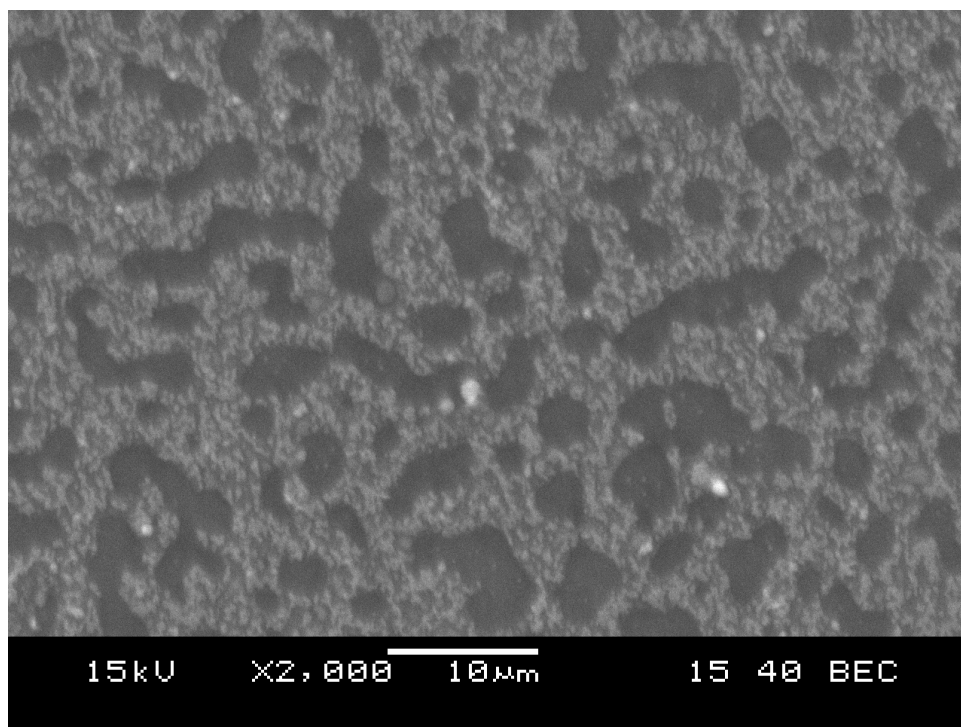


Figure 54: Typical Phase Structure of an Annealed Blend

Table 21: Phase Area Statistics in μm^2

Blend Number	Average	Top Quartile	Median	Bottom Quartile
1	21.63	33.56	14.62	8.86
2	15.51	22.74	14.10	6.06
3	30.87	43.33	27.10	11.33
4	7.26	10.40	6.25	3.32
5	51.58	52.38	40.25	10.60
6	12.93	16.84	10.71	5.98
7	5.68	8.35	4.85	2.56
8	79.25	81.66	42.25	13.62
9	19.57	24.40	15.24	7.86
10	20.16	27.15	20.78	10.06
11	10.82	16.33	9.34	6.82
12	34.81	93.21	25.07	11.85
13	32.08	46.94	24.05	10.90

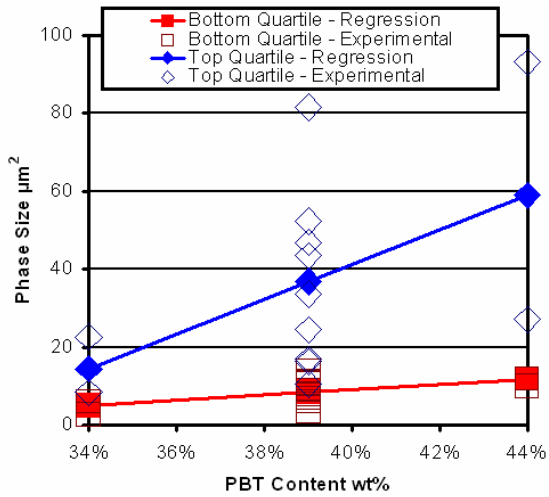


Figure 55: Phase Size Regression Results

Table 22: Phase Size Regression Results

	Bottom Quartile	Top Quartile
Regression Significance	96%	91%
Fit	Excellent	Excellent
Units	μm^2	μm^2
β_0 Intercept	8.4	36.7
β_3 N	---	---
β_4 N²/Q	---	---
β_5 1/Q	---	---
β_7 Composition	2.6	17.4 (91%)*

*Coefficient significance in model is greater than 95% unless otherwise indicated.

4.3 Processing Environment

4.3.1 Specific Energy Consumption (SEC)

Term 2 of Meijer equation [128] for specific energy consumption simplifies to N^2/Q . It can be seen in Figure 56 that this term provides a good fit for the specific energy consumption measured at the time of compounding. Table 23 shows that, as expected, no other variables were found to be significant, partially validating the fitting procedure.

4.3.2 Die Pressure and Blend Temperature at Extruder Exit

Die pressure and melt-exit-temperature are closely related as both measurements are taken at the same point in the extruder. In Tables 24 and 25, the regression model results for both response variables are given. Two starting assumptions are possible. First, SEC is important and degree of fill is not as in Equation 51. Conversely, the degree of fill is important and SEC is not, Equation 52. For both die pressure and melt-exit temperature, the models resulting from Equation 52 provide a better fit with fewer parameters. The use of Equation 51 results in unexpected dependences which is most likely due to the co-dependence between the two remaining variables and the excluded extruder fill parameter. To verify this hypothesis, the physical implications of the two competing models are examined.

Under Equation 51 die pressure, (y), increases with increasing specific energy consumption (β_4) and residence time (β_5). A physically possible explanation for this model is that both regressors result in increased melt temperature and therefore decreased viscosity.

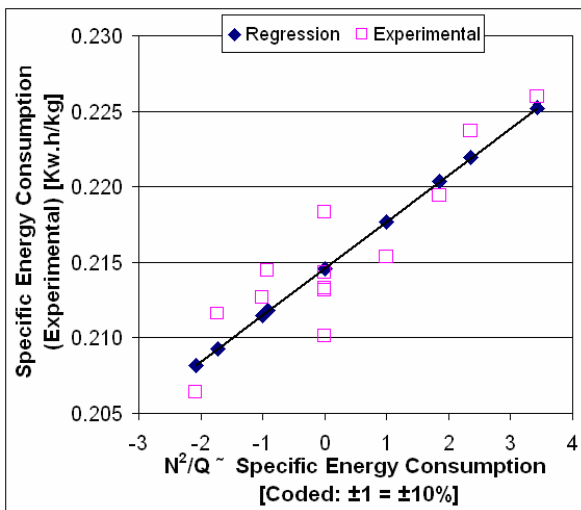


Figure 56: SEC Regression Results

Table 23: SEC Regression Results

	SEC
Regression Significance	>99%
Fit	OK
Units	Kwh/kg
β_0 Intercept	0.21
β_3 N	---
β_4 N^2/Q	0.0031
β_5 $1/Q$	---
β_7 Composition	---

The die pressure model using Equation 51 would predict a temperature increase but when Tables 24 and 25 are compared, we see that this is not the case. The result from Equation 52, states that as the filled volume in the extruder, (β_2), is increased, die pressure increases and temperature decreases. This is exactly as expected based on the physics confirming the initial hypothesis that Equation 52 provides the accurate predictions.

According to the analysis in Tables 24 and 25, neither equation affects the composition term, (β_7), as demonstrated by the similar results regardless of the model used. As was expected, higher PBT content results in a lower viscosity blend and therefore lower die pressure. Decreasing temperature at the extruder exit point with increasing PBT content is consistent with the PBT latent heat of fusion being a significant factor in temperature control. Figures 56 and 57 plot the relationship between the processing environment and its most important influencing factors. The regression results in each of these plots represent the model developed using Equation 52.

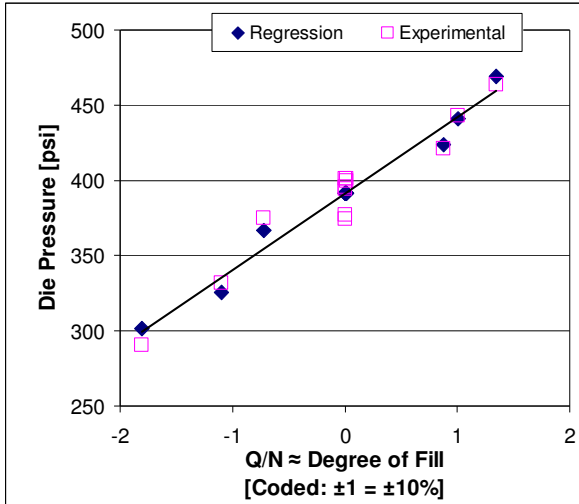


Figure 57: Die Pressure Regression Results

Table 24: Die Pressure Regression Results

Equation	51	52
Regression Significance	>99%	>99%
Fit	Excellent	Excellent
Units	psi	psi
β_0 Intercept	396	391
β_2 N/Q	N/A	49.5
β_3 N	---	---
β_4 N ² /Q	-22.6	N/A
β_5 1/Q	-24.6	---
β_7 Composition	-8.8 (93%)*	-8.5 (94%)*

*Coefficient significance in model is greater than 95% unless otherwise indicated.

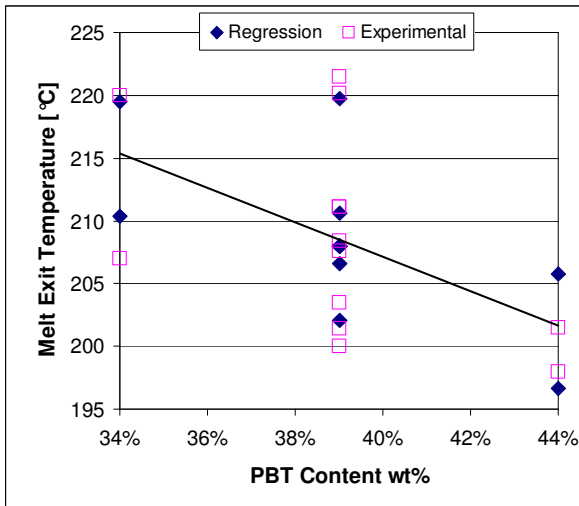


Figure 58: Melt Exit Temperature Results

Table 25: Melt Exit Temperature Results

Equation	51	52
Regression Significance	96%	>99%
Fit	Excellent	Excellent
Units	°C	°C
β_0 Intercept	208	208
β_2 N/Q	N/A	-5.5
β_3 N	4.6 (92%)*	---
β_4 N ² /Q	---	N/A
β_5 1/Q	6.5 (94%)*	---
β_7 Composition	-6.5	-6.3

*Coefficient significance in model is greater than 95% unless otherwise indicated.

4.4 Effects of Processing

4.4.1 Molecular Weight

The molecular weight rule of mixtures result was produced assuming that the effects of additives on the molecular weight distribution are negligible. In particular it is assumed that the impact modifier present in the blend was insoluble when GPC solutions were prepared. The changes in molecular weight distribution in Figure 59 between the blend and raw polymer rule-of-mixtures results are interpreted in light of these assumptions. The main thing observed is a small reduction in molecular weight with most of the change concentrated in the largest chains. As PBT is the main contributor to the high molecular weight end of the spectrum this suggests greater degradation of PBT than PC. Preferential degradation of the low viscosity component and the high molecular weight chains is consistent with mechanical degradation in the extruder as described in section 1.3.7. No major changes are observed in the low molecular weight range indicating that the end-group-attack co-polymer formation mechanism was not extremely significant.

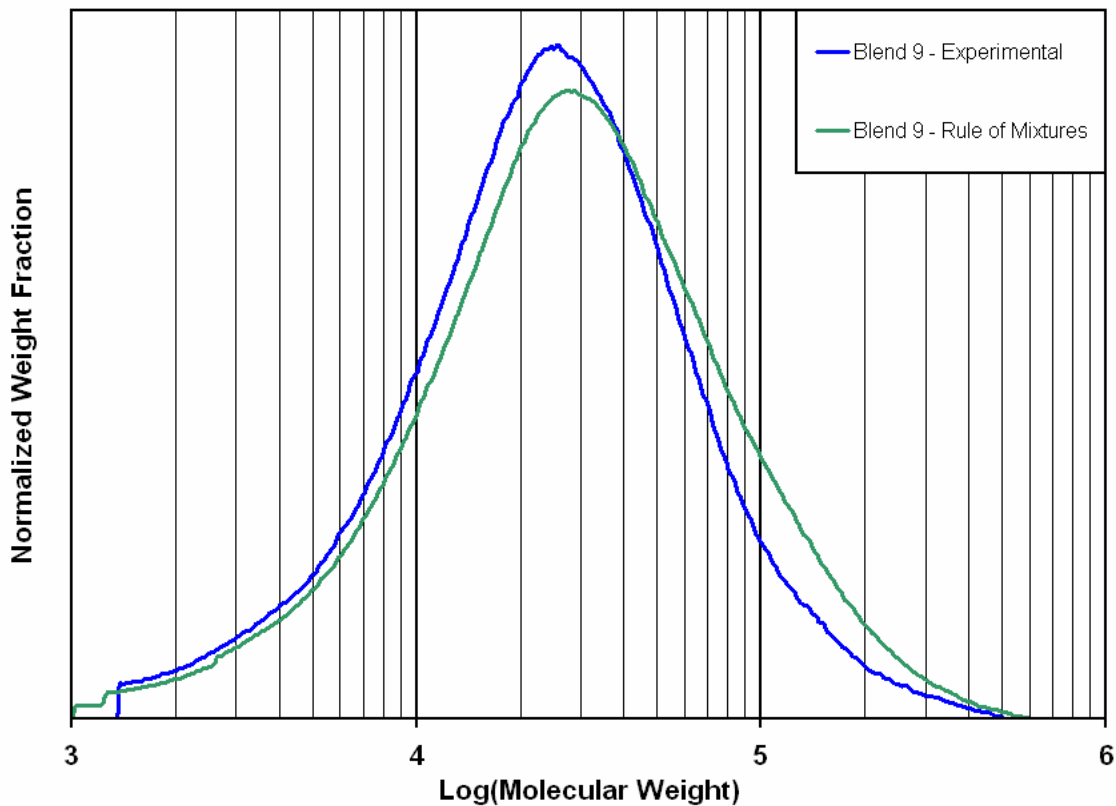


Figure 59: Molecular Weight Change due to Blending

4.4.2 Volumetric Melt Flow Rate

The poor fit observed for the MVR results in Table 26 may indicate that an important term is missing from the model. The second set of results fit using Equation 52 shows that degree of fill is not the missing parameter. The model results indicate that composition is the most important factor controlling MVR, followed by SEC. Figure 60 graphically compares the model to the experimental results.

4.4.3 Phase Size

No statistically significant phase size changes due to processing were observed. This does not necessarily rule out significant effects. Larger than anticipated random scatter was observed and has the potential to mask significant effects due to the small sample size. More results are necessary to conclusively say if there is any effect of processing on the annealed phase size. Examination of the images in Figure 61 indicates that there may be decreases in phase size with increasing extruder fill. Variations in image quality and contrast make even this visual determination difficult.

4.4.4 PBT Melting Temperatures

No consistent pattern of processing effects on melting temperature is observed between the two heating rates in Tables 27 and 28. This may be due to melting kinetic differences between the two tests. However, as all the effects are smaller than what is practically

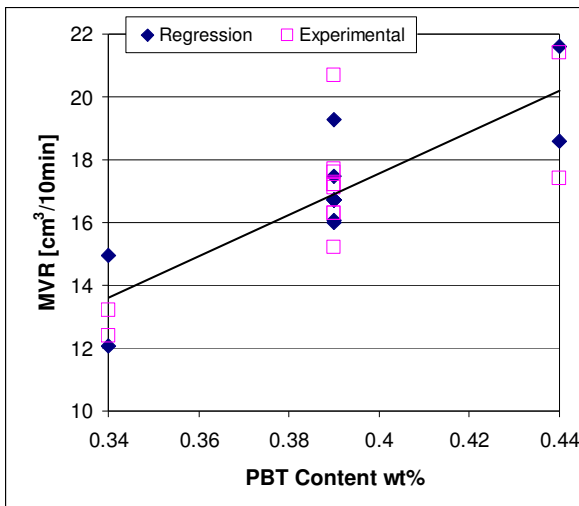


Figure 60: MVR Regression Results

Table 26: MVR Regression Results

Regression Significance	>99%	>99%
Fit	Poor	Poor
Units	cm ³ /10min	cm ³ /10min
β_0 Intercept	16.7±0.9	16.8
β_2 N/Q	N/A	---
β_3 N	---	1.4
β_4 N ² /Q	0.7±0.6	N/A
β_5 1/Q	---	1.4
β_7 Composition	2.5±1.3	2.3

significant the exact reason for this discrepancy is not of great importance. As a decrease rather than an increase in melting temperature would be expected if transesterification were the cause [65], the small increase in melting temperature with increased residence time is not associated with this reaction.

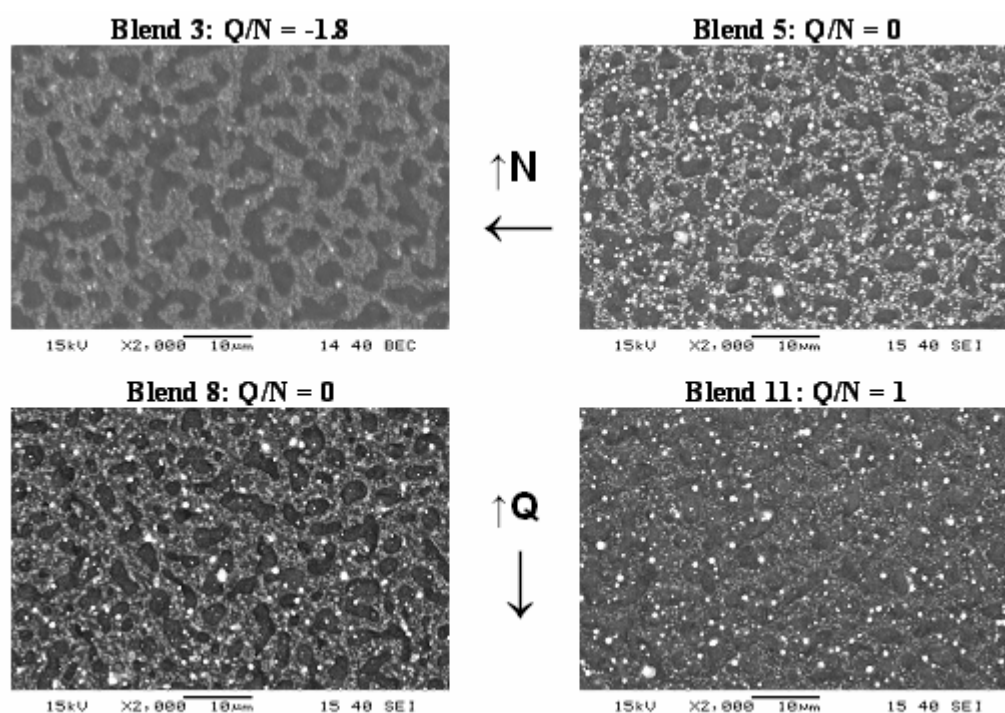


Figure 61: Blends with identical composition but different processing.

Table 27: Main Melting Regression Results

DSC Rate	5 °C/min	10 °C/min
Regression Significance	97%	98%
Fit	Excellent	Ok
Units	°C	°C
β_0 Intercept	220.1±0.1	218.5
β_3 N	---	---
β_4 N ² /Q	---	0.06
β_5 1/Q	0.17±0.16	---
β_7 Composition	---	0.09

Table 28: Small Melting Regression Results

DSC Rate	5 °C/min	10 °C/min
Regression Significance	>99%	N/A
Fit	Good	Excellent
Units	°C	°C
β_0 Intercept	212.2±0.1	211.9
β_3 N	---	---
β_4 N ² /Q	---	---
β_5 1/Q	0.31±0.25	---
β_7 Composition	0.34±0.20	---

4.4.5 Fraction PC-Rich-Phase

Table 29 shows the regression analysis results of the heat capacity change over the glass transition range. The results show that both composition and screw speed have similar effects on the heat capacity change measured at the PC-rich-phase glass transition. It is known that the height of the step change (e.g. Figure 9 Section 1.4.2) over the glass transition is proportional to the weight fraction of the phase in the blend. This implies that the observed five percent increase in the weight fraction of the PC-rich phase is indeed significant. The effects of three linearly dependent terms in Equation 49 are combined in the screw speed term. These relate to specific energy consumption, residence time and shear rate. According to our analysis the other terms related to specific energy consumption and residence time are not significant, leaving shear rate as the only possibility for the influence of screw speed. One known effect of the shear rate is to reduce the molecular weight which in turn could affect the PC-rich phase composition and corresponding weight fraction. However, it is clear that the phase composition has not changed based on the glass transition temperature results.

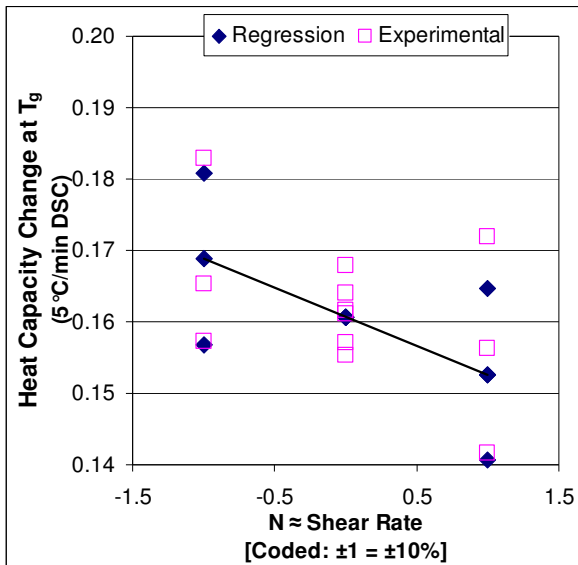


Table 29: PC-Rich-Phase Regression Results

DSC Rate	5°C/min	10°C/min
Regression Significance	99%	98%
Fit	Good	Ok
Units	J/(g·°C)	J/(g·°C)
β₀ Intercept	0.161	0.138
β₃ N	-0.008	-0.008
β₄ N²/Q	---	---
β₅ 1/Q	---	---
β₇ Composition	-0.009	-0.010

Figure 62: PC-Rich-Phase Regression Results

5.0 CONCLUSIONS AND RECOMMENDATIONS

Based on the limited sample set of PC/PBT blends studied for a large scale co-rotating screw extruder, and without reference to the joint confidence intervals in Appendix I, the following conclusions have been made:

5.1 Blend Properties

The blend crystallinity increased after processing as compared to pure PBT. The increase is due to the differences in initial small melting peaks observed using differential scanning calorimetry. As there is no statistical difference in the main peak area before and after processing it is concluded that blending increased the population of low melting point crystallites without affecting the high melting point ones. This is likely caused by improved nucleation as indicated by an increased blend crystallization temperature. Improved nucleation may result from an interaction with PC or with one of the proprietary additives. A small increase in both melting temperatures was observed in the blend; however, it is not expected to be practically significant. The observed crystallization and melting results are consistent with low blend co-polymer content.

Two amorphous phases are predicted based on glass transition data. The composition of these phases is constant with respect to processing and overall blend composition. Of the mixing rules used to calculate phase composition, the Utracki-Jukes equation provided the best fit. The empirical constant was found to be 0.41 with PBT as the second polymer. Glass transition temperatures were similar to those of other low co-polymer content PC/PBT blends of similar molecular weight polymers. Based on comparisons with phase diagrams in the literature, all the blend compositions and processing conditions studied in this work are expected to reside in the two-phase region.

A continuous PC-rich- phase was visible only in the annealed blends. The PBT-rich-phase size was found to increase with increasing PBT content with the average phase area varying between 6 and 79 μm^2 .

5.2 Processing Conditions

The model term N^2/Q was closely correlated with specific energy consumption. This is consistent with the Meijer equations [128]. The most significant influencing factors on die pressure and blend temperature at the die section were found to be extruder degree of fill and blend composition. Blend composition had the most significant effect on temperature, with temperature decreasing with increasing PBT. This is attributed to the energy requirements for PBT melting. Die pressure is most affected by extruder fill, with pressure increasing with increasing fill.

A small decrease in molecular weight was observed after processing, concentrated at the upper end of the molecular weight distribution. This is attributed to mechanical degradation. No practically significant processing effects on PBT melting temperature were measured. The effects of processing conditions on phase size are not considered to be statistically significant, perhaps due to the larger than expected scatter. More study is recommended if practically significant changes in phase size with processing are to be entirely dismissed.

The heat capacity change at the PC-rich-phase glass transition was influenced equally by blend composition and screw speed. The blend composition effect is expected as the heat capacity change is proportional to the weight fraction of material undergoing transition. It was also found that the fraction of PC-rich phase was affected by screw speed, specifically by the shear rate. Although high shear rates can in turn reduce the blend molecular weight and modify phase composition, the glass transitions measurements did not detect compositional changes.

5.3 Recommendations

1. The as-received samples did not provide sufficient phase size or contrast to image with the SEM equipment available for this work. If the phase structure of the extruded pellets is of interest, it is recommended that a TEM study be conducted or an SEM be used with higher resolution to achieve magnifications greater than 10,000X.
2. To better evaluate the quality of the above models discussion of the joint confidence intervals presented in Appendix I should be integrated into future presentations of this work.
3. The commonly used Fox equation provided a poor representation of the blend composition. Use of the Utracki-Jukes equation is recommended for phase composition estimation using the glass transition temperature.

REFERENCES

1. A.W. Birley, Xin Yue Chen (1985) "Further Studies of Polycarbonate-Poly(butylene terephthalate) Blends" British Polymer Journal, **17**, p297-306
2. Huiyu Bai, Yong Zhang, Yinxi Zang, Xiangfu Zang, Wen Zhou (2005) "Toughening Modification of PBT/PC Blends by PTW" Polymer Testing, **24**, p235-240
3. J.M.R.C.A. Santos, J.T. Guthrie (2005) "Polymer blends: the PC-PBT case" Journal of Materials Chemistry, **16**, p237-245
4. L.A. Utracki (1990), "Polymer Alloys and Blends: Thermodynamics and Rheology" Oxford University Press, New York, p8-9
5. Vahid Noeei Ancheh "A Study of Polycarbonate / Poly (butylene terephthalate) Compounding in a Twin Screw Extruder", Masters Thesis, University of Waterloo, 2008
6. L.A. Utracki (1990), p20
7. I. Homfe, G. Pompe, K.J. Eichhorn (1997) "Ordered structures and progressive transesterification in PC/PBT melt blends studied by FTi.r. spectroscopy combined with d.s.c. and n.m.r." Polymer, **38**, p2321-2327
8. J. Jang, K. Sim (1998) "Crystallization Behaviour in Poly(ether Imide)/Poly(butylenes Terephthalate) Blends using a Spectroscopic Method" Polymer Testing, **17**, p507-521
9. D.G. Hamilton, R.R. Galluci (1993) "NOTE: The Effects of Molecular Weight on Polycarbonate-Polybutylene Terephthalate Blends" Journal of Applied Polymer Science, **48**, p2249-2252
10. J. Mark, K. Ngai, W. Graessley, L. Mandelkern, E. Samulski, J. Koenig, G. Wignall, (2004) "Physical Propertis of Polymers", 3rd Ed, Cambridge University Press, p102-104, p213-p214, p253
11. P.C. Hiemenz (1984) "Polymer Chemistry: The Basic Conseptis", CRC Press, New York, p103-106, p164
12. P.C. Hiemenz, (1984), p174-298
13. P.C. Hiemenz (1984), p41-42
14. P.C Hiemenz, (1984), p42, p174-298
15. G. Beaucage, (2005) "Determination of Molecular Weight, MTEN 732: Polymer Characterization –Course Material ", University of Cincinnati
"http://www.eng.uc.edu/~gbeaucag/Classes/Characterization/MolecularWeighthtml/Molecular Weight.pdf" 2007/09/26 09:45
16. G. Sitaramatah, (1965) "Polymer-Solvent Interactions of Bisphenol A Polycarbonate in Different Solvents" Journal Of Polymer Science: Part A, **3**, p2743-2757
17. P.C. Hiemenz (1984), p590-597
18. P.C. Hiemenz (1984), p604-610
19. P.C. Hiemenz (1984), p642-652
20. G. Montaudo, C. Puglisi, F. Samperi (1993) "Chemical Reactions Occurring in the Thermal Treatment of Polymer Blends Investigated by Direct Pyrolysis Mass Spectrometry: Polycarbonate/ Polybutyleneterephthalate" Journal of Polymer Science: Part A Chemistry, **31**, p13-25
21. G. Montaudo, C. Puglisi, F. Samperi (1998) "Mechanism of Exchange in PBT/PC and PET/PC Blends. Composition of the Copolymer Formed in the Melt Mixing Process" Macromolecules, **31**, p650-661

-
22. Huiyu Bai, Yong Zhang, Yinxi Zang, Xiangfu Zang, Wen Zhou (2006) "Toughening Modification of PBT/PC Blends with PTW and POE" Journal of Applied Polymer Science, **101**, p54-62
 23. S. Nabar, D.D. Kale (2007) "Rheology and Transestrification between Polycarbonate and Polyesters" Journal of Applied Polymer Science, **104**, p2039-2047
 24. D.C. Wahrmund, D.R. Paul, J.W. Barlow (1978) "Polyester-Polycarbonate Blends. I. Poly(butylene Terephthalate)" Journal of Applied Polymer Science, **22**, p2155-2164
 25. J. Devaux, P. Godard, J.P. Mercier (1982) "The Transesterification of Bisphenol A Polycarbonate (PC) and Polybutylene Terephthalate (PBTP): A New Route to Block Copolycondensates" Polymer Engineering and Science, **22**, p229-233
 26. D. Delimoy, B. Goffaux, J. Devaux, R. Legras (1995) "Thermal and morphological behaviours of bisphenol A polycarbonate / poly(butylene terephthalate) blends" Polymer, **36**, p3255-3266
 27. P. Sanchez, P.M. Remiro, J. Nazabal (1993) "Physical Properties and Structure of Unreacted PC/PBT Blends" Journal of Applied Polymer Science, **50**, p995-1005
 28. P.G. Kelleher, R.P. Wentz, D.R. Falcone (1982) "Hydrolysis of poly(butylene terephthalate)" Polymer Engineering and Science, **22**, p260-264
 29. A.S. Goje (2006) "Auto-Catalyzed Hydrolytic Depolymerization of Poly(Butylene Terephthalate) Waste at High Temperature", Polymer-Plastics Technology and Engineering, **45**, p171-181
 30. I. Ghorbel, N. Akele, F. ThomINETTE, P. Spiteri, J. Verdu, (1995) "Hydrolytic Aging of Polycarbonate. II. Hydrolysis Kinetics, Effect of Static Stresses" Journal of Applied Polymer Science, **55**, p173-179
 31. GE Plastics "Lexan Processing Guide"
 32. GE Plastics "XENOY PC/PBT Processing Guide"
 33. J. Wu, Y-W. Mai, A.F. Yee, (1994) "Fracture toughness and fracture mechanisms of polybutylene-terephthalate / polycarbonate / impact-modifier blends, Part III: Fracture toughness and mechanisms of PBT/PC blends without impact modifiers" Journal of Materials Science, **29**, p4510-4522
 34. M. Pellow-Jarman, M. Hetem (1995) "The effect of the poly(butylenes terephthalate) constituent of the reactions occurring in poly(butylenes terephthalate) / polycarbonate polymer blends below their decomposition temperature" Plastics, Rubber and Composites Processing and Applications, **23**, p31-41
 35. G. Pompe, L. Häussler (1997) "Investigations of Transesterification in PC/PBT Melt Blends and the Proof of Immiscibility of PC and PBT at Completely Suppressed Transesterification" Journal of Polymer Science: Part B: Polymer Physics, **35**, p2161-2168
 36. A.N. Wilkinson, D. Cole, S.B. Tattum (1995) "The effects of transesterification on structure development in PC-PBT blends" Polymer Bulletin, **35**, p751-757
 37. S.P. Mishra, P. Venkidusamy (1995) "Structural and Thermal Behaviour of PC/PBT Blends" Journal of Applied Polymer Science, **58**, p2229-2234
 38. S.B. Tattum, D. Cole, A.N. Wilkinson (2000) "Controlled Transesterification and Its Effects on Structure Development in Polycarbonate-Poly(Butylene Terephthalate) Melt Blends" Journal of Macromolecular Science: Physics, **39**, p459-479

-
39. J. Wu, K.Wang, D. Yu (2003) "Fracture toughness and fracture mechanisms of PBT/PC/IM blends Part V: Effect of PBT-PC interfacial strength on the fracture and tensile properties of the PBT/PC blends" Journal of Materials Science, **38**, p183-191
 40. A.B. Bestul (1954), "Kinetics of Capillary Shear Degradation in Concentrated Polymer Solutions" Journal of Chemical Physics, **24**, p1196-1201
 41. A. Ram, A. Kadim (1970) "Shear Degradation of Polymer Solutions" Journal of Applied Polymer Science, **14**, p2145-2156
 42. E.M.S. Sanchez (2007) "Ageing of PC/PBT blend: Mechanical properties and recycling possibility" Polymer Testing, **26**, p378-387
 43. A.T. Riga, L. Judovits (2001) "Materials Characterization by Dynamic and Modulated Thermal Analytical Techniques" ASTM, STP 1402
 44. E.A. Turi, (1981) "Thermal Characterization of Polymeric Materials" Academic Press, New York, p185-186
 45. K.-H. Illers, (1980) "Heat of fusion and specific volume of poly(ethelene terephthalate) and poly(butylele terephthalate)", Colloid & Polymer Sci. **258**, p117-124,
 46. Y. Y. Cheng, M. Brillhart, P. Cebe (1997) "Modulated differential scanning calorimetry study of blends of poly(butylene terephthalate) with polycarbonate", Thermochemica Acta **304**, p369-378
 47. J. Runt, D. M. Miley, X. Zhang, K. P. Gallagher, K. McFeaters, J. Fishburn (1992) "Crystallization of Poly(butylene terephthalate) and its Blends with Polyarylate" Macromolecules, **25**, p1929-1934
 48. S.Z.D. Cheng, R. Pan, B. Wunderlich (1988) "Thermal analysis of poly(butylene terephthalate) for heat capacity, rigid-amorphous content, and transition behaviour" Makromol. Chem. **189**, p2443-2458
 49. M.E. Nichols, R.E. Robertson (1992) "The Multiple Melting Endotherms from Poly (butylene Terephthalate)" Journal of Polymer Science: Part B Polymer Physics, **30**, p755-768
 50. R.S. Stein, A. Misra (1980) "Morphological Studies on Polybutylene Terephthalate" Journal of Polymer Science: Polymer Phys. Ed., **18**, p327-342
 51. L. Delbreilh, E. Dargent, J. Grenet, J-M Saiter, A. Bernes, C. Lacabanne, (2007) "Study of poly(bisphnol A carbonate) relaxation kinetics at the glass transition temperature" European Polymer Journal, **43**, p249-254
 52. J. Robertson (2001) "Thermal Degradation Studies of Polycarbonate" Dissertation, Virginia Polytechnic
 53. J. Mark et al (2004), p212-213
 54. E.A. Turi (1981), p141-142
 55. E.A. Turi (1981), p126-131
 56. J. Mark et al (2004), p245-247
 57. L.A. Utracki (1990), p55
 58. R.S. Halder, M. Joshi, A. Misra (1990) "Morphological Studies on the Blends of Poly(butylenes Terephthalate) and Bisphenol-A Polycarbonate" Journal of Applied Polymer Science, **39**, p1251-1264
 59. J. Mark et al (2004), p246-247
 60. J. Mark et al (2004), p209
 61. J. Mark et al (2004), p261
 62. P.C. Hiemenz (1984), p204-206

-
63. P.C. Hiemenz (1984), p216
 64. J. Mark et al (2004), p204
 65. J. Mark et al (2004), p217-219
 66. J. Mark et al (2004), p254
 67. J. Mark et al (2004), p261-267
 68. J. Mark et al (2004), p72
 69. E.A. Turi (1981), p170-171
 70. J. Mark et al (2004), p75-79
 71. P.C. Hiemenz (1984), p244-248
 72. E.A. Turi (1981), p418-420
 73. J. Mark et al (2004), p101-114
 74. J. Mark et al (2004), p102-103
 75. L.A. Utracki (1990), p93-94
 76. L.A. Utracki (1990), p94-99
 77. L.A. Utracki (1990), p2-3
 78. L.A. Utracki (1990), p30-43
 79. L.A. Utracki (1990), p43-52
 80. L.A. Utracki (1990), p64-117
 81. M. Okamoto, T. Inoue (1994) "Phase separation mechanism and structure development in poly(butylenes terephthalate)/polycarbonate blends" Polymer, **35**, p257-261
 82. Y-Y. Cheng, M. Brillhart, P. Cebe, M. Capel (1996) "X-Ray Scattering and Thermal Analysis Study of the Effects of Molecular Weight on Phase Structure in Blends of Poly(butylene terephthalate) with Polycarbonate" Journal of Polymer Science: Part B: Polymer Physics, **34**, p2953-2965
 83. J. Santos, J. Guthrie (2005) "Analysis of interactions in multicomponent polymeric systems: The key-role of inverse gas chromatography" Materials Science and Engineering R, **50**, p79-107
 84. J. Mark et al (2004), p154-158
 85. J. Mark et al (2004), p188-190,197
 86. L.A. Utracki (1990), p147
 87. L.A. Utracki (1990), p132-133
 88. L.A. Utracki (1990), p140
 89. J. Mark et al (2004), p178
 90. J.M Dealy (1990), "Melt Rheology and its Role in Plastics Processing", Van Nostrand Reinhold, New York, p269-270
 91. J.M. Dealy (1990), p317-329
 92. L.A. Utracki (1990), p25
 93. P.C. Hiemenz (1984), p81-83
 94. J.M. Dealy (1990), p270-278
 95. J. Mark et al (2004), p163-166
 96. L.A. Utracki (1990), p231-244
 97. P.C Hiemenz (1984), p84-88
 98. P.C. Hiemenz (1984), p91-103
 99. J. Mark et al (2004), p191-192
 100. J. Mark et al (2004), p168-169

-
101. P.C. Hiemenz (1984), p107-113
 102. P.C. Hiemenz (1984), p116-120
 103. P.C. Hiemenz (1984), p120-124
 104. J. Mark et al (2004), p193-201
 105. P.C. Hiemenz (1984), p103-107
 106. J. Mark et al (2004), p189-190
 107. L.A. Utracki (1990), p131-181
 108. L.A. Utracki (1990), p148-149
 109. L.A. Utracki (1990), p167-170
 110. L.A. Utracki (1990), p181
 111. L.A. Utracki (1990), p162
 112. L.A. Utracki (1990), p161
 113. L.A. Utracki (1990), p176-180
 114. J. Mark et al (2004), p267
 115. G. Aravinthan, D.D. Kale (2005) “Blends of Poly(ethylene terephthalate) and Poly(butylenes terephthalate)”, Journal of Applied Polymer Science, **98**, p75–82
 116. A. Marcincin, E. Kormendy, M. Hricova, A. Rusnak, P.A. Arun (2006) “Rheological Behaviour of Polyester Blend and Mechanical Properties of the Polypropylene–Polyester Blend Fibres” Journal of Applied Polymer Science, **102**, p4222–4227
 117. E. Boudreaux, J.A. Cuculo (1982) “A Comparison of the Flow Behaviour of Linear Polyethylene, Poly(butylene Terephthalate), and Poly (ethylene Terephthalate)” Journal of Applied Polymer Science, **27**, p301-318
 118. L. Scatteia, P. Scarfato, D. Acierno (2004) “Rheology of PBT-layered silicate nanocomposites prepared by melt compounding” Plastics, Rubbers and Composites, **33**, p85-91
 119. G. Mago, F.T. Fisher, D.M. Kalyon (2006) “Effect Of Shearing On The Crystallization Behaviour Of Poly (Butylene Terephthalate) And PBT Nanocomposites” ASME, Proceedings of IMECE2006
 120. J. Wu, D.-M. Wang, A.F. Yu (2000) “Fracture toughness and fracture mechanisms of PBT/PC/IM blends Part IV: Impact toughness and failure mechanisms of PBT/PC blends without impact modifier” Journal of Materials Science, **35**, p307-315
 121. K. Wang, J. Wu, H. Zeng (2001) “Microstructures and fracture behavior of glass-fiber reinforced PBT/PC/E-GMA elastomer blends 1: microstructures” Composites Science and Technology, **61**, p1529-1538
 122. H. Bai, Y. Zhang, Y. Zang, X. Zang, W. Zhou (2006) “Crystallization Kinetics of Toughed Poly(butylenes terephthalate)/Polycarbonate Blends” Journal of Applied Polymer Science, **101**, p1295-1308
 123. R.S. Hadler, M. Joshi, A. Misra (1990) “Morphological Studies on the Blends of Poly(butylenes Terephthalate) and Bisphenol-A Polycarbonate” Journal of Applied Polymer Science, **39**, p1251-1264
 124. S.S. Pesetskii, B. Jurkowski, V.N. Koval (2002) “Polycarbonate/Polyalkylene Terephthalate Blends: Interphase Interactions and Impact Strength” Journal of Applied Polymer Science, **84**, p1277-1285
 125. A.N. Wilkinson, S.B. Tattum, A.J. Ryan (1997) “Melting, reaction and recrystallization in a reactive PC-PBT blend” Polymer, **38**, p1923-1928

-
126. P. Marchese, A. Celli, M. Fiorini (2004) "Relationships between the Molecular Architecture, Crystallization Capacity, and Miscibility in Poly(butylenes terephthalate) / Polycarbonate Blends: A Comparison with Poly(ethylene terephthalate) / Polycarbonate Blends", Journal of Polymer Science: Part B: Polymer Physics, **42**, p2821-2832
127. J.M. Dealy (1990), p480-489
128. H.E.H. Meijer, P.H.M. Elemans (1988) "The Modeling of Continuous Mixers. Part I: The Corotating Twin-Screw Extruder" Polymer Engineering and Science, **28**, p275-290
129. L.A. Utracki (1990), p16-19
130. J. Gao, G.C. Walsh, D. Bigio (2000) "Mean Residence Time Analysis for Twin Screw Extruders" Polymer Engineering and Science, **40**, p227-237
131. I.O. Mohamed, R.Y. Ofoli, R.G. Morgan (1990) "Modeling the Average Shear Rate in a Co-Rotating Twin Screw Extruder" Journal of Food Process Engineering, **12**, p227-246
132. Jordi FLP, (2008) "GPC Report Number: J3021 – Continued"
133. S.S. Rao (2002) "Applied numerical Methods for Engineers and Scientists" Prentice Hall, New Jersey, p198-199, p399
134. G. Hohne, W. Hemminger, H.-J. Flammersheim (1996) "Differential Scanning Calorimetry, An Introduction for Practitioners" Springer, Berlin, p9
135. G. Hohne, W. Hemminger, H.-J. Flammersheim (1996), 21-25
136. M. Sorai, (2004) "Calorimetry & Thermal Analysis" John Wiley & Sons, Chichester, p221
137. A. Riga, D. Young, G. Mlachak, P. Kovach (1997) "Thermoanalytical Evaluation Of Readily Available Reference Polymers" Journal of Thermal Analysis, **49**, p425-435
138. C. Schick, M. Merzlyakov, A. Minakov, A. Wurm (2000) "Crystallization Of Polymers Studied By Temperature Modulated Calorimetric Measurements At Different Frequencies" Journal of Thermal Analysis and Calorimetry, **59**, p279-288
139. L.A. Utracki (1990), p98
140. E.A. Turi (1981), p170
141. D.A. Ditmars, S. Ishihara, S.S. Chang, G. Bernstein, E.D. West (1982) "Enthalpy and Heat-Capacity Standard Reference Material: Synthetic Sapphire (α -Al₂O₃) from 10 to 2250 K", Journal of Research of the National Bureau of Standards, **87**, p159-163
142. L.A. Utracki (1990), p114-117
143. S.Y. Hobbs, M.E.J. Dekkers, V.H. Watkins (1988) "Toughened blends of poly(butylenes terephthalate) and BPA polycarbonate: Part 1 Morphology" Journal Of Materials Science, **23**, p1219-1224
144. L.C. Sawyer, D.T. Grubb (1987) "Polymer Microscopy" Chapman and Hall, New York, p89,
145. B. Ohlsson, B. Tornell (1990) "The Use of RuO₄ in Studies of Polymer Blends by Scanning Electron Microscopy" Journal of Applied Polymer Science, **41**, p1189-1196
146. University of Waterloo ME 632 Course Notes, Summer 2008
147. D.C. Montgomery (2005), "Design and Analysis of Experiments" John Wiley & Sons, p373-400

APPENDIX A: FTIR Analysis of PC/ PBT Blends

A.D. Rogalsky, #20072715

Dept of Mechanical & Mechatronics Engineering, University of Waterloo, Waterloo, Ontario, Canada, N2L 3G1, adrogals@uwaterloo.ca

Introduction

Blends of polycarbonate, PC, and poly(butylene terephthalate), PBT, are used primarily for automotive parts, particularly bumpers [1]. They are valued for their high impact and solvent resistance as well as stiffness at elevated temperatures. A titanium based polymerization catalyst present in commercial PBT also catalyses an exchange reaction with PC. Initially it leads to block co-polymers but at high reaction extent a statistical co-polymer is produced [2]. Formation of block co-polymer is beneficial to strength and solvent resistance but its compatibilizing effect improves inter-phase adhesion too much, lowering impact strength. Furthermore, blend solvent resistance is mainly provided by PBT crystallinity which is reduced by large reaction extents. For these reasons an attempt is made to limit or totally suppress the reaction in most commercial blends.

Transesterification extent, percent crystallinity, phase size and phase composition are expected to be the main factors affecting blend properties. To predict blend performance, techniques that can quantify these factors are necessary. Reaction extent and other chemical changes can be characterized by NMR, Raman IR and FTIR. For crystallinity, FTIR, Raman IR, DSC and wide angle x-ray are good techniques. Optical and electron microscopy are good at characterizing phase size, but FTIR and Raman IR microscopy are better at providing phase composition. In good scientific studies several complementary techniques are often used to provide a cross check for data [3]. Spectroscopic IR techniques have such broad applicability that they are good choices to limit the number of experiments necessary. Raman has some distinct advantages however it has not been used with PC/PBT blends necessitating that the focus of this discussion be on FTIR.

Fundamentals

PC & PBT chemical structures can be seen in Figures 1 and 2 respectively. PC does not crystallize under commercial processing conditions while PBT is semi-crystalline. Thermal treatment produces the ' α ' crystal form characterized by a gosh-trans-gosh, g-t-g, conformation of the aliphatic chain. Deformation produces the ' β ' crystal form. This form is more difficult to differentiate chemically from the amorphous fraction as both are characterized by a t-t-t conformation [4,5]. The main PC and PBT peaks as well as an assignment of associated chemical structures are given in tables 1 and 2 respectively. Figures 3 and 4 show spectra of the two polymers in the mid IR range.

Given known peaks, quantitative determination of concentrations can be accomplished using the Beer-Lambert law as rearranged by Lambert et al. [6]. The basic parameters are the peak absorbance of the species to be measured, A , the molar absorbance associated with this peak, α , and the sample thickness, S . Equation 1 can be used to directly determine the concentration, X , if sample thickness is known. If a reference peak is available equation 2 can be used. Reference peaks may be based on the addition of a known tracer concentration or provided by a material peak unaffected by the process being studied. In the latter case the reference concentration is 1, as the peak is provided by 100% of the sample. A special case is represented by mutually exclusive peaks such as those associated with the amorphous and crystalline phases in a semi-crystalline polymer or the two separate constituents of a polymer

blend. As the concentrations are known to sum to 100%, the Beer-Lambert law can be rearranged into the form of equation 3.

$$X_1 = \frac{A_1}{\alpha_1 \cdot S} \quad [6] \quad \text{Equation 1}$$

$$X_1 = X_r \frac{\alpha_r \cdot A_1}{\alpha_1 \cdot A_r} \quad [6] \quad \text{Equation 2}$$

$$\frac{1}{X_1} = 1 + \frac{\alpha_1 \cdot A_2}{\alpha_2 \cdot A_1} \quad [6] \quad \text{Equation 3}$$

Proper sample preparation is necessary for good results. PC/PBT blends range from translucent to opaque due to PBT crystallinity. Jang and Sim overcame poor IR transmission in a PBT blend through use of attenuated total reflection [5]. As this technique only samples the surface of a specimen it can be used with opaque materials, however results may differ from those of the bulk material. To obtain information about the bulk material Pellow-Jarman and Hetem used powdered sample pressed in KBr pellets [7]. This technique works by diluting the sample with an IR transparent solid. For 100 mg of KBr approximately 1 mg of sample is used. Sample particles are reduced to less than 2 μ m to avoid IR scattering [3]. A drawback of pressed pellets is that deformation destroys most existing microstructure and may convert α crystalline PBT into its β form. To observe un-deformed microstructure, hot pressed thin films might be used, however Pellow-Jarman and Hetem were unable to obtain thin enough films [7]. Excellent results were obtained by Homfe et al. on 2-3 μ m thick microtome slices, suggesting that for quantitative analysis of un-deformed microstructure this is the best technique [4]. Sample thickness for these very thin sections can be determined using equation 4, where n is the number of interference fringes, η is the refractive index, (the indices of PBT and PC are almost identical), and λ_1 and λ_2 are the wavelength range over which the interference fringes have been counted.

$$S = \frac{n}{2\eta} \left(\frac{\lambda_1 \cdot \lambda_2}{\lambda_1 - \lambda_2} \right) \quad [3] \quad \text{Equation 4}$$

Application - Composition Determination and Chemical Mapping

To determine composition characteristic peaks for the two polymers must be found. Both polymers have carbonyl groups which produce strong peaks in the 1730-1860 cm^{-1} range and no other nearby peaks of similar significance [8]. Carbonyl stretching IR bands are at 1775-1780 cm^{-1} and 1720 cm^{-1} for PC and PBT respectively [4, 8, 9]. Both Tattum et al., figure 5, and Hopfe et al., figure 6, have published calibration curves for these bands from which the constants in the Beer-Lambert law can be derived. For best results, calibration curves from the same instrument and experimental conditions should be used. A standard FTIR instrument and these curves suffice to find bulk composition, however for blends this is usually known in advance. What is generally of interest is the composition and distribution of individual phases.

To sample individual phases, a microscope fitted with a computer controlled XY table is used to scan the sample in a grid. A small aperture controls the size of the area being sampled allowing quantitative analysis of the results to build a false color image of composition [3]. Diffraction gives the theoretical limit of $\lambda/2$ for pixel size. In conventional equipment 2λ is the practical limit due to the limited light that passes through a smaller aperture [10]. For the limiting 1780 cm^{-1} band, wavelength is 5.6 μ m resulting in a limiting pixel size of approximately 12 μ m. In un-reacted PC/PBT blends the phase size is

approximately 5-10 μm as determined by TEM [9]. As the pixel size is on the same order as the phase size, composition maps are unlikely to show much useful detail. Hopfe et al., have published measurements of compositional differences between phases using a 20 μm aperture size [4]. Specific details of the sampling procedure and statistical analysis used are not provided, however care would have to be taken to prevent the scan area overlapping phase boundaries and biasing the measurement. To overcome these difficulties a more intense light source such as a laser or synchrotron might be used. They have been used to overcome throughput issues in other IR applications [10]. Raman IR could be even better as it uses 0.4-0.6 μm laser allowing for a <1 μm limiting pixel size [3].

Application - Crystallinity Determination

PBT α crystallinity is of primary interest in work on compounding and molding. A promising IR Band for its determination exists at 917 cm^{-1} [4, 11]. It is almost non-existent in the amorphous and β crystal phases, but is sharp in the α phase [11]. See figure 7. Interference from PC is not expected as PC does not have any large peaks between 900 and 1000 cm^{-1} [8]. Other promising peaks near and including one at 1458 cm^{-1} have been identified [4, 5]. See figures 8 and 9. Unfortunately the PC spectrum is not as flat in this region [8], making analysis more complicated. The PBT ring deformation peak at 872 cm^{-1} might provide a useful internal reference for use with equation 2. Homfe et al. reported it to be unaffected by temperature changes or crystallinity up to the polymer decomposition temperature but in their own figure it decreases markedly with increasing temperature calling this into doubt [4]. See figure 8.

As in phase mapping, calibration curves based on samples with known composition are necessary for the determination of the molar absorbency or its ratio. None are reported for PBT in the recent literature necessitating another technique be used with FTIR to establish these curves before crystallinity can be quantitatively determined. Wide angle X-ray can not be done as rapidly as FTIR but has been used successfully by Lamderti and Brucato with poly(propylene) to produce calibration curves for FTIR [6]. Another option is DSC which quantifies crystallinity by detecting heat flow during melting and crystallization. DSC has been used to determine crystallinity of PC/PBT blends by the author as well as Tattum et al. [9], Hompe et al. [4] and Mishra and Colleague [12]. The fast crystallization kinetics of PBT can result in changes in crystallinity on the time scale of a DSC scan, however with careful control of temperature cycle this should not be a major issue. FTIR, which does not suffer from these issues, can provide a useful cross check once calibration curves have been established.

Transesterification Determination and Limitations

If the exchange reaction is not totally suppressed, products other than the original polymer repeat unit are formed [2]. Table 3 presents the reaction products and their IR band assignments. Most of these bands are close to the existing carbonyl bands of the parent polymer making isolation of them difficult. Tattum et al. were unable to de-convolute the 1770 and 1740 peaks below a reaction extent of 37% [9] while Hopfe et al. required co-polymer contents as high as 23 mol% to clearly distinguish the 1760 cm^{-1} band. More promising is the 1070 cm^{-1} band which is further from major PC and PBT peaks allowing co-polymer concentrations as low as 3.5 mol% to be detected. Unfortunately significant changes in material properties are already expected at this reaction extent [4]. In commercial blends where significant changes are to be avoided, a more sensitive check of stability is required. Characterization of extremely small reaction extents is possible by NMR, however better resolution may be available with FTIR as well. At low reaction extent only highly insoluble

block co-polymers are formed [2]. Assuming a reasonable molecular weight, the signal from un-reacted chain elements in these co-polymers will be several orders of magnitude larger than that of the reaction products. Solvent extraction of one of the polymers followed by IR analysis of the insoluble residue should provide a good estimate of co-polymer content. Birley and Chen conducted such an experiment and though they did not use it to estimate co-polymer content they did find that the PC content in PBT rich insoluble residue increased with reaction time [1].

Conclusions

Good IR bands and calibration curves are available for composition determination. Conventional FTIR pixel size is too large to determine phase distribution, but phase composition might be determined. For phase analysis microtoming is best sample preparation technique. IR bands associated with α crystallinity have been identified, but calibration curves are not available. At present another technique such as DSC or wide angle x-ray must be used in conjunction with FTIR to characterize crystallinity in PC/PBT blends. For quantifying small amounts of transesterification in stabilized blends standard FTIR sample preparation is inadequate. NMR is the proven technique; however solvent extraction followed by IR analysis is promising. For routine investigation of PC/PBT blends FTIR currently poses several challenges however these challenges are what provide the greatest potential for original research.

References

1. Birley, Chen "Further Studies of Polycarbonate-Poly(butylene terephthalate) Blends" British Polymer Journal, 17, (1985)
2. Devaux, Godard, Mercier "The Transesterification of Bisphenol A Polycarbonate (PC) and Polybutylene Terephthalate (PBTP): A New Route to Block Copolycondensates" Polymer Engineering and Science, 22, 229-233 (1982)
3. Robinson, Frame, Frame II "Undergraduate Instrumental Analysis" 6th Ed. Marcel Dekker, New York (2005)
4. Homfe, Pompe, Eichhorn "Ordered structures and progressive transesterification in PC/PBT melt blends studied by FTIR spectroscopy combined with d.s.c. and n.m.r." Polymer, 38, 2321-2327 (1997)
5. Jang, Sim "Crystallization Behaviour in Poly(ether Imide)/Poly(butylene Terephthalate) Blends using a Spectroscopic Method" Polymer Testing, 17, 507-521 (1998)
6. Lamberti, Brucato "Real-Time Orientation and Crystallinity Measurements during the Isotactic Polypropylene Film-Casting Process" Journal of Polymer Science: Part B: Polymer Physics, 41, 998-1008 (2003)
7. Pellow-Jarman, Hetem "The effect of the poly(butylene terephthalate) constituent on the reactions occurring in poly(butylene terephthalate)/polycarbonate polymer blends below their decomposition temperature" Plastics, Rubber and Composites Processing and Applications, 23, 31-41 (1995)
8. Kuptov, Zhizhin "Handbook of Fourier Transform Raman and Infrared Spectra of Polymers" Elsevier, Amsterdam (1998)
9. Tattum, Cole, Wilkinson "Controlled Transesterification and Its Effects on Structure Development in Polycarbonate-Poly(Butylene Terephthalate) Melt Blends" Journal of Macromolecular Science: Physics, 39, 459-479 (2000)
10. Mark, Nagai, Graessley, Mandelkern, Smulski, Koenig, Wignall "Physical Properties of Polymers" 3rd Ed, Cambridge University Press, Cambridge (2004)
11. Gillette, Dirlikov, Koenig, Lando "An infra-red study of model compounds of poly(tetramethylene terephthalate)" Polymer, 23, 1759-1764 (1982)
12. Mishra, Venkidusamy "Structural and Thermal Behaviour of PC/PBT Blends" Journal of Applied Polymer Science, 58, 2229-2234 (1995)

Tables and Figures

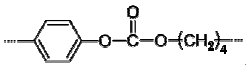
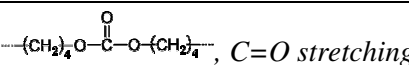
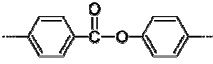
Table 1: PC Peak Assignment

Assignment	Wave-number (cm ⁻¹)
C-H stretching in C-CH ₃	2970-2990 [12]
Aromatic carbonate C=O stretching	1780 [9, 12, 2], 1775 [7]
In-plane ring C-H stretching	1510 [7, 12]
O-C-O	1150-1290 [7, 12]
O-C-O	1010 [7]
ring C-C-C stretching	880 [12]
Out of plane ring deformation	833 [7]
C=O out of plane bending	840 [12]
C=O in plane bending	550 [12]

Table 2: PBT Peak Assignment

Assignment	Wave-number (cm ⁻¹)
Aliphatic CH ₂ symmetric stretch	2840-2860 [8]
Aliphatic ester C=O stretching	1720 [9, 7, 2]
Associated with Crystallinity	1714 [7]
In-plane ring deformation	1504 [7]
CH ₂ bending t-t-t conformation, β crystalline	1485 [7]
CH ₂ bending t-t-t conformation, β crystalline, amorphous state	1470 [7, 8]
CH ₂ bending g-t-g conformation, α crystalline	1452, 1458-1460 [7, 8]
In-plane ring deformation	1410 [7]
CH ₂ wagging t-t-t conformation, β crystalline	1393 [7]
CH ₂ wagging g-t-g conformation, α crystalline	1386 [7]
CH ₂ twisting, α crystalline	1320-1322 [7, 8]
C-O-C	1260 [7]
CH ₂ wagging t-t-t conformation, β crystalline	1208 [7]
CH ₂ wagging g-t-g conformation, α crystalline	1173 [7]
In-plane ring deformation	1018, 1108 [7]
Skeleton and rocking vibrations t-t-t conformation, β crystalline	960 [7, 8]
Skeleton and rocking vibrations g-t-g conformation, α crystalline	917-918 [7, 8]
Out of plane ring deformation, not dependent on crystallinity	872 [7]
Skeleton and rocking vibrations t-t-t conformation	842 [7]
Skeleton and rocking vibrations g-t-g conformation	811 [7]
coupled vibration of carbonyl and out of plane ring	728 [7]

Table 3: Reaction Products Peak Assignment

Assignment	Wave-number (cm ⁻¹)
Aliphatic-Aromatic Carbonate,  , C=O stretching	1770 [7, 2]
Aliphatic-Aliphatic Carbonate,  , C=O stretching	1763 [7]
Aromatic Ester,  , C=O stretching	1740, 1070-1080 [12, 2]

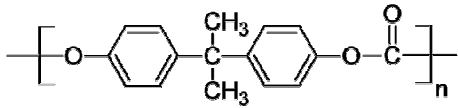


Figure 1: Polycarbonate Repeat Unit [8]

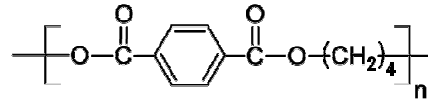


Figure 2: Poly(butylene terephthalate) [8]

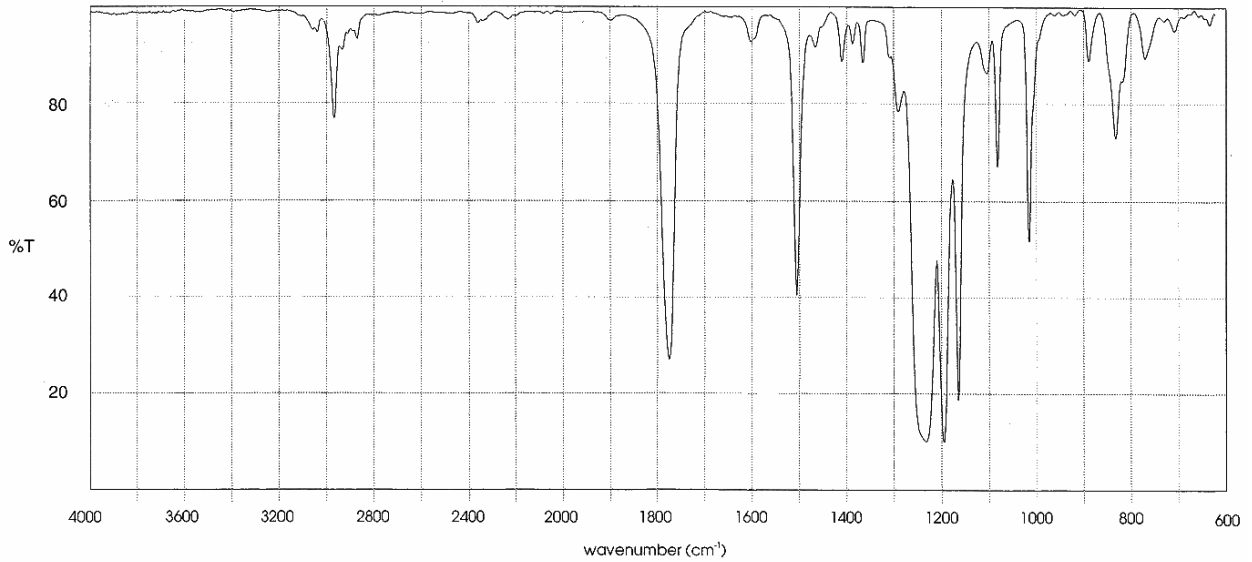


Figure 3: FTIR Spectrum of PC

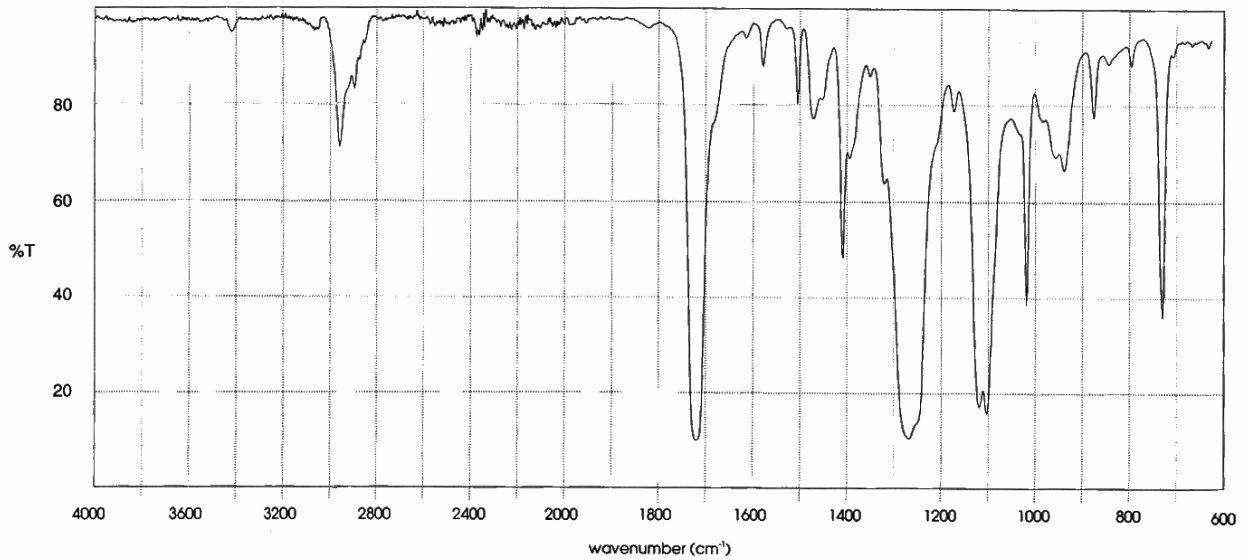


Figure 4: FTIR Spectrum of PBT

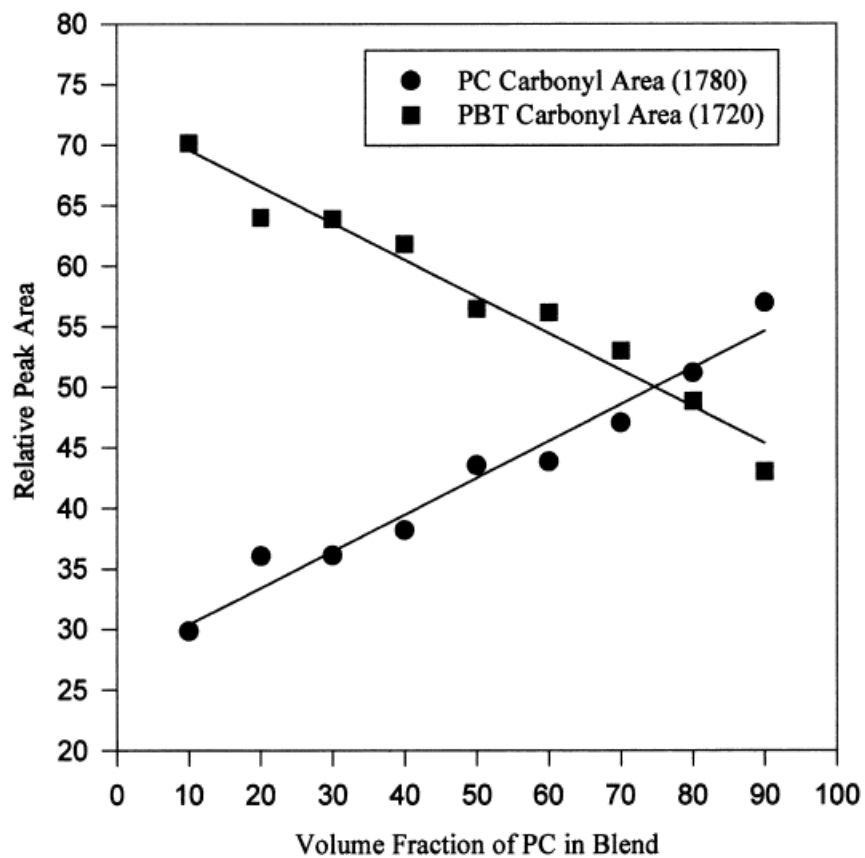


Figure 5: Calibration curve for volume fraction in un-reacted PC / PBT blends [9]

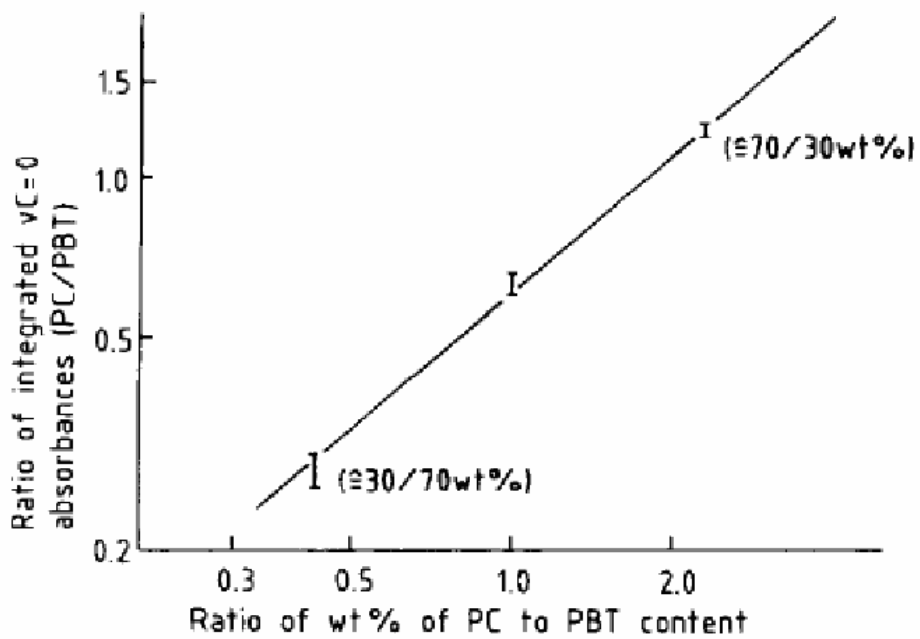


Figure 6: Calibration curve for wt% in un-reacted PC / PBT blends [7]

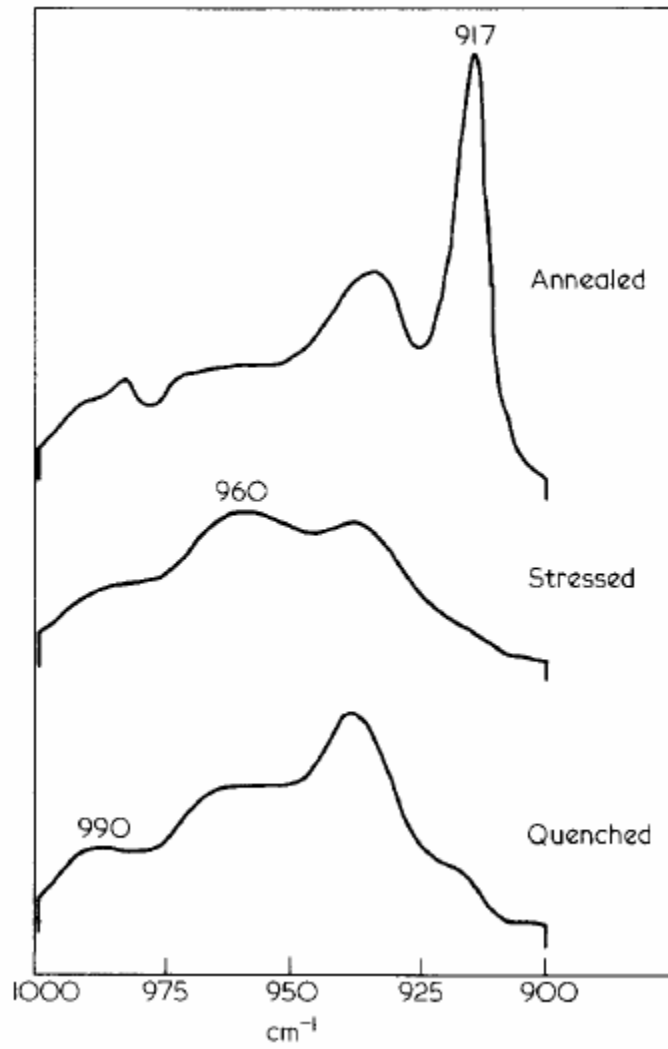


Figure 7: IR Scan of PBT, annealed and stressed represent the α and β crystal forms respectively [11]

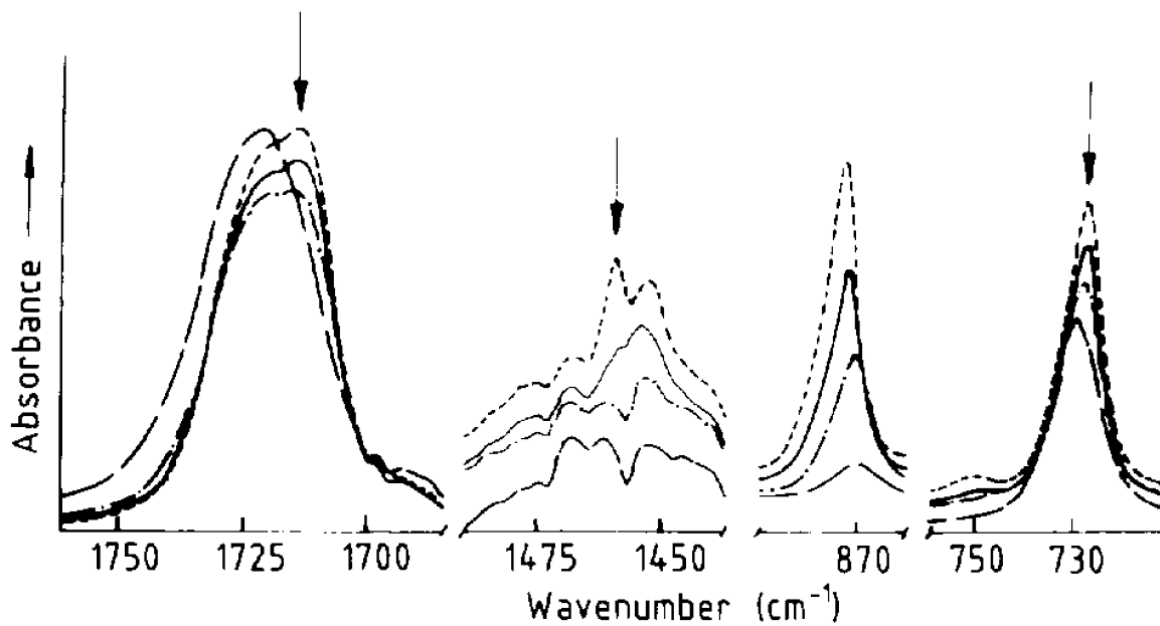


Figure 8: IR Spectra of Pure PBT at different Temperatures, 20°C (---), 90°C (—), 190°C (- · -), 230°C (— — —) [7]

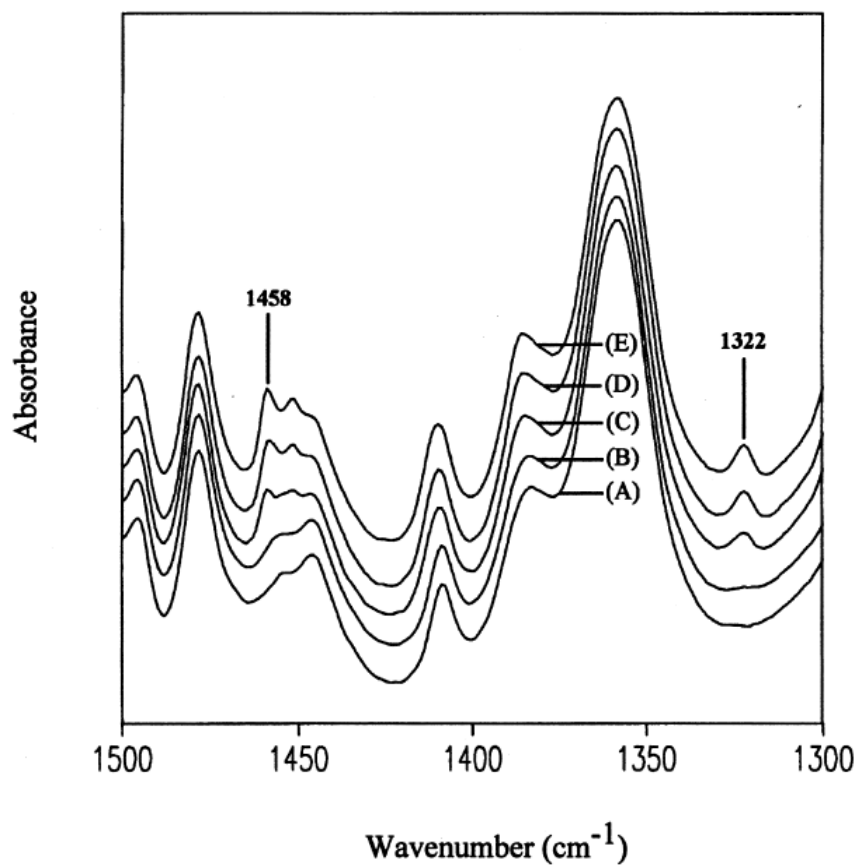


Figure 9: Effect of annealing at 200°C on the FT-IR spectra of PEI/PBT blend: (A) 0 min, (B) 5 min, (C) 10 min, (D) 30 min, (E) 60 min. [8]

APPENDIX B: Universal Analysis Macros for Data Analysis

ExportData

- Outputs Data Text File From Universal Analysis

- 1: Function Signal Selection
- 2: Select Item 3 Y2 Signal Temperature (°C)
- 3: Select Item 5 Y2 Type Derivative (time)
- 4: Button OK Signal Selection
- 5: Function Export File and Plot Signals
- 6: Button Windows (ANSI)
- 7: Button Finish >> Export Data File

SecondaryAnalysis

- Finds: First cycle PBT Tg and melting, Second cycle PBT crystallization
- Exports results to Excel

- 1: Function Open Data File
- 2: Button OK Data File Information
- 3: Function Cycle List
- 4: Uncheck Item 3 Cycle 3
- 5: Button OK Data Cycle Selection
- 6: Function Integrate Peak Sig Tangent
- 7: Cursor Point 1 (220.0, 0.315147)
- 8: Cursor Point 2 (205.0, 0.312712)
- 9: Cursor Point 3 (155.0, 0.301564)
- 10: Cursor Point 4 (150.0, 0.210037)
- 11: Function Accept Cursor Limits
- 12: Function Integrate Peak Sig Tangent
- 13: Cursor Point 1 (245.0, -0.315561)
- 14: Cursor Point 2 (236.0, -0.307815)
- 15: Cursor Point 3 (200.0, -0.309494)
- 16: Cursor Point 4 (175.0, -0.292254)
- 17: Function Accept Cursor Limits
- 18: Function Glass/Step Transition
- 19: Cursor Point 1 (12.5498, -.0882019)
- 20: Cursor Point 2 (74.8239, -0.112137)
- 21: Function Accept Cursor Limits
- 22: Function Results Options
- 23: Check Report heading
- 24: Check Result type
- 25: Check Result separator
- 26: Check Result notes

- 27: Check Column name
- 28: Check Column units
- 29: Check Multiplex value
- 30: Uncheck Signal name
- 31: Uncheck File name
- 32: Uncheck Sample ID
- 33: Button OK Result Options
- 34: Function Results Spreadsheet
- 35: Function Close Data File

PrimaryAnalysis

- Finds: Third cycle PBT Tg, PC Tg and PBT melting peaks, splitting peaks with a vertical line.
- Exports results to Excel

- 1: Function Open Data File
- 2: Button OK Data File Information
- 3: Function Cycle List
- 4: Uncheck Item 1 Cycle 1
- 5: Uncheck Item 2 Cycle 2
- 6: Button OK Data Cycle Selection
- 7: Function Glass/Step Transition
- 8: Cursor Point 1 (10.0, -.0914504)
- 9: Cursor Point 2 (100.0, -0.125527)
- 10: Function Accept Cursor Limits
- 11: Function Glass/Step Transition
- 12: Cursor Point 1 (100.0, -0.125527)
- 13: Cursor Point 2 (180.0, -0.164022)
- 14: Function Accept Cursor Limits
- 15: Function Integrate Peak Sig Tangent
- 16: Cursor Point 1 (150.0, -0.153258)
- 17: Cursor Point 2 (170.0, -0.159921)
- 18: Cursor Point 3 (240.0, -0.16833)
- 19: Cursor Point 4 (249.0, -0.171208)
- 20: Function Accept Cursor Limits
- 21: Select Label 3
- 22: Mouse Down Right (0.790698, 0.841936)
- 23: Function Copy Text
- 24: Assign MainPeakTemp = Clipboard(1)
- 25: Assign MainPeakTemp = MainPeakTemp - 0.2
- 26: Assign x_cursor[2] = MainPeakTemp

27: Function Peak Maximum
 28: Cursor Point 1 (150.0, -0.170219)
 29: Function Accept Cursor Limits
 30: Select Label 1
 31: Mouse Down Right (0.656218, 0.701613)
 32: Function Copy Text
 33: Assign x_cursor[1] = Clipboard(1)
 34: Function Integrate Peak Perpendicular Drop
 35: Function Accept Cursor Limits
 36: Dialog (Confirmation No Jump End) "Is Analysis Ok?"
 37: Function Results Options
 38: Check Report heading
 39: Check Result type
 40: Check Result separator
 41: Check Result notes
 42: Check Column name
 43: Check Column units
 44: Check Multiplex value
 45: Uncheck Signal name
 46: Uncheck File name
 47: Uncheck Sample ID
 48: Button OK Result Options
 49: Function Results Spreadsheet
 50: Function Close Data File

PCAnalysis

- Finds: Third cycle PC Tg
 - Exports results to Excel

1: Function Open Data File
 2: Button OK Data File Information
 3: Function Cycle List
 4: Uncheck Item 1 Cycle 1
 5: Uncheck Item 2 Cycle 2
 6: Button OK Data Cycle Selection
 7: Function Glass/Step Transition
 8: Cursor Point 1 (25.0, -.0944787)
 9: Cursor Point 2 (220.0, -0.163439)
 10: Function Accept Cursor Limits
 11: Function Results Options
 12: Check Report heading
 13: Check Result type
 14: Check Result separator

15: Check Result notes
 16: Check Column name
 17: Check Column units
 18: Check Multiplex value
 19: Uncheck Signal name
 20: Uncheck File name
 21: Uncheck Sample ID
 22: Button OK Result Options
 23: Function Results Spreadsheet
 24: Function Close Data File

PBTAnalysis

- Finds: Second Cycle PBT Crystallization, Third cycle PBT Tg, and PBT melting peaks, splitting peaks with a vertical line.
 - Exports results to Excel

1: Function Open Data File
 2: Button OK Data File Information
 3: Function Cycle List
 4: Uncheck Item 1 Cycle 1
 5: Uncheck Item 2 Cycle 2
 6: Button OK Data Cycle Selection
 7: Function Glass/Step Transition
 8: Cursor Point 1 (15.0, -0.125527)
 9: Cursor Point 2 (80.0, -0.164022)
 10: Function Accept Cursor Limits
 11: Function Integrate Peak Sig Tangent
 12: Cursor Point 1 (100.0, -0.153258)
 13: Cursor Point 2 (150.0, -0.159921)
 14: Cursor Point 3 (240.0, -0.16833)
 15: Cursor Point 4 (249.0, -0.171208)
 16: Function Accept Cursor Limits
 17: Select Label 3
 18: Mouse Down Right (0.790698, 0.841936)
 19: Function Copy Text
 20: Assign MainPeakTemp = Clipboard(1)
 21: Assign MainPeakTemp = MainPeakTemp - 0.2
 22: Assign x_cursor[2] = MainPeakTemp
 23: Function Peak Maximum
 24: Cursor Point 1 (150.0, -0.170219)
 25: Function Accept Cursor Limits
 26: Select Label 1

27: Mouse Down Right (0.656218,
0.701613)
28: Function Copy Text
29: Assign x_cursor[1] = Clipboard(1)
30: Function Integrate Peak Perpendicular
Drop
31: Function Accept Cursor Limits
32: Function Cycle List
33: Check Item 2 Cycle 2
34: Button OK Data Cycle Selection
35: Function Integrate Peak Sig Tangent
36: Cursor Point 1 (140.0, 0.146476)
37: Cursor Point 2 (150.0, 0.13663)
38: Cursor Point 3 (210.0, 0.175944)
39: Cursor Point 4 (220.0, 0.181621)
40: Function Accept Cursor Limits

41: Dialog (Confirmation No Jump End)
"Is Analysis Ok?"
42: Function Results Options
43: Check Report heading
44: Check Result type
45: Check Result separator
46: Check Result notes
47: Check Column name
48: Check Column units
49: Check Multiplex value
50: Uncheck Signal name
51: Uncheck File name
52: Uncheck Sample ID
53: Button OK Result Options
54: Function Results Spreadsheet
55: Function Close Data File

APPENDIX C: DSC Curve Analysis Results

Notes:

1. Blend number is given in the form “Blend Number-Sample Number”. Ave stands for average, Sd for standard deviation, Cv for coefficient of variation, numeric values stand for individual samples. Cv is the ratio of standard deviation over average.
2. ΔC_p stands for the heat capacity change at glass transition.
3. ΔQ is the measured energy associated with a transition.
4. Blend numbers PBT, PC1 and PC2 represent pure polymer.
5. “---”Indicates no result could be found.

Table C1: PBT Results, 10°C/Min Heating and Cooling Rates

Blend Number	Glass Transition		Crystallization		Small Melting		Main Melting		Melting Total ΔQ
	Midpoint	ΔC_p	Onset	ΔQ	Onset	ΔQ	Onset	ΔQ	
---	°C	J/(gK)	°C	J/g	°C	J/g	°C	J/g	J/g
1-01	47.26	0.1008	193.96	17.07	211.53	1.16	218.34	16.83	17.99
1-02	47.45	0.0835	193.79	15.56	211.59	1.12	218.58	15.81	16.93
1-03	46.68	0.1080	193.75	16.73	211.58	1.31	218.40	16.77	18.08
1-04	46.50	0.1156	194.00	16.51	211.57	1.27	218.39	17.12	18.38
1-05	47.08	0.1139	194.13	17.15	211.62	1.26	218.46	17.21	18.47
1-06	47.06	0.1099	193.64	16.62	211.67	1.13	218.41	16.74	17.86
1-Ave	47.01	0.1053	193.88	16.61	211.59	1.21	218.43	16.75	17.95
1-Sd	0.36	0.0119	0.18	0.57	0.05	0.08	0.08	0.50	0.55
1-Cv	0.76%	11.28%	0.09%	3.44%	0.02%	6.84%	0.04%	2.97%	3.07%
2-01	48.43	0.1311	194.47	12.97	211.34	1.20	218.37	15.20	16.41
2-02	45.69	0.1148	194.68	14.69	211.24	1.01	218.32	14.92	15.94
2-03	48.27	0.1031	193.81	14.14	211.16	0.60	218.45	15.44	16.04
2-04	49.82	0.0963	194.51	14.49	211.29	1.05	218.24	15.19	16.24
2-05	50.03	0.1147	194.48	14.52	211.92	1.09	218.71	14.77	15.86
2-06	46.81	0.1100	195.01	14.35	211.41	1.07	218.45	15.07	16.14
2-Ave	48.18	0.1117	194.49	14.19	211.39	1.00	218.42	15.10	16.11
2-Sd	1.69	0.0119	0.39	0.63	0.27	0.21	0.16	0.23	0.20
2-Cv	3.51%	10.67%	0.20%	4.42%	0.13%	20.57%	0.07%	1.56%	1.25%
3-01	54.03	0.1287	195.57	18.12	212.41	1.50	219.13	18.71	20.21
3-02	47.11	0.1058	195.52	16.47	212.46	1.34	219.09	16.88	18.22
3-03	46.26	0.1201	195.14	16.57	212.05	1.35	218.65	17.23	18.58
3-04	47.45	0.0973	195.38	17.41	212.22	1.44	218.84	16.93	18.37
3-05	52.97	0.1440	195.70	16.90	211.75	1.52	218.60	17.21	18.73
3-06	46.92	0.1473	194.94	16.57	212.70	1.16	218.65	17.58	18.73
3-Ave	49.12	0.1239	195.38	17.01	212.27	1.38	218.83	17.42	18.81
3-Sd	3.43	0.0201	0.29	0.65	0.34	0.13	0.23	0.68	0.72
3-Cv	6.98%	16.25%	0.15%	3.80%	0.16%	9.65%	0.11%	3.89%	3.81%

Table C1: Continued... PBT Results

Blend Number	Glass Transition		Crystallization		Small Melting		Main Melting		Melting Total ΔQ
	Midpoint	ΔC_p	Onset	ΔQ	Onset	ΔQ	Onset	ΔQ	
---	$^{\circ}\text{C}$	J/(gK)	$^{\circ}\text{C}$	J/g	$^{\circ}\text{C}$	J/g	$^{\circ}\text{C}$	J/g	J/g
4-01	48.42	0.1090	195.15	17.16	211.94	1.64	218.63	17.08	18.72
4-02	50.70	0.0504	194.41	15.61	212.88	1.17	218.98	14.62	15.78
4-03	46.72	0.1332	194.39	15.96	212.40	1.12	218.57	16.33	17.45
4-04	46.60	0.1370	195.03	16.69	212.38	1.47	218.57	17.27	18.74
4-05	51.14	0.1253	194.84	15.96	212.62	1.23	218.89	15.97	17.20
4-06	44.74	0.1516	194.83	16.78	211.70	1.41	218.33	17.12	18.53
4-Ave	48.05	0.1177	194.78	16.36	212.32	1.34	218.66	16.40	17.74
4-Sd	2.51	0.0358	0.31	0.60	0.43	0.20	0.24	1.01	1.17
4-Cv	5.23%	30.45%	0.16%	3.68%	0.20%	14.88%	0.11%	6.16%	6.58%
5-01	45.14	0.1453	194.39	16.97	212.14	1.45	218.34	16.88	18.33
5-02	52.04	0.1458	194.50	16.35	212.23	1.35	218.30	16.91	18.26
5-03	50.24	0.1081	194.82	15.88	211.67	1.53	218.36	16.84	18.37
5-04	47.02	0.0585	194.47	15.28	212.48	1.23	219.03	15.01	16.24
5-05	50.21	0.1371	193.92	16.44	211.76	1.13	218.32	16.27	17.39
5-06	50.58	0.1386	194.72	15.93	212.06	1.30	218.58	16.68	17.97
5-Ave	49.21	0.1222	194.47	16.14	212.06	1.33	218.49	16.43	17.76
5-Sd	2.58	0.0342	0.31	0.58	0.30	0.14	0.28	0.74	0.83
5-Cv	5.25%	27.97%	0.16%	3.58%	0.14%	10.87%	0.13%	4.48%	4.67%
6-01	47.98	0.1221	194.18	16.53	211.90	1.35	218.25	16.29	17.64
6-02	46.82	0.1396	194.37	16.59	211.95	1.36	218.45	16.93	18.29
6-03	50.57	0.1229	194.68	16.29	212.43	1.39	219.01	16.39	17.77
6-04	49.61	0.1340	194.47	16.81	212.07	1.35	218.65	17.18	18.52
6-05	50.23	0.1184	194.17	17.05	212.08	1.12	218.48	16.89	18.01
6-06	45.95	0.1085	194.48	16.45	211.91	1.36	218.50	16.11	17.47
6-Ave	48.53	0.1243	194.39	16.62	212.06	1.32	218.56	16.63	17.95
6-Sd	1.90	0.0111	0.20	0.27	0.20	0.10	0.26	0.43	0.40
6-Cv	3.92%	8.96%	0.10%	1.63%	0.09%	7.41%	0.12%	2.56%	2.23%
7-01	46.80	0.0937	194.29	13.52	211.82	0.92	218.21	14.83	15.75
7-02	47.39	0.1172	194.55	13.88	211.83	0.87	218.27	14.73	15.60
7-03	54.11	0.1287	194.52	13.83	211.74	0.98	218.30	14.07	15.05
7-04	51.31	0.0987	193.96	13.42	212.14	0.85	218.79	13.40	14.25
7-05	46.25	0.1174	194.53	14.02	211.74	0.97	218.18	14.42	15.38
7-06	50.94	0.1026	194.74	14.26	211.28	1.10	218.04	14.82	15.92
7-Ave	49.47	0.1097	194.43	13.82	211.76	0.95	218.30	14.38	15.33
7-Sd	3.13	0.0134	0.27	0.31	0.28	0.09	0.26	0.56	0.61
7-Cv	6.32%	12.26%	0.14%	2.26%	0.13%	9.47%	0.12%	3.91%	3.96%
8-01	48.28	0.0946	194.06	15.90	212.37	1.18	218.86	16.43	17.61
8-02	51.80	0.1017	194.22	16.52	211.95	1.24	218.67	15.88	17.12
8-03	47.11	0.1338	194.34	17.14	211.80	1.43	218.52	17.51	18.93
8-04	50.90	0.1091	194.58	17.09	212.03	1.37	218.62	17.74	19.11
8-05	48.46	0.0631	194.59	16.98	211.56	1.39	218.38	16.90	18.29
8-06	50.17	0.1344	194.35	16.10	212.00	1.21	218.68	16.60	17.81
8-Ave	49.45	0.1061	194.36	16.62	211.95	1.30	218.62	16.84	18.15
8-Sd	1.79	0.0268	0.21	0.53	0.27	0.11	0.16	0.69	0.78
8-Cv	3.61%	25.21%	0.11%	3.21%	0.13%	8.14%	0.07%	4.12%	4.28%

Table C1: Continued... PBT Results

Blend Number	Glass Transition		Crystallization		Small Melting		Main Melting		Melting Total ΔQ
	Midpoint	ΔC_p	Onset	ΔQ	Onset	ΔQ	Onset	ΔQ	
---	$^{\circ}C$	J/(gK)	$^{\circ}C$	J/g	$^{\circ}C$	J/g	$^{\circ}C$	J/g	J/g
9-01	50.76	0.1305	194.14	16.03	211.79	1.00	218.56	16.05	17.05
9-02	45.92	0.1090	194.01	18.00	212.09	1.23	218.15	18.48	19.71
9-03	49.98	0.1058	194.34	16.81	211.89	1.12	218.46	16.70	17.82
9-04	47.62	0.1289	194.25	16.41	211.28	1.24	218.33	17.18	18.42
9-05	53.39	0.1300	194.33	19.87	211.42	1.44	218.43	16.97	18.41
9-06	47.16	0.1404	194.46	16.68	211.50	1.18	218.43	16.97	18.14
9-Ave	49.14	0.1241	194.26	17.30	211.66	1.20	218.39	17.06	18.26
9-Sd	2.76	0.0136	0.16	1.42	0.31	0.15	0.14	0.80	0.87
9-Cv	5.61%	10.97%	0.08%	8.23%	0.15%	12.15%	0.06%	4.69%	4.79%
10-01	46.12	0.1420	194.51	18.62	211.80	1.50	218.54	18.53	20.03
10-02	53.77	0.1199	194.38	17.84	212.54	1.30	219.04	18.01	19.31
10-03	45.37	0.1091	194.00	17.98	212.19	1.15	219.02	17.71	18.85
10-04	47.62	0.1300	194.58	18.66	211.88	1.25	218.44	18.87	20.12
10-05	48.98	0.1012	194.18	18.59	211.75	1.25	218.66	18.97	20.22
10-06	49.85	0.1297	194.46	19.30	211.90	1.45	218.55	19.15	20.60
10-Ave	48.62	0.1220	194.35	18.50	212.01	1.32	218.71	18.54	19.86
10-Sd	3.03	0.0150	0.22	0.53	0.30	0.14	0.26	0.57	0.65
10-Cv	6.24%	12.31%	0.11%	2.85%	0.14%	10.30%	0.12%	3.09%	3.26%
11-01	51.47	0.1226	196.50	17.28	210.83	1.39	218.59	18.12	19.51
11-02	46.93	0.1052	193.97	16.32	211.36	1.28	218.24	16.54	17.83
11-03	47.76	0.1151	195.91	16.88	212.27	1.15	218.31	17.81	18.96
11-04	48.23	0.1125	194.06	15.93	211.70	1.24	218.48	16.11	17.35
11-05	49.22	0.0944	194.37	18.09	212.93	1.02	218.85	16.59	17.61
11-06	55.53	0.1356	196.49	17.13	210.53	1.64	218.58	17.95	19.58
11-Ave	49.86	0.1142	195.22	16.94	211.60	1.29	218.51	17.19	18.47
11-Sd	3.19	0.0142	1.21	0.76	0.90	0.21	0.22	0.87	1.00
11-Cv	6.39%	12.40%	0.62%	4.48%	0.42%	16.52%	0.10%	5.06%	5.39%
12-01	48.97	0.0989	194.16	18.67	212.07	1.59	218.60	18.62	20.20
12-02	51.69	0.1193	194.20	18.86	211.74	1.55	218.41	18.59	20.14
12-03	49.78	0.1209	193.49	17.96	212.23	1.28	218.67	17.73	19.01
12-04	47.95	0.1228	194.05	18.47	211.90	1.53	218.49	18.37	19.90
12-05	46.92	0.1297	193.91	17.95	211.86	1.54	218.45	18.53	20.07
12-06	49.92	0.1253	193.61	18.41	211.73	1.34	218.49	18.00	19.35
12-Ave	49.21	0.1195	193.90	18.39	211.92	1.47	218.52	18.31	19.78
12-Sd	1.67	0.0107	0.29	0.37	0.20	0.13	0.10	0.36	0.49
12-Cv	3.38%	8.97%	0.15%	2.01%	0.09%	8.68%	0.04%	1.98%	2.46%
13-01	49.56	0.1014	193.44	16.10	211.49	1.08	218.50	16.80	17.88
13-02	50.03	0.1314	193.85	16.95	211.31	1.29	218.44	16.77	18.06
13-03	51.94	0.1079	194.11	16.24	211.56	1.02	218.64	16.30	17.32
13-04	50.33	0.1345	193.81	15.25	211.39	1.05	218.36	16.49	17.54
13-05	48.46	0.1079	194.24	16.74	211.24	1.25	218.56	16.67	17.92
13-06	49.58	0.0781	193.56	17.66	211.92	0.97	219.12	14.71	15.68
13-Ave	49.98	0.1102	193.84	16.49	211.49	1.11	218.60	16.29	17.40
13-Sd	1.15	0.0208	0.31	0.82	0.24	0.13	0.27	0.80	0.89
13-Cv	2.30%	18.86%	0.16%	5.00%	0.11%	11.73%	0.12%	4.89%	5.09%

Table C2: PC Results, 10°C/Min Heating and Cooling Rates

Blend Number	Glass Transition		Blend Number	Glass Transition		Blend Number	Glass Transition	
	Midpoint	ΔC_p		Midpoint	ΔC_p		Midpoint	ΔC_p
---	°C	J/(gK)	---	°C	J/(gK)	---	°C	J/(gK)
01-01	136.19	0.1413	06-01	136.56	0.1405	12-01	136.83	0.0957
01-02	138.12	0.1121	06-02	135.83	0.1369	12-02	136.75	0.1415
01-03	137.53	0.1130	06-03	138.45	0.1474	12-03	137.19	0.1199
01-04	137.75	0.1373	06-04	135.70	0.1039	12-04	136.03	0.1428
01-05	136.66	0.1287	06-05	136.27	0.1432	12-05	138.85	0.1228
01-06	137.24	0.1524	06-06	137.79	0.1198	12-06	137.01	0.1082
1-Ave	137.25	0.1308	6-Ave	136.77	0.1320	12-Ave	137.11	0.1218
1-Sd	0.72	0.0161	6-Sd	1.11	0.0167	12-Sd	0.94	0.0184
1-Cv	0.52%	12.28%	6-Cv	0.81%	12.67%	12-Cv	0.69%	15.13%
02-01	137.12	0.1334	07-01	137.22	0.1582	13-01	137.27	0.1464
02-02	136.51	0.1346	07-02	137.94	0.1883	13-02	136.99	0.1455
02-03	138.83	0.1921	07-03	136.51	0.1770	13-03	138.41	0.1352
02-04	137.43	0.1283	07-04	139.36	0.1570	13-04	136.97	0.1165
02-05	138.52	0.1195	07-05	136.56	0.1702	13-05	138.64	0.1379
02-06	137.12	0.1490	07-06	134.71	0.1606	13-06	138.31	0.1492
2-Ave	137.59	0.1428	7-Ave	137.05	0.1686	13-Ave	137.77	0.1385
2-Sd	0.90	0.0260	7-Sd	1.56	0.0124	13-Sd	0.77	0.0120
2-Cv	0.65%	18.20%	7-Cv	1.14%	7.35%	13-Cv	0.56%	8.67%
03-01	137.48	0.1253	08-01	138.77	0.1398			
03-02	138.26	0.1283	08-02	137.45	0.1447			
03-03	136.79	0.1206	08-03	138.98	0.1445			
03-04	136.97	0.1207	08-04	138.39	0.1878			
03-05	138.14	0.1301	08-05	134.94	0.1274			
03-06	137.75	0.1279	08-06	138.92	0.1407			
3-Ave	137.57	0.1255	8-Ave	137.91	0.1475			
3-Sd	0.60	0.0040	8-Sd	1.56	0.0207			
3-Cv	0.44%	3.22%	8-Cv	1.13%	14.06%			
04-01	136.67	0.1197	09-01	138.24	0.1318			
04-02	137.15	0.1408	09-02	137.48	0.1224			
04-03	137.25	0.1564	09-03	136.15	0.1404			
04-04	136.66	0.1489	09-04	136.36	0.1450			
04-05	139.87	0.1337	09-05	136.38	0.1115			
04-06	138.26	0.1294	09-06	137.19	0.1242			
4-Ave	137.64	0.1382	9-Ave	136.97	0.1292			
4-Sd	1.24	0.0134	9-Sd	0.81	0.0124			
4-Cv	0.90%	9.67%	9-Cv	0.59%	9.58%			
05-01	137.76	0.1446	10-01	137.20	0.1256			
05-02	138.48	0.1594	10-02	139.19	0.1120			
05-03	135.92	0.1226	10-03	137.61	0.1440			
05-04	137.74	0.1293	10-04	136.14	0.1147			
05-05	137.69	0.1795	10-05	135.36	0.1193			
05-06	137.10	0.1572	10-06	135.53	0.1163			
5-Ave	137.45	0.1488	10-Ave	136.84	0.1220			
5-Sd	0.87	0.0210	10-Sd	1.46	0.0117			
5-Cv	0.63%	14.13%	10-Cv	1.07%	9.63%			

Table C3: PBT Results, 5°C/Min Heating and Cooling Rates

Blend Number	Glass Transition		Crystallization		Small Melting		Main Melting		Melting Total ΔQ J/g
	Midpoint °C	ΔC_p J/(gK)	Onset °C	ΔQ J/g	Onset °C	ΔQ J/g	Onset °C	ΔQ J/g	

1-11	50.90	0.0325	198.21	20.11	212.00	4.84	220.12	12.83	17.67
1-12	47.93	0.1355	197.95	20.72	212.02	4.88	219.96	12.96	17.85
1-13	0.00	0.0000	198.16	18.57	212.17	4.45	219.96	11.93	16.37
1-Ave	32.94	0.0560	198.11	19.80	212.06	4.72	220.01	12.57	17.30
1-Sd	28.57	0.0707	0.14	1.11	0.09	0.24	0.09	0.56	0.81
1-Cv	86.72%	126.34%	0.07%	5.60%	0.04%	5.10%	0.04%	4.46%	4.67%
2-11	49.07	0.0436	198.61	16.92	211.75	4.32	220.14	11.16	15.48
2-12	54.29	0.0584	198.54	18.09	211.56	2.78	219.92	11.59	14.37
2-13	53.92	0.1128	198.29	18.50	210.99	4.34	219.57	12.01	16.36
2-Ave	52.43	0.0716	198.48	17.84	211.43	3.81	219.88	11.59	15.40
2-Sd	2.91	0.0364	0.17	0.82	0.40	0.90	0.29	0.43	1.00
2-Cv	5.56%	50.89%	0.08%	4.60%	0.19%	23.49%	0.13%	3.67%	6.47%
3-11	49.47	0.0845	199.45	20.42	212.44	5.40	220.26	13.45	18.85
3-12	48.92	0.0667	198.67	19.87	212.53	4.68	220.66	12.98	17.66
3-13	46.34	0.0239	199.31	20.29	212.25	4.60	220.36	13.65	18.25
3-Ave	48.24	0.0583	199.14	20.19	212.41	4.89	220.43	13.36	18.25
3-Sd	1.67	0.0312	0.42	0.29	0.14	0.44	0.21	0.34	0.60
3-Cv	3.46%	53.41%	0.21%	1.42%	0.07%	9.02%	0.09%	2.57%	3.26%
4-11	45.58	0.0343	198.73	19.93	212.79	5.55	220.37	12.35	17.89
4-12	50.86	0.0393	197.95	19.03	212.24	4.49	220.21	12.41	16.90
4-13	45.92	0.0824	198.97	20.51	212.71	5.44	220.26	12.70	18.13
4-Ave	47.45	0.0520	198.55	19.82	212.58	5.16	220.28	12.49	17.64
4-Sd	2.96	0.0264	0.53	0.75	0.30	0.58	0.08	0.19	0.65
4-Cv	6.23%	50.82%	0.27%	3.76%	0.14%	11.26%	0.04%	1.50%	3.70%
5-11	50.59	0.0846	198.45	20.09	212.52	5.59	220.14	12.53	18.12
5-12	51.59	0.0597	198.66	20.45	212.56	5.58	220.14	12.45	18.04
5-13	50.86	0.0130	198.46	20.20	212.54	5.59	220.14	12.60	18.19
5-Ave	51.01	0.0524	198.52	20.25	212.54	5.59	220.14	12.53	18.12
5-Sd	0.52	0.0364	0.12	0.18	0.02	0.00	0.00	0.08	0.08
5-Cv	1.01%	69.36%	0.06%	0.91%	0.01%	0.07%	0.00%	0.60%	0.41%
6-11	51.24	0.0121	198.50	20.34	212.49	5.33	220.15	12.51	17.83
6-12	51.38	0.0043	198.48	20.09	212.69	5.69	220.25	12.47	18.16
6-13	49.41	0.0171	197.97	18.99	212.01	4.76	220.12	12.29	17.04
6-Ave	50.68	0.0112	198.32	19.81	212.40	5.26	220.17	12.42	17.68
6-Sd	1.10	0.0065	0.30	0.72	0.35	0.47	0.07	0.12	0.58
6-Cv	2.17%	57.79%	0.15%	3.63%	0.16%	8.98%	0.03%	0.94%	3.26%
7-11	49.89	0.0640	198.46	16.59	212.10	4.59	220.10	10.64	15.23
7-12	44.24	0.1021	198.28	16.91	211.12	4.07	219.86	11.52	15.58
7-13	48.76	0.0373	198.36	17.68	211.78	4.64	219.83	11.14	15.78
7-Ave	47.63	0.0678	198.37	17.06	211.67	4.43	219.93	11.10	15.53
7-Sd	2.99	0.0326	0.09	0.56	0.50	0.32	0.15	0.44	0.28
7-Cv	6.28%	48.03%	0.05%	3.28%	0.24%	7.13%	0.07%	3.98%	1.79%

Table C3: Continued... PBT Results

Blend Number	Glass Transition		Crystallization		Small Melting		Main Melting		Melting Total ΔQ
	Midpoint °C	ΔC_p J/(gK)	Onset °C	ΔQ J/g	Onset °C	ΔQ J/g	Onset °C	ΔQ J/g	
---	°C	J/(gK)	°C	J/g	°C	J/g	°C	J/g	J/g
8-11	47.65	0.0586	197.63	18.96	212.11	4.36	220.21	12.78	17.14
8-12	50.18	0.1162	198.51	20.27	212.54	5.39	220.30	12.66	18.05
8-13	48.86	0.0837	197.84	20.87	211.70	4.60	219.96	13.82	18.42
8-Ave	48.90	0.0862	197.99	20.03	212.12	4.78	220.16	13.09	17.87
8-Sd	1.27	0.0289	0.46	0.98	0.42	0.54	0.18	0.64	0.66
8-Cv	2.59%	33.52%	0.23%	4.88%	0.20%	11.25%	0.08%	4.87%	3.69%
9-11	50.97	0.0526	198.29	20.21	212.46	5.24	220.32	12.95	18.19
9-12	46.79	0.0969	198.43	20.55	212.12	5.01	220.07	13.27	18.28
9-13	52.12	0.0884	197.91	19.42	211.89	4.41	220.13	13.21	17.62
9-Ave	49.96	0.0793	198.21	20.06	212.16	4.89	220.17	13.14	18.03
9-Sd	2.80	0.0235	0.27	0.58	0.29	0.43	0.13	0.17	0.36
9-Cv	5.61%	29.64%	0.14%	2.89%	0.14%	8.75%	0.06%	1.29%	1.99%
10-11	50.07	0.0808	198.54	22.91	212.68	5.91	220.28	14.68	20.59
10-12	49.78	0.0570	198.74	23.32	212.62	5.83	220.29	14.65	20.48
10-13	50.51	0.0519	198.10	22.41	212.49	5.44	220.21	14.54	19.99
10-Ave	50.12	0.0633	198.46	22.88	212.60	5.73	220.26	14.62	20.35
10-Sd	0.37	0.0155	0.33	0.46	0.10	0.25	0.04	0.07	0.32
10-Cv	0.73%	24.43%	0.16%	1.99%	0.05%	4.37%	0.02%	0.50%	1.57%
11-11	62.40	0.0991	200.16	22.59	211.49	4.22	219.53	15.84	20.06
11-12	50.28	0.0474	197.34	19.33	211.71	4.28	219.98	13.40	17.68
11-13	---	---	199.89	21.87	211.56	4.26	219.91	15.28	19.55
11-Ave	56.34	0.0732	199.13	21.26	211.59	4.25	219.81	14.84	19.10
11-Sd	8.57	0.0366	1.56	1.71	0.11	0.03	0.24	1.28	1.25
11-Cv	15.21%	49.94%	0.78%	8.05%	0.05%	0.74%	0.11%	8.61%	6.56%
12-11	47.18	0.1220	198.14	22.55	212.56	5.69	220.21	14.33	20.03
12-12	51.79	0.0859	198.24	23.14	212.12	4.08	219.96	14.33	18.41
12-13	48.62	0.0239	198.17	22.27	212.85	5.93	220.24	13.92	19.84
12-Ave	49.20	0.0773	198.18	22.65	212.51	5.23	220.14	14.19	19.43
12-Sd	2.36	0.0496	0.05	0.44	0.37	1.00	0.15	0.24	0.89
12-Cv	4.79%	64.18%	0.03%	1.96%	0.17%	19.17%	0.07%	1.67%	4.56%
13-11	52.07	0.0191	197.92	20.15	212.12	4.60	220.24	13.06	17.66
13-12	---	---	198.35	20.27	211.94	4.38	220.06	13.40	17.79
13-13	49.20	0.0203	198.04	19.88	212.19	4.51	220.22	12.97	17.48
13-Ave	50.64	0.0197	198.10	20.10	212.08	4.50	220.17	13.14	17.64
13-Sd	2.03	0.0008	0.22	0.20	0.13	0.11	0.10	0.23	0.16
13-Cv	4.01%	4.02%	0.11%	0.99%	0.06%	2.38%	0.04%	1.73%	0.88%
PBT-11	44.04	0.1787	193.45	47.22	210.00	5.74	219.21	33.67	39.41
PBT-12	40.38	0.1566	198.30	49.12	210.76	7.90	219.59	32.60	40.51
PBT-13	43.64	0.1566	192.27	45.51	209.92	6.06	218.99	30.42	36.48
PBT-Ave	42.69	0.1640	194.67	47.28	210.23	6.57	219.26	32.23	38.80
PBT-Sd	2.01	0.0128	3.20	1.81	0.46	1.17	0.30	1.66	2.08
PBT-Cv	4.70%	7.78%	1.64%	3.82%	0.22%	17.77%	0.14%	5.14%	5.37%

Table C4: PC Results, 10°C/Min Heating and Cooling Rates

Blend Number	Glass Transition		Blend Number	Glass Transition		Blend Number	Glass Transition	
	Midpoint	ΔC_p		Midpoint	ΔC_p		Midpoint	ΔC_p
---	°C	J/(gK)	---	°C	J/(gK)	---	°C	J/(gK)
01-11	137.00	0.1539	06-11	137.34	0.1535	12-11	133.27	0.1612
01-12	138.26	0.1652	06-12	137.45	0.1579	12-12	138.51	0.1743
01-13	137.18	0.1524	06-13	138.89	0.1546	12-13	136.58	0.1478
1-Ave	137.48	0.1572	6-Ave	137.89	0.1553	12-Ave	136.12	0.1611
1-Sd	0.68	0.0070	6-Sd	0.86	0.0023	12-Sd	2.65	0.0133
1-Cv	0.50%	4.45%	6-Cv	0.63%	1.47%	12-Cv	1.95%	8.22%
02-11	138.89	0.1518	07-11	137.62	0.1922	13-11	138.38	0.1619
02-12	136.55	0.1929	07-12	140.07	0.1821	13-12	136.13	0.1609
02-13	136.64	0.1711	07-13	139.72	0.1743	13-13	138.12	0.1730
2-Ave	137.36	0.1719	7-Ave	139.14	0.1829	13-Ave	137.54	0.1653
2-Sd	1.33	0.0206	7-Sd	1.33	0.0090	13-Sd	1.23	0.0067
2-Cv	0.97%	11.96%	7-Cv	0.95%	4.91%	13-Cv	0.89%	4.06%
03-11	137.26	0.1468	08-11	140.33	0.1496	PC1-11	149.48	0.2674
03-12	140.06	0.1487	08-12	138.02	0.1171	PC1-12	150.35	0.2669
03-13	139.21	0.1734	08-13	140.04	0.1517	PC1-13	150.75	0.2541
3-Ave	138.84	0.1563	8-Ave	139.46	0.1395	PC1-Ave	150.19	0.2628
3-Sd	1.44	0.0148	8-Sd	1.26	0.0194	PC1-Sd	0.65	0.0075
3-Cv	1.03%	9.49%	8-Cv	0.90%	13.91%	PC1-Cv	0.43%	2.87%
04-11	138.46	0.1528	09-11	138.67	0.1595	PC2-11	145.71	0.3142
04-12	140.30	0.1808	09-12	137.97	0.1564	PC2-12	145.42	0.2713
04-13	138.78	0.1584	09-13	138.22	0.1687	PC2-13	145.70	0.2703
4-Ave	139.18	0.1640	9-Ave	138.29	0.1615	PC2-Ave	145.61	0.2853
4-Sd	0.98	0.0148	9-Sd	0.35	0.0064	PC2-Sd	0.16	0.0251
4-Cv	0.71%	9.03%	9-Cv	0.26%	3.96%	PC2-Cv	0.11%	8.79%
05-11	136.69	0.1645	10-11	137.87	0.1184			
05-12	137.70	0.1593	10-12	137.49	0.1447			
05-13	136.96	0.1478	10-13	138.30	0.1615			
5-Ave	137.12	0.1572	10-Ave	137.89	0.1415			
5-Sd	0.52	0.0085	10-Sd	0.41	0.0217			
5-Cv	0.38%	5.44%	10-Cv	0.29%	15.35%			

APPENDIX D: Blend and Phase Composition from DSC

Notes:

1. DSC Heating and Cooling Rates were all 5°C/min
2. Midpoint Values for T_g were used.
3. ΔC_p stands for the heat capacity change at glass transition

Table D1: Blended PC Parameters

Equation	T _g	Equation	ΔC_p
	°C		J/(g·K)
11	147.98	44	0.2735
12	147.99		
13	147.77		

Table D2: Phase Compositions using the Fox Equation (Equation 11)

Blend Number	Amorphous Phases								Blend			
	PC Rich				PBT Rich				Total PC	Amorous PBT	Eq. 42 Crystalline PBT	Total PBT
	PC	PBT	Eq. 44 Δc_p	Eq. 43 Phase in Blend	PC	PBT	Eq. 44 Δc_p	Eq. 43 Phase in Blend				
---	wt%	wt%	J/(g·°C)	wt%	wt%	wt%	J/(g·°C)	wt%	wt%	wt%	wt%	wt%
1	97%	3.1%	0.28	57%	19%	81%	0.34	25%	60%	22%	12%	34%
2	97%	3.1%	0.28	62%	26%	74%	0.33	22%	66%	18%	11%	29%
3	97%	2.7%	0.28	57%	16%	84%	0.34	17%	58%	16%	13%	29%
4	97%	2.6%	0.28	60%	14%	86%	0.34	15%	60%	15%	13%	27%
5	97%	3.2%	0.28	57%	23%	77%	0.33	16%	59%	14%	13%	27%
6	97%	3.0%	0.28	56%	22%	78%	0.33	3%	55%	4%	13%	17%
7	97%	2.6%	0.28	66%	15%	85%	0.34	20%	68%	19%	11%	30%
8	98%	2.5%	0.28	51%	18%	82%	0.34	26%	54%	22%	13%	35%
9	97%	2.8%	0.28	59%	20%	80%	0.33	24%	62%	21%	13%	33%
10	97%	3.0%	0.28	51%	21%	79%	0.33	19%	54%	17%	15%	31%
11	96%	3.5%	0.28	58%	34%	66%	0.32	23%	64%	17%	14%	31%
12	97%	3.1%	0.28	60%	19%	81%	0.34	23%	62%	21%	14%	34%
13	97%	3.1%	0.28	61%	22%	78%	0.33	6%	60%	7%	13%	19%

Table D3: Phase Compositions using the Utracki & Jukes Equation (Equation 12)

Blend Number	Amorphous Phases								Blend			
	PC Rich				PBT Rich				Total PC	Amorous PBT	Eq. 42 Crystalline PBT	Total PBT
	PC	PBT	Eq. 44 Δc_p	Eq. 43 Phase in Blend	PC	PBT	Eq. 44 Δc_p	Eq. 43 Phase in Blend				
---	wt%	wt%	J/(g·°C)	wt%	wt%	wt%	J/(g·°C)	wt%	wt%	wt%	wt%	
1	94%	5.9%	0.28	57%	12%	88%	0.34	25%	56%	25%	12%	37%
2	94%	6.0%	0.28	62%	17%	83%	0.34	21%	62%	21%	11%	32%
3	95%	5.1%	0.28	56%	10%	90%	0.34	17%	55%	18%	13%	31%
4	95%	4.9%	0.28	59%	9%	91%	0.34	15%	58%	17%	13%	29%
5	94%	6.1%	0.28	57%	14%	86%	0.34	15%	55%	17%	13%	30%
6	94%	5.7%	0.28	56%	14%	86%	0.34	3%	53%	6%	13%	19%
7	95%	5.0%	0.28	66%	9%	91%	0.34	20%	64%	21%	11%	32%
8	95%	4.8%	0.28	50%	11%	89%	0.34	25%	51%	25%	13%	38%
9	95%	5.5%	0.28	58%	13%	87%	0.34	23%	58%	24%	13%	36%
10	94%	5.7%	0.28	51%	13%	87%	0.34	19%	50%	19%	15%	34%
11	93%	6.7%	0.28	58%	22%	78%	0.33	22%	59%	21%	14%	35%
12	94%	5.9%	0.28	59%	11%	89%	0.34	23%	59%	24%	14%	37%
13	94%	6.0%	0.28	60%	14%	86%	0.34	6%	58%	9%	13%	21%

Table D4: Phase Compositions using the Utracki & Jukes Equation (Equation 13), $k = 0.41$ when PBT is 2

Blend Number	Amorphous Phases								Blend			
	PC Rich				PBT Rich				Total PC	Amorous PBT	Eq. 42 Crystalline PBT	Total PBT
	PC	PBT	Eq. 44 Δc_p	Eq. 43 Phase in Blend	PC	PBT	Eq. 44 Δc_p	Eq. 43 Phase in Blend				
---	wt%	wt%	J/(g·°C)	wt%	wt%	wt%	J/(g·°C)	wt%	wt%	wt%	wt%	
1	87%	13.2%	0.28	55%	5%	95%	0.35	24%	49%	30%	12%	43%
2	87%	13.3%	0.28	61%	7%	93%	0.34	21%	54%	27%	11%	38%
3	88%	11.5%	0.28	55%	4%	96%	0.35	17%	50%	22%	13%	36%
4	89%	11.1%	0.28	58%	4%	96%	0.35	15%	52%	21%	13%	33%
5	86%	13.6%	0.28	55%	6%	94%	0.35	15%	49%	22%	13%	35%
6	87%	12.7%	0.28	55%	6%	94%	0.35	3%	48%	10%	13%	23%
7	89%	11.1%	0.28	65%	4%	96%	0.35	20%	58%	26%	11%	37%
8	89%	10.7%	0.28	50%	5%	95%	0.35	25%	45%	29%	13%	42%
9	88%	12.2%	0.28	57%	6%	94%	0.35	23%	51%	29%	13%	42%
10	87%	12.7%	0.28	50%	6%	94%	0.35	18%	45%	24%	15%	38%
11	85%	14.8%	0.28	57%	10%	90%	0.34	21%	50%	28%	14%	41%
12	87%	13.1%	0.28	58%	5%	95%	0.35	22%	52%	29%	14%	43%
13	87%	13.3%	0.28	59%	6%	94%	0.35	6%	52%	13%	13%	26%

APPENDIX E: Rule of Mixtures DSC Curve Superposition

Figure E1: Blend 1, the T_g Region (a), T_m Region (b)

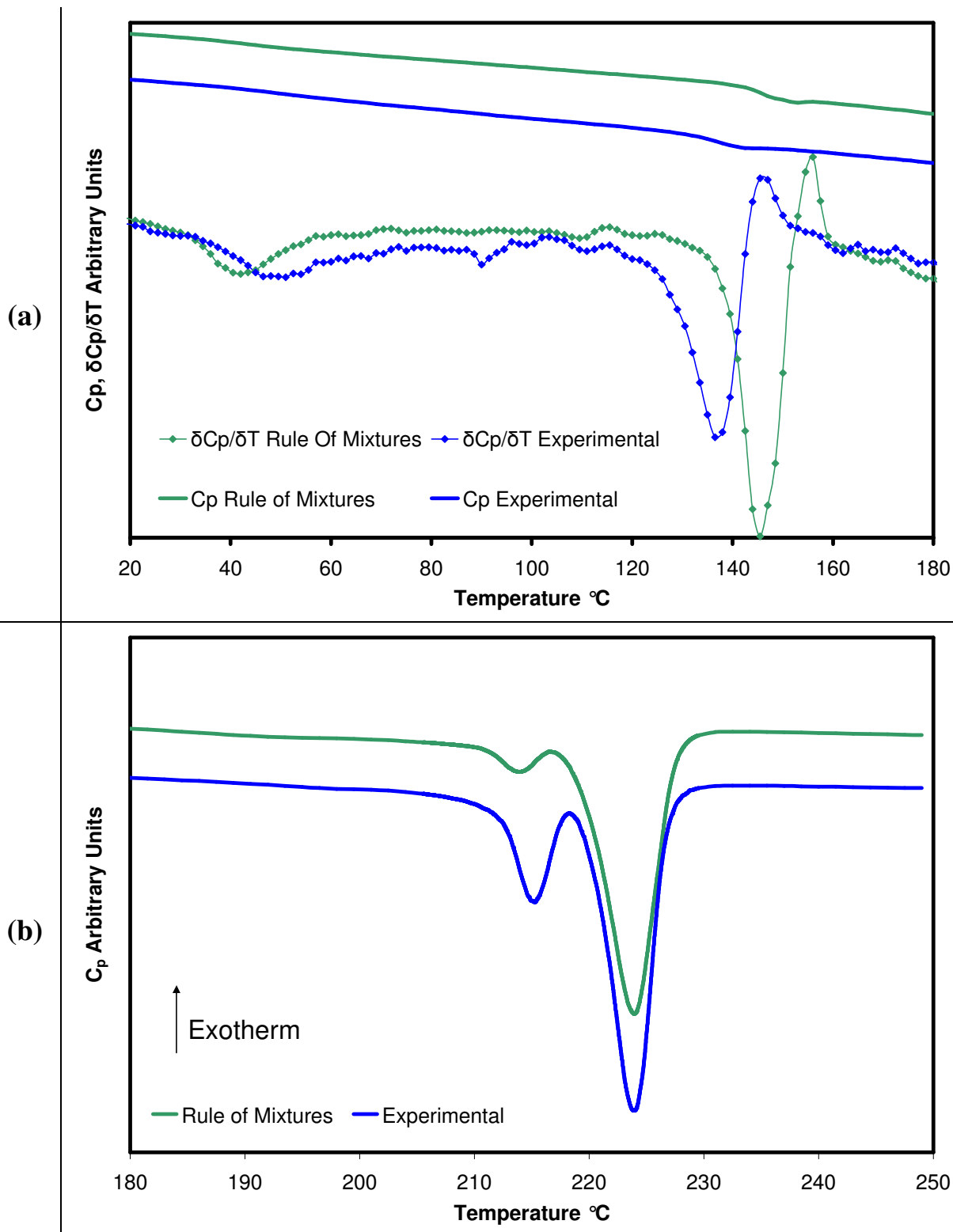


Figure E2: Blend 2, T_g Region (a), T_m Region (b)

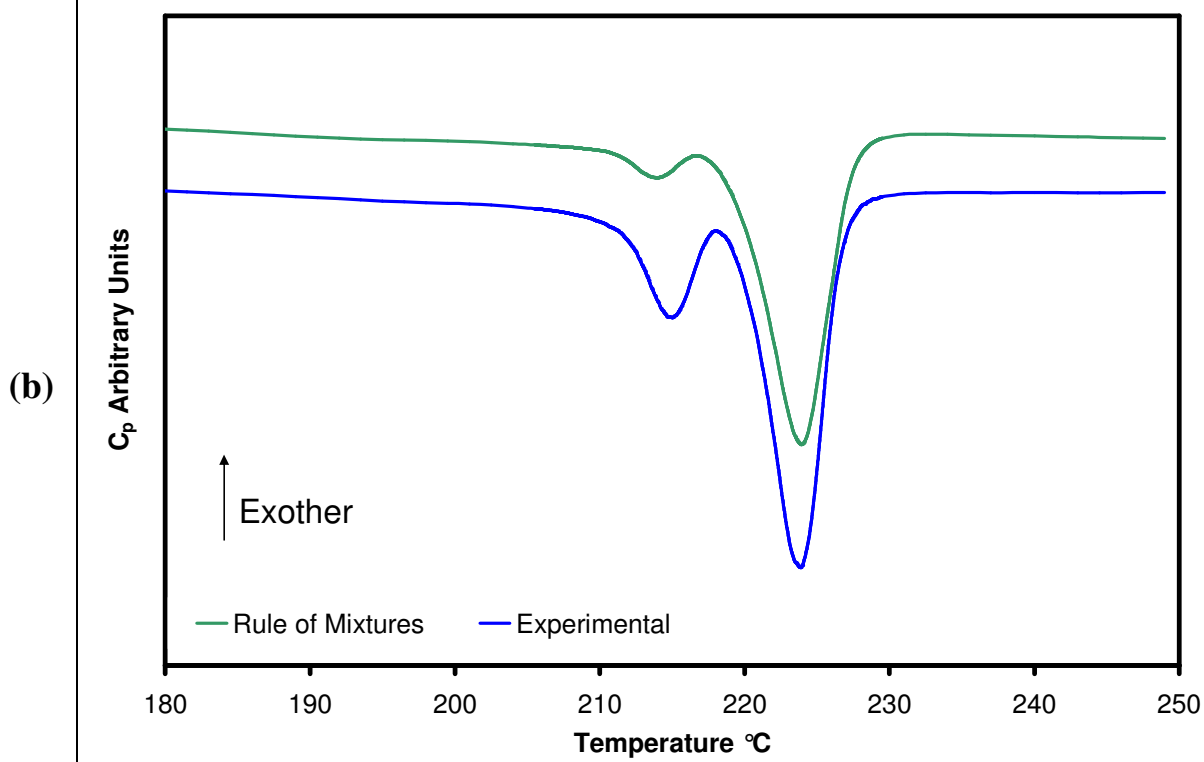
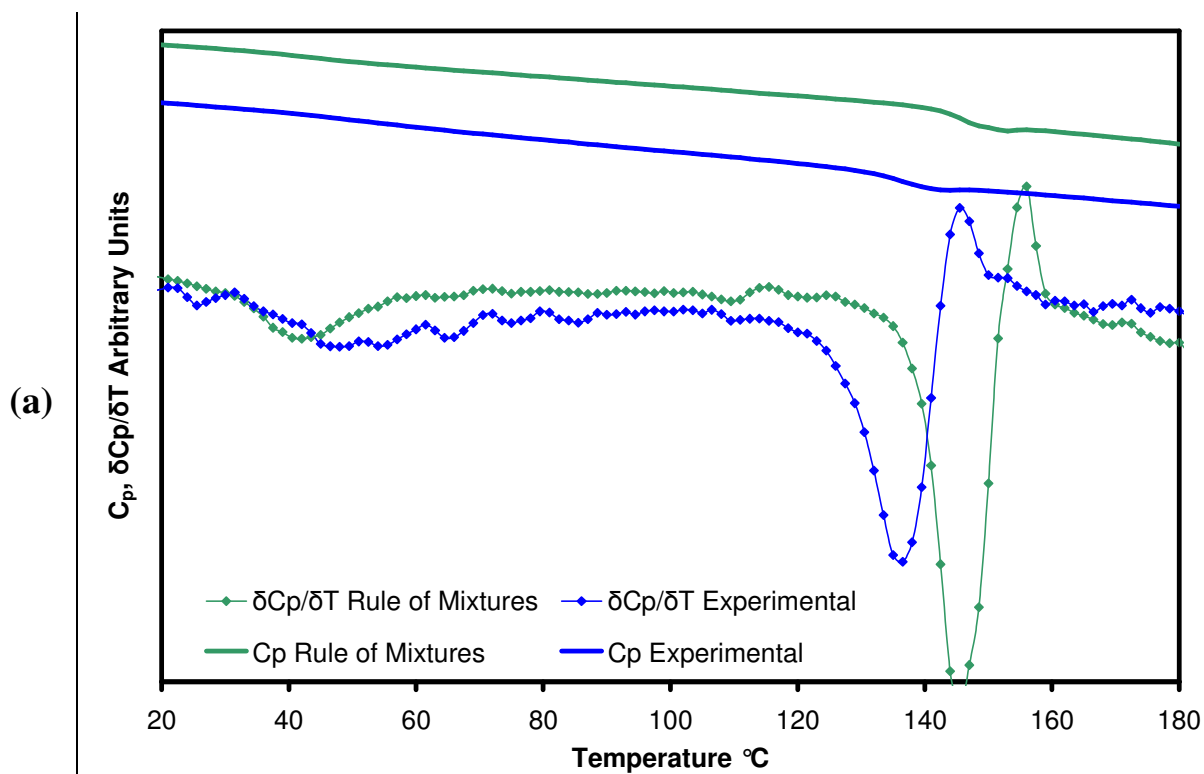


Figure E3: Blend 3, T_g Region (a), T_m Region (b)

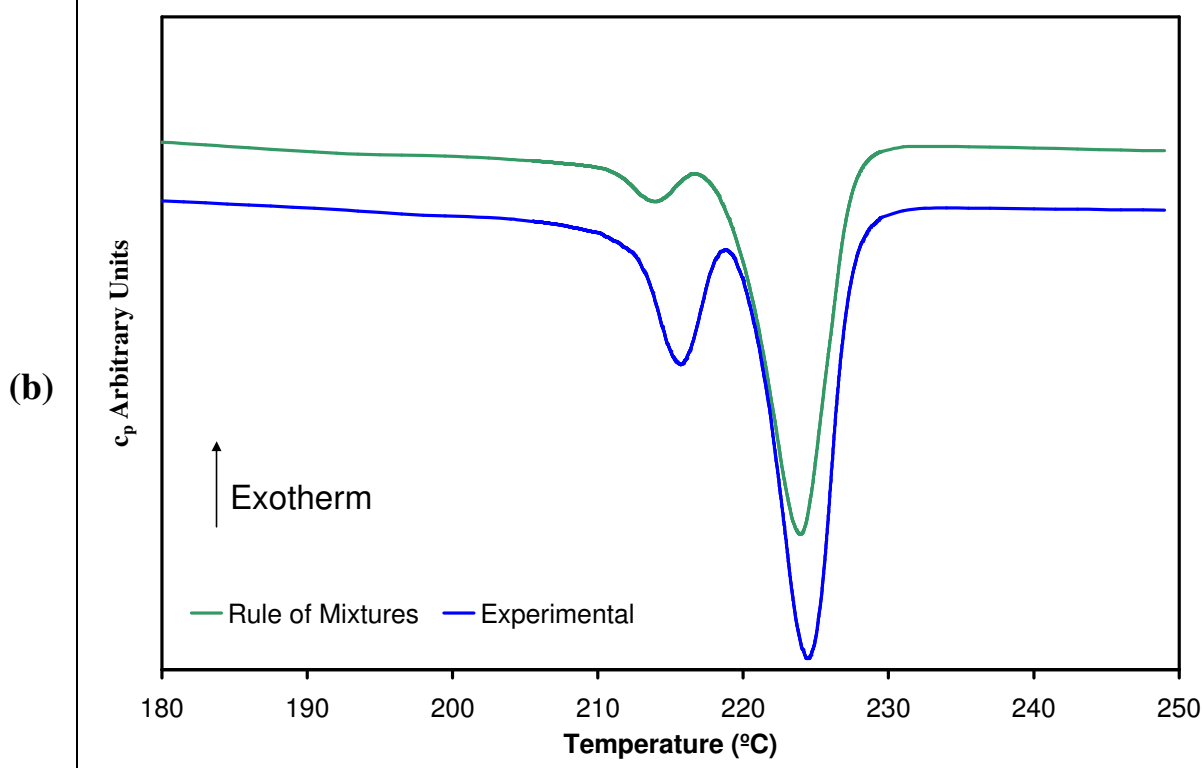
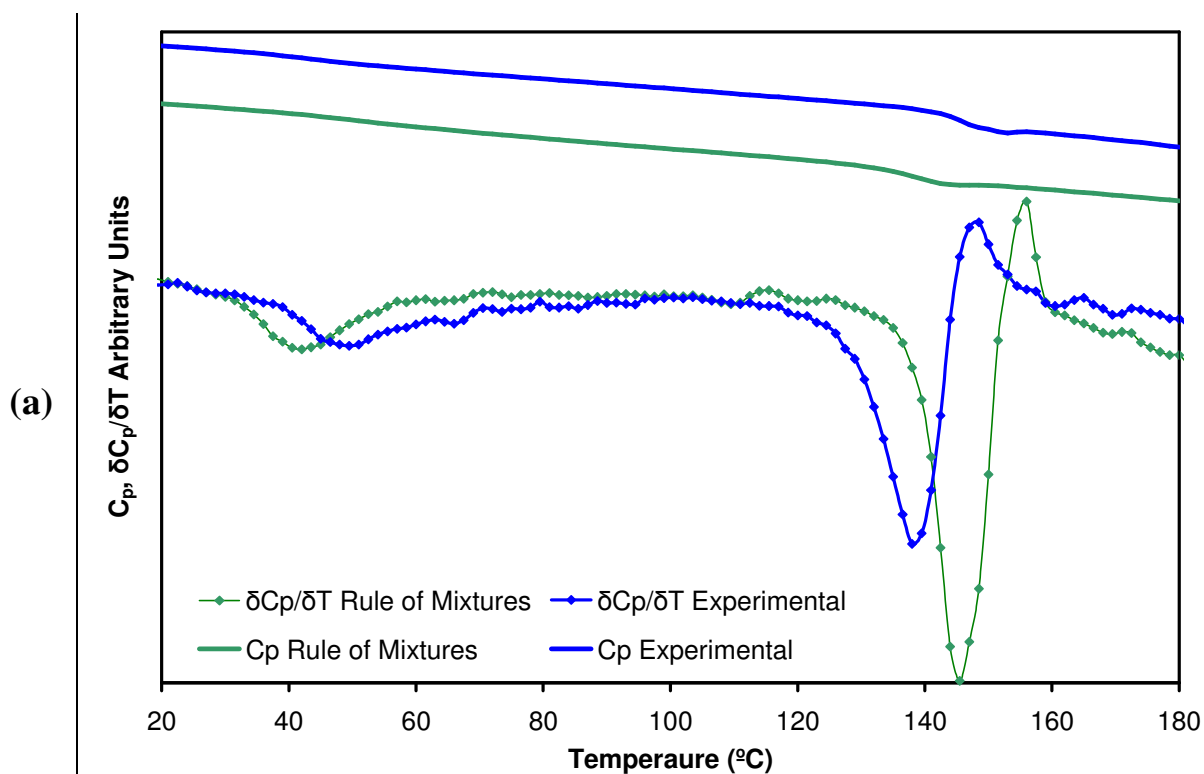


Figure E4: Blend 4, T_g Region (a), T_m Region (b)

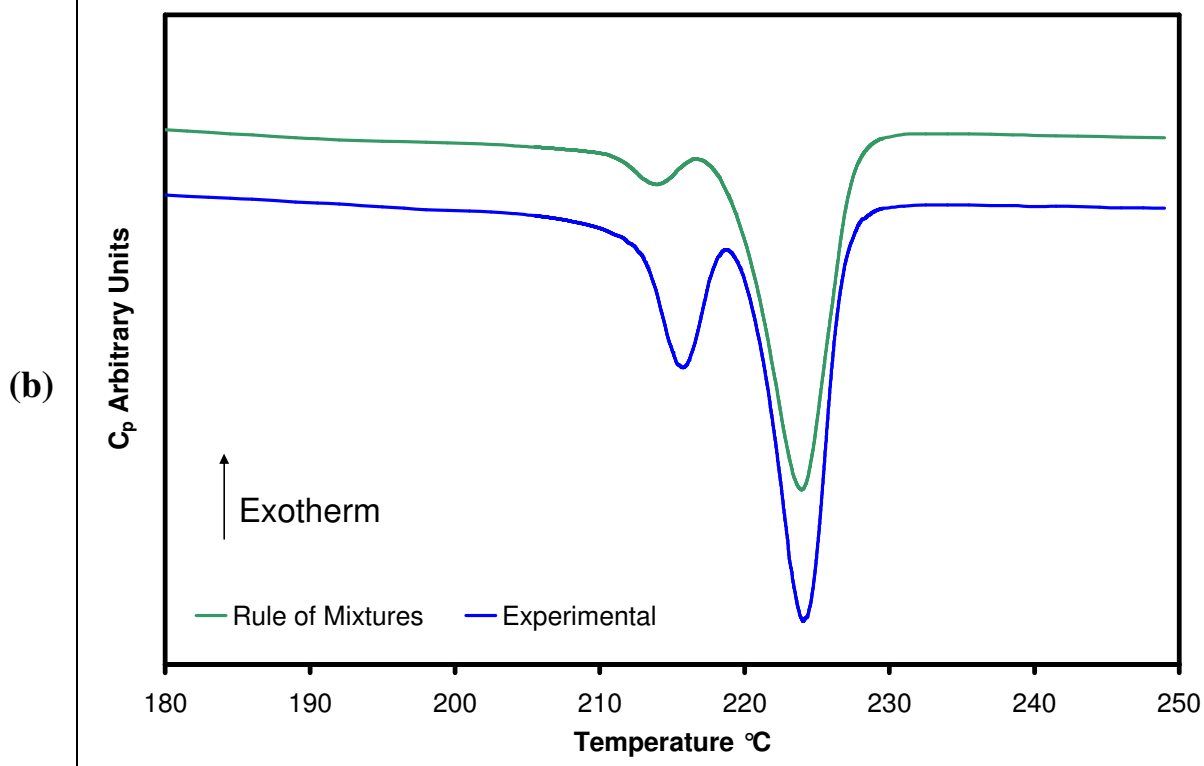
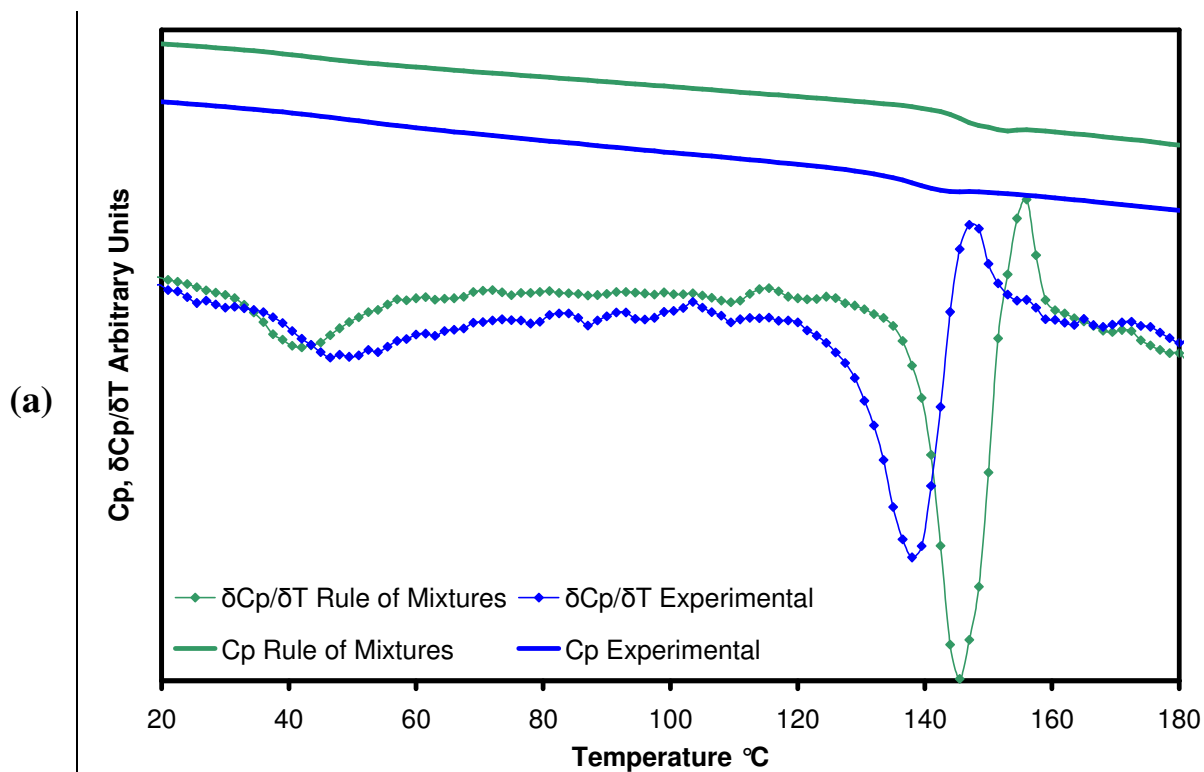


Figure E5: Blend 5, T_g Region (a), T_m Region (b)

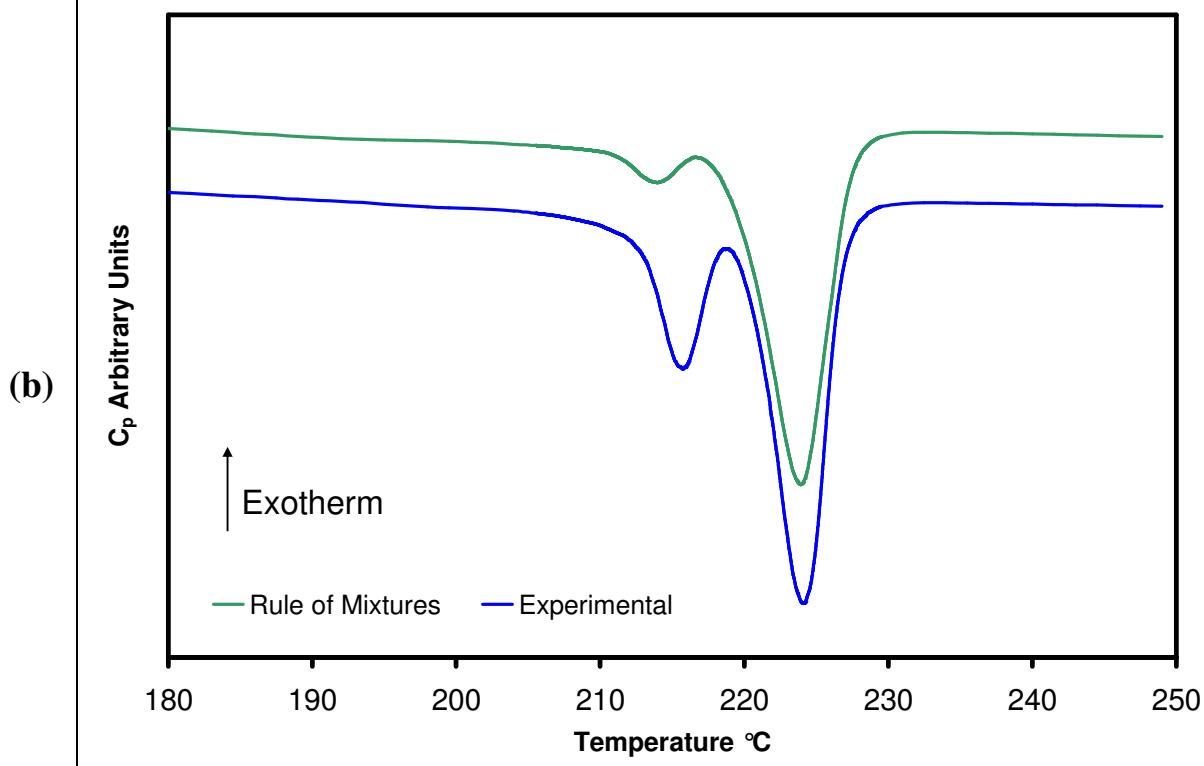
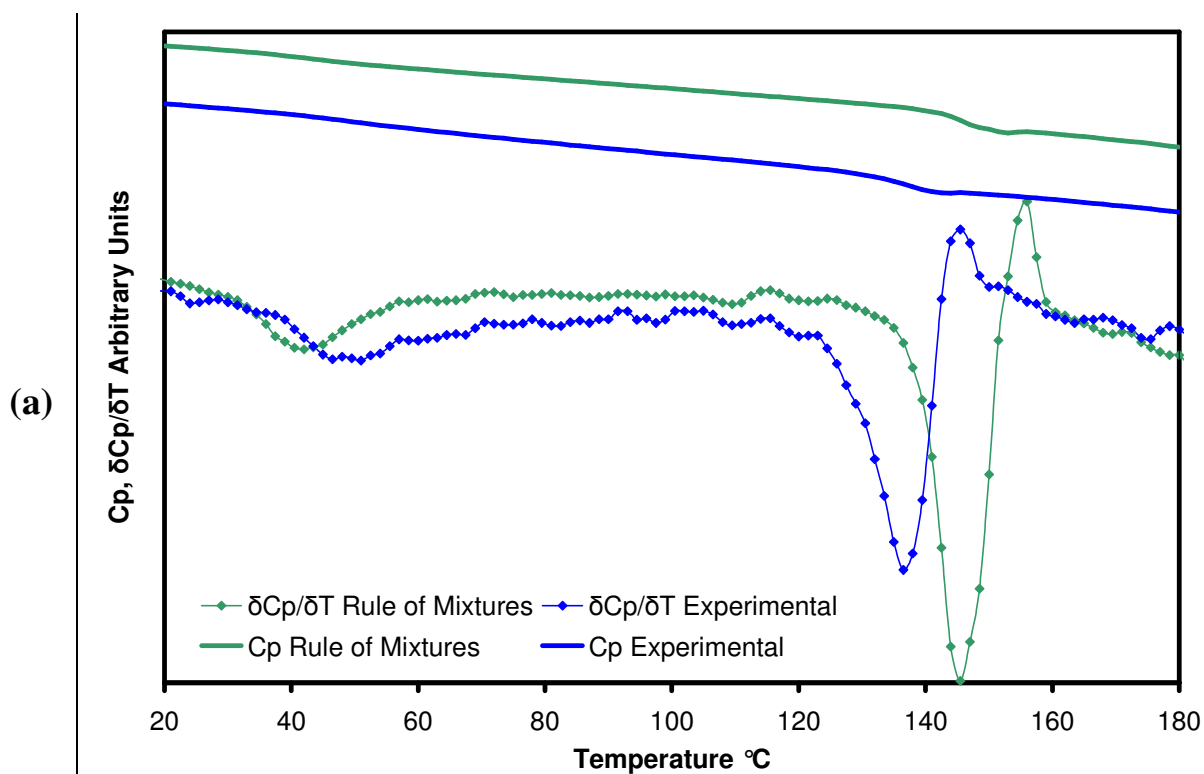


Figure E6: Blend 6, T_g Region (a), T_m Region (b)

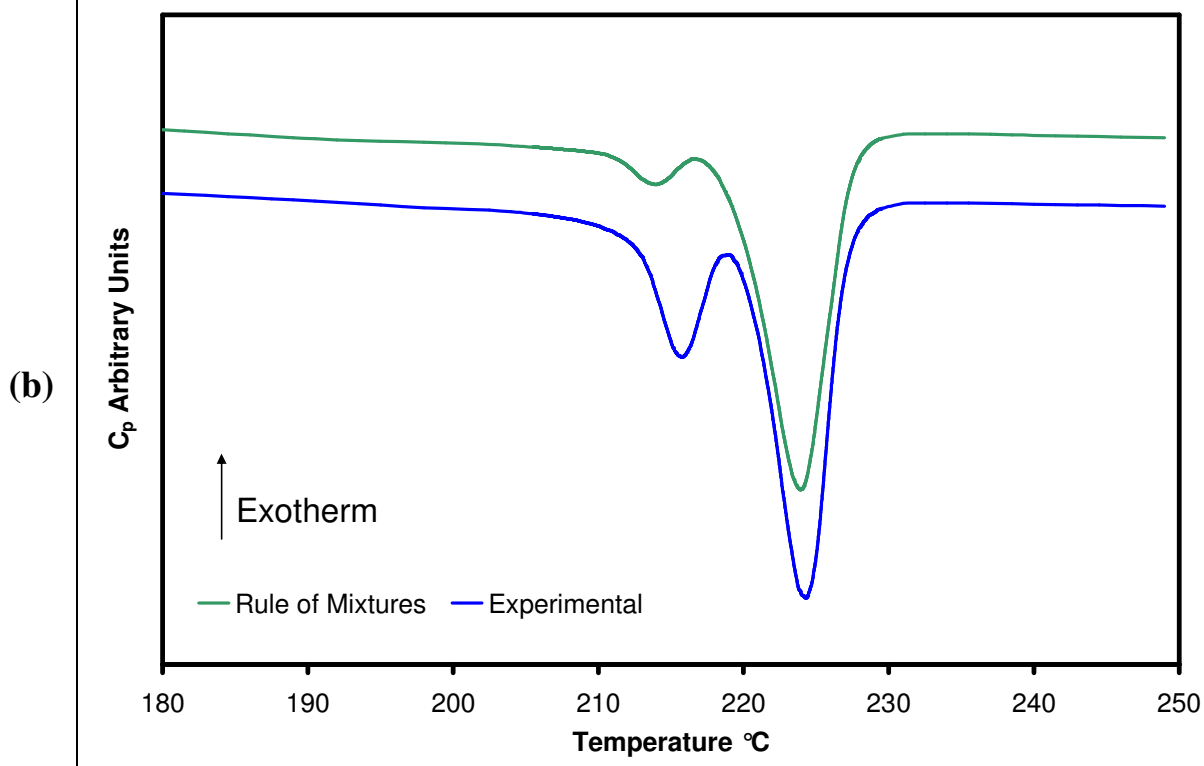
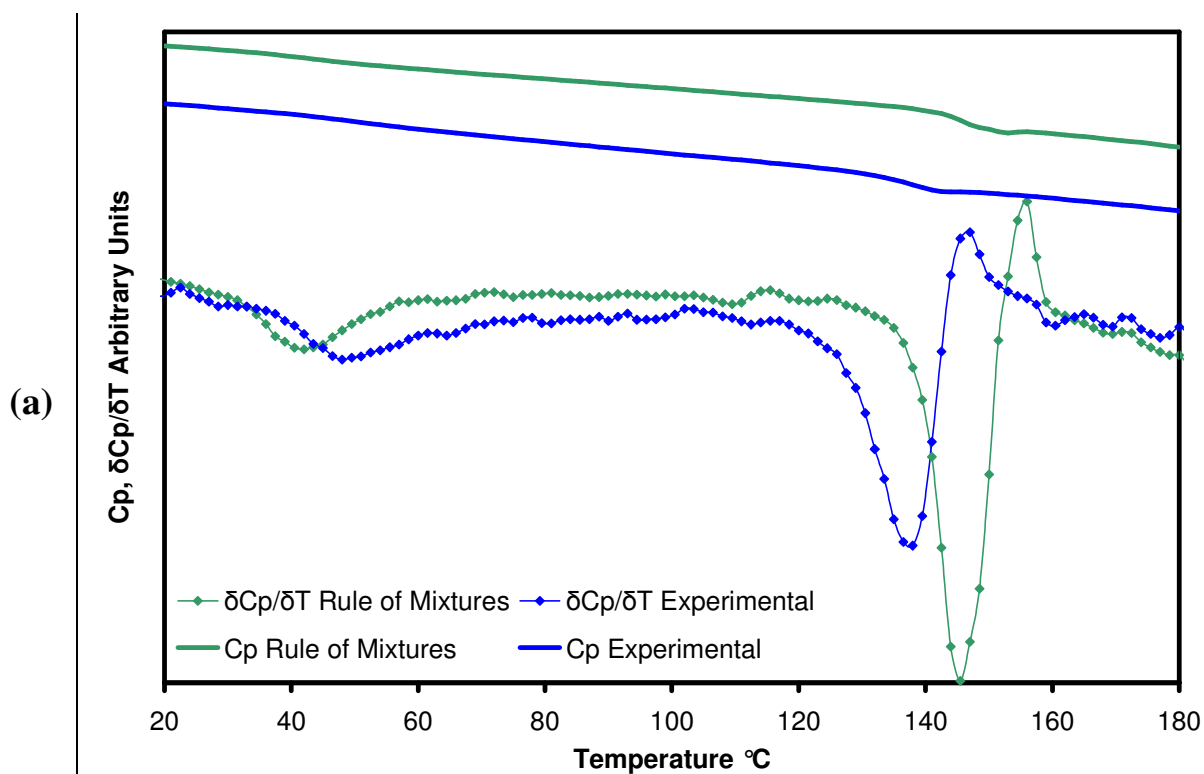


Figure E7: Blend 7, T_g Region (a), T_m Region (b)

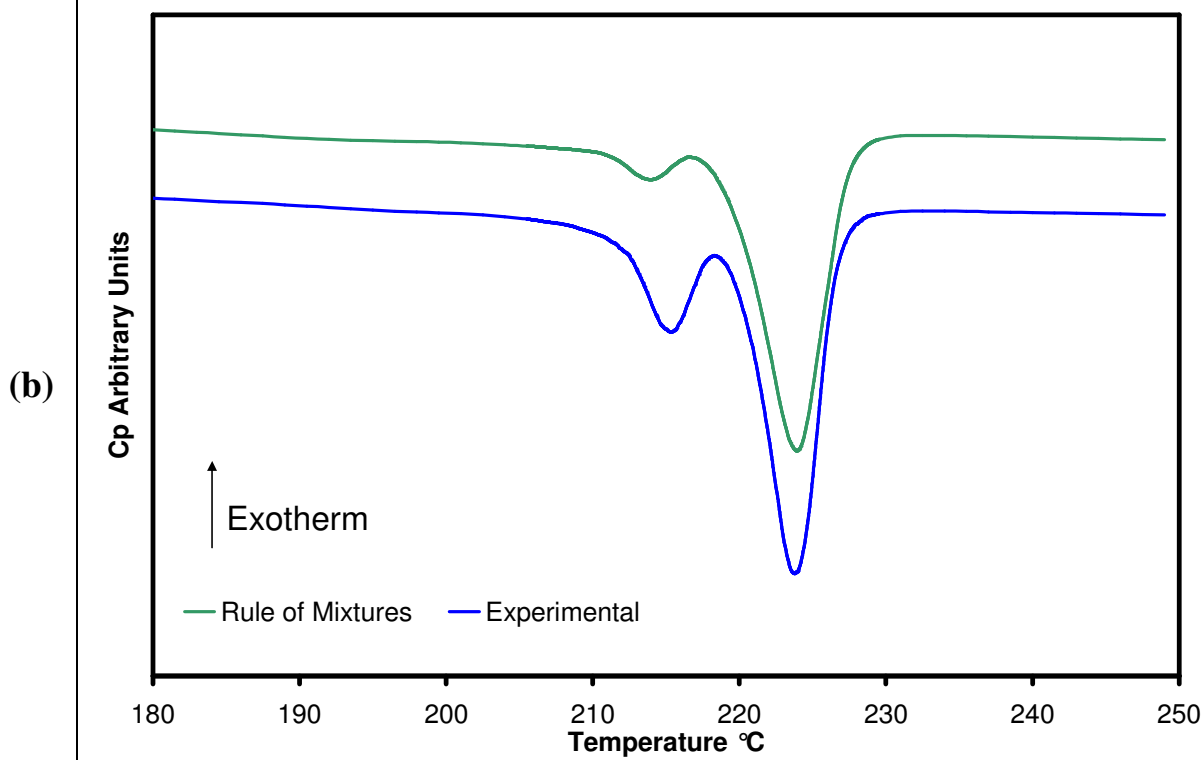
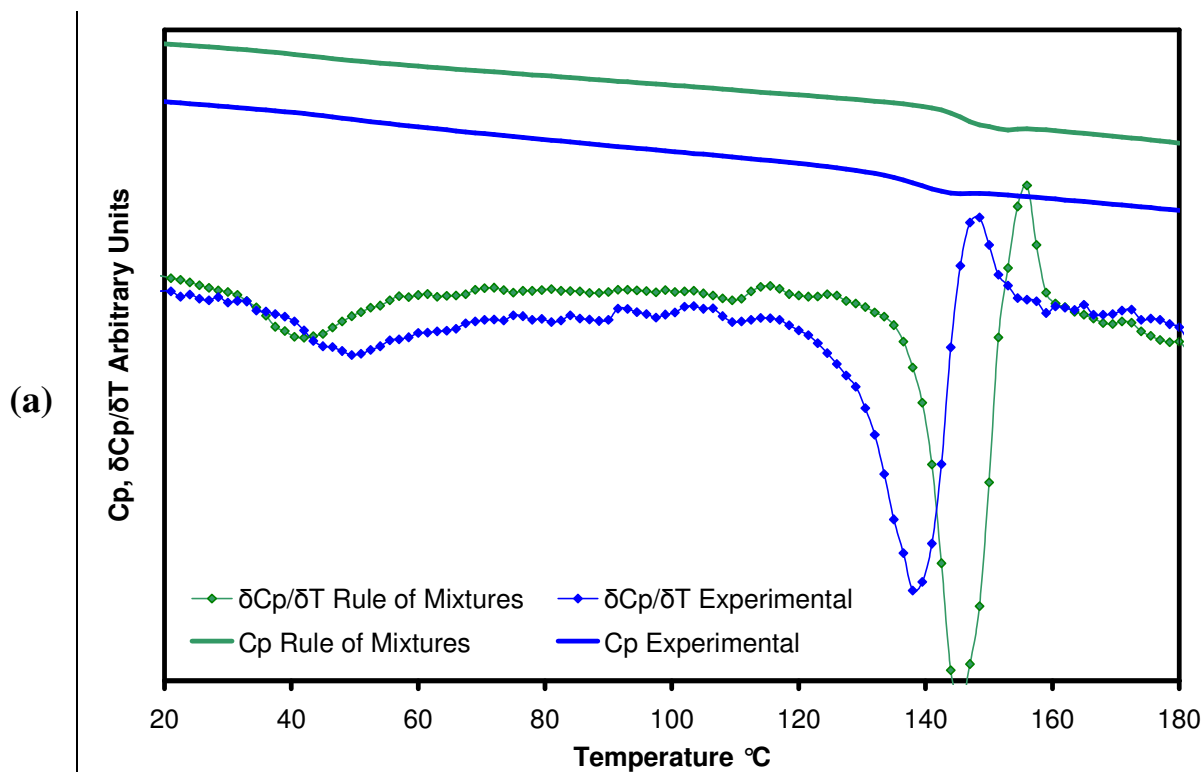


Figure E8: Blend 8, T_g Region (a), T_m Region (b)

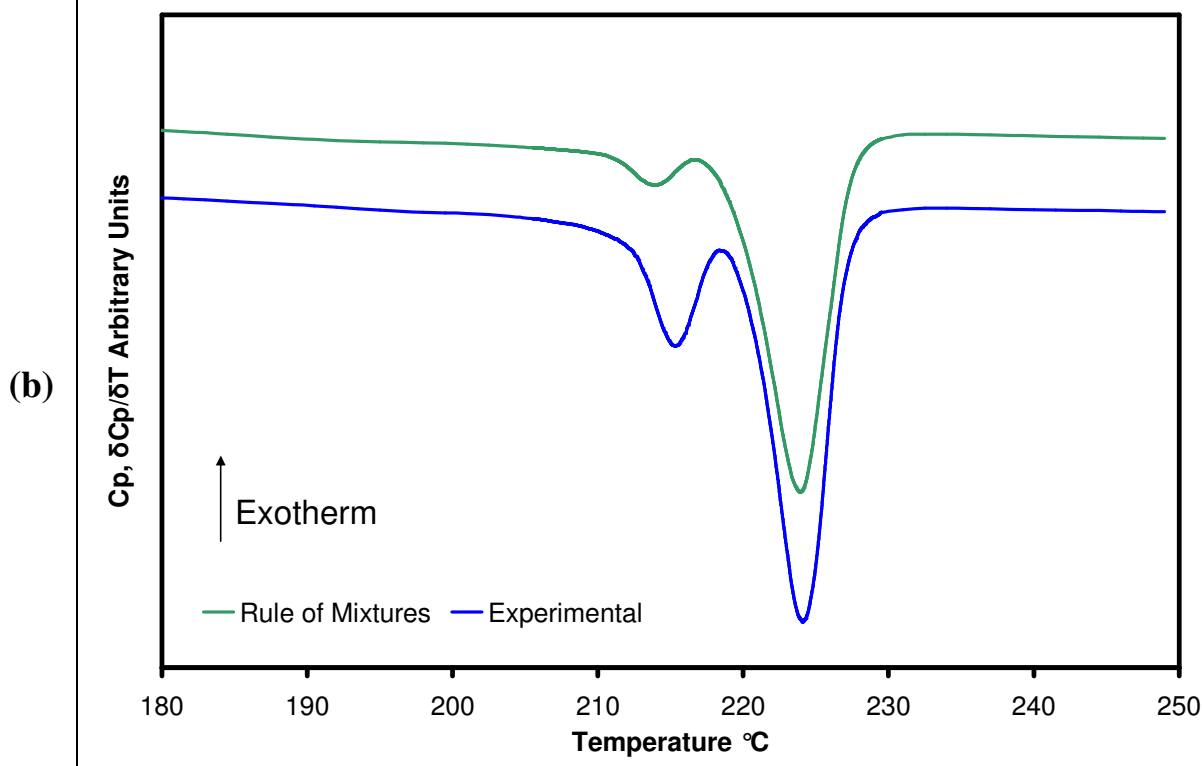
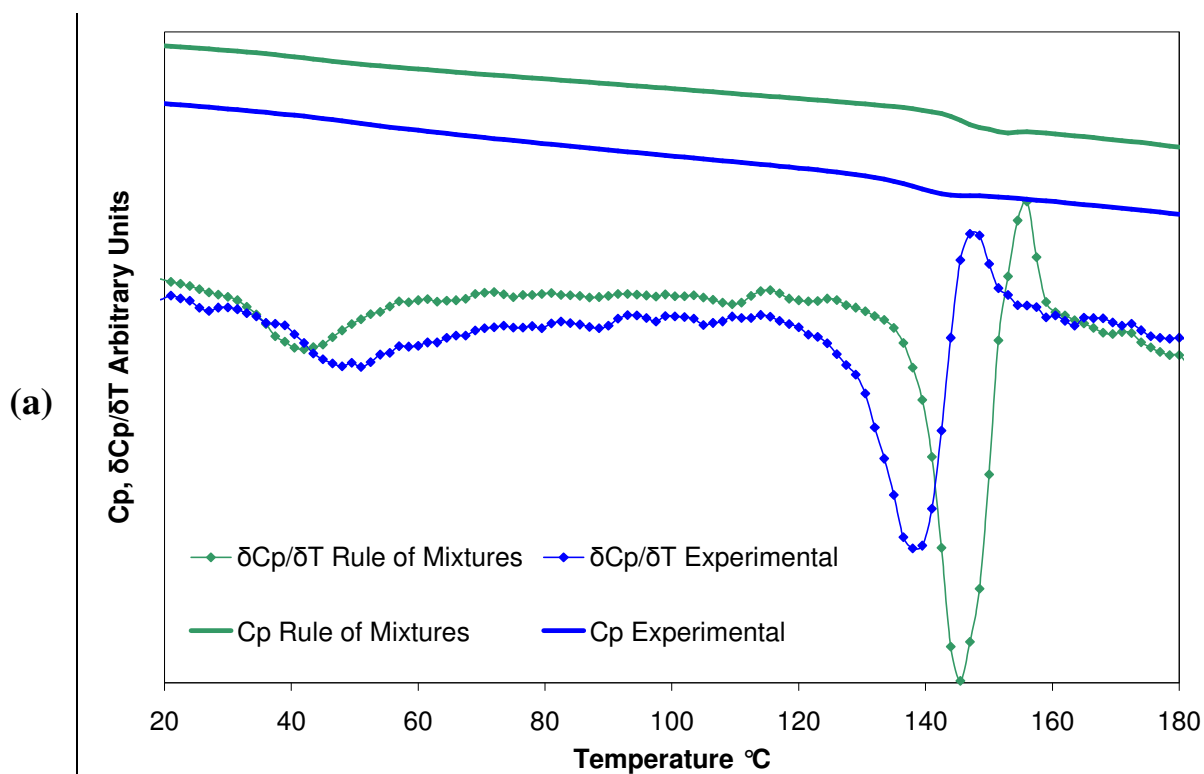


Figure E9: Blend 9, T_g Region (a), T_m Region (b)

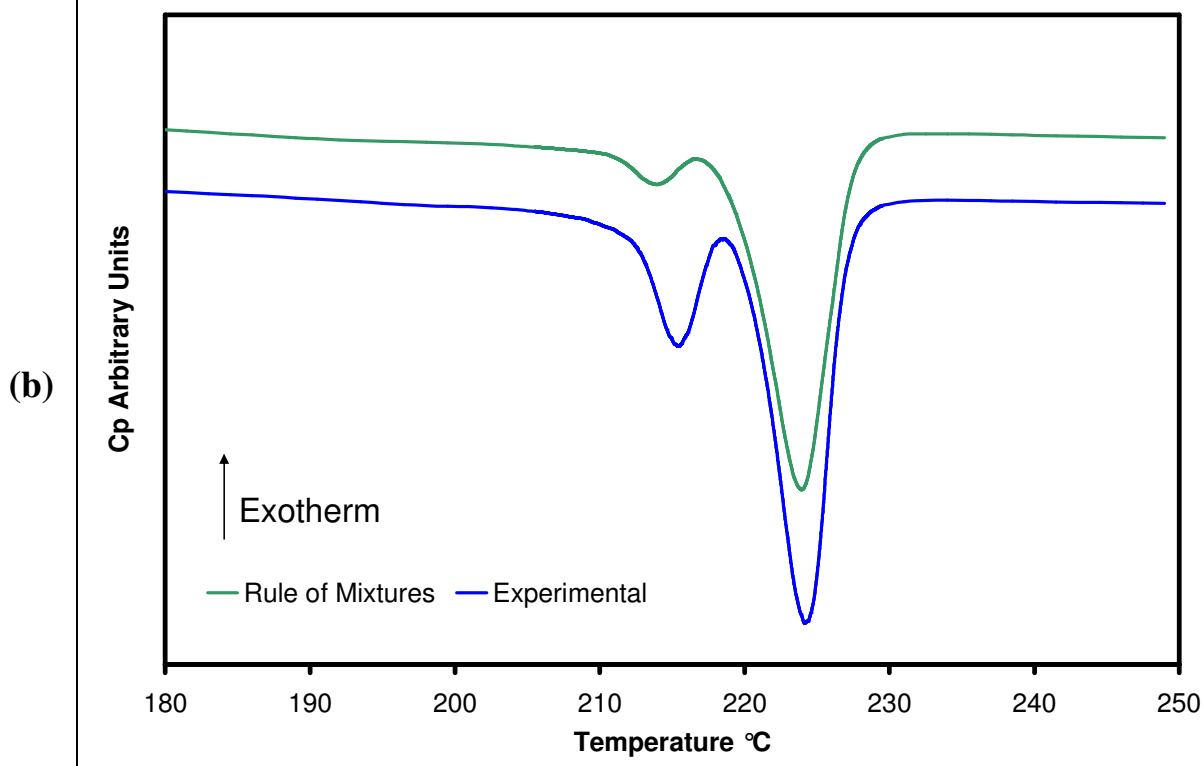
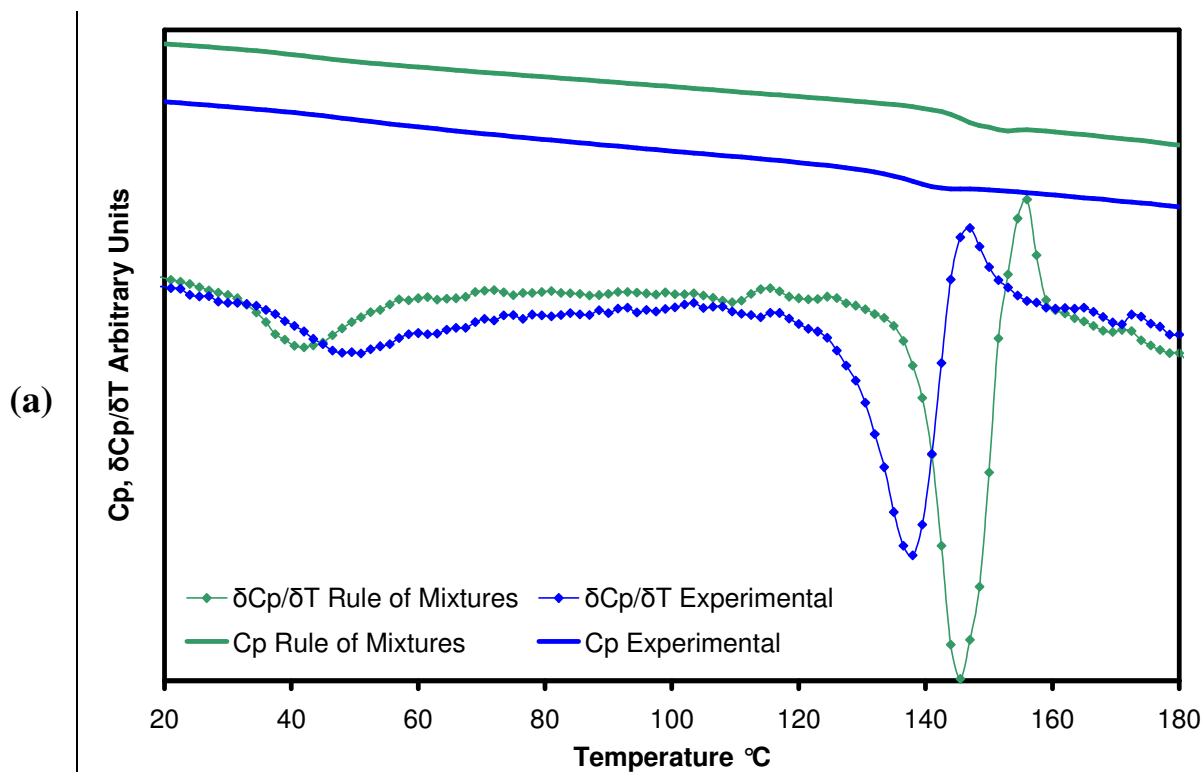


Figure E10: Blend 10, T_g Region (a), T_m Region (b)

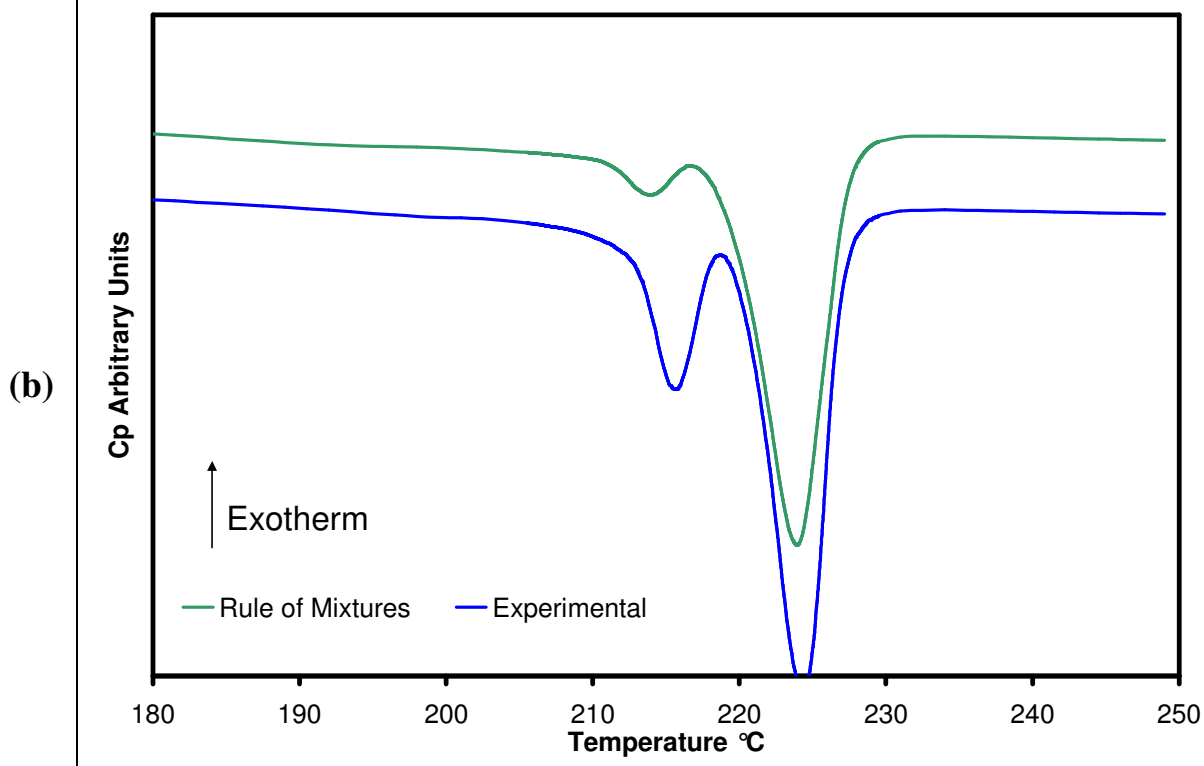
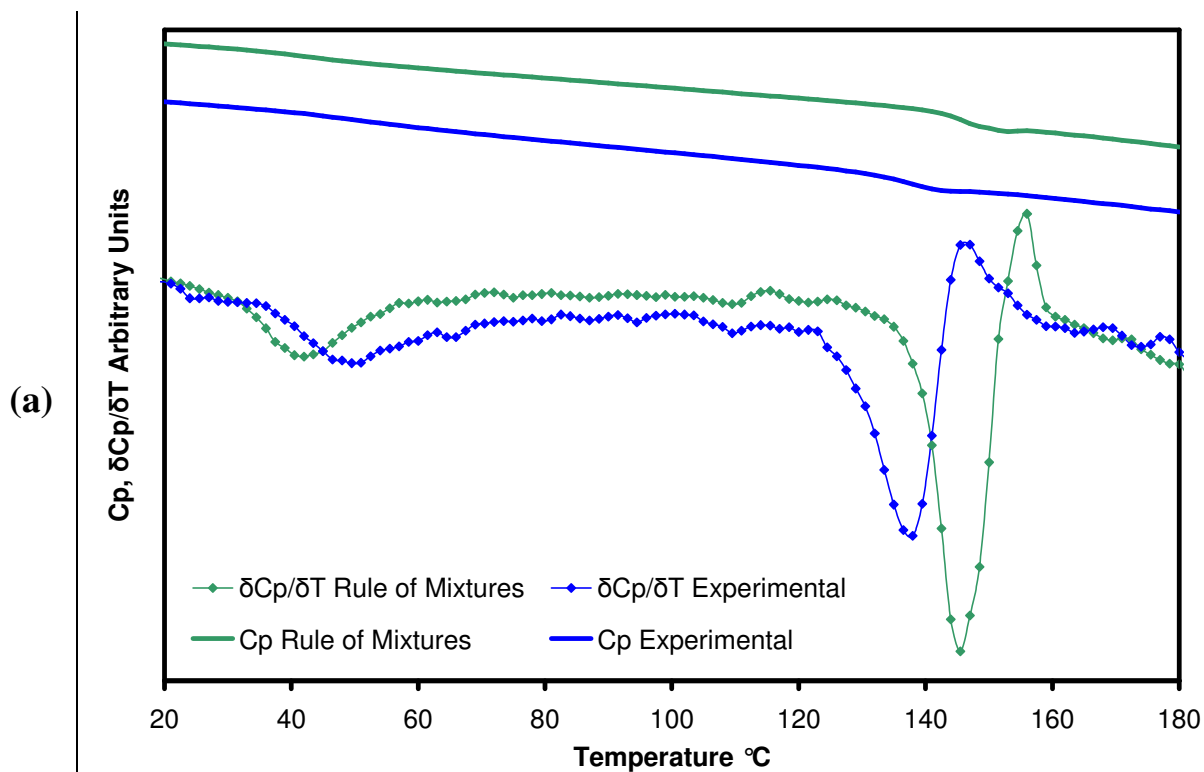


Figure E11: Blend 11, T_g Region (a), T_m Region (b)

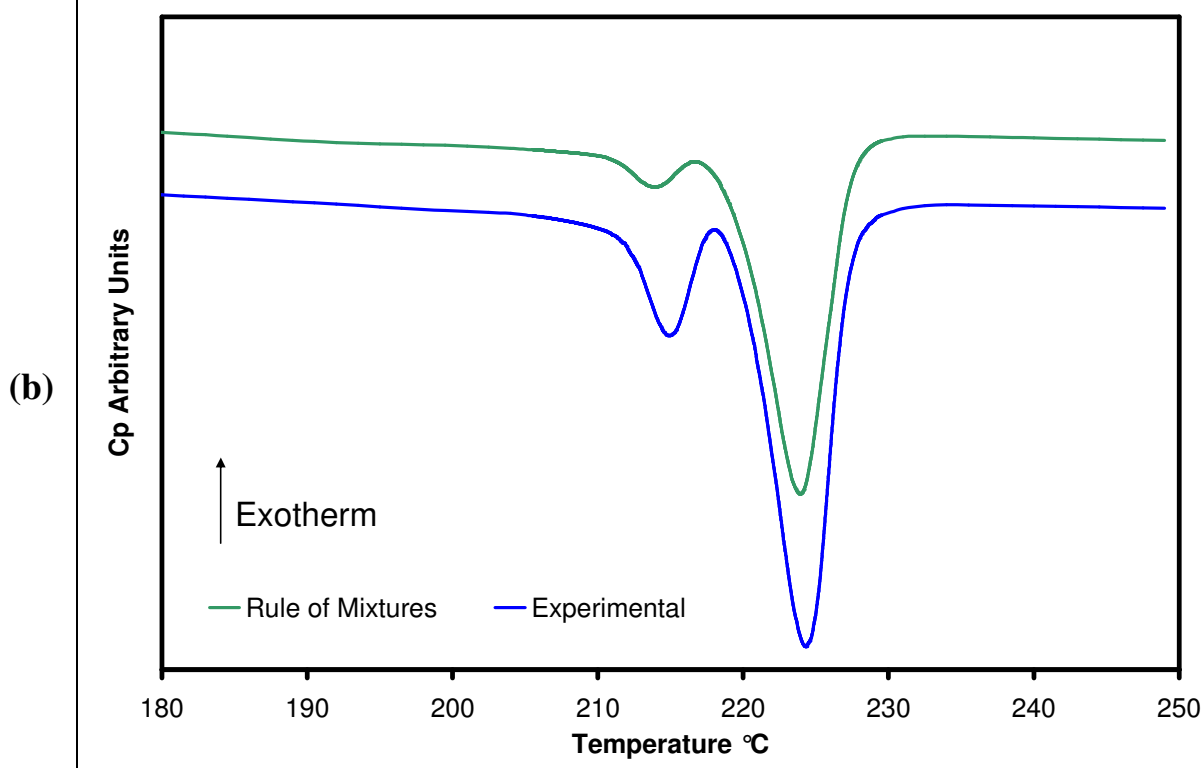
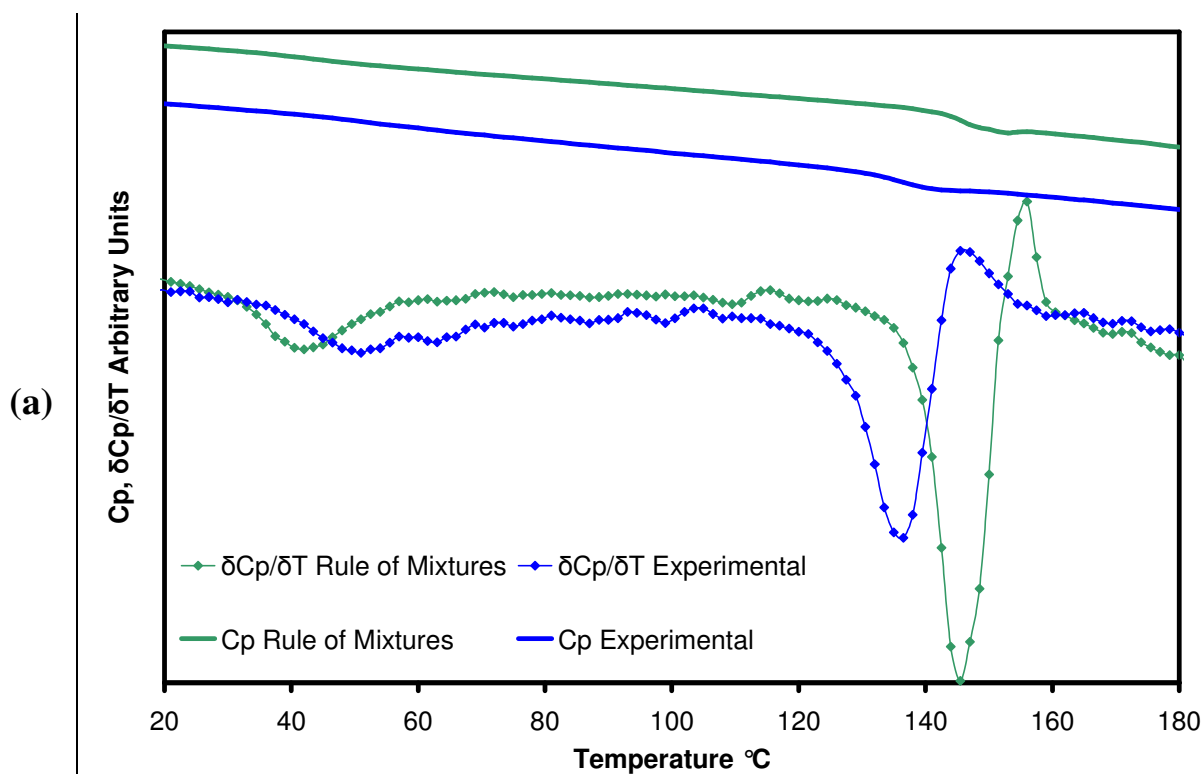


Figure E12: Blend 12, T_g Region (a), T_m Region (b)

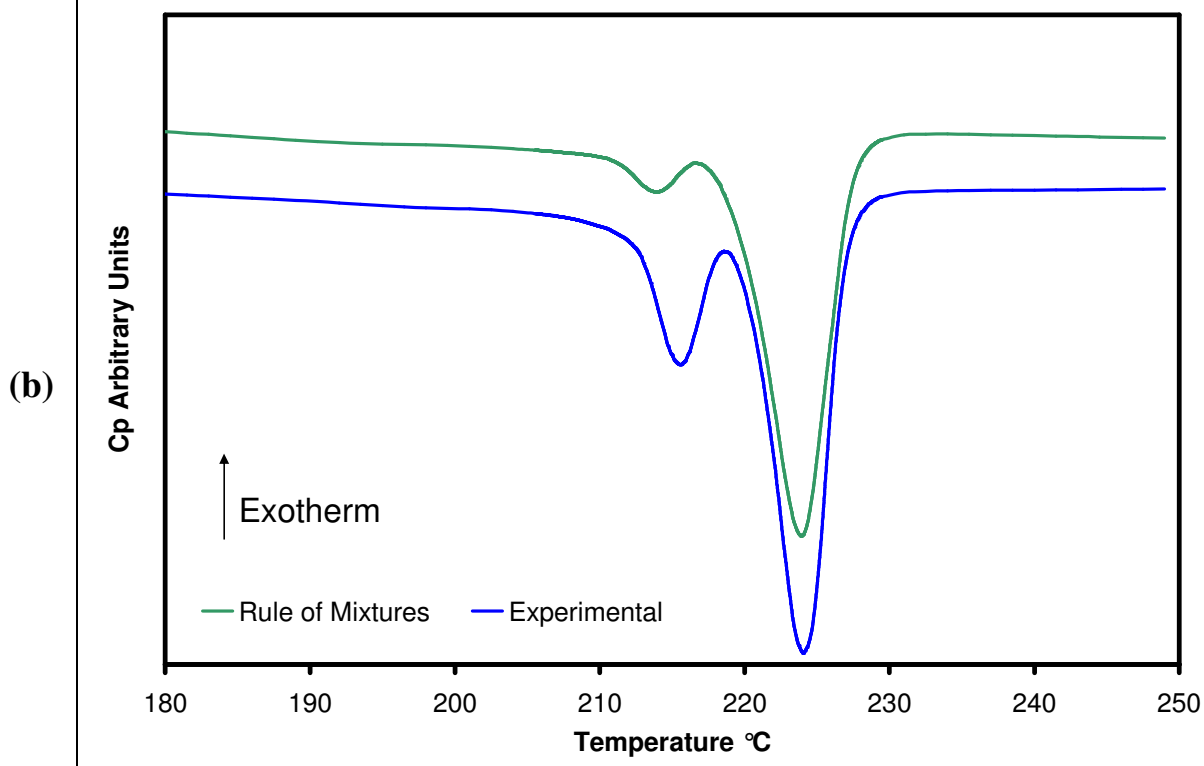
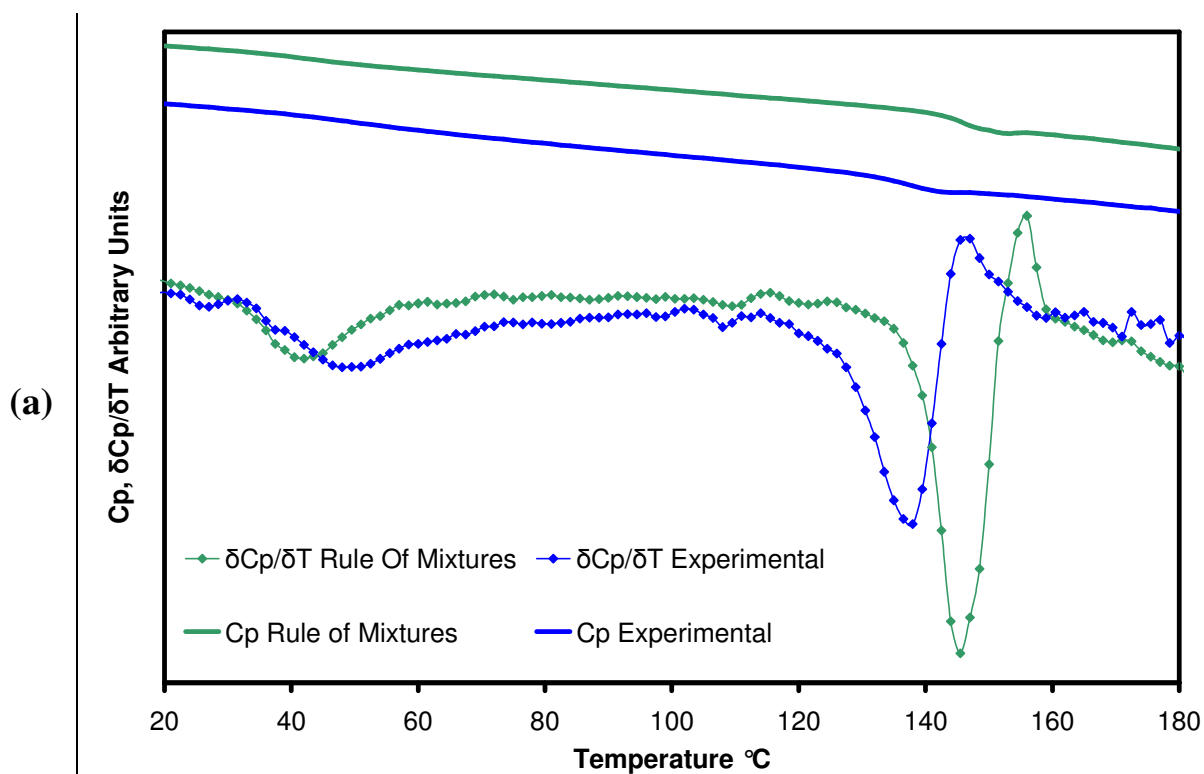
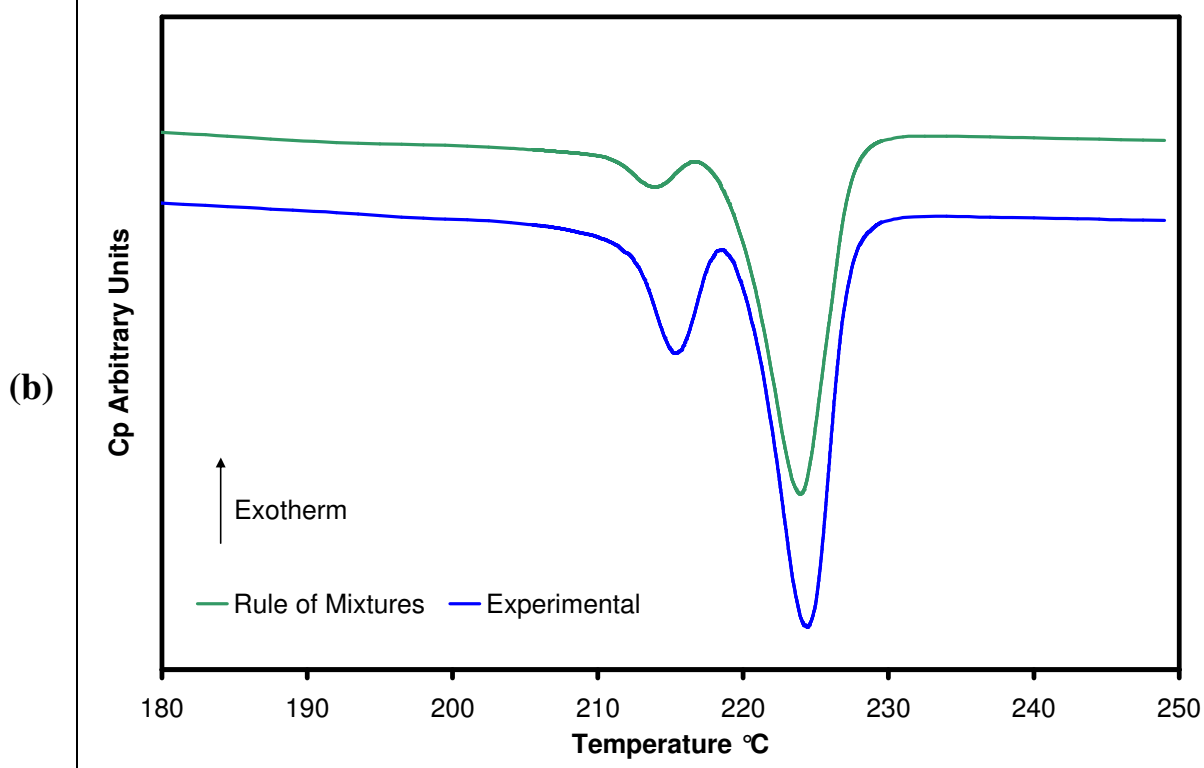
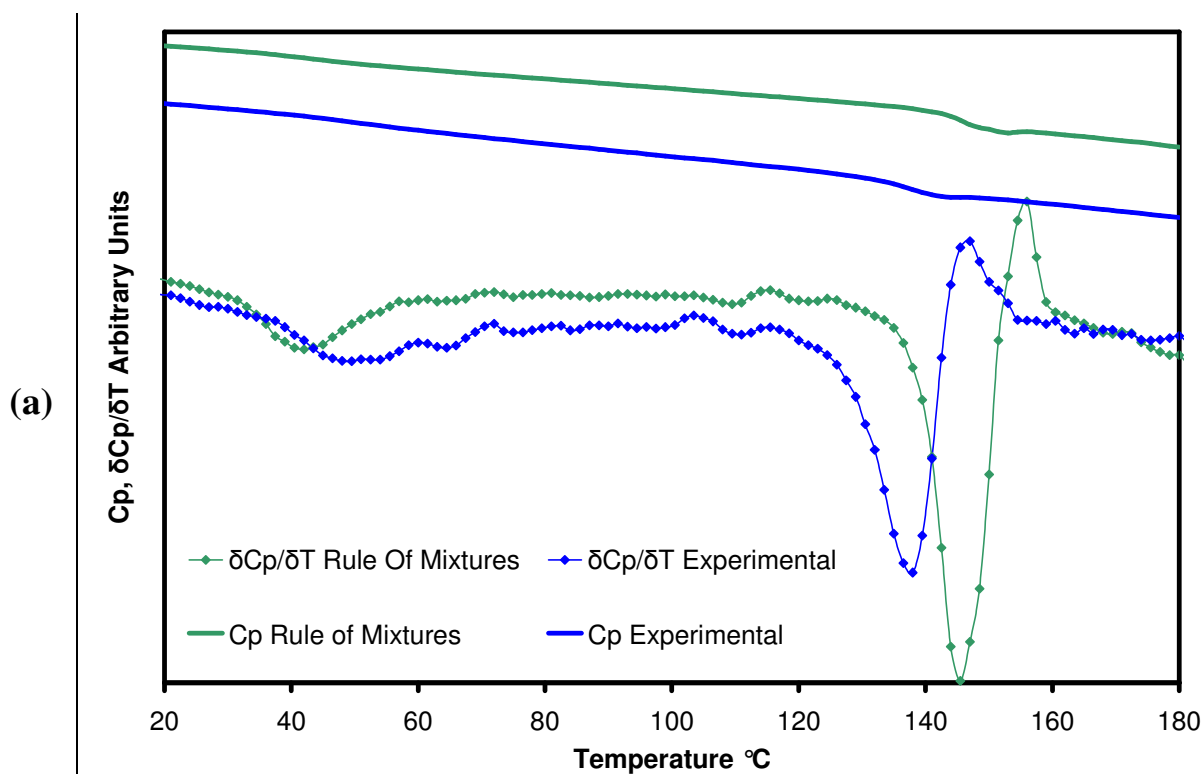


Figure E13: Blend 13, T_g Region (a), T_m Region (b)



APPENDIX F: Material Safety Data Sheets for Staining Compounds

SIGMA-ALDRICH		Material Safety Data Sheet	
		Version 3.1 Revision Date 11/19/2007 Print Date 05/29/2008	
1. PRODUCT AND COMPANY IDENTIFICATION			
Product name	:	Sodium (meta)periodate	
Product Number	:	71859	
Brand	:	Fluka	
Company	:	Sigma-Aldrich Canada, Ltd 2149 Winston Park Drive OAKVILLE ON L6H 6J8 CANADA	
Telephone	:	+1 9058299500	
Fax	:	+1 9058299292	
Emergency Phone #	:	800-424-9300	
2. COMPOSITION/INFORMATION ON INGREDIENTS			
Synonyms	:	Sodium periodate	
Formula	:	IO ₄ .Na	
Molecular Weight	:	213.89 g/mol	
CAS-No.	EC-No.	Index-No.	Concentration
Sodium periodate			
7790-28-5	232-197-6	-	-
3. HAZARDS IDENTIFICATION			
WHMIS Classification			
D1B	Toxic Material Causing Immediate and	Toxic by ingestion	
D2B	Serious Toxic Effects	Irritant	
HMIS Classification			
Health Hazard: 2			
Flammability: 0			
Physical hazards: 3			
NFPA Rating			
Health Hazard: 2			
Fire : 0			
Reactivity Hazard: 3			
Special hazard.: OX			
Potential Health Effects			
Fluka - 71859	Sigma-Aldrich Corporation www.sigma-aldrich.com		Page 1 of 5

Inhalation Skin Eyes Ingestion	May be harmful if inhaled. Causes respiratory tract irritation. May be harmful if absorbed through skin. Causes skin irritation. Causes eye irritation. Toxic if swallowed.
4. FIRST AID MEASURES	
<p>General advice Consult a physician. Show this safety data sheet to the doctor in attendance. Move out of dangerous area.</p> <p>If inhaled If breathed in, move person into fresh air. If not breathing give artificial respiration. Consult a physician.</p> <p>In case of skin contact Wash off with soap and plenty of water. Consult a physician.</p> <p>In case of eye contact Rinse thoroughly with plenty of water for at least 15 minutes and consult a physician.</p> <p>If swallowed Never give anything by mouth to an unconscious person. Rinse mouth with water. Consult a physician.</p>	
5. FIRE-FIGHTING MEASURES	
<p>Flammable properties Flash point no data available Ignition temperature no data available</p> <p>Suitable extinguishing media Use water spray, alcohol-resistant foam, dry chemical or carbon dioxide.</p> <p>Special protective equipment for fire-fighters Wear self contained breathing apparatus for fire fighting if necessary.</p> <p>Further information Use water spray to cool unopened containers.</p>	
6. ACCIDENTAL RELEASE MEASURES	
<p>Personal precautions Use personal protective equipment. Avoid dust formation. Avoid breathing dust. Ensure adequate ventilation. Evacuate personnel to safe areas.</p> <p>Environmental precautions Do not let product enter drains.</p> <p>Methods for cleaning up Pick up and arrange disposal without creating dust. Keep in suitable, closed containers for disposal.</p>	
7. HANDLING AND STORAGE	
<p>Handling Avoid contact with skin and eyes. Avoid formation of dust and aerosols. Provide appropriate exhaust ventilation at places where dust is formed. Keep away from sources of ignition - No smoking. Keep away from combustible material.</p> <p>Storage Keep container tightly closed in a dry and well-ventilated place. Light sensitive. hygroscopic</p>	
<p>Fluka - 71859</p> <p style="text-align: center;">Sigma-Aldrich Corporation www.sigma-aldrich.com</p> <p style="text-align: right;">Page 2 of 5</p>	

8. EXPOSURE CONTROLS / PERSONAL PROTECTION

Contains no substances with occupational exposure limit values.

Personal protective equipment

Respiratory protection

Where risk assessment shows air-purifying respirators are appropriate use a full-face particle respirator type N100 (US) or type P3 (EN 143) respirator cartridges as a backup to engineering controls. If the respirator is the sole means of protection, use a full-face supplied air respirator. Where risk assessment shows air-purifying respirators are appropriate use a dust mask type N95 (US) or type P1 (EN 143) respirator. Use respirators and components tested and approved under appropriate government standards such as NIOSH (US) or CEN (EU).

Hand protection

Handle with gloves.

Eye protection

Safety glasses

Skin and body protection

Choose body protection according to the amount and concentration of the dangerous substance at the work place.

Hygiene measures

Handle in accordance with good industrial hygiene and safety practice. Wash hands before breaks and at the end of workday.

9. PHYSICAL AND CHEMICAL PROPERTIES

Appearance

Form	crystalline
Colour	white

Safety data

pH	3.5 - 5.5 at 107 g/l at 25 °C (77 °F)
Melting point	300 °C (572 °F)
Boiling point	no data available
Flash point	no data available
Ignition temperature	no data available
Lower explosion limit	no data available
Upper explosion limit	no data available
Density	3.860 g/cm ³
Water solubility	107 g/l at 20 °C (68 °F) - completely soluble

10. STABILITY AND REACTIVITY

Storage stability

Stable under recommended storage conditions. hygroscopic

Conditions to avoid

Exposure to light.

Materials to avoid

Organic materials, Forms shock-sensitive mixtures with certain other materials., Reducing agents, Powdered metals, Magnesium

Hazardous decomposition products
Hazardous decomposition products formed under fire conditions. - Hydrogen iodide, Iodine, iodine oxides, Sodium oxides

11. TOXICOLOGICAL INFORMATION

Acute toxicity

LD50 Oral - rat - 264 mg/kg

Irritation and corrosion

no data available

Sensitisation

no data available

Chronic exposure

IARC: No component of this product present at levels greater than or equal to 0.1% is identified as probable, possible or confirmed human carcinogen by IARC.

Signs and Symptoms of Exposure

To the best of our knowledge, the chemical, physical, and toxicological properties have not been thoroughly investigated.

Potential Health Effects

Inhalation	May be harmful if inhaled. Causes respiratory tract irritation.
Skin	May be harmful if absorbed through skin. Causes skin irritation.
Eyes	Causes eye irritation.
Ingestion	Toxic if swallowed.

12. ECOLOGICAL INFORMATION

Elimination information (persistence and degradability)

no data available

Ecotoxicity effects

no data available

Further information on ecology

no data available

13. DISPOSAL CONSIDERATIONS

Product

Observe all federal, state, and local environmental regulations. Contact a licensed professional waste disposal service to dispose of this material. Dissolve or mix the material with a combustible solvent and burn in a chemical incinerator equipped with an afterburner and scrubber.

Contaminated packaging

Dispose of as unused product.

14. TRANSPORT INFORMATION

DOT (US)

UN-Number: 3087 Class: 5.1 (6.1)

Packing group: II

Proper shipping name: Oxidizing solid, toxic, n.o.s. (Sodium periodate)

IMDG

UN-Number: 3087 Class: 5.1 (6.1) Packing group: II EMS-No: F-A, S-Q

Proper shipping name: OXIDIZING SOLID, TOXIC, N.O.S. (Sodium periodate)

Marine pollutant: No

IATA

UN-Number: 3087 Class: 5.1 (6.1) Packing group: II

Proper shipping name: Oxidizing solid, toxic n.o.s. (Sodium periodate)

15. REGULATORY INFORMATION

TSCA Status

On TSCA Inventory

DSL Status

All components of this product are on the Canadian DSL list.

WHMIS Classification

D1B	Toxic Material Causing Immediate and	Toxic by ingestion
D2B	Serious Toxic Effects	Irritant

16. OTHER INFORMATION

Further information

Copyright 2007 Sigma-Aldrich Co. License granted to make unlimited paper copies for internal use only. The above information is believed to be correct but does not purport to be all inclusive and shall be used only as a guide. The information in this document is based on the present state of our knowledge and is applicable to the product with regard to appropriate safety precautions. It does not represent any guarantee of the properties of the product. Sigma-Aldrich Co., shall not be held liable for any damage resulting from handling or from contact with the above product. See reverse side of invoice or packing slip for additional terms and conditions of sale.

SIGMA-ALDRICH

MATERIAL SAFETY DATA SHEET

Date Printed: 05/29/2008
Date Updated: 01/29/2006
Version 1.5

Section 1 - Product and Company Information

Product Name RUTHENIUM(III) CHLORIDE HYDRATE,
REAGENTPLUS
Product Number 206229
Brand ALDRICH
Company Sigma-Aldrich Canada, Ltd
Address 2149 Winston Park Drive
Oakville ON L6H 6J8 CA
Technical Phone: 9058299500
Fax: 9058299292
Emergency Phone: 800-424-9300

Section 2 - Composition/Information on Ingredient

Substance Name	CAS #	SARA 313
RUTHENIUM(III) CHLORIDE HYDRATE	14898-67-0	No
Formula	RuCl3.xH2O	

Section 3 - Hazards Identification

EMERGENCY OVERVIEW

Corrosive.
Causes burns.

HMIS RATING

HEALTH: 3
FLAMMABILITY: 0
REACTIVITY: 1

NFPA RATING

HEALTH: 3
FLAMMABILITY: 0
REACTIVITY: 1

For additional information on toxicity, please refer to Section 11.

Section 4 - First Aid Measures

ORAL EXPOSURE

If swallowed, wash out mouth with water provided person is conscious. Call a physician immediately.

INHALATION EXPOSURE

If inhaled, remove to fresh air. If not breathing give artificial respiration. If breathing is difficult, give oxygen.

DERMAL EXPOSURE

In case of skin contact, flush with copious amounts of water for at least 15 minutes. Remove contaminated clothing and shoes. Call a physician.

EYE EXPOSURE

In case of contact with eyes, flush with copious amounts of water for at least 15 minutes. Assure adequate flushing by separating the eyelids with fingers. Call a physician.

Section 5 - Fire Fighting Measures

FLASH POINT

N/A

AUTOIGNITION TEMP

N/A

FLAMMABILITY

N/A

EXTINGUISHING MEDIA

Suitable: Dry chemical powder.

FIREFIGHTING

Protective Equipment: Wear self-contained breathing apparatus and protective clothing to prevent contact with skin and eyes.
Specific Hazard(s): Emits toxic fumes under fire conditions.

Section 6 - Accidental Release Measures

PROCEDURE TO BE FOLLOWED IN CASE OF LEAK OR SPILL

Evacuate area.

PROCEDURE(S) OF PERSONAL PRECAUTION(S)

Wear self-contained breathing apparatus, rubber boots, and heavy rubber gloves.

METHODS FOR CLEANING UP

Sweep up, place in a bag and hold for waste disposal. Ventilate area and wash spill site after material pickup is complete.

Section 7 - Handling and Storage

HANDLING

User Exposure: Do not breathe dust. Do not get in eyes, on skin, on clothing. Avoid prolonged or repeated exposure.

STORAGE

Suitable: Keep tightly closed.

SPECIAL REQUIREMENTS

Hygroscopic.

Section 8 - Exposure Controls / PPE

ENGINEERING CONTROLS

Safety shower and eye bath. Use only in a chemical fume hood.

PERSONAL PROTECTIVE EQUIPMENT

Respiratory: Use respirators and components tested and approved under appropriate government standards such as NIOSH (US) or CEN (EU). Where risk assessment shows air-purifying respirators are appropriate use a full-face particle respirator type N100 (US) or type P3 (EN 143) respirator cartridges as a backup to engineering controls. If the respirator is the sole means of protection, use a

full-face supplied air respirator.
Hand: Compatible chemical-resistant gloves.
Eye: Chemical safety goggles.

GENERAL HYGIENE MEASURES

Wash contaminated clothing before reuse. Discard contaminated shoes. Wash thoroughly after handling.

Section 9 - Physical/Chemical Properties

Appearance	Physical State: Solid Color: Deep grey Form: Powder	
Property	Value	At Temperature or Pressure
Molecular Weight	207.43 AMU	
pH	N/A	
BP/BP Range	N/A	
MP/MP Range	N/A	
Freezing Point	N/A	
Vapor Pressure	N/A	
Vapor Density	N/A	
Saturated Vapor Conc.	N/A	
SG/Density	N/A	
Bulk Density	N/A	
Odor Threshold	N/A	
Volatile%	N/A	
VOC Content	N/A	
Water Content	N/A	
Solvent Content	N/A	
Evaporation Rate	N/A	
Viscosity	N/A	
Surface Tension	N/A	
Partition Coefficient	N/A	
Decomposition Temp.	N/A	
Flash Point	N/A	
Explosion Limits	N/A	
Flammability	N/A	
Autoignition Temp	N/A	
Refractive Index	N/A	
Optical Rotation	N/A	
Miscellaneous Data	N/A	
Solubility	N/A	

N/A = not available

Section 10 - Stability and Reactivity

STABILITY

Stable: Stable.
Materials to Avoid: Zinc.

HAZARDOUS DECOMPOSITION PRODUCTS

Hazardous Decomposition Products: Hydrogen chloride gas.

HAZARDOUS POLYMERIZATION

Hazardous Polymerization: Will not occur

Section 11 - Toxicological Information

ROUTE OF EXPOSURE

Skin Contact: Causes burns.
Skin Absorption: May be harmful if absorbed through the skin.
Eye Contact: Causes burns.
Inhalation: Material is extremely destructive to the tissue of the mucous membranes and upper respiratory tract. May be harmful if inhaled.
Ingestion: May be harmful if swallowed.

SIGNS AND SYMPTOMS OF EXPOSURE

Material is extremely destructive to tissue of the mucous membranes and upper respiratory tract, eyes, and skin. Inhalation may result in spasm, inflammation and edema of the larynx and bronchi, chemical pneumonitis, and pulmonary edema. Symptoms of exposure may include burning sensation, coughing, wheezing, laryngitis, shortness of breath, headache, nausea, and vomiting. To the best of our knowledge, the chemical, physical, and toxicological properties have not been thoroughly investigated.

Section 12 - Ecological Information

No data available.

Section 13 - Disposal Considerations

APPROPRIATE METHOD OF DISPOSAL OF SUBSTANCE OR PREPARATION

Contact a licensed professional waste disposal service to dispose of this material. Dissolve or mix the material with a combustible solvent and burn in a chemical incinerator equipped with an afterburner and scrubber. Observe all federal, state, and local environmental regulations.

Section 14 - Transport Information

DOT

Proper Shipping Name: Corrosive solid, acidic, inorganic, n.o.s.
UN#: 3260
Class: 8
Packing Group: Packing Group II
Hazard Label: Corrosive
PIH: Not PIH

IATA

Proper Shipping Name: Corrosive solid, acidic, inorganic, n.o.s.
IATA UN Number: 3260
Hazard Class: 8
Packing Group: II

Section 15 - Regulatory Information

EU ADDITIONAL CLASSIFICATION

Symbol of Danger: C
Indication of Danger: Corrosive.
R: 34
Risk Statements: Causes burns.
S: 26-36/37/39-45
Safety Statements: In case of contact with eyes, rinse immediately with plenty of water and seek medical advice. Wear suitable protective clothing, gloves, and eye/face protection. In case of accident or if you feel unwell, seek medical advice

immediately (show the label where possible).

US CLASSIFICATION AND LABEL TEXT

Indication of Danger: Corrosive.

Risk Statements: Causes burns.

Safety Statements: In case of contact with eyes, rinse immediately with plenty of water and seek medical advice. Wear suitable protective clothing, gloves, and eye/face protection. In case of accident or if you feel unwell, seek medical advice immediately (show the label where possible).

UNITED STATES REGULATORY INFORMATION

SARA LISTED: No

CANADA REGULATORY INFORMATION

WHMIS Classification: This product has been classified in accordance with the hazard criteria of the CPR, and the MSDS contains all the information required by the CPR.

DSL: No

NDSL: No

Section 16 - Other Information

DISCLAIMER

For R&D use only. Not for drug, household or other uses.

WARRANTY

The above information is believed to be correct but does not purport to be all inclusive and shall be used only as a guide. The information in this document is based on the present state of our knowledge and is applicable to the product with regard to appropriate safety precautions. It does not represent any guarantee of the properties of the product. Sigma-Aldrich Inc., shall not be held liable for any damage resulting from handling or from contact with the above product. See reverse side of invoice or packing slip for additional terms and conditions of sale. Copyright 2008 Sigma-Aldrich Co. License granted to make unlimited paper copies for internal use only.

APPENDIX G: SEM Images of Annealed Blend

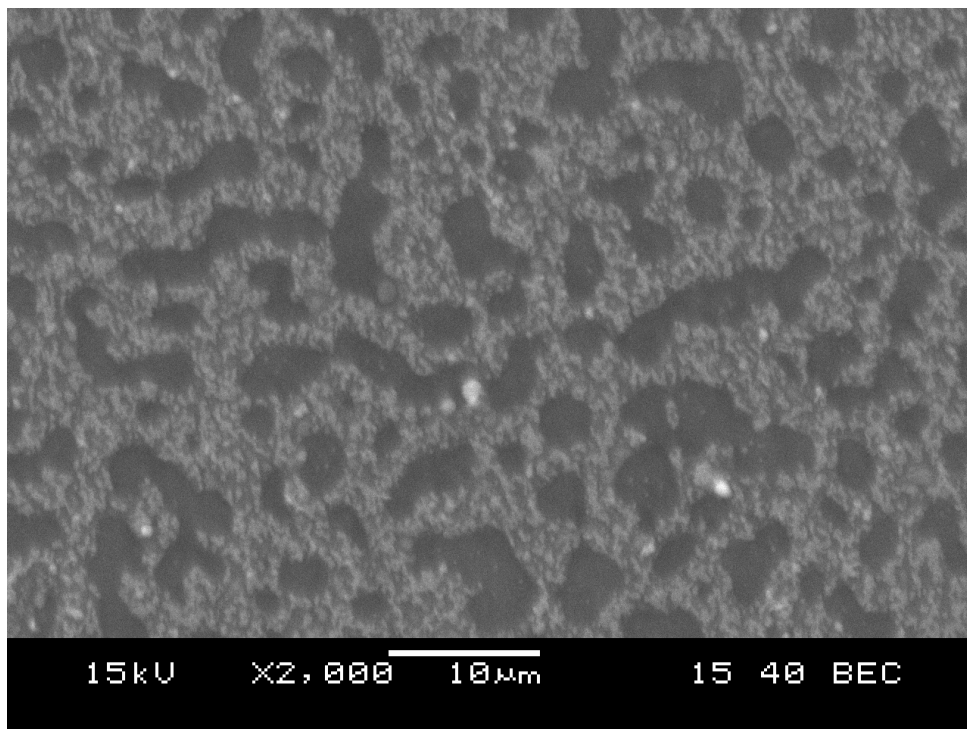


Figure G1: Blend 1 SEM Result

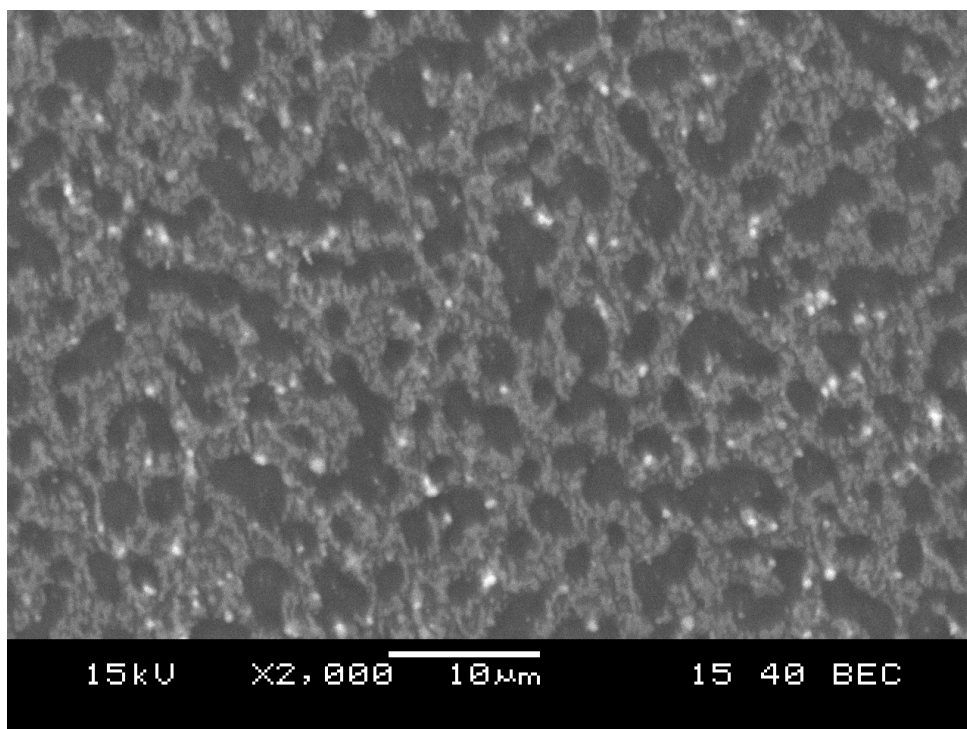


Figure G2: Blend 2 SEM Result

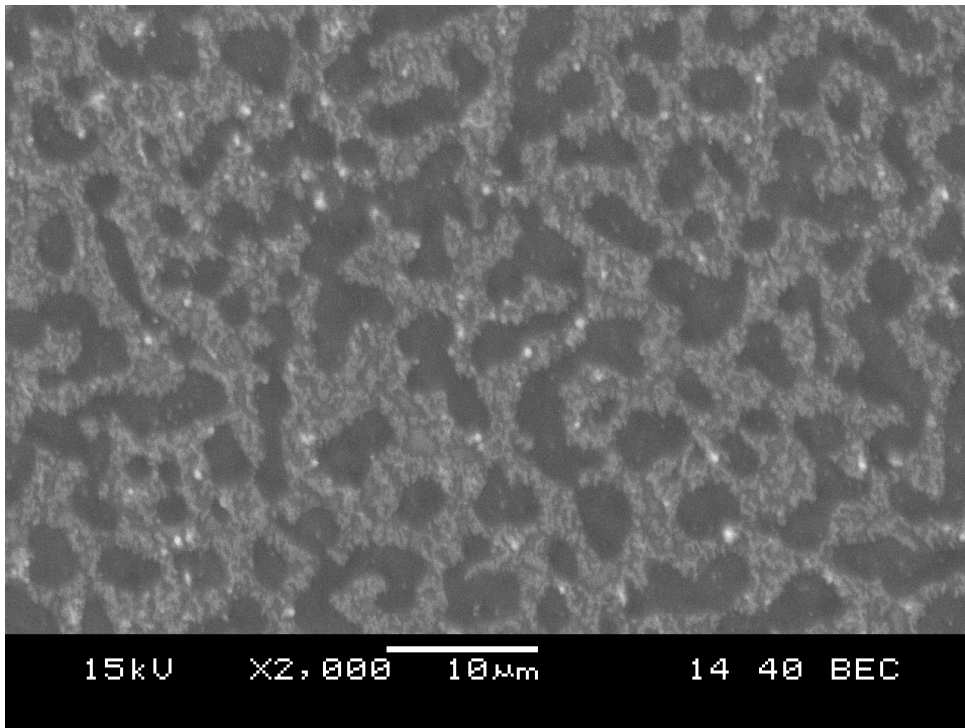


Figure G3: Blend 3 SEM Result

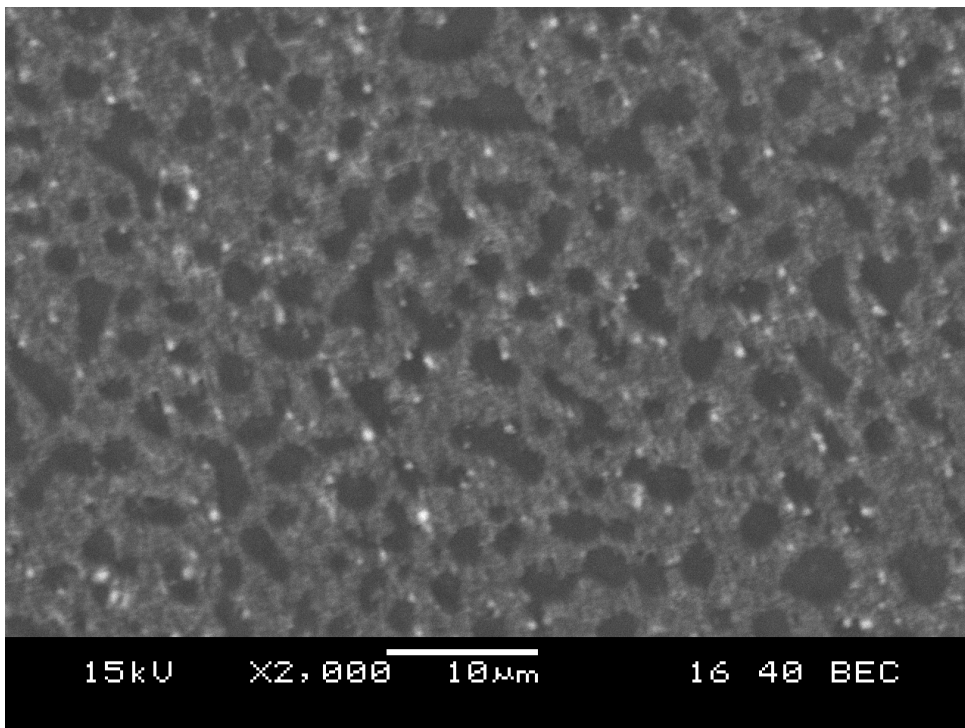


Figure G4: Blend 4 SEM Result

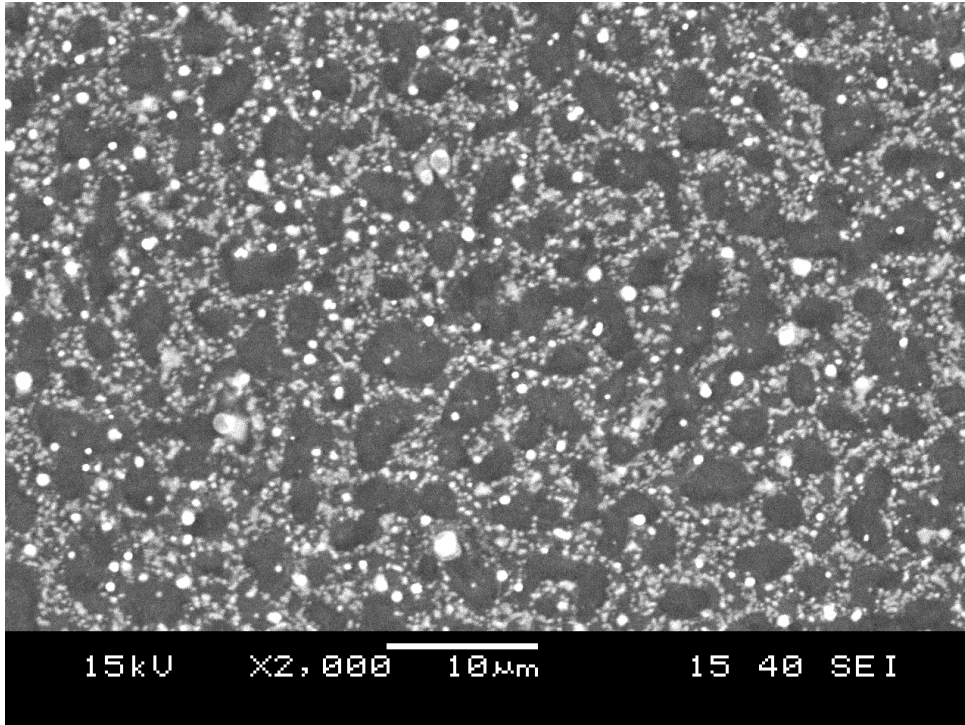


Figure G5: Blend 5 SEM Result

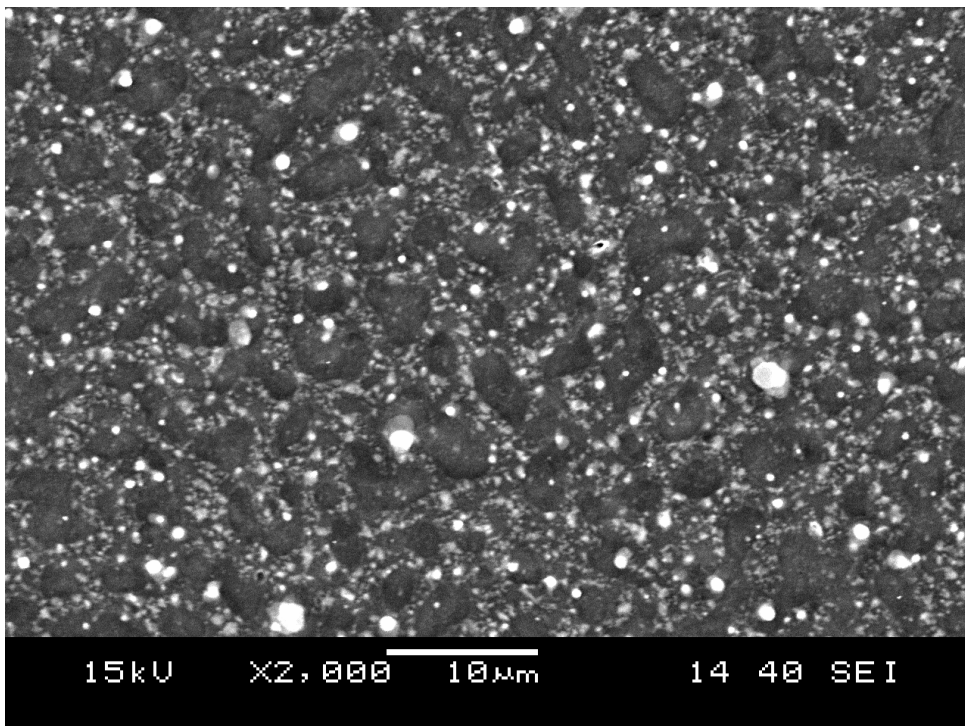


Figure G6: Blend 6 SEM Result

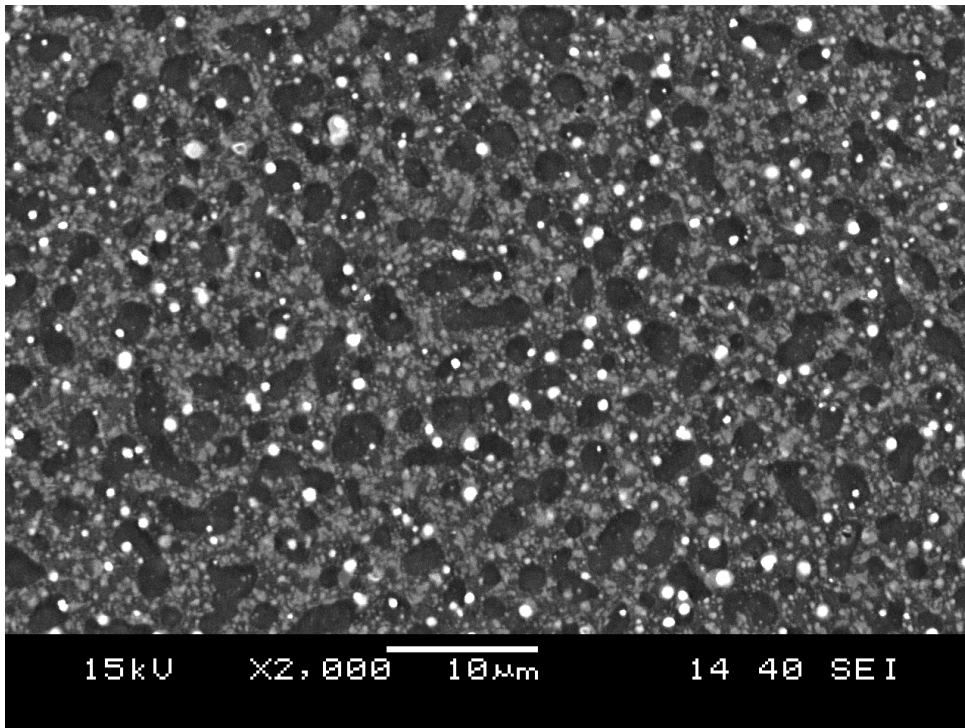


Figure G7: Blend 7 SEM Result

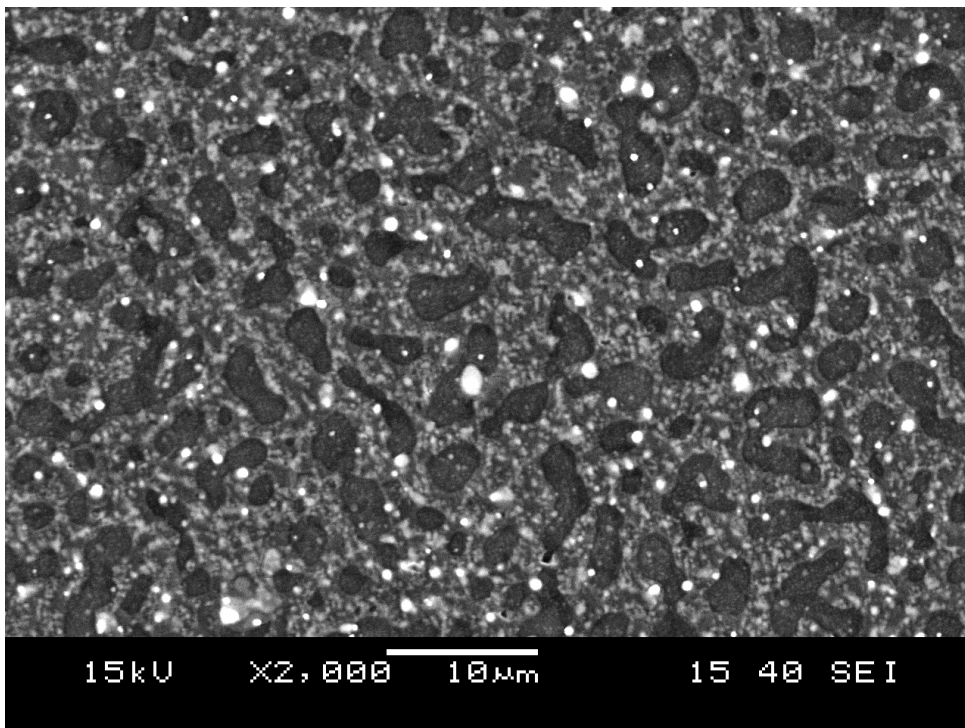


Figure G8: Blend 8 SEM Result

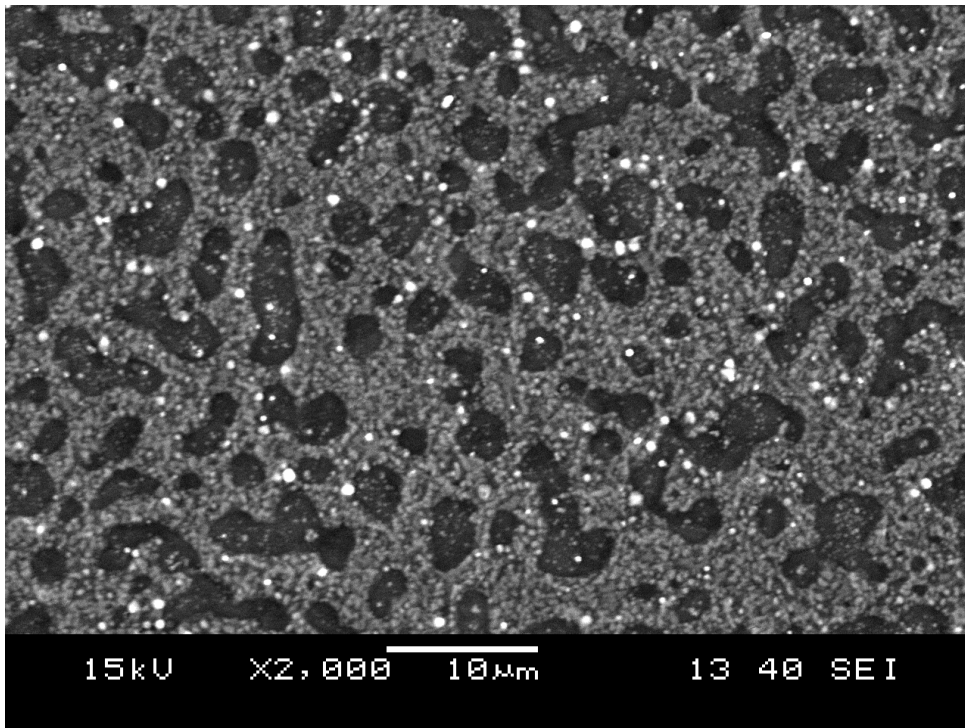


Figure G9: Blend 9 SEM Result

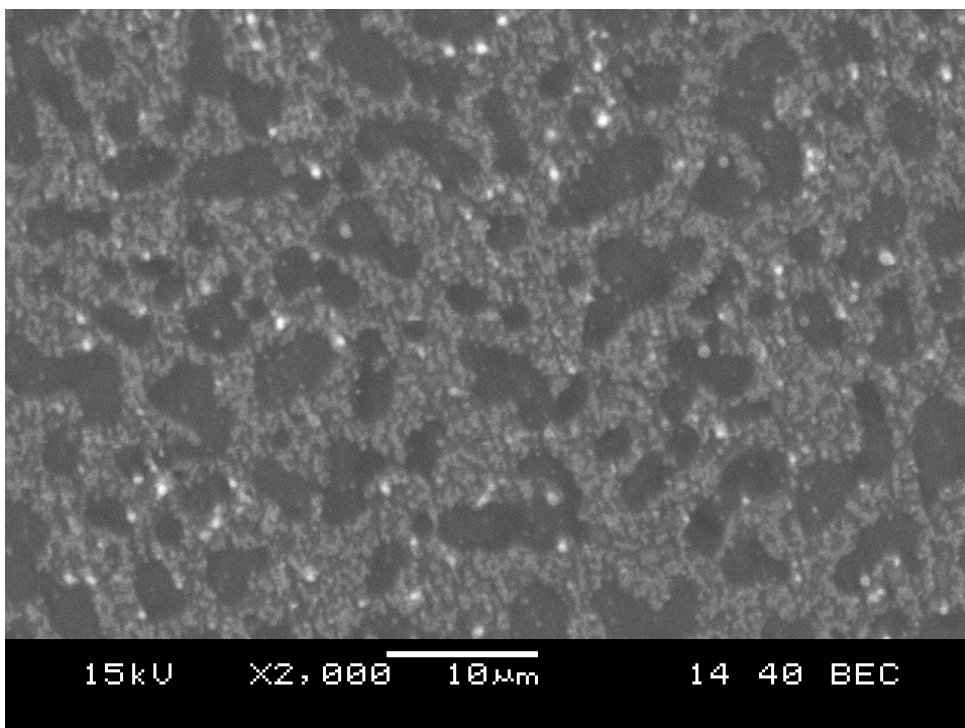


Figure G10: Blend 10 SEM Result

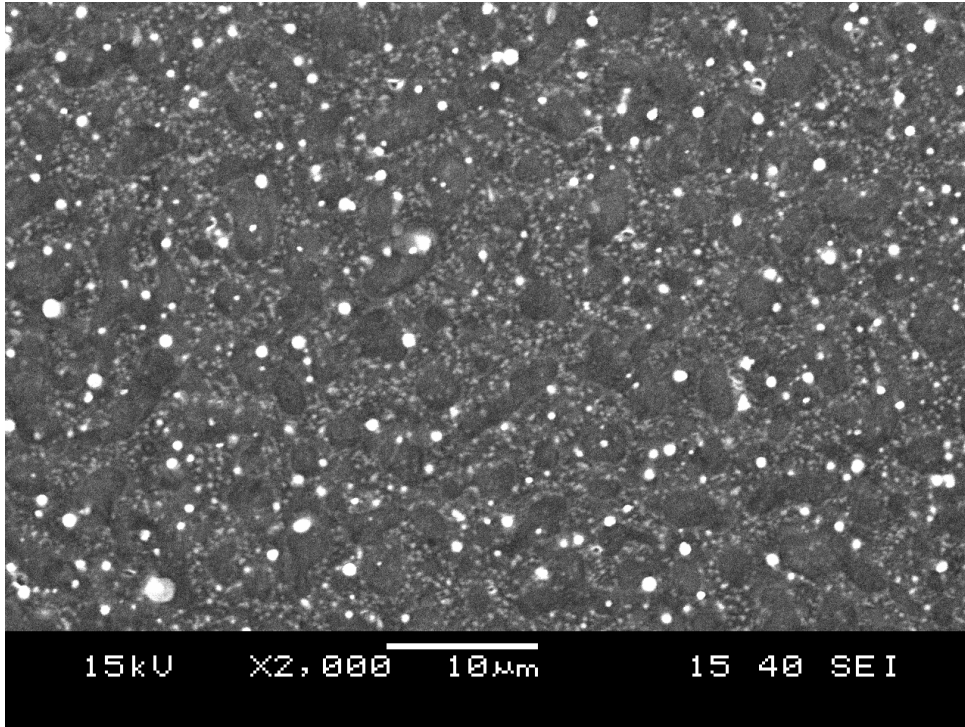


Figure G11: Blend 11 SEM Result

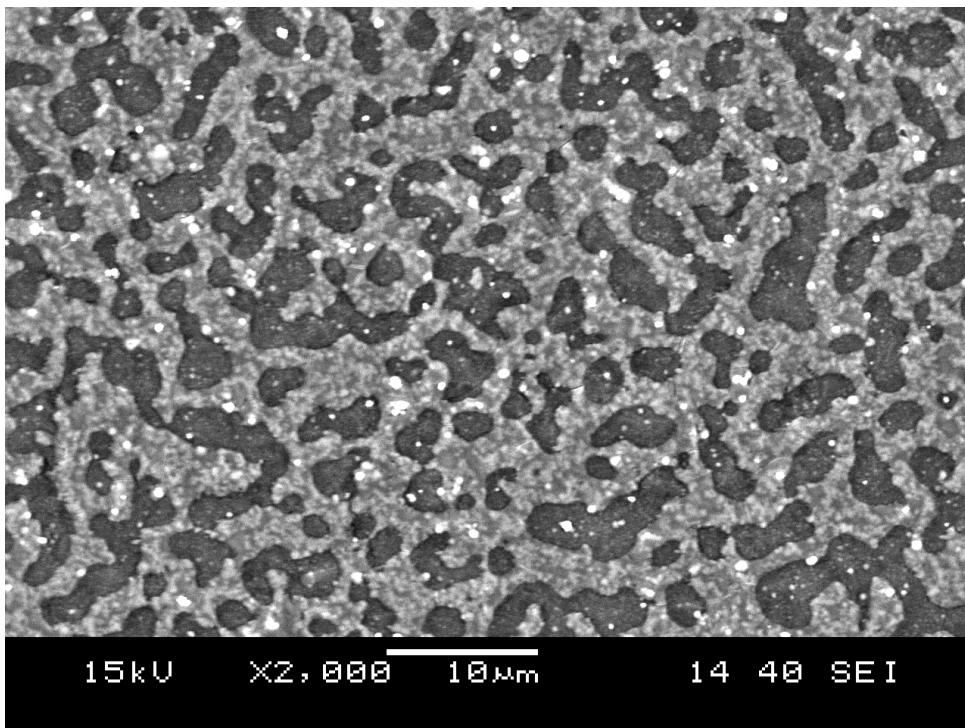


Figure G12: Blend 12 SEM Result

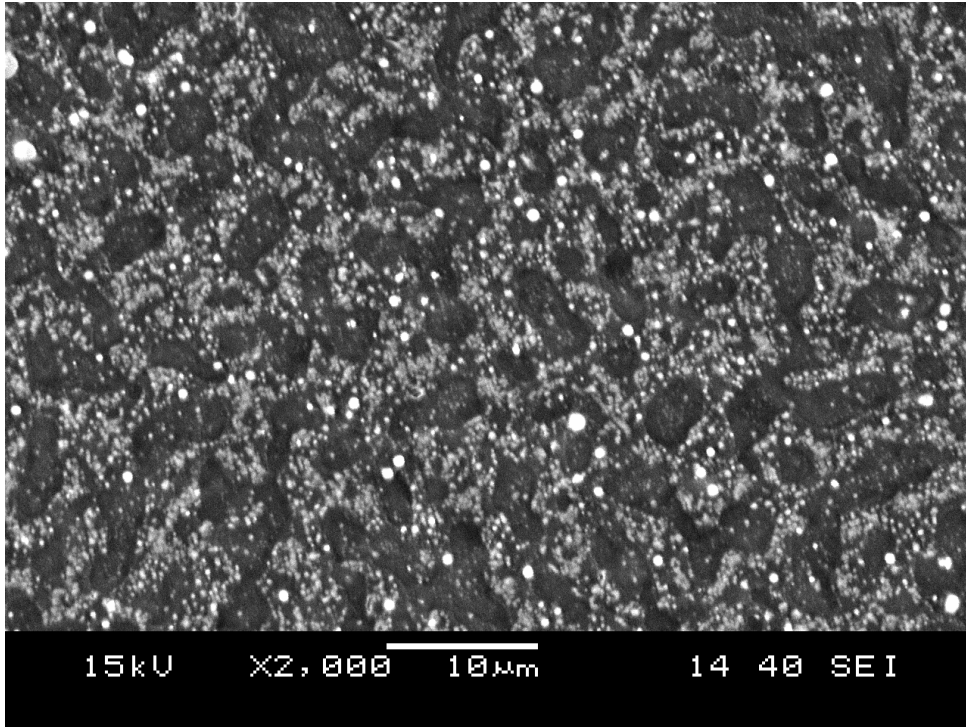


Figure G13: Blend 13 SEM Result

APPENDIX H: Linear Regression MATLAB Code

```
% Program to analyze data from DSC Experiments
% Author: Allan Rogalsky
% All Equation References are to D.C. Montgomery "Design and Analysis of
% Experiments" 6th Edition, John Wiley & Sons, 2005

% Erase Workspace
clear

% Read in x matrix.
Xave = dlmread([pwd '\RegresionX.txt']);

% Read in Y matrix.
Yave = dlmread([pwd '\RegresionY.txt']);

% Read in Coded Value Matrix
C = dlmread([pwd '\RegresionC.txt']);

% Initalize Statistical Constants
kmax = length(Xave(1,:)); %Maximum Number of Regresor Variables
n = length(Xave(:,1)); %Number of Data Points
m = length(Yave(1,:)); %Number of Data Sets

%Initalize Analisis Veriablles
B = zeros(kmax,m); %B Coefishant Matrix
SS = zeros(4, m); %Sum of Squares: 1 - SSr, 2 - SSe, 3 - SSlof, 4 - SSpe
MS = zeros(4, m); %Mean Squares: 1 - MSr, 2 - SSe, 3 - MSlof, 4 - MSpe
Fo = zeros(2, m); %F values: 1 = Fr, 2 - Flof
to = zeros(kmax, m); %t values for individual B Coefishants
df = zeros(4, m); %Degrees of Freedom

%Main Analisis Loop
for i = 1:m
    if sum(Yave(:,i)) ~= 0
        k = sum(C(:,i)); %Number of regresor variables
        X = zeros(n,k); %Initalize X matrix to be used
        index = 1;
        for j = 1:kmax
            if C(j,i) == 1
                X(:,index) = Xave(:,j); %If regresor used populate col
                index = index + 1;
            end
        end
        end

        %Sort X into unique subsets
        temp = sortrows([X Yave(:,i)]);
        X = temp(:,1:k);
        Yave(:,i) = temp(:,k+1);

        %Calculate B values (10-13)
        Btemp = inv(X'*X)*X'*Yave(:,i);

        %Fill Global B matrix
```

```

index = 1;
for j = 1:kmax
    if C(j,i) == 1
        B(j,i) = Btemp(index);    %If regresor used populate B value
        index = index + 1;
    end
end

%Calculate SS Regression (10-23)
SS(1,i) = Btemp'*X'*Yave(:,i) - sum(Yave(:,i))^2/n;

%Calcualte SS Residual(10-24)
SS(2,i) = Yave(:,i)'*Yave(:,i) - Btemp'*X'*Yave(:,i);

%Loop to Find:
    %Number of Unique Data Sets (Levels)
    %df Pure Error
    %SS Lack of Fit (10-60)
    %SS Pure Error (10-58)
levels = 0;    %initalize levels
df4 = 0;    %initalize df pure error
ntemp = 0;    %initalize counter for number of points per level
for j = 1:n
    ntemp = ntemp + 1;
    if (j==n) || (isequal(X(j,:),X(j+1,:)) == 0) %If last in level
        levels = levels + 1;    %Increase Level Counter
        df4 = df4 + ntemp - 1;    %Add to Degree of Freedom Counter

        %Calcualte SS Lack of Fit (10-60)
        SS(3,i) = SS(3, i) + ntemp*(mean(Yave(j-ntemp+1:j,i)) -
X(j,:)*Btemp)^2;

        %Calculate SS Pure Error (10-58)
        for jj = j-ntemp+1:j
            SS(4,i) = SS(4,i) + (Yave(jj,i) - mean(Yave(j-
ntemp+1:j,i)))^2;
        end

        ntemp = 0;    %Reset Counter
    end
end

%Calculate Degrees of Freedom
df(1,i) = k - 1;    %Df Regression
df(2,i) = n - k;    %Df Residual Error
df(3,i) = levels - k;    %Df Lack of Fit
df(4,i) = df4;    %Df Pure Error (10-59)

%Calculate Mean Squares
MS(:,i) = SS(:,i)./df(:,i);

%Calculate F ratios
Fo(1,i) = MS(1,i)/MS(2,i);
Fo(2,i) = MS(3,i)/MS(4,i);

```



```

        %Check Individual Beta Values for significance (10-28)
        index = 1;
        BigX = inv(X'*X);
        for j = 1:kmax
            if (C(j,i) == 1)
                to(j,i)=B(j,i)/sqrt (MS (2,i)*BigX(index,index));
                index = index + 1;
            end
        end
    end
end

end

%Create FormatString for Output
FormatString = '\n';
for i = 1:kmax
    FormatString=['% 12.4f' FormatString];
    if (i < kmax)
        FormatString=[',' FormatString];
    end
end
end

%Write output file for B values
fid = fopen([pwd '\RegresionB.txt'],'wt');
fprintf(fid, FormatString, B);
fclose(fid);

%Write output file for SS
fid = fopen([pwd '\RegresionSS.txt'],'wt');
fprintf(fid, '% 12.4f,% 12.4f,% 12.4f,% 12.4f\n', SS);
fclose(fid);

%Write output file for MS
fid = fopen([pwd '\RegresionMS.txt'],'wt');
fprintf(fid, FormatString, MS);
fclose(fid);

%Write output file for Fo
fid = fopen([pwd '\RegresionF.txt'],'wt');
fprintf(fid, '% 15.6f,% 12.6f\n', Fo);
fclose(fid);

%Write output file for 'to'
fid = fopen([pwd '\RegresionT.txt'],'wt');
fprintf(fid, FormatString, to);
fclose(fid);

%Write output file for 'df'
fid = fopen([pwd '\RegresionD.txt'],'wt');
fprintf(fid, '% 5.0f,% 5.0f,% 5.0f,% 5.0f\n', df);
fclose(fid);

%end program
return

```

APPENDIX I: Joint Confidence Intervals for Regression Results

Procedure:

Joint Confidence Intervals were generated using equation I1 where n is the number of samples, p is the number of parameters in the fit equation, $\hat{\beta}$ is a $1 \times p$ column vector representing the best fit regression coefficients, β is a $1 \times p$ column vector representing possible values for the regression coefficients, X is a $p \times n$ matrix containing the coded factor/levels for the experiment, MS_{Res} is the mean square residuals from the regression analysis, and $F_{\alpha, p, n-p}$ is the F distribution value for a confidence level of $(1-\alpha) \times 100\%$ [1].

$$\frac{(\hat{\beta} - \beta)' X' X (\hat{\beta} - \beta)}{pMS_{Res}} = F_{\alpha, p, n-p} \quad [1] \quad \text{Equation I1}$$

The following diagrams are produced by varying pairs of coefficients and setting all others to their nominal values. The general equation of the ellipse defining the confidence boundary is given in equation I2 for a pair of coefficients at matrix positions, a, b where $a \neq b$, the $1 \times p$ column vector $\beta^{simplified} = (\hat{\beta} - \beta)$ and the $p \times p$ square matrix $X^{square} = X'X$.

$$A(\hat{\beta}_a - \beta_a)^2 + B(\hat{\beta}_a - \beta_a)(\hat{\beta}_b - \beta_b) + C(\hat{\beta}_b - \beta_b)^2 + D(\hat{\beta}_a - \beta_a) + E(\hat{\beta}_b - \beta_b) + F = 0$$

$$A = X_{a,a}^{square}$$

$$B = 2X_{a,b}^{square}$$

$$C = X_{b,b}^{square}$$

Equation I2

$$D = \sum_{i \neq a, b} (\beta_i^{simplified} X_{i,a}^{square})$$

$$E = \sum_{i \neq a, b} (\beta_i^{simplified} X_{i,b}^{square})$$

$$F = \sum_{i \neq a, b} \left(\beta_i^{simplified} \sum_{ii \neq a, b} (\beta_{ii}^{simplified} X_{i,ii}^{square}) \right) - pMS_{Res} F_{\alpha, p, n-p}$$

This is a general ellipse at some arbitrary angle θ relative to the axis, and centered at some arbitrary point (h, k). Equations I3 to I11 give the translations necessary to put the ellipse in its standard form, equation I12, under a transformed coordinate system x, y.

$$\theta = \frac{1}{2} \tan^{-1} \left(\frac{B}{A-C} \right) \quad \text{Equation I3}$$

$$A' = A \cos^2 \theta + \frac{1}{2} B \sin 2\theta + C \sin^2 \theta \quad \text{Equation I4}$$

$$B' = 0 \quad \text{Equation I5}$$

$$C' = C \cos^2 \theta - \frac{1}{2} B \sin 2\theta + A \sin^2 \theta \quad \text{Equation I6}$$

$$E' = D \cos \theta + E \sin \theta \quad \text{Equation I7}$$

$$D' = E \cos \theta - D \sin \theta \quad \text{Equation I8}$$

$$D' = E \cos \theta - D \sin \theta \quad \text{Equation I9}$$

$$h = -\frac{1}{2} \frac{D'}{A'} \quad \text{Equation I10}$$

$$k = -\frac{1}{2} \frac{E'}{C'} \quad \text{Equation I11}$$

$$F' = F - A'h^2 - B'k^2 \quad \text{Equation I12}$$

$$A'x^2 + B'y^2 = -F'$$

From here, points can be easily generated using equations I13, and transformed back into the original coordinate system using equations I14 and I15.

$$y = \pm \sqrt{\frac{F' - A'x^2}{C'}}, \quad -\sqrt{\frac{F'}{A'}} \leq x \leq \sqrt{\frac{F'}{A'}} \quad \text{Equation I13}$$

$$\beta_a = \hat{\beta}_a - [(x+h)\cos \theta - (y+k)\sin \theta] \quad \text{Equation I14}$$

$$\beta_b = \hat{\beta}_b - [(k+h)\sin \theta + (y+k)\cos \theta] \quad \text{Equation I15}$$

Reference:

1. D.C Montgomery, E.A. Peck, G.G. Vining “Introduction to Linear Regression Analysis” John Wiley & Sons, New York, p107

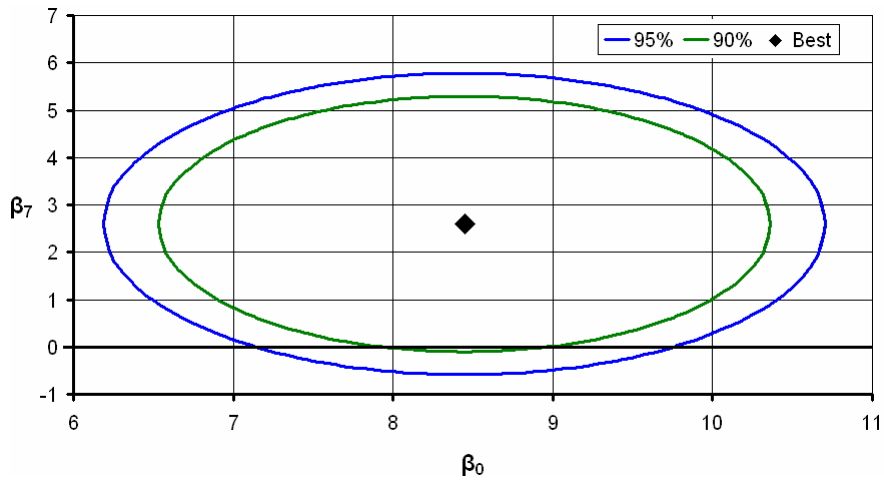


Figure 11: Bottom Quartile Phase Size, Composition (β_7) versus Intercept (β_0)

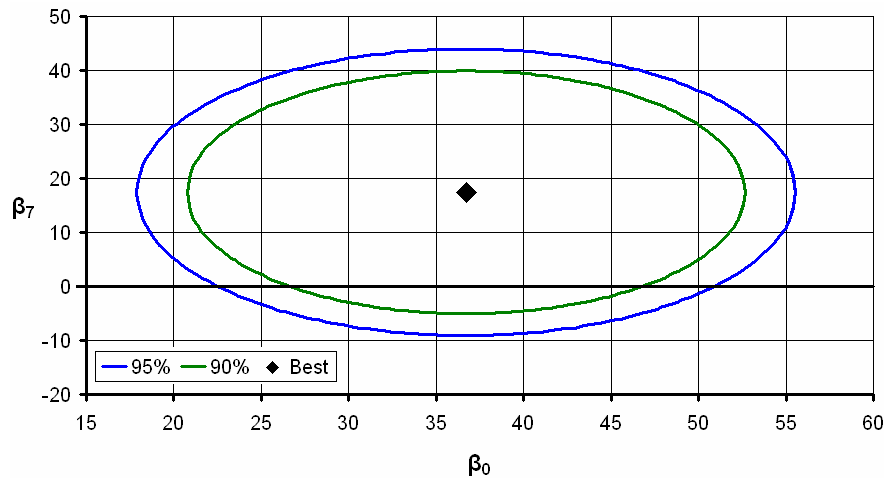


Figure 12: Top Quartile Phase Size, Composition (β_7) versus Intercept (β_0)

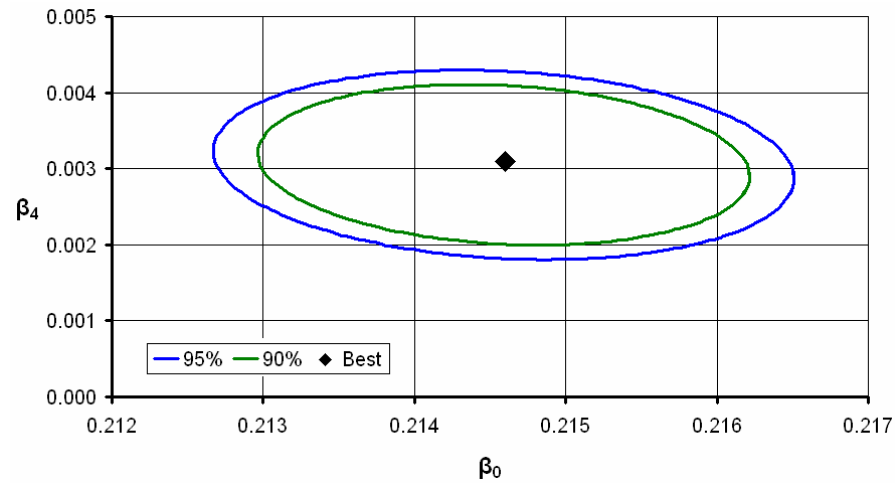


Figure 13: Specific Energy Consumption, N^2/Q (β_4) versus Intercept (β_0)

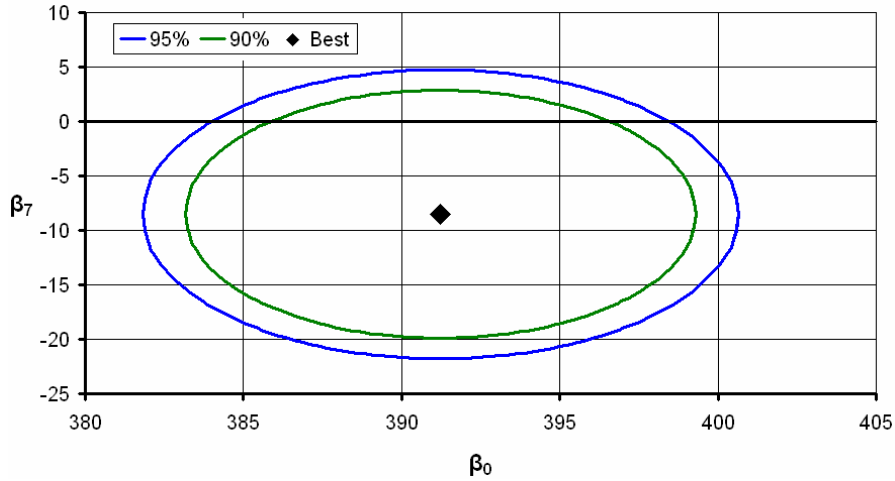


Figure I4: Die Pressure, Composition (β_7) versus Intercept (β_0)

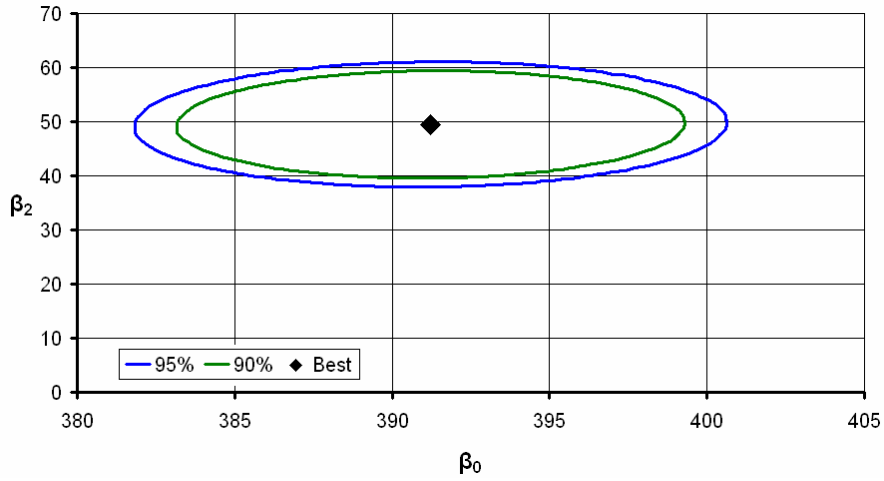


Figure I5: Die Pressure, N/Q (β_2) versus Intercept (β_0)

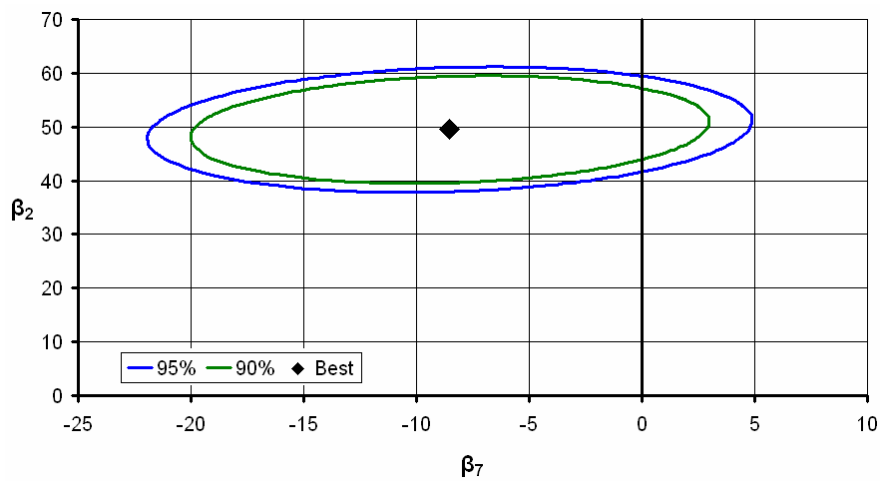


Figure I6: Die Pressure, N/Q (β_2) versus Composition (β_7)

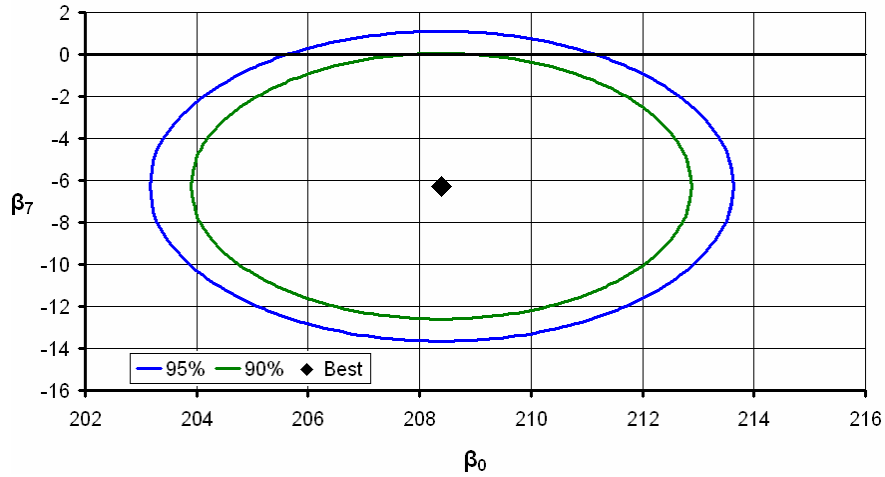


Figure I7: Melt Exit Temperature, Composition (β_7) versus Intercept (β_0)

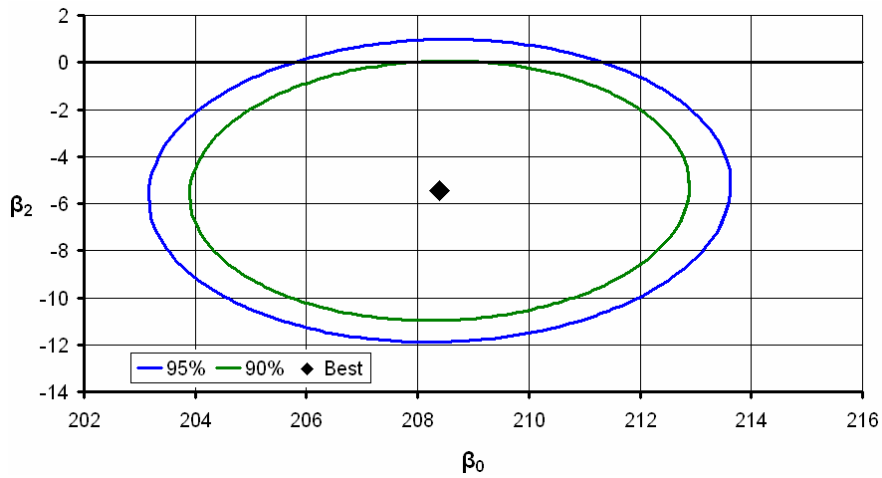


Figure I8: Melt Exit Temperature, N/Q (β_2) versus Intercept (β_0)

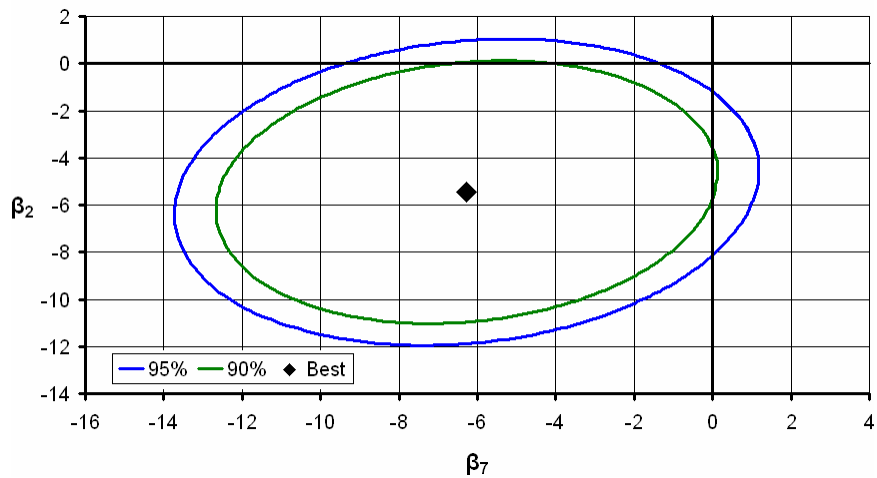


Figure I9: Melt Exit Temperature, N/Q (β_2) versus Composition (β_7)

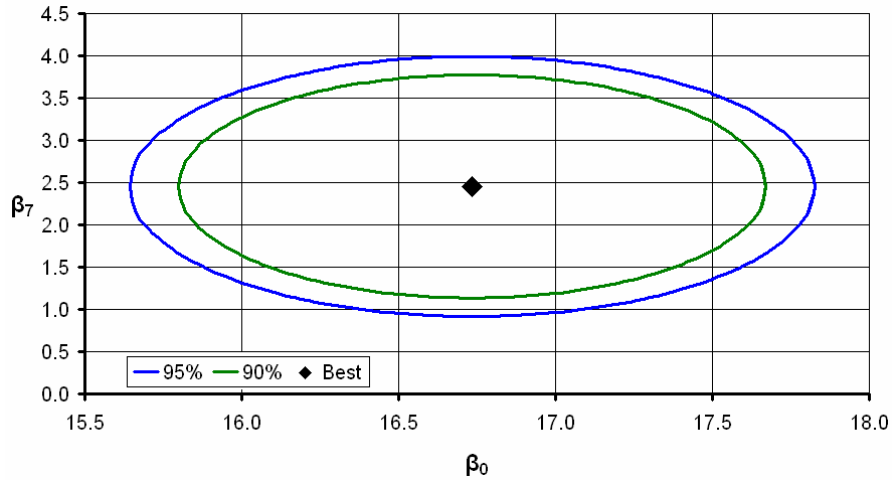


Figure I10: Volumetric Melt Flow Rate, Composition (β_7) versus Intercept (β_0)

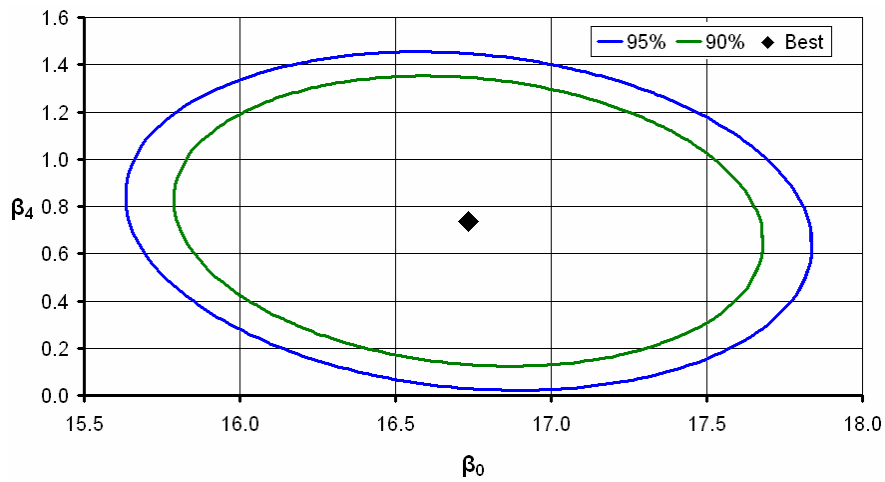


Figure I11: Volumetric Melt Flow Rate, N^2/Q (β_4) versus Intercept (β_0)

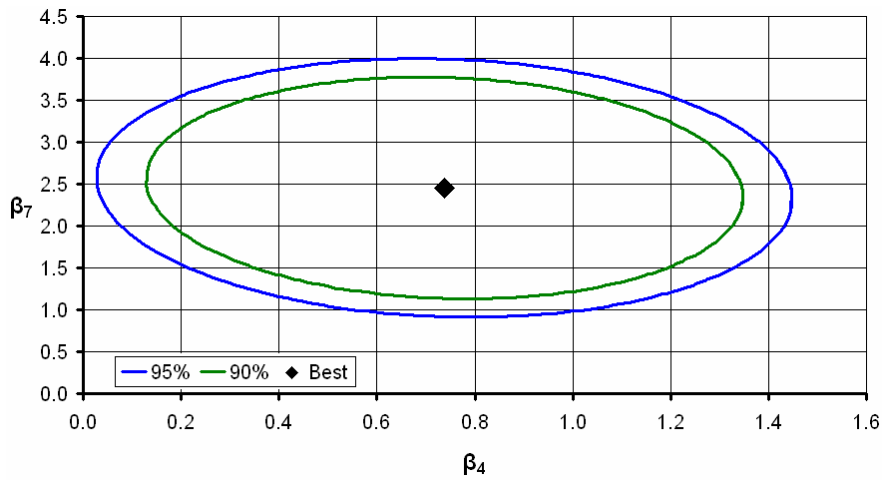


Figure I12: Volumetric Melt Flow Rate, N^2/Q (β_4) versus Composition (β_7)

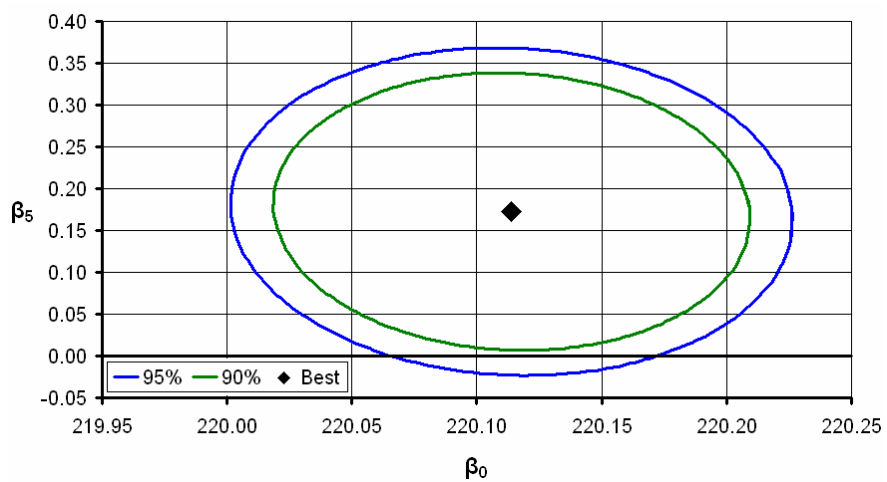


Figure I13: Main Melting Temperature 5°C/min DSC, 1/Q (β_5) versus Intercept (β_0)

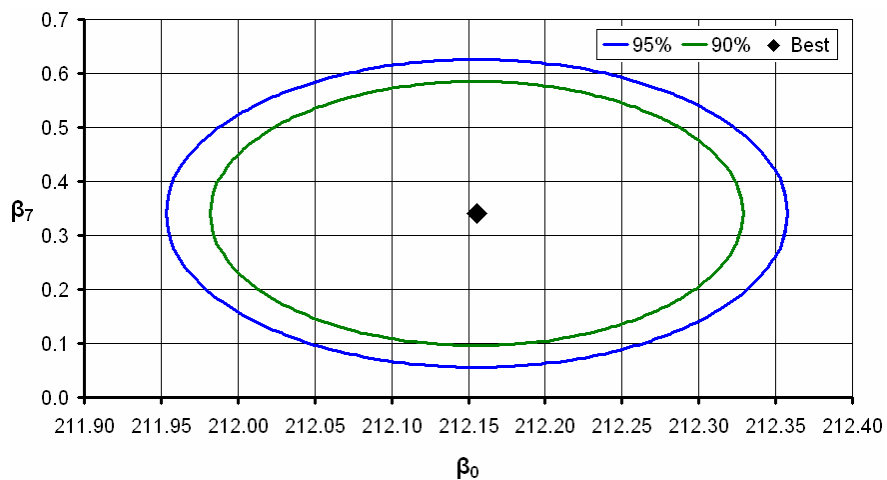


Figure I14: Small Melting Temperature 5°C/min DSC, Composition (β_7) versus Intercept (β_0)

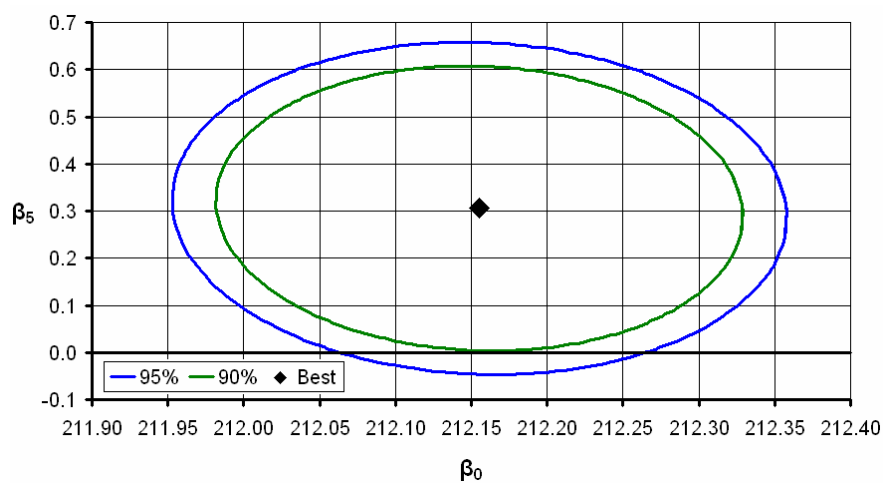


Figure I15: Small Melting Temperature 5°C/min DSC, 1/Q (β_5) versus Intercept (β_0)

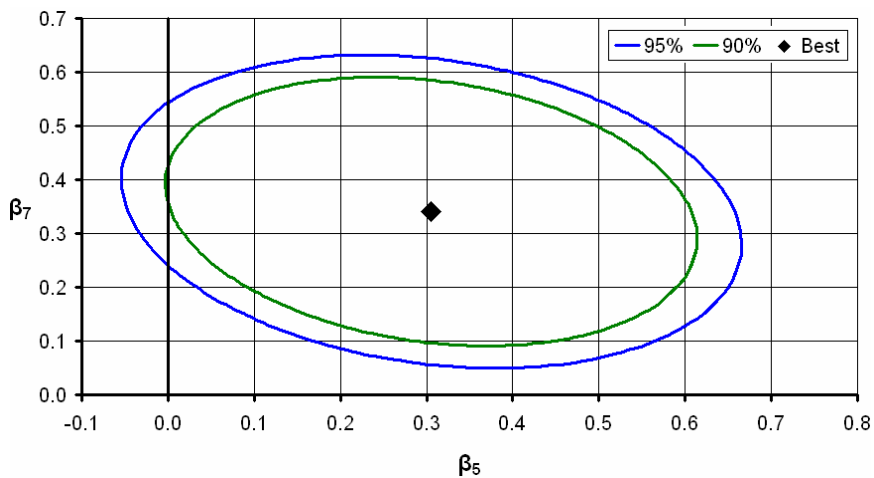


Figure I16: Small Melting Temperature 5°C/min DSC, 1/Q (β_5) versus Composition (β_7)

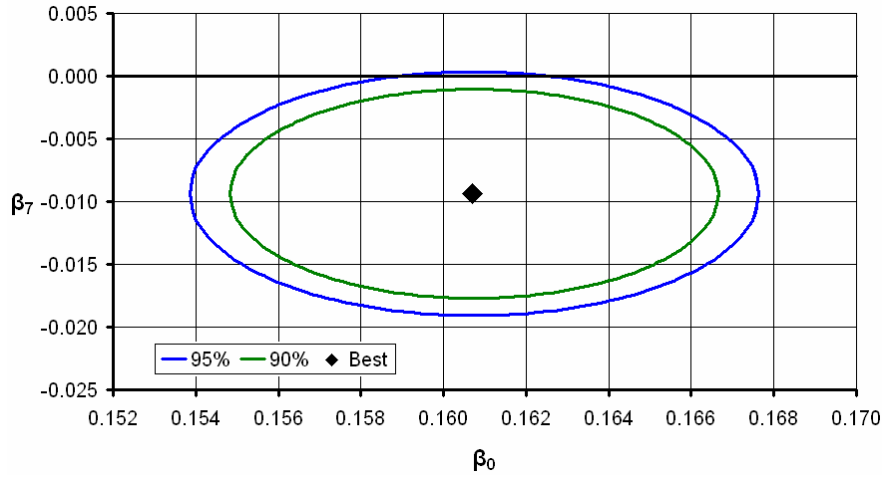


Figure I17: PC-Rich Phase 5°C/min DSC, Composition (β_7) versus Intercept (β_0)

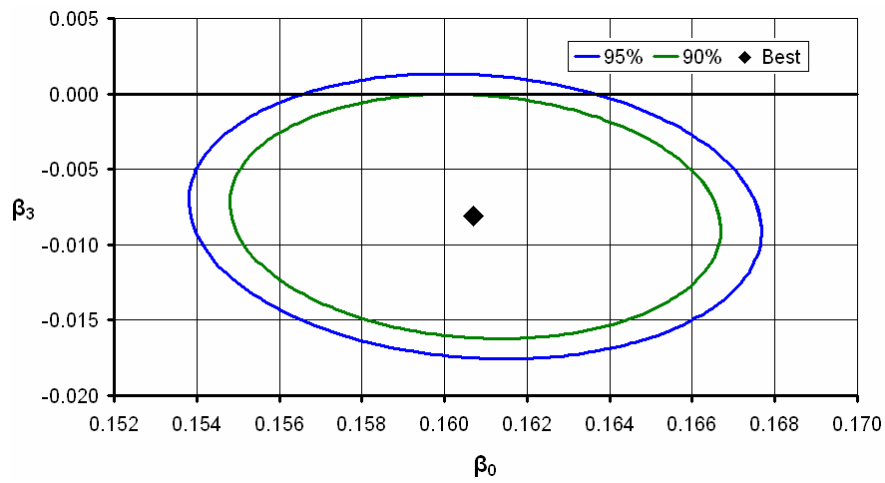


Figure I18: PC-Rich Phase 5°C/min DSC, N (β_3) versus Intercept (β_0)

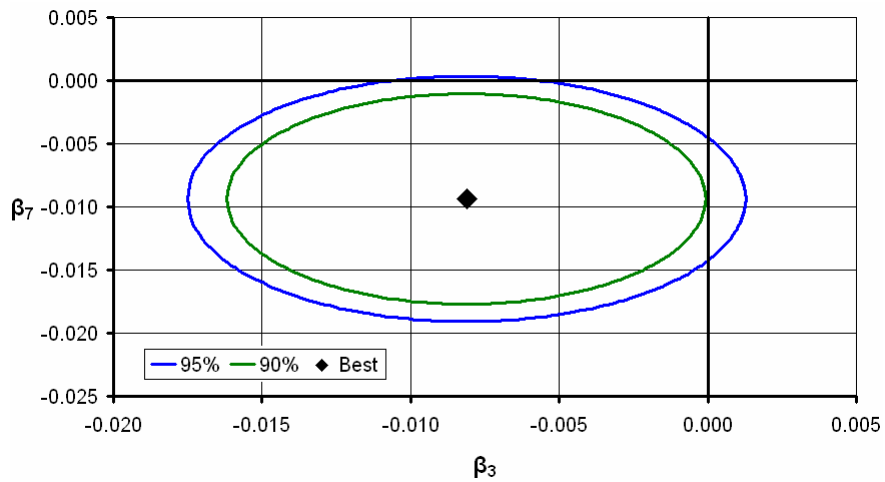


Figure I19: PC-Rich Phase 5°C/min DSC, Composition (β_7) versus N (β_3)